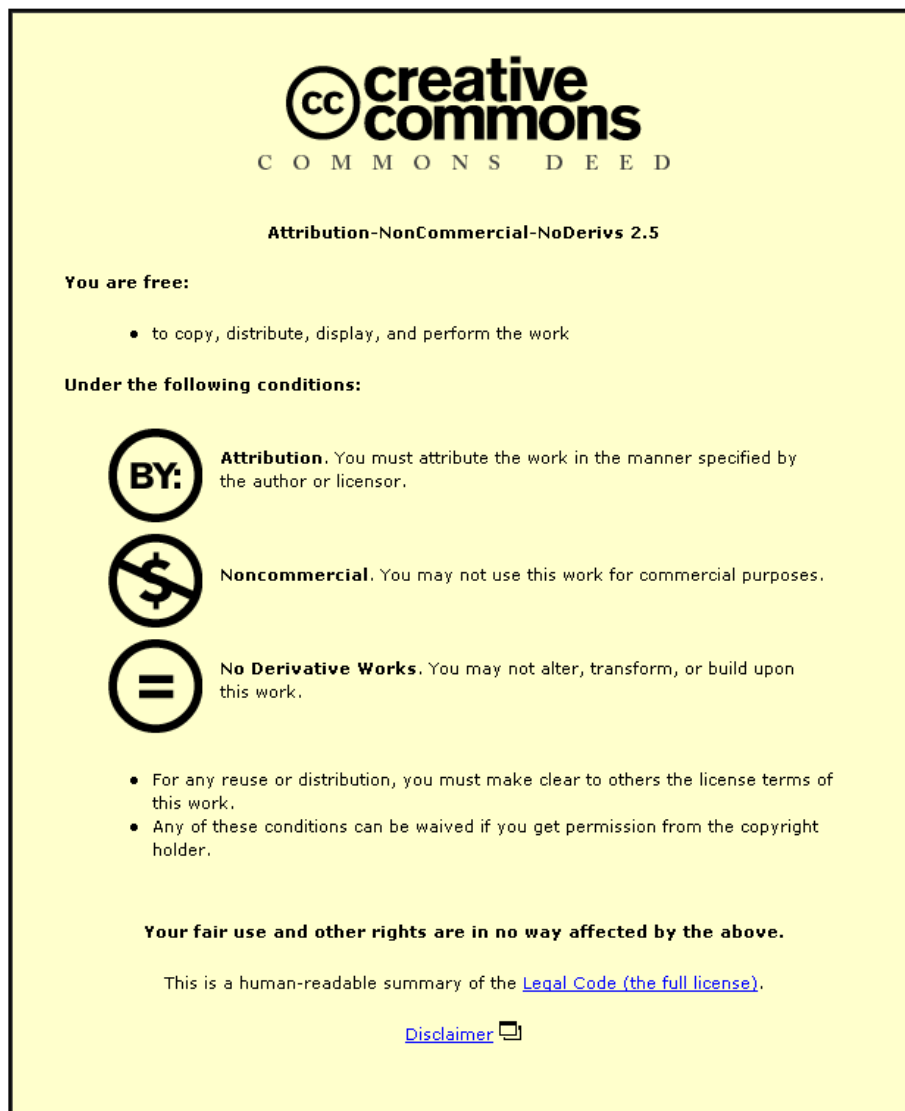


This item was submitted to Loughborough University as a PhD thesis by the author and is made available in the Institutional Repository (<https://dspace.lboro.ac.uk/>) under the following Creative Commons Licence conditions.



For the full text of this licence, please go to:
<http://creativecommons.org/licenses/by-nc-nd/2.5/>



Pilkington Library

Author/Filing Title PETIRAKSAKUL

Vol. No. Class Mark T

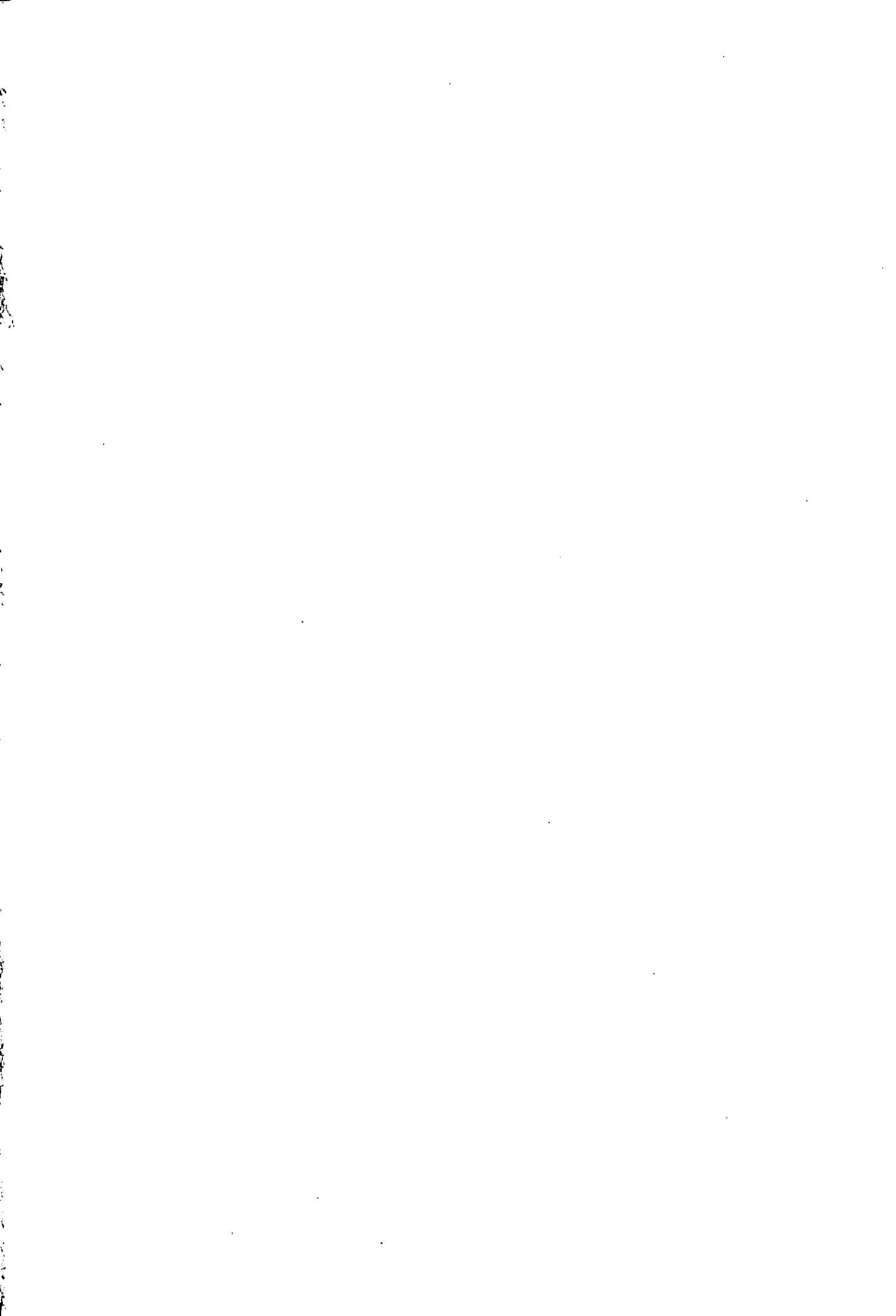
**Please note that fines are charged on ALL
overdue items.**

14 NOV 2000 11 JAN 2001	LOAN COPY	
----------------------------	-----------	--

FOR REFERENCE ONLY

0402219945





**Effect of Stearate/Stearic acid Coating on
Filled High Density Polyethylene Properties**

by

Pinsupha Petiraksakul

A Doctoral thesis submitted in partial fulfilment of the requirements
for the award of the degree of Doctor of Philosophy
of the Loughborough University

January 2000

Supervisor: Dr. Marianne Gilbert

Institute of Polymer Technology and Materials Engineering

© P. Petiraksakul, 2000

 Loughborough University Pitt Rivers Library
Date May 00
Class
Acc No. 040221994

M0001675LB

ABSTRACT

High density polyethylene (HDPE) is a widely used plastic but it is also a combustible material. One way of reducing flammability is to add fillers, such as magnesium hydroxide ($Mg(OH)_2$). However, this has a deleterious effect on the mechanical properties of composites. It has been found that one possible method of restoring mechanical properties is to modify the filler particles with coating agents, such as stearic acid. In the present work, this idea was taken a stage further with the use of various metal stearates (e.g. magnesium stearate, calcium stearate, and zinc stearate) for modifying filler. The fillers examined were magnesium hydroxide and calcium carbonate. A filler loading of 40% w/w was used in all samples. Samples were moulded into a variety of shapes for mechanical testing. Such tests included, tensile, flexural, and impact testing. To obtain deeper understanding of the effect of the coating agents on the fillers, a variety of fundamental tests were carried out. These included Diffuse Reflectance FTIR (DRIFT), Thermal Analysis using a DSC cell, X-ray Diffraction (XRD), contact angle measurement.

Unfilled HDPE, uncoated filled-HDPE, and coated filled-HDPE were compared using uncoated filled-HDPE as a base line. Uncoated filled-HDPE is more brittle than unfilled HDPE. Surface modification of filler improves the toughness properties. Comparing coated filled-compounds, stearic acid and zinc stearate caused a small improvement, magnesium stearate improved the properties significantly with calcium carbonate while calcium stearate gave the best results for coating magnesium hydroxide. One monolayer coating gave the best compound properties compared to other degrees of coating. Although, tensile/flexural strength was not greatly affected elongation at yield, extension at maximum load, and impact properties increased significantly.

DSC was used to observe the disappearance and conversion of coating agents as coating proceeded. X-ray diffraction showed the effect of injection moulding on the orientation of the filler and polymer. During coating of the filler particles, XRD and DSC were used to follow incorporation of stearate particles to produce the monolayer coverage. Surface free energy results showed that surface modification of filler resulted in the reduction of hydrophilicity of filler leading to tougher composites compared with uncoated filled-compounds.

Keywords: high density polyethylene, magnesium hydroxide, calcium carbonate, filled polymer, filler, metal stearate, stearic acid, surface modification, coating, DRIFT, DSC, X-ray diffraction, contact angle, surface free energy, mechanical properties, preferred orientation.

ACKNOWLEDGEMENTS

I would be grateful to thank all these people who give me their help and full support during studying at IPTME particularly to Dr Marianne Gilbert my kindly supervisor and the director of department for her excellent help, support, and encouragement, Dr D H Ross for all his help, support, advice, especially with X-ray diffraction; without his expert help it would not have been possible to understand in X-ray diffraction and crystal structures at all. Thank you David. Thanks also go to Prof. D J Hourston my director of research, Dr I Mathieson of ISST for her help with all the XPS experimental work and analysis, Mr N F Miller for his help, friendship, and computer assistance. I would like to thank for all IPTME staff as the following: Miss J Lennie (secretary of institute), Mr A Trotter (processing), Mr F Page (SEM), Mr R Owens (characterisation), Mr T Atkinson (photographic printing), Mr A McCormack (electrical assistance), Mr M R Shaheedullah (film scanning), all my friends at Loughborough University, and many others who have not their names in here.

Thank to Ramkumhaeng University, Bangkok, Thailand for supporting me to study here and all of the Thai Government students' office staff who give me full assistance.

Special thanks go to Prof. Dhawat my great dad and Mrs Supa Poonotoke my wonderful mum for all of their love, support, advice, and encouragement.

Finally, thanks go to Anurak, my lovely husband, and his family who always give excellent support, encouragement, and assistance.

CONTENTS

	<i>Page</i>
ABSTRACT	<i>i</i>
ACKNOWLEDGEMENTS	<i>ii</i>
CONTENTS	<i>iii</i>
LIST OF FIGURES	<i>viii</i>
LIST OF TABLES	<i>xiii</i>
NOMENCLATURE	<i>xiv</i>
CHAPTER 1 : INTRODUCTION	1
1.1 Introduction	1
1.2 Objectives	4
CHAPTER 2 : LITERATURE REVIEW	5
2.1 General	5
2.2 Polyethylene	5
2.3 Fillers	9
2.3.1 Calcium carbonate as a general purpose filler	9
2.3.2 Magnesium hydroxide as a flame retardant filler	13
2.4 Surface modification	19
2.4.1 Mechanism of surface modification	21
2.5 Surface modifiers	23
2.5.1 Organosilicon compounds	23
2.5.2 Organotitanates	24
2.5.3 Unsaturated polymeric acids	26
2.5.4 Organophosphates	26
2.5.5 Fatty acids	27

	<i>Page</i>
2.6 Characterisation techniques	31
2.6.1 Fourier transform infrared spectroscopy (FTIR)	32
2.6.2 X-Ray diffraction (XRD)	37
2.6.3 X-Ray photoelectron spectroscopy (XPS)	41
2.6.4 Surface energy analysis	43
2.7 Modification of mechanical properties	48
2.7.1 Effect on tensile and flexural properties	49
2.7.2 Effect on impact properties	51
2.7.3 Effect on crystallisation	52
CHAPTER 3 : EXPERIMENTAL	57
3.1 General	57
3.2 Materials	57
3.2.1 Polymer	57
3.2.2 Fillers	57
3.2.3 Coating agents	58
3.3 Sample preparation	58
3.3.1 Surface modification of fillers	58
3.3.2 Compounding	62
3.3.3 Injection moulding	65
3.4 Physical property characterisation	66
3.4.1 Fourier transform infrared spectroscopy (FTIR)	67
3.4.2 Thermal analysis	71
3.4.3 X-Ray diffraction (XRD)	74
3.4.4 Contact angle measurement	77
3.4.5 X-Ray photoelectron spectroscopy (XPS)	79
3.4.6 Scanning electron microscopy (SEM)	81
3.4.7 Ash determination	82

	<i>Page</i>
3.5 Mechanical property characterisation	84
3.5.1 Reversion measurement	85
3.5.2 Melt flow index determination	86
3.5.3 Tensile property determination	86
3.5.4 Flexural property determination	88
3.5.5 Falling weight impact properties	89
CHAPTER 4 : RESULTS AND DISCUSSION: SERIES I	91
4.1 General	91
4.2 Characteristic of a coating process	94
4.2.1 Effect of temperature on a coating process	94
4.2.2 Effect of various concentrations of coating agents on the coating process	101
4.3 Characterisation of coated fillers	107
4.3.1 Differential scanning calorimetry (DSC)	107
4.3.2 X-Ray diffraction (XRD)	114
4.3.3 Contact angle measurement	120
4.4 Effect of filler coating on compound properties	121
4.4.1 Filler content	122
4.4.2 Tensile properties	124
4.4.3 Flexural properties	130
4.4.4 Impact properties	135
4.4.5 Crystallisation properties	140
4.4.6 Reversion measurement	143
4.4.7 Filler/polymer orientations	144
4.4.8 Surface free energy	153
4.5 Summary	154

	<i>Page</i>
CHAPTER 5 : RESULTS AND DISCUSSION: SERIES II	156
5.1 Characterisation of coated fillers	157
5.1.1 Fourier transform infrared spectroscopy (FTIR)	157
5.1.2 Thermal analysis	163
5.1.3 X-Ray diffraction (XRD)	169
5.1.4 Contact angle measurement	174
5.1.5 X-Ray photoelectron spectroscopy (XPS)	176
5.2 Effect of coating agents on filled compound properties	181
5.2.1 Filler contents	181
5.2.2 Tensile properties	182
5.2.3 Flexural properties	187
5.2.4 Impact properties	191
5.2.5 Crystallisation properties	195
5.2.6 Reversion measurement	197
5.2.7 Filler/polymer orientation	198
5.2.8 Surface free energy	204
5.2.9 Specific energy	205
5.2.10 Microstructure and morphology	206
5.2.11 Wavelength dispersive X-Ray mapping (WDXM)	211
5.3 Effect of coating agents on polymer properties	215
5.3.1 Polymer/coating agent contents	215
5.3.2 Tensile properties	215
5.3.3 Flexural properties	217
5.3.4 Impact properties	218
5.3.5 Crystallisation properties	219
5.3.6 Reversion measurement	220
5.3.7 Polymer orientation	220
5.3.8 Surface free energy	221

	<i>Page</i>
5.3.9 Specific energy	222
5.3.10 Melt flow index (MFI)	222
5.4 Summary	223
5.4.1 Characterisation and mechanical properties	223
5.4.2 Structure/properties/interactions	224
CHAPTER 6 : CONCLUSIONS AND SUGGESTIONS FOR FURTHER WORK	226
6.1 Conclusions	226
6.2 Suggestions for further work	228
REFERENCES	230
APPENDIX A MACHINE PARAMETERS	243
APPENDIX B SUMMARISED RESULTS (SERIES I)	250
APPENDIX C SUMMARISED RESULTS (SERIES II)	262
APPENDIX D CALCULATIONS	269
APPENDIX E DSC TRACES	276
APPENDIX F FTIR AND XPS SPECTRA	291
APPENDIX G X-RAY DIFFRACTION PATTERNS	301
APPENDIX H MICROGRAPHS	311
APPENDIX I LIST OF PUBLICATIONS	313

LIST OF FIGURES

<i>Description</i>	<i>Page</i>
Figure 2.1: Molecular structure of polyethylene.	6
Figure 2.2: HDPE orthorhombic unit cell.	8
Figure 2.3: The unit cell of calcite.	10
Figure 2.4: Single layer of the brucite structure.	14
Figure 2.5: Different structures of surface monolayers on filler surfaces.	20
Figure 2.6: Diagrammatic representation of the unit cell of a stearic acid crystal.	29
Figure 2.7: Illustrative molecular structure and the corresponding infrared carbonyl frequency of monolayer and multilayer γ -MPS molecules.	35
Figure 2.8: Diagrams of crystal axes and reference axes.	39
Figure 2.9: Diagrammatic of a drop liquid deposited on a horizontal flat solid surface.	45
Figure 3.1: Fielder mixer.	60
Figure 3.2: The typical apparatus of compounder.	63
Figure 3.3: Injected specimen obtained from a) a four part mould, b) a four pieces tensile mould.	66
Figure 3.4: Schematic diagrams of FTIR apparatus.	68
Figure 3.5: FTIR spectrum of magnesium hydroxide coated with 6.2%w/w magnesium stearate.	70
Figure 3.6: A Soxhlet extraction apparatus.	71
Figure 3.7: DSC apparatus.	72
Figure 3.8: The thermogram of high density polyethylene.	73
Figure 3.9: Basic layout of a diffractometer.	75
Figure 3.10: The X-ray patterns of $Mg(OH)_2$ filled HDPE.	77
Figure 3.11: Diagrammatic of a contact angle measurement.	78
Figure 3.12: The basic elements of X-ray photoelectron spectroscopy.	80
Figure 3.13: Layout of the SEM.	82
Figure 3.14: Polymer, filler, and coating agent content determination.	83
Figure 3.15: Diagram of apparatus for measuring Melt Flow Index.	86
Figure 3.16: Flexural test in tensile machine.	88
Figure 3.17: Impact Falling Weight equipment.	90
Figure 4.1: Temperature against time for $Mg(OH)_2$ coated with 6.2% magnesium stearate in the Waring blender.	94
Figure 4.2: Temperature against time for $Mg(OH)_2$ coated with 6.4% calcium stearate in the Waring blender.	95
Figure 4.3: FTIR spectra of $Mg(OH)_2$ coated with 6.2% w/w magnesium stearate taken from the Waring blender after 5 and 40 minutes.	96
Figure 4.4: FTIR spectra of $Mg(OH)_2$ coated with 6.4% w/w calcium stearate taken from the Waring blender after 5 and 40 minutes.	97

<i>Description</i>	<i>Page</i>
Figure 4.5: Plot of CH/OH ratio versus coating time for Mg(OH) ₂ coated with 6.2% w/w magnesium stearate at various voltages in the Waring blender.	99
Figure 4.6: Plot of RCOO ⁻ /OH ratio versus coating time for Mg(OH) ₂ coated with 6.2% w/w magnesium stearate at various voltages in the Waring blender.	99
Figure 4.7: Plot of CH/OH ratio versus coating time for Mg(OH) ₂ coated with 6.4% w/w calcium stearate at various voltages in the Waring blender.	100
Figure 4.8: Plot of RCOO ⁻ /OH ratio versus coating time for Mg(OH) ₂ coated with 6.4% w/w calcium stearate at various voltages in the Waring blender.	100
Figure 4.9: Temperature against coating time in the Fielder mixer.	102
Figure 4.10: FTIR spectra of Mg(OH) ₂ uncoated and coated with 3.1%, 6.2%, and 9.3% magnesium stearate after coating 40 minutes in the Fielder mixer.	103
Figure 4.11: FTIR spectra of Mg(OH) ₂ uncoated and coated with 3.2%, 6.4%, and 9.6% calcium stearate after coating 40 minutes in the Fielder mixer.	103
Figure 4.12: Plot of CH/OH ratio versus coating time for Mg(OH) ₂ coated with various concentrations of magnesium stearate and stearic acid in the Fielder mixer.	105
Figure 4.13: Plot of RCOO ⁻ /OH ratio versus coating time for Mg(OH) ₂ coated with various concentrations of magnesium stearate and stearic acid in the Fielder mixer.	106
Figure 4.14: Plot of CH/OH ratio versus coating time for Mg(OH) ₂ coated with various concentrations of calcium stearate in the Fielder mixer.	106
Figure 4.15: Plot of RCOO ⁻ /OH ratio versus coating time for Mg(OH) ₂ coated with various concentrations of calcium stearate in the Fielder mixer.	107
Figure 4.16: Plots of free components against coating time for magnesium hydroxide coated with magnesium stearate a: 3.1% w/w, b: 6.2% w/w, and c: 9.3% w/w.	111
Figure 4.17: Plot of free component against coating time for magnesium hydroxide coated with 6.4% w/w calcium stearate at different voltages supplied in the Waring mixer.	112
Figure 4.18: Plots of free components against coating time for magnesium hydroxide coated with calcium stearate a: 3.2% w/w, b: 6.4% w/w, and c: 9.6% w/w.	114

<i>Description</i>	<i>Page</i>
Figure 4.19: X-ray patterns of magnesium hydroxide coated with various of magnesium stearate concentrations at coating time of 5 min.	116
Figure 4.20: X-ray patterns of magnesium hydroxide coated with various of magnesium stearate concentrations at coating time of 40 min.	117
Figure 4.21: X-ray patterns of magnesium hydroxide coated with various of calcium stearate concentrations at coating time of 5 min.	119
Figure 4.22: X-ray patterns of magnesium hydroxide coated with various of calcium stearate concentrations at coating time of 40 min.	119
Figure 4.23: Tensile properties of unfilled and Mg(OH) ₂ filled HDPE at the different coating levels of magnesium stearate and stearic acid.	128
Figure 4.24: Tensile properties of unfilled and Mg(OH) ₂ filled HDPE at the different coating levels of calcium stearate.	129
Figure 4.25: Flexural properties of unfilled and Mg(OH) ₂ filled HDPE at different coating levels of Mg stearate and stearic acid.	132
Figure 4.26: Flexural properties of unfilled and Mg(OH) ₂ filled HDPE at different coating levels of calcium stearate.	134
Figure 4.27: Falling Weight Impact properties of unfilled and Mg(OH) ₂ filled HDPE with different levels of magnesium stearate and stearic.	136
Figure 4.28: Falling Weight Impact properties of unfilled and Mg(OH) ₂ filled HDPE with different levels of calcium stearate.	138
Figure 4.29: The proposed mechanisms of coating filler.	140
Figure 4.30: %Reversion test of unfilled and Mg(OH) ₂ filled HDPE at different coating levels of magnesium stearate and stearic acid.	143
Figure 4.31: %Reversion test of unfilled and Mg(OH) ₂ filled HDPE at different coating levels of calcium stearate.	144
Figure 4.32: Orthorhombic structure for polyethylene.	146
Figure 4.33 Hexagonal close packed structure for magnesium hydroxide.	147
Figure 4.34: Scheme of test sample showing places and directions of the X-ray diffraction measurements and the mutual orientation of the magnesium hydroxide and PE crystals.	147
Figure 4.35: Plot of peak intensity ratio of PE200/110 for unfilled and Mg(OH) ₂ filled HDPE with various magnesium stearate concentrations.	148
Figure 4.36: Plot of peak intensity ratio of MH001/101 for unfilled and Mg(OH) ₂ filled HDPE with various magnesium stearate concentrations.	150
Figure 4.37: Plot of peak intensity ratio of PE200/110 for unfilled and Mg(OH) ₂ filled HDPE with various calcium stearate concentrations.	151
Figure 4.38: Plot of peak intensity ratio of MH001/101 for unfilled and Mg(OH) ₂ filled HDPE with various calcium stearate concentrations.	152

<i>Description</i>	<i>Page</i>
Figure 5.1: FTIR spectra of $Mg(OH)_2$ uncoated/coated with various coating agent types.	158
Figure 5.2: CH/OH ratio versus time for magnesium hydroxide coated with metal stearates and stearic acid in the Fielder high speed mixer.	159
Figure 5.3: RCOO/OH ratio versus time for magnesium hydroxide coated with metal stearates and stearic acid in the Fielder high speed mixer.	160
Figure 5.4: FTIR spectra of $CaCO_3$ uncoated and coated with various coating agent types.	161
Figure 5.5: CH/CO ratio versus time for calcium carbonate coated with metal stearates and stearic acid in the Fielder high speed mixer.	161
Figure 5.6: Free components versus coating time for magnesium hydroxide coated with one monolayer of different coating agent types.	166
Figure 5.7: Free components versus coating time for calcium carbonate coated with one monolayer of different coating agent types.	168
Figure 5.8: X-ray diffraction patterns of magnesium hydroxide added with 6.2% w/w magnesium stearate at various coating time.	170
Figure 5.9: X-ray diffraction patterns of magnesium hydroxide coated with 6.2% w/w magnesium stearate at various coating time.	171
Figure 5.10: X-ray diffraction patterns of magnesium hydroxide coated with 6.4% w/w calcium stearate at various coating time.	172
Figure 5.11: X-ray diffraction patterns of magnesium hydroxide coated with 6.7% w/w zinc stearate at various coating time.	173
Figure 5.12: X-ray diffraction patterns of magnesium hydroxide coated with 6.0% w/w stearic acid at various coating time.	174
Figure 5.13: High energy resolution carbon 1s photoelectron peaks for uncoated and coated magnesium hydroxide with various magnesium stearate concentrations.	177
Figure 5.14: High energy resolution carbon 1s photoelectron peaks for uncoated and coated magnesium hydroxide with various coating agent types.	178
Figure 5.15: High energy resolution carbon 1s photoelectron peaks for uncoated and coated calcium carbonate with various coating agent types.	180
Figure 5.16: Tensile properties of unfilled and $Mg(OH)_2$ filled HDPE containing various coating agent types.	184
Figure 5.17: Tensile properties of unfilled and $CaCO_3$ filled HDPE containing various coating agent types.	186
Figure 5.18: Flexural properties of unfilled and $Mg(OH)_2$ filled HDPE containing various coating agent types.	188
Figure 5.19: Flexural properties of unfilled and $CaCO_3$ filled HDPE containing various coating agent types.	191

<i>Description</i>	<i>Page</i>
Figure 5.20: Impact properties of high density polyethylene filled with 40% Mg(OH) ₂ , uncoated and coated with different types of coating agents.	192
Figure 5.21: Impact properties of high density polyethylene filled with 40% CaCO ₃ , uncoated/coated with different types of coating agents.	194
Figure 5.22: %Reversion test of unfilled and Mg(OH) ₂ filled HDPE containing various coating agent types.	197
Figure 5.23: %Reversion test of unfilled and CaCO ₃ filled HDPE containing various coating agent types.	198
Figure 5.24: Peak intensity ratio of PE200/110 of unfilled HDPE and Mg(OH) ₂ filled compounds containing various coating agent types.	200
Figure 5.25: Peak intensity ratio of MH001/101 for pure magnesium hydroxide and Mg(OH) ₂ filled compounds containing various coating agents types.	201
Figure 5.26: Peak intensity ratio of PE200/110 for unfilled HDPE and CaCO ₃ filled compounds containing various coating agent types.	202
Figure 5.27: Peak intensity ratio of CC104/110 for pure calcium carbonated and CaCO ₃ filled compounds containing various coating agent types	203
Figure 5.28: Rhombohedral structure; plane axes of calcium carbonate.	203
Figure 5.29: Scheme of a test sample showing places and directions of the X-ray diffraction measurements and the mutual orientation of calcium carbonate and polyethylene crystals.	204
Figure 5.30: Microstructure of HDPE compounds containing uncoated and coated magnesium hydroxide.	208
Figure 5.31: Microstructure of HDPE compounds containing uncoated and coated calcium carbonate.	210
Figure 5.32: Micrographs of Mg and Ca mapping for HDPE compounds containing uncoated and coated magnesium hydroxide.	212
Figure 5.33: Micrographs of Mg and Ca mapping for HDPE compounds containing uncoated and coated calcium carbonate.	213
Figure 5.34: Tensile properties of unfilled HDPE and HDPE compounds containing various coating agent types.	216
Figure 5.35: Flexural properties of unfilled HDPE and HDPE compounds containing various coating agent types.	218
Figure 5.36: Impact properties of unfilled HDPE and HDPE compounds containing various coating agents.	219
Figure 5.37: %Reversion of HDPE filled with various coating agents.	220
Figure 5.38: Plot of the peak intensity ratio of PE200/110 for HDPE unfilled and filled with various coating agents.	221

LIST OF TABLES

<i>Description</i>	<i>Page</i>
Table 3.1: Technical specification of fillers.	58
Table 3.2: Technical data of coating agents.	58
Table 3.3: Filler formulations used for Series I-a.	61
Table 3.4: Filler formulations used for Series I-b.	62
Table 3.5: Filler formulations used for Series II-a.	62
Table 3.6: Filler formulations used for Series II-b.	62
Table 3.7: Setting temperatures of the barrel.	63
Table 3.8: Compound formulations used for Series I-a.	64
Table 3.9: Compound formulations used for Series I-b.	64
Table 3.10: Compound formulations used for Series II-a.	64
Table 3.11: Compound formulations used for Series II-b.	65
Table 3.12: Compound formulations used for Series II-c.	65
Table 3.13: The surface tension of liquids.	78
Table 4.1: Melting properties of coating agents.	91
Table 4.2: Contact angles and surface energy of pure coating agent, uncoated filler, and coated filler with various calcium stearate concentrations.	120
Table 4.3: Filler and coating contents for unfilled HDPE and HDPE compounds containing Mg(OH) ₂ coated with various concentrations of magnesium stearate and stearic acid.	123
Table 4.4: Filler and coating contents for unfilled HDPE and HDPE compounds containing Mg(OH) ₂ coated with various concentrations of calcium stearate.	124
Table 4.5: Crystallisation properties for unfilled HDPE and Mg(OH) ₂ filled HDPE containing various concentrations of magnesium stearate and stearic acid.	142
Table 4.6: Crystallisation properties for unfilled HDPE and Mg(OH) ₂ filled HDPE containing various concentrations of calcium stearate.	142
Table 4.7: Contact angles and surface free energy of calcium stearate filled-HDPE.	153
Table 5.1: Contact angles and surface free energy of studied substances.	175
Table 5.2: Surface compositions of uncoated and coated magnesium hydroxide.	176
Table 5.3: Surface compositions of uncoated and coated calcium carbonate.	180
Table 5.4: Filler and coating agent contents.	182
Table 5.5: Crystallisation properties for unfilled HDPE and Mg(OH) ₂ /CaCO ₃ filled HDPE containing various coating agents.	196
Table 5.6: Contact angles and surface free energy of samples.	205
Table 5.7: Specific energy of compounding machine for HDPE compounds.	206
Table 5.8: Polymer/coating agent contents.	215
Table 5.9: Crystallisation properties for HDPE compounds with and without various coating agents.	219
Table 5.10: Contact angles and surface free energy of HDPE containing coating agent.	222
Table 5.11: Specific energy of compounding machine for HDPE compounds.	222
Table 5.12: Melt flow indices of HDPE unfilled and filled with various coating agents.	223

NOMENCLATURE

<i>Symbols</i>	<i>Descriptions</i>	<i>Unit</i>
a, b, c	: axial translations (unit cell constants)	[Å]
A_0	: original area of specimen	[m ²]
A_a	: cross section area of acid	[nm ² /molecule]
b_1	: specimen width	[mm]
d	: average particle diameter	[m]
d_{hkl}	: interplanar spacing for hkl planes	[Å]
E	: Young's modulus	[N/mm ²]
E_b	: binding energy	[eV]
E_F	: flexural modulus	[N/mm ²]
f_c	: percent of crystallinity	[%]
F	: applied force	[N]
F_m	: force at the mid-point	[N]
ΔH_m	: enthalpy of fusion for semi-crystalline polymer	[J/g]
ΔH_{mc}	: enthalpy of fusion for completely crystalline polymer	[J/g]
h	: Plank's constant	[Js]
h_1	: specimen thickness	[mm]
K	: stress concentration factor	[-]
k	: slope of plot of tensile strength	[-]
KE	: kinetic energy	[eV]
L	: length of interest during the test	[mm]
L_0	: initial length	[mm]
L_1	: final length	[mm]
L_m	: monolayer coverage	[g _{acid} /g _{filler}]
MW_a	: molecular mass of the acid	[g/mole]
N_A	: Avogadro's number	[molecules/mol]
R_m	: maximum reversion value	[%]
S_f	: specific area of filler	[nm ² /g]
T_c	: recrystallisation temperature	[°C]
T_m	: melting temperature	[°C]
T_{sm}	: onset of melting temperature	[°C]
T_{sc}	: onset of recrystallisation temperature	[°C]
V_p	: volume fraction of filler	[-]
W_{SL}	: work of adhesion	[mJ/m ²]

Symbols	Descriptions	Unit
W_{SL}^H	: hydrogen bonding at interfacial between solid and liquid	[mJ/m ²]
W_{SL}^π	: π -bond at interfacial between solid and liquid	[mJ/m ²]
W_{SL}^P	: polar interaction at interfacial between solid and liquid	[mJ/m ²]
W_{SL}^E	: electrostatic interaction at interfacial between solid and liquid	[mJ/m ²]
Greek	Descriptions	Unit
α, β, γ	: angles between crystal axes	[degree]
δ	: central deflection	[mm]
ε	: strain	[-]
$\Delta\varepsilon$: difference in strain between two points	[-]
ν	: frequency of light	[s ⁻¹]
2θ	: angle of deviation of diffracted rays from the incident X-ray	[degree]
θ_1	: contact angle	[degree]
λ	: X-ray wavelength	[Å]
ϕ_s	: correction factor for the spectrometer function	[-]
σ	: stress	[N/mm ²]
$\Delta\sigma$: difference in stress between two points	[N/mm ²]
σ_c	: composite tensile strength	[N/mm ²]
σ_F	: flexural stress	[N/mm ²]
σ_m	: matrix tensile strength	[N/mm ²]
γ_L	: surface tension of liquid	[mJ/m ²]
γ_S	: surface tension of solid	[mJ/m ²]
γ_{SL}	: interfacial tension between the solid and the liquid	[mJ/m ²]
γ_S^D	: dispersion energy of solid	[mJ/m ²]
γ_L^D	: dispersion energy of liquid	[mJ/m ²]
γ_S^P	: polar part of the surface free energy of solid	[mJ/m ²]
γ_L^P	: polar part of the surface free energy of liquid	[mJ/m ²]
γ_{SL}^D	: dispersion energy of interface between solid and liquid	[mJ/m ²]
γ_S^+	: electron-acceptor parameter of the surface tension of solid	[mJ/m ²]
γ_S^-	: electron-donor parameter of the surface tension of solid	[mJ/m ²]
γ_L^+	: electron-acceptor parameter of the surface tension of liquid	[mJ/m ²]
γ_L^-	: electron donor parameter of the surface tension of liquid	[mJ/m ²]

C H A P T E R 1

INTRODUCTION

1.1 INTRODUCTION

Plastics were produced industrially beginning in the nineteenth century and they have been used in many applications. Polyethylene is one of the most popular polyolefins derived from oils. It was accidentally discovered in the ICI laboratories in the UK in 1933 and was commercialised in the early 1950s [1]. There are three grades of polyethylene; low density (LDPE) produced by polymerisation using a free radical source at high pressures, linear low density (LLDPE) produced by various techniques designed to give chains with limited short chain branching, and high density (HDPE) produced by the Ziegler process [1]. The applications for polyethylene are cold water piping, toys, housewares, packaging, films, bottles, and containers, etc. Polyethylene was also introduced in the cable industry as an electrical insulator as it is a nonpolar material, with properties, including low dielectric constant, which were almost independent of temperature and frequency. In particular, wire and cable works require materials which have high environmental durability and good insulation properties, thus high density polyethylene is used as an excellent electrical insulator which has increased in demand continuously over the years. However, high density polyethylene still has limitations in use. Like linear alkanes, high density polyethylene is a linear hydrocarbon polymer, therefore, it sputters and burns readily unless combined with flame retardant materials which generally result in lower ignition sensitivity and lower flammability of composites.

A number of flame retardants which have been used in the plastics industry, such as the organophosphates, can change polymer decomposition chemistry by inducing the formation of a surface char layer. This layer both insulates the product from further

thermal degradation and obstructs the flow of combustible vapours from inside the product to the gas phase where combustion would occur. Halogen-containing species, and other additives, can be selected to vaporise at the same temperature as polymer fragments. During burning, the halogens can help to decrease the concentration of the free radicals which propagate flames in the reactive area, thus these materials are effective at reducing the flame intensity and burning rate, respectively, even when used at low levels of the filler addition. However, the burning of halogenated materials produces toxic and corrosive smoke, which results in damage to electronic components and can also cause loss of life. The incineration of halogenated waste products can also produce dioxin and furan like species, therefore, the use of halogenated-flame retardants is becoming less popular. Halogen-free flame retardants, such as aluminium trihydroxide ($\text{Al}(\text{OH})_3$) and magnesium hydroxide ($\text{Mg}(\text{OH})_2$), are an alternative type of additive to reduce hazards from unwanted fires. The incorporation of these additives into polymers can increase the heat capacity of compounds, therefore, the enthalpy needed to bring the polymer to a temperature at which fracture of chemical bonds occurs is increased. The endothermic volatilisation of bound water is a significant function of this family of retardants. Aluminium trihydroxide is widely used in thermosets and some thermoplastics as an effective smoke suppressant. It is, however, not suitable to be incorporated into polyolefins processed at high temperature as it has a relatively low decomposition temperature. This has led to a surge of interest in other more stable materials, such as magnesium hydroxide, which decomposes at 330°C , which is 100°C higher than aluminium hydroxide, therefore $\text{Mg}(\text{OH})_2$ can be incorporated into polymers processed at high temperature [2].

To obtain effective fire retardant with halogenated fillers requires a loading, typically of 2-10 %w/w. However, to obtain equivalent fire retardant with metal hydroxide fillers requires a loading of 40-60 %w/w, which results in poor mechanical properties of composites [3-6]. The restoration of the mechanical properties can be achieved by treating the filler surface with coating agents such as silanes, titanates, and fatty acids.

These coating agents can aid the wetting of filler in a nonpolar polymer matrix resulting in a better dispersion of the filler in the compound. For the surface treatment of alkaline fillers, such as magnesium hydroxide and calcium carbonate, fatty acids are the most common coating agents used to give strong surface interaction between basic groups of filler and acid groups of fatty acid. This type of coating is cheap, easily applied and is widely used. Benefits, include easier processing and being capable of decreasing water adsorption of fillers. Fatty acids commonly used contain hydrocarbon chains only 16-18 atoms long which is too short to entangle with the matrix to give strong adhesion between the filler surface and polymer resin [7]. They are also unable to react chemically with the matrix, and so are generally weakly interacting and produce low bond strengths between filler and matrix. A common example of fatty acids is stearic acid.

While many researches have been concerned with the study of magnesium hydroxide as a flame retardant and smoke suppressant in plastics, little has been published concerning the effects of magnesium hydroxide coated with stearic acid and other fatty acids on mechanical properties of the composites. Also metal stearates have not yet been considered as an alternative. It is, therefore, desirable to understand further the effects of surface modification of magnesium hydroxide and calcium carbonate coated with metal stearates, on mechanical properties of 40% filled high density polyethylene composites. The thesis will be focused on two separate areas. First, the effects of $Mg(OH)_2$ coated with various amounts of magnesium and calcium stearates on mechanical properties of filled HDPE composites will be studied (Series I). The second study will be concerned on the use of various types of coating agents on $Mg(OH)_2$ and $CaCO_3$ filled HDPE (Series II). The effect of the coating agent alone on mechanical properties of HDPE compounds will also be investigated. Magnesium, calcium, and zinc stearates, and stearic acid will be used as coating agents.

1.2 OBJECTIVES

In order to produce a filled HDPE that is effective in commercial and functional terms a number of objectives that need investigating can be suggested.

1. To study the amount of coating agent required to form a monolayer on the filler surface.
2. To understand the nature of the coating agents and their effects on the filler surface.
3. To investigate the effects of different combinations of fillers and coating agents on mechanical properties of the composites.
4. To relate the surface treatment and the surface free energies of the various components to the improvement of mechanical properties of the composites.

CHAPTER 2

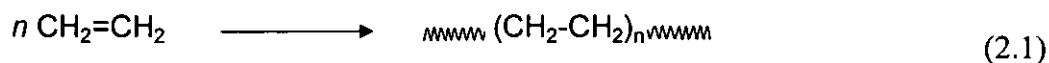
LITERATURE REVIEW

2.1 GENERAL

This chapter focuses on polyethylenes and their properties. Filler and surface modifier properties are introduced together with the characterisation methods (for fillers and composites) involving techniques such as Fourier Transform Infrared Spectroscopy (FTIR), X-ray diffraction (XRD), X-ray photoelectron spectroscopy (XPS), and contact angle measurement (surface energy analysis). Furthermore, the modification of mechanical properties and processing performance of filled thermoplastics are also considered.

2.2 POLYETHYLENE

Polyethylene (PE) is a thermoplastic material which easily softens when heated and solidifies on cooling. This property influences the capacity for processing and recycling of thermoplastics. The main attractive features of polyethylene include its low price, excellent electrical insulation properties, very good chemical resistance, good processibility, toughness, flexibility and transparency in thin films. Consequently polyethylene has become the largest volume commercial polymer in the world. Polyethylene is a linear polymer and is produced from ethylene by addition polymerisation. Its general formula is $-(CH_2-CH_2)_n-$ and the fundamental polymerisation reaction can be expressed as Equation (2.1):



Polyethylenes are divided into four groups. Firstly, low density polyethylene (LDPE) contains alkyl substituents, or short-chain branches and long-chain branches on the

chain backbone. LDPE is a homopolymer synthesised by free-radical polymerisation at high pressure. Branches are formed by molecular rearrangements of the polyethylene backbone while the chains are growing. The branches normally contain 2-8 carbon atoms of alkyl substituents, most often 4, thus these polyethylenes are associated with copolymers of ethylene and a mixture of α -olefins which contain a considerable amount of 1-hexene. Low density polyethylenes have densities of about $0.910\text{-}0.930\text{ g/cm}^3$ and a melting point of $105\text{-}115^\circ\text{C}$ [8]. The degree of crystallinity of a typical commercial grade is 45-55% and these products usually contain 15-25 short-chain branches per 1000 carbon atoms. As a result of the substitution of the alkyl groups, the formation of long-chain branches as long as the backbone chain occurs from grafting of polymer chains to inert chains before they have been removed from the reactor. The LDPE molecular structure is shown in Figure 2.1.

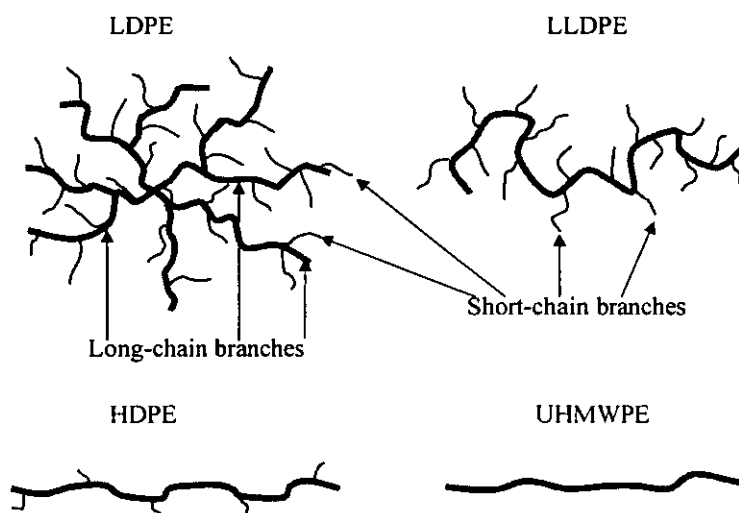


Figure 2.1: Molecular structure of polyethylenes.

The second group is linear low density polyethylene (LLDPE) and medium density polyethylene (MDPE) containing linear molecules without long-chain branches. Short-chain branches in the LLDPE molecule are obtained with the polymerisation of ethylene with other α -olefins. The length and number of these short-chain branches relate directly to the molecular weight and concentration of the α -olefin monomer. It is believed that increasing length of a short-chain branch may obstruct molecular

chain folding and hence reduce the growth of crystal lamella as it solidifies. This hindrance may increase the number of interlamellar tie-molecules, resulting in a stronger product [9]. Typically, linear low density polyethylenes have densities of 0.915-0.970 g/cm³ and a crystallinity of about 25-75 % [10]. Most of these products are made using the Ziegler-type catalysts.

Ultrahigh molecular weight polyethylene (UHMWPE) is high density polyethylene which has a molecular weight over 3×10^6 and a crystallinity of about 45% [10]. UHMWPE and high density polyethylene are chemically identical as both are straight chain linear polymers. The Ziegler catalyst process is used for UHMWPE polymerisation which can be a batch or continuous process. Typically most UHMWPE is produced by a slurry process, however, both solution and bulk processes are applicable.

The final polyethylene group is high density polyethylene (HDPE) which is usually produced using the Ziegler-type or Phillips catalysts. It is a homopolymer containing a small number of chain branches. The chain branches are freely introduced by the co-polymerisation of ethylene with α -olefins or are manifested in chains as a result of side reactions for a particular polymerisation mechanism. The most regular linear structure is produced using chromium oxide-based catalysts [11]. The HDPE molecule consists of two chain ends, one is usually a methyl group, and the other chain end is either a similar saturated group if hydrogen is used as a chain-transfer agent in the polymerisation, or it contains a double bond. Typically, the double-bond structure is vinyl, vinylidene, and trans-vinylene [8]. Vinyl groups are formed during the chain-transfer reaction to ethylene, and the other groups are produced during similar reactions at branching points and in double-bond isomerisations. HDPE is a semi-crystalline polymer with crystallinities of 60-80% [12] and densities of 0.940-0.970 g/cm³. The local chain conformation of HDPE is all trans, corresponding to the flat zigzag chain configuration [10, 13, 14], which has a C-C bond length of 1.54 Å, a C-C-C angle of 112°, and a length of ethylene unit of 2.53 Å. A number of HDPE crystalline structures is possible, the principal form is an orthorhombic shape and contains two

repeat units, one in the centre and $\frac{1}{4}$ at each corner. The cell parameters are: $a = 7.40 \text{ \AA}$, $b = 4.93 \text{ \AA}$, $c = 2.53 \text{ \AA}$ and the chain axes are aligned in the c axis direction which is parallel to the 200 plane and perpendicular to the 001 plane [15-18]. The HDPE unit cell is shown in Figure 2.2. The theoretical density of the HDPE crystal is 1.00 g/cm^3 . A second crystalline modification is pseudomonoclinic with unit-cell parameters: $a = 4.05 \text{ \AA}$, $b = 4.85 \text{ \AA}$, $c = 2.54 \text{ \AA}$, $\alpha = \beta = 90^\circ$, $\gamma = 105^\circ$, and has a theoretical density of 0.956 g/cm^3 [8]. This modification usually forms during low temperature processing. Another unstable crystalline modification of PE is triclinic, with $a = 4.28 \text{ \AA}$, $b = 4.80 \text{ \AA}$, $c = 2.45 \text{ \AA}$, $\alpha = 90^\circ$, $\beta = 110^\circ$, $\gamma = 108^\circ$, and has a density of 1.00 g/cm^3 [8].

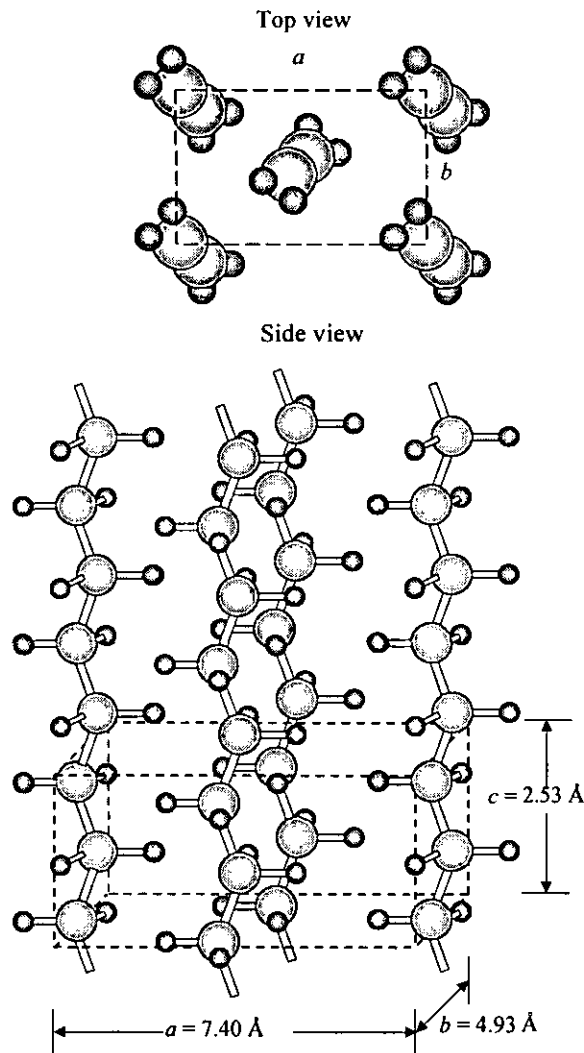


Figure 2.2: HDPE orthorhombic unit cell showing the unit cell parameters a , b and c [17].

2.3 FILLERS

Fillers are defined as solid substances which are added to plastics to promote better mechanical properties, higher bulk and density of composites, and also low product cost. There are a variety of filler types, such as mineral powders, carbon black, metallic powders, glass fibres, and flame-retardant fillers, etc. The use of fillers depends on both polymer and filler properties and the possibility of producing good quality and low price products. Polyethylene is a combustible material and it is relatively easily ignited. The fillers that have usually been used and researched are mineral powders and flame retardant fillers. In this section, calcium carbonate and magnesium hydroxide are described as a general purpose filler and a flame retardant filler respectively, together with their effects on the properties of the filled thermoplastic composites.

2.3.1 CALCIUM CARBONATE AS A GENERAL PURPOSE FILLER

Calcium carbonate has the chemical formula CaCO_3 and a molecular weight of 100. CaCO_3 is found naturally in different crystalline forms and with various degrees of chemical purity [19]. Calcium carbonate has three crystal modifications, aragonite, calcite and vaterite, but only the calcite form is ordinarily used as a thermoplastic filler. Calcite crystal structure is a perfect rhombohedrally-centred hexagon [20, 21], with lattice parameters $a = 4.990 \text{ \AA}$, $c = 17.002 \text{ \AA}$ [22]. The unit cell of calcite is illustrated in Figure 2.3 [23]. The Ca atoms are situated at the points of a face-centred rhombohedron. The CO_3 ions are situated midway between Ca atoms along rows parallel to the rhombohedral cleavage edges; thus one CO_3 group is situated at the body centre of the rhombohedron. The CO_3 ions are trigonal in form, planar parallel to 001 plane, and each group is turned 60° with respect to the next one. Calcite is a soft mineral with a Mohs hardness of 3.0, and is birefringent having refractive indices of 1.65 and 1.48, and a specific gravity of 2.70 [24]. It has a melting point of 1339°C at 102.5 atm but decomposes at 900°C into calcium oxide and carbon dioxide at

atmospheric pressure [25]. Solubility of calcium carbonate in water at 25°C is 0.0015 g/100 ml. The origin of calcite is the deposition of shells and skeletons of sea animals on the sea bottom or the metamorphosis of limestone by dissolution and recrystallisation. Aragonite is the orthorhombic form and sometimes may appear naturally as needle-shaped prisms or spherulites depending on its environmental conditions. It can be transformed into calcite when heated to 400°C [26]. Aragonite has a specific gravity of 2.93 and its hardness is 3.5-4.0 Mohs. It decomposes at 825°C.

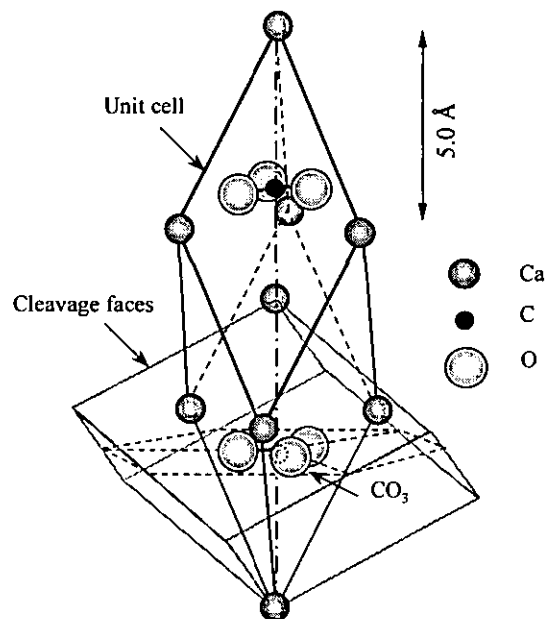


Figure 2.3: The unit cell of calcite [23].

The quarried calcium carbonate is cut into segments small enough to be crushed. The small pieces are then screened for size grading of unwanted substances. The screened calcium carbonate is milled by roll and ball mills. The milled particles are conveyed to agitator tanks having a continuous agitation system and fully filled with water. The agitation system encourages fine particles to float up to the top of the tanks where they are easily removed into sedimentation tanks. In these tanks, the calcium carbonate fine particles settle out as slurry at the bottom of the tanks and are then pumped to a dryer. The slurries are dried giving final products which have a particle size of 1-3 μm [25].

Calcium carbonate is the most common filler used for thermoplastics as it gives remarkable advantages as follows:

- high chemical purity, no heavy metal ions that can catalyse the degradation in polymers;
- calcitic structure with relatively low specific surface, without any great absorptive effect on plasticizer and other additives;
- high degree of whiteness, hence the possibility of partial substitution of expensive white pigments;
- coloration in pastel shades is possible, also at high filler contents;
- non-abrasive, gentle on machine parts (Mohs hardness 3);
- good dispersibility (in particular coated grades) with only slight influence on the mechanical and electrical properties of the final products;
- increase in stiffness and modulus of elasticity;
- reduced shrinkage;
- higher colour fastness;
- improvement in the surface of the article;
- low plate-out (deposition of mixture ingredients);
- increased impact strength, in particular through the use of coated grades;
- improvement in stability and aging resistance, particularly when using coated grade;
- non-toxic, odourless, tasteless, heat resistance up to 600°C;
- low price;
- beneficial increase in weight and volume.

The addition of calcium carbonate to polyethylene (PE) gives a lower specific heat and higher thermal conductivity than unfilled PE, which results in a higher throughput during extrusion and injection moulding. This addition also leads to an increase in hardness, stiffness, heat deflection temperature, slip resistance and resistance to stress cracking and a reduction of melt index, shrinkage, elongation, water vapour and oxygen permeability.

The use of calcium carbonate in polypropylene (PP) gives a composite with higher chemical and stress cracking resistance at high temperature and greater stiffness at room temperature. However it increases the brittleness of PP at temperatures below 0°C. Furthermore, PP filled with calcium carbonate results in higher stiffness and dimensional stability at shorter cycle times in injection moulding due to the higher thermal conductivity of the composite. For polypropylene films, calcium carbonate improves the deep drawing properties. In PP cord and tape production, the addition of calcium carbonate helps to avoid undesirable splicing and produces a cleaning action in the extruder die.

Calcium carbonate can also be used in polyvinyl chloride (PVC). As it has high chemical purity, it has no heavy metals which would have a catalytic effect on the aging properties of PVC. Compared to unfilled PVC, filled CaCO_3 gives lower shrinkage, lower plate-out and higher stiffness. PVC filled with CaCO_3 also permits an increase of output rate, a better surface of finished products, and a lower lubricant requirement. Like CaCO_3 filled PE, the incorporation of CaCO_3 into PVC can improve both electrical and dielectric properties of the filled composite and can reduce the amount of plasticiser required. Improvements in dry handling, the prevention of sticking to calendar rolls, and a reduction in the cost of the final products are also achieved. In addition, the CaCO_3 serves as a hydrochloric acid acceptor which could absorb some of the hydrochloric acid generated in the decomposition of the PVC [26].

The addition of large amounts (typically up to 60% by weight) of calcium carbonate filler, which is a non-combustible material, to a polymer compound can slightly reduce flammability and smoke by diluting the quantity of combustible polymer available for combustion and providing a “heat-sink” in the composites [27]. The quantity of smoke evolved relative to the sample weight of the composite can decrease in proportion to the content of the filler. The addition of 50% CaCO_3 to PP

and 60% CaCO₃ to polyester can also increase smoke-suppressant activity of the filled composites by diluting the volume of the combustible materials with the filler [3, 20, 28].

2.3.2 MAGNESIUM HYDROXIDE AS A FLAME RETARDANT FILLER

Magnesium hydroxide has the chemical formula Mg(OH)₂ and molecular weight of 58.3. Magnesium hydroxide occurs naturally as the mineral brucite which was discovered in 1814 by Bruce at Hoboken (New Jersey) [30]. Magnesium hydroxide is a white, odourless, and low toxicity crystalline material. After processing it has an average particle size of 1-10 μm and a specific gravity of approximately 2.36 [8]. It is soft and non-abrasive with a Mohs hardness of about 2.5 and has a refractive index of 1.57 [24]. Magnesium hydroxide is practically insoluble in water and alcohol but it is soluble in dilute acid and ammonium salt solution [31]. It starts to decompose endothermically and loses water at about 330°C as shown in Equation (2.2) [8].



Crystals of brucite are trigonal (hexagonal) with lattice parameters $a = 3.174 \text{ \AA}$, and $c = 4.769 \text{ \AA}$, and its basal plane lies in the 001 plane direction. This crystallographic structure consists of close packed hydroxyl anions with magnesium cations occupying half of the octahedral holes. Brucite has a layer structure in which each layer consists of two sheets of OH in hexagonal close packing, with a sheet of Mg atoms between them as shown in Figure 2.4 [32]. Each Mg atom is in sixfold co-ordination between OH, and each OH fits into three OH groups from the next layer. The layers are held together by weak secondary forces between adjacent OH sheets. Brucite has a strong positive refraction. The plate-like crystals of brucite are soft, and exhibit a foliated structure and lustre. The electrical conductivity of brucite is approximately nil [30]. Magnesium hydroxide is potentially available in a number of product forms, which are still being developed and optimised for flame retardant uses.

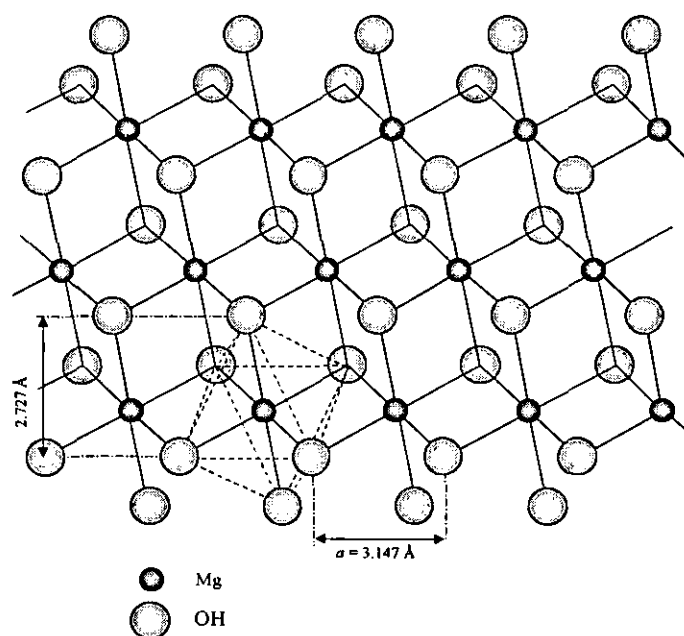
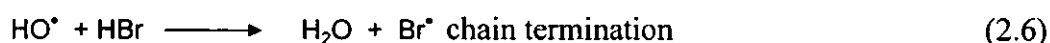
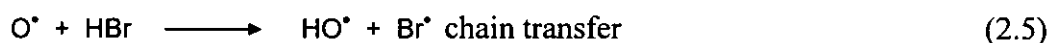
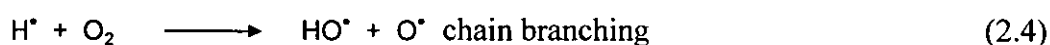
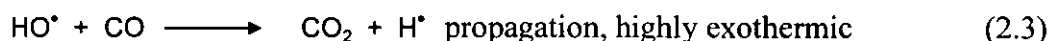


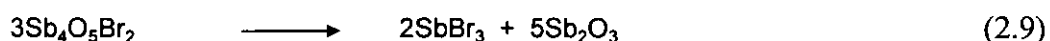
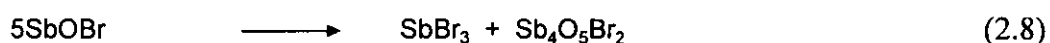
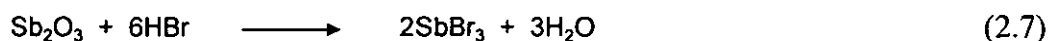
Figure 2.4: Single layer of the brucite structure with Mg in octahedral coordination with (OH); the hexagonal a axis is horizontal [32].

The mechanism of action of flame retardants is not understood in detail, but a general picture of a burning piece of plastic gives some insight into four basic steps: pyrolysis, ignition, combustion and heat transfer. Pyrolysis occurs in the solid phase to generate gaseous decomposition products. When these mix with the surrounding air, ignition occurs at a certain combustion temperature and fuel-air composition. Heat from the resulting combustion is fed back to the solid cycle [33]. Before magnesium hydroxide was used as flame retardant filler, organohalogen- and organophosphorus-containing compounds were the first flame retardants for plastic materials. During combustion of thermoplastics, free radicals are formed by pyrolysis. Halogen compounds are believed to act primarily in the combustion zone through the formulation of hydrogen halides [33]. The reactions of free radical chains which are involved in the oxidation of a fuel are terminated by hydrogen halide formation [34, 35]. The hydrogen halides inhibit flammability by reacting with the hydroxyl and hydrogen chain propagating radical species to give less reactive halide radicals (Equation 2.6). These compounds also lead to an increase of a char formation. It is presumed that the following reactions take place when organobromine compounds are used as flame retardants:



It is supposed that organophosphoric compounds generally promote heavy charring through the formation of phosphoric acids which react with the polymer and produce a char layer, resulting in a surface protection of the combustible material, and formation of water and also non-flammable gases [36].

Another group of flame retardants involve halogen-antimony synergism, which has been observed in many cases. A synergism may be defined as a case in which the effect of two components taken together is greater than the sum of their effects taken separately. Antimony trioxide is an important component of thermoplastics containing halogen compounds. It is believed that synergism between antimony trioxide and organobromine compounds might produce antimony tribromide [34, 37]. The tribromide forms a dense white smoke which snuffs the flame by excluding oxygen from the front of the flame. By the action of water released during the combustion (Equation 2.7), antimony tribromide is decomposed to antimony oxybromide (SbOBr) and hydrobromic acid (HBr) which is able to convert from the highly reactive and chain-carrying hydroxy radical into the less reactive bromine radical. The antimony oxybromide can give self-reactions and produce antimony tribromide as well as higher oxybromides at temperatures of about 250-285°C (Equation 2.8). The higher oxybromides are converted back into antimony oxide and released again as antimony tribromide at temperatures around 500°C (Equation 2.9).



Small amounts of organohalogen-, organophosphorus-containing flame retardants and also synergism between these with antimony in thermoplastics can reduce compound combustibility, and their use has little effect on the mechanical properties of the composites. Typically, 4-23 wt% halogenated, 1-10 wt% phosphorus containing, and between 25-50 wt% antimony oxide in halogenated compounds can be used in applications of flame retardants for polymers [37]. Although organohalogen, organophosphorus compounds, halogen-containing flame retardants, and antimony compounds have many advantages in the flame retardancy of polymer composites, the combustion of these compounds produces considerable amounts of smoke and toxic fume emissions, therefore considerable interest has been stimulated in the development of alternative halogen-free fire retardant systems. An inert or non-halogenated flame retardant and a smoke suppressant material such as aluminium hydroxide ($\text{Al}(\text{OH})_3$) is an alternative type which reduces the problems of toxic and corrosive smoke during the burning of thermoplastic composites. It is believed that the burning mechanism of a polymer containing aluminium hydroxide is an endothermic dehydration [6, 38]. In the burning process, volatile polymer fragments are produced through an endothermic cracking reaction in the pyrolysis zone by a portion of the heat of combustion transferred back to the polymer. These volatile products travel to the combustion zone, where they react exothermically with oxygen. By acting as a heat sink and sacrificially absorbing a portion of the heat of combustion transmitted back to the condensed phase, aluminium hydroxide retards pyrolysis and hence reduces the burning rate. Dilution of combustion gases by water vapour and participation of water in condensed phase reactions occurs. Typically, aluminium hydroxide must be used at high loadings (33-60 wt% or greater) to provide the required degree of flame retardancy [39]. However, aluminium hydroxide has a limitation in use, as it decomposes at 180°C (Equation 2.10), it cannot be used with polymers processed at high temperatures.



Magnesium hydroxide ($\text{Mg}(\text{OH})_2$), another metal hydroxide, is an inert flame retardant which has thermal stability inherently greater than $\text{Al}(\text{OH})_3$, thus it can be successfully used as a filler in thermoplastics which are melt processed at temperatures where the incorporation of $\text{Al}(\text{OH})_3$ cannot be achieved due to problems of premature decomposition. Magnesium hydroxide decomposes endothermically at a temperature of about 330°C (Equation 2.2) to release water of hydration which contributes to its flame retarding action [3, 38].

Since the decomposition of magnesium hydroxide is an endothermic reaction, it also withdraws heat from a polymer substrate resulting in the reduction of the rate of thermal degradation. Vaporisation of the liquid water released from the decomposition into the gaseous phase is generally considered to provide a beneficial effect through cooling of volatiles produced by the polymer decomposition and dilution of the fuel supply present in the gas phase [5, 40]. The combined effects of endothermic decomposition and water release, result in a significant reduction in heat release rate of magnesium hydroxide-filled polymers [5]. However, the flame retardancy of magnesium hydroxide in polymers depends not only on the endothermic decomposition and accompanying water release mentioned earlier but also on other considerations. These include:

- formation of a stable oxide char residue over the polymer substrate which is capable of absorbing many species;
- protection of the polymer from the heat source [5];
- limiting thermal feedback and supply of oxygen to the degrading polymer [41];
- dilution of combustible material within the composition;
- the relative decomposition temperatures of polymer and filler;
- the influence of the filler on dripping behaviour may also be relevant in some polymer systems [3, 4, 20, 38].

The mechanism of smoke suppression in polymers containing magnesium hydroxide filler requires an understanding of soot formation during combustion of organic

matter. More specifically it requires consideration of the mechanism of carbon formation and destruction within the flame, carbon deposition on the polymer substrate in areas converted by the flame and subsequent carbon volatilisation on exposure to oxygen as presented in a number of reactions as follows:



A reaction between carbon and steam (produced during the decomposition of magnesium hydroxide) might occur which would result in increased carbon monoxide emissions as shown in Equation (2.13). However, it has been observed that carbon monoxide evolution during smoke testing of compositions under flaming conditions implied that polymer containing magnesium hydroxide gave lower carbon monoxide emissions than corresponding material filled with magnesium oxide. This supports the idea that the water did not take part in the water gas reaction resulting in an increase in the level of carbon monoxide emission [3, 5].

Hornsby and Watson [4] studied magnesium hydroxide as a combined flame retardant and smoke suppressant filler for polypropylene. They found that at high filler loadings the filler conferred good fire retardancy combined with excellent smoke suppressant characteristics without evolution of toxic or corrosive decomposition by-products originating from the filler phase. The addition of high levels of magnesium hydroxide to PP, polyester, and polyamides was shown to result in a significant improvement in flame retardancy of polymers and a considerable reduction in smoke emission. These results were supported by many workers [29, 42-44]. At a loading of 50-60%, $\text{Mg}(\text{OH})_2$ was able to promote char formulation and decrease smoke from the final products. The reduction of smoke was directly proportional to the $\text{Mg}(\text{OH})_2$ loading. A stronger char was observed when the level of $\text{Mg}(\text{OH})_2$ was increased [45]. It is evident, therefore, that high loadings of magnesium hydroxide are generally

required to optimise combustibility and smoke suppression characteristics of filled polymer composites.

However, incorporation of high levels of inorganic fillers into polymers usually causes deterioration of mechanical properties such as ductility, impact strength, and other features which often decide the practical importance of these composites. The reduced mechanical properties can be improved by surface modification of fillers with suitable modifiers as discussed in the following section.

2.4 SURFACE MODIFICATION

Surface modification is defined as the result of the interaction of an organic compound with a filler, pigment or reinforcement surface, to alter the organophilic nature of the surface [46]. It can increase the force of adhesion at a polymer/filler interface. This force has been shown to exert a considerable influence on mechanical responses, and a correlation between the acid-base characteristics of filler and polymer [47].

The modification of the surface of fillers may be accomplished by direct treatment of the surface, i.e. the filler may be precoated, or by an indirect method which is the addition of coating agents during compounding, allowing the coating agent to make its way to the filler surface (*in-situ* coating). Some of the various possibilities that can be encountered with short mono-functional coating molecules are illustrated in Figure 2.5 [7]. (a) shows the situation where the reactive sites are much more widely spaced than the area occupied by the coating agent. Complete surface reaction is possible, but much of the surface is uncoated and may be able to adsorb other types of molecules. (b) shows the reverse situation, the reactive sites are very close together and steric factors prevent the coating reacting with all the sites. In this case it has complete coverage but incomplete reaction, and the surface may still be able to adsorb and interact strongly with small molecules such as water. (c) shows the ideal situation

where the spacing is such that complete geometric coverage exactly corresponds to complete surface reaction. While this situation may be thought unlikely, it seems that stearic acid coating on calcium carbonate comes very close to it and this may explain the great success of this filler-coating combination.

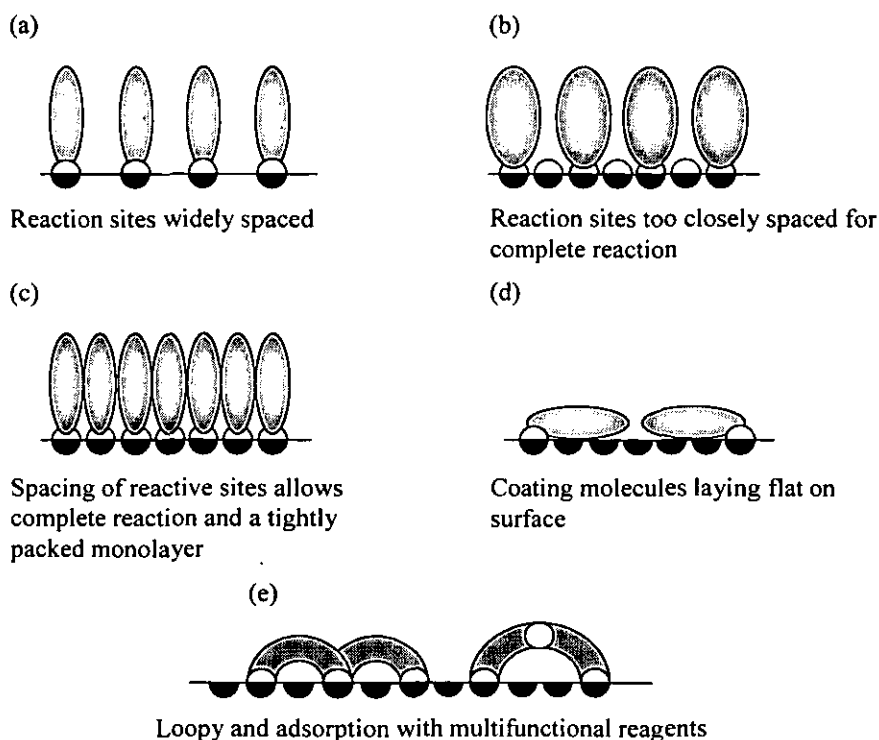


Figure 2.5: Different structures of surface monolayers on filler surfaces depending on bulk and functionality of the adsorbing molecule, and the density of surface reactive sites [7].

A further area of confusion is in assessing molecular orientation at the surface. Most molecules have a number of possible orientations, which makes calculation of geometric coverage difficult. This is especially true of some organosilane coupling agents where the functionality intended to react with the matrix may in some circumstances be strongly adsorbed on to the filler surface, resulting in flat or bridged rather than vertical orientation. Even long-chain carboxylic acids may adsorb flat rather than vertically at low coverages. This situation is illustrated in (d). Loopy adsorption such as illustrated in (e) is possible when multifunctional adsorbates are used.

2.4.1 MECHANISMS OF SURFACE MODIFICATION

2.4.1.1 Chemisorption. Chemisorption is a process which involves bonding of an agent to a surface without the formation of a primary chemical bond. It is the mechanism by which many complexes form to produce permanent combinations. Most filler surfaces are electronegative and will form complexes with compounds such as metallic salts, amino compounds, and others which have electropositive sites. The mechanism seems to be related to van der Waals bonding forces, which are of low order. Chemisorption is often promoted by adsorbed water, which can interact in the basic or acidic mode and therefore act as an intermediary regardless of the nature of the underlying surface. As the water is displaced in the process, the bonding may have various degrees of hydrolytic resistance. Ionic and covalent bonding will, under most circumstances, produce greater stability or resistance to an imposed stress because of the greater bond strengths [48].

2.4.1.2 Ionic bonding. Ionic bonds are generated when opposite charges (a cation and anion) attract each other, two atoms that have gained and lost electrons are pulled together into a bond. Ionic bonding is one type of primary chemical bonding that is common to many fillers, especially calcium carbonate and magnesium hydroxide, and depends on the isoelectric point of the filler surface and the dissociation constant of the reactant. In non-aqueous systems, stearic acid, for example, will react with magnesium hydroxide [48]:



If the concentration of stearic acid is enough to saturate the surface, the magnesium is bonded through residual coordination with oxygens of the Mg ions of the crystal. The surface of the mineral then consists of an exposed layer of 18 carbon chains. When fully reacted under extreme conditions, the modified filler is permanently hydrophobic and hydrolysis-resistant. Cationics, illustrated by amines, react with

acidic surfaces by separating a proton (hydrogen ion) to form a positively charged group which is attached to the negative oxygen of the precursor hydroxyl group, releasing a molecule water. Typically, this reaction occurs with the silicate mineral fillers. Quaternary ammonium compounds are used in water slurries of fillers or added directly to filler and matrix compounds to produce similar ionic complexes.

2.4.1.3 Covalent bonding. Covalent bonds are usually formed between non-metals. Two atoms share one or more electrons in order to complete their outer shell of electrons. By sharing the electrons, both atoms have eight electrons in their outer shell creating a stable molecule. For example, the reaction of organosilanes with radicals of silica or alumina hydroxyls (silanol or aluminol) on filler surfaces results in a covalent bond between the silica of the silane and the oxygen of the filler surface and then releases an alcohol or acid. The reaction is promoted by water through hydrolysis. As with all reactions of this type, there always exists a degree of complication due to competing self-condensation of the modifiers, reaction with surface impurities, and conditions under which surface modification is conducted [49].

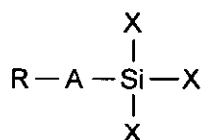
2.4.1.3 Other Chemical Bonding. Many filler surfaces are catalytically active, essentially in nonaqueous media and at processing temperatures during composite fabrication. Alumina and calcined kaolin are examples of catalytic agents that can split esters to yield highly charged fragments or polymerise unsaturated polymers and interact with each other with the formation of van der Waals forces. Metallic fillers form co-ordination complexes with some polar modifiers such as chlorophosphonates. Dipole bonding occurs with molecules containing chlorine and hydrogen atoms of chlorinated hydrocarbons. Depending on the proton donating potential of the medium in which surface modification is conducted or that of the filler surface, ether linkages can be protonated to yield positively charged sites adsorbed by negatively charged filler surfaces [50].

2.5 SURFACE MODIFIERS

Many inorganic fillers are not highly compatible with the polymer medium in which they are dispersed. In order to improve interfacial adhesion between the filler and polymer, chemical additives called surface modifiers are usually added. These modifiers can be subdivided into coupling agents and coating agents. The coupling agents have groups capable of reacting to form an intermolecular bridge between the filler surface and the polymer matrix. Generally the coupling agent molecule consists of an inorganic functional group and an organic functional group. The inorganic functional group reacts with inorganic filler surfaces while the organic functionality is attracted to the polymer medium. Coating agents generally possess both polar and nonpolar groups in their molecule. The polar groups of coating agents attracts to inorganic filler surface while the nonpolar groups will usually improve the interfacial force by forming bonds to the polymer matrix by the van der Waals forces. A number of surface modifiers have been used in thermoplastic industries, such as organosilicon compounds, organotitanates, unsaturated polymeric acids, organo-phosphates, and fatty acids.

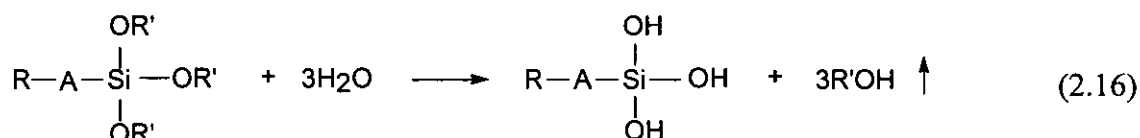
2.5.1 ORGANOSILICON COMPOUNDS

Organosilicon compounds are extensively used for modifying the surface of mineral fillers. The compounds used have the general formula:

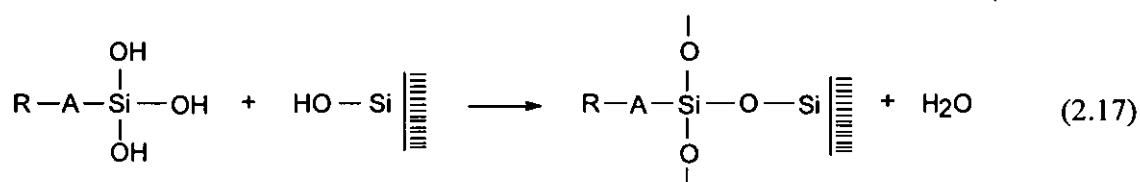


R represents an organo functional group which will be attracted to the polymer matrix through a hydrolytically stable carbon-silicon bond. These groups are “organophillic” and may be vinyl, amino, methacrylate or epoxy groups, etc. Different plastics may require a silane with different organo functional groups for obtaining best results. -A- simply represents an aliphatic linkage between the organic group R and the inorganic

group. The X usually represents either halogen or alkoxy groups which hydrolyse on exposure to moisture evolving alcohol and leaving the inorganic reactive group to react with surface hydroxyls of the filler to produce a stable bond. Then, strong bonds are produced with the polymer matrix as well as with the filler surface and these materials are known as silane coupling agents.



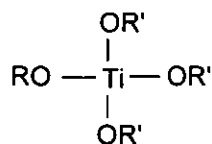
The loss of the alcohol unblocks the silane functional groups which in turn are free to react with silanol groups present on siliceous filler surfaces.



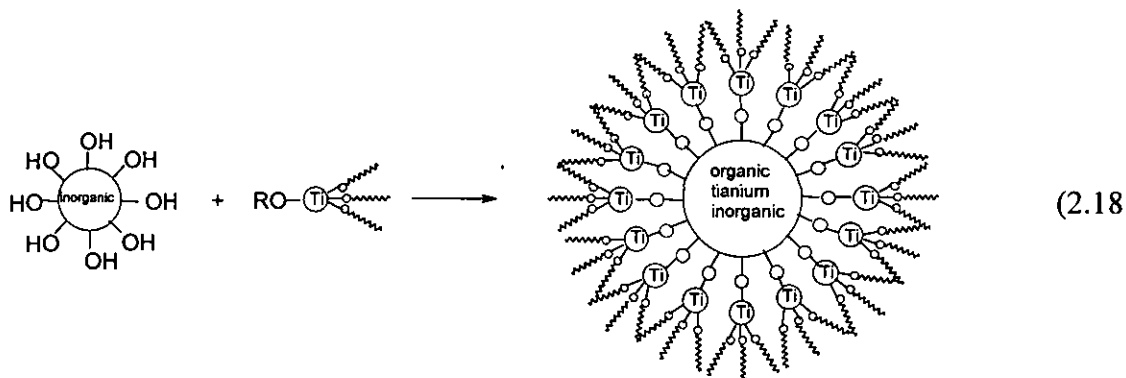
Silane coupling agents are much more widely used in particulate-filled composites than non-reactive compounds. This is because of their ability to improve filler/polymer adhesion as well as improving dispersion and reducing hydrophilicity of fillers. In the simple model, a monolayer is envisaged in which an end of the silane coupling agent bonds to the filler and the other end reacts with the polymer matrix. Unfortunately, the real situation is much more complex as discussed in many papers in recent years [4, 51-53].

2.5.2 ORGANOTITANATES

The organotitanate class of surface modifier has aroused great interest in recent years. They can be regarded as derivatives of orthotitanic acid. One common general structure is shown below.



These coupling agents are unique in that reactions with the free photons at the inorganic interface result in the formation of a monomolecular organic layer around the filler particle or fibre as shown in Equation (2.18). In concept, the organotitanates are similar to silanes that they act as molecular bridges at the interface between two substances, usually an inorganic filler and an organic polymer matrix. Organotitanate molecules consist of alkoxy groups (OR'). These groups readily hydrolyse to become titanium hydroxy groups and condense with surface hydroxyls of the filler. They also carry other organic groups, which are more hydrolytically stable and may also contain some reactive functional groups to bond with organophilic sites of the polymer matrix.

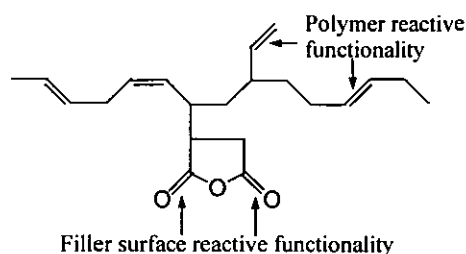


Depending on their chemical nature, organotitanates can be precoated from organic or aqueous solution, dry-blended or used *in situ*. However, their relevant chemistry is different from those of silanes. The most important factor is that, unlike the silicon to carbon bond, the titanium to carbon bond is very unstable and cannot be used to attach organic groups permanently for surface treatment applications. The organotitanates are thus generally based on tetra-substituted titanium where all the substituents are linked by titanium-oxygen-carbon bonds and their chemistry is dominated by the hydrolytic sensitivity of alkoxy radicals. Titanates are very active chemicals and they can exhibit a variety of cross-linking and catalytic effects in polymeric systems, which

may in part contribute to their effectiveness as filler treatments. A number of research papers have been published in various areas [54-57].

2.5.3 UNSATURATED POLYMERIC ACIDS

Unsaturated polymeric acid is one of the coupling agents that is used for coating mineral filler used in elastomers. The structure of a typical unsaturated polymeric acid anhydride surface modifier based on maleinized polybutadiene (MPBD) is shown below.



It is believed that the anhydride groups react with the filler surface, probably through salt formation, whereas the residual unsaturated groups are available to take part in the curing or cross-linking processes. This type of additive can be used either precoated on to a filler or added separately during compounding, when it is believed to diffuse to and react with the filler surface during processing operations [58, 59].

2.5.4 ORGANOPHOSPHATES

Organophosphates have been proposed as a filler treatments, especially organo-functional dihydrogen phosphates obtained by phosphorylation of organic hydroxy compounds using phosphorus trichloride. The general formula of organophosphates is $(RO-PO_3H_2)$, where R is either a simple hydrocarbon (ethyl, butyl, hexyl, octyl) or contains additional functionality such as vinyl, methacryloxy, or chloro groups. These modifiers have been the subject of a number of papers by various workers [60-62].

2.5.5 FATTY ACIDS

The term fatty acid was originally applied principally to the saturated monobasic carboxylic acids [63]. Both saturated and unsaturated types of fatty acids which contain an even number of carbon atoms in straight chain compounds (R) with the general formula RCOOH occur naturally. Chain lengths range from two to over 80 carbon atoms although they are most commonly between C₁₂ and C₂₂. Fatty acids and their derivatives are introduced in the thermoplastic industry as coating agents as they can improve filler dispersion leading to a reduction of melt viscosity, modulus and an improvement of impact properties of composites. Stearic acid is the most widely used fatty acid. This section, therefore, focuses only on stearic acid and its derivatives.

2.5.5.1. Stearic acid. Stearic (octadecanoic) acid is the most widely used fatty acid for filler coating. It is the highest molecular weight saturated fatty acid occurring abundantly in natural fats and has a molecular formula as CH₃(CH₂)₁₆COOH. Stearic acid is a waxy crystalline solid melting at 69.6°C. It is practically insoluble in water (0.00029 g/100 ml of water at 20°C), but fairly soluble in chloroform (50 g/100 ml). It is produced commercially by several processes depending on the desired purity and the use for which it is intended. For the filler coating, a more homogenous product containing 95% or more of stearic acid, is produced by fractional distillation or crystallisation from solvent of the mixed acids [64].

To understand how stearic acid is adsorbed on filler particles, the adsorption and conformation of stearic acid on the surfaces has been widely studied especially by using the Langmuir-Blodgett (LB) technique [65]. A Langmuir-Blodgett film of material is applied to the subphase surface by first dissolving it in a solvent. The solvent should be able to dissolve an adequate quantity of the monolayer material (concentrations of 0.1-1.0 mg/ml are typical). The solvent must not react chemically within a reasonable time so that no trace remains in the condensed layer. Solvents which are commonly used for monolayer-spreading include n-hexane, chloroform and diethylether. The structure of the stearic acid molecule consists essentially of 16 CH₂

groups forming a long hydrocarbon chain. One end of the chain terminates in a hydrophilic COOH group and the other end is a simple methyl group. The molecule aligns perpendicular to the polar surface [66]. Under these conditions, the surface area occupied per molecule is approximately 21.0 \AA^2 [67]. Moreover, the single crystal long-chain of fatty acids and their derivatives has been investigated by using X-ray diffraction. The more important conclusions include the following [64]:

- X-ray diffraction patterns of long-chain compounds reveal the existence of two small spacings (*a*- and *b*-axis) which have about the same values for all substances in a homologous series. A third spacing (*c*-axis) of greater length increases proportionally to the number of CH₂ groups in the particular compound. All spacings suggest that the unit cell is a long prism, which has the same cross section for all substances in the series. The spacing, which indicates the length of prism, is designated the long spacing and is a measure of the length of the carbon chain. It is the most characteristic feature of the diffraction pattern of long-chain compounds.
- Normally, the diameters of the carbon and oxygen atoms in an acid molecule would give a maximum distance for 18-carbon atoms of about 30.0 \AA while the measured long spacing of stearic acid is 38.7 \AA . Therefore, the unit cell of stearic acid must contain more than one molecule. Half of this measured distance, however, would be considerably less than the theoretical length. Therefore, it was concluded that the unit cell must consist of two molecules between parallel planes and that the atoms in these chains must be arranged in a zigzag pattern.
- From crystallographic measurements of a single crystal of stearic acid, the results showed that stearic-acid crystallises in the monoclinic prismatic system of the space group C_{2h}. Diagrammatic representation of the unit cell of a stearic acid crystal is shown in Figure 2.6. The axial dimensions of the elementary parallelepiped are; $a = 5.546 \text{ \AA}$, $b = 7.381 \text{ \AA}$, and $c = 48.840 \text{ \AA}$. The *b*-axis is perpendicular to the plane *ac* but the *c*-axis is inclined to produce the angle β between the *a*- and *c*-axis of $68^\circ 38'$. The density is slightly more than 1.05 g/cm^3 ; thus the unit cell of stearic acid consists of four molecules. The rectangular base of the cell has the dimension $7.4 \times 5.6 \text{ \AA}$ or an area of 41.4 \AA^2 . For a unit cell, the

molecules arrange their ends at the corners and in the centre of this rectangle. The area is a measure of the space occupied by the base of two molecules so that each molecule stands on a base of average 20.7 \AA^2 .

- From observation it is concluded that the unit cell of stearic acid produces the double layer formation by having the two layers oppositely oriented, the active groups of the bottom layer being directed toward the active groups of the upper layer. Normally stearic acid crystallises with the chain axis vertical to the 001 planes.

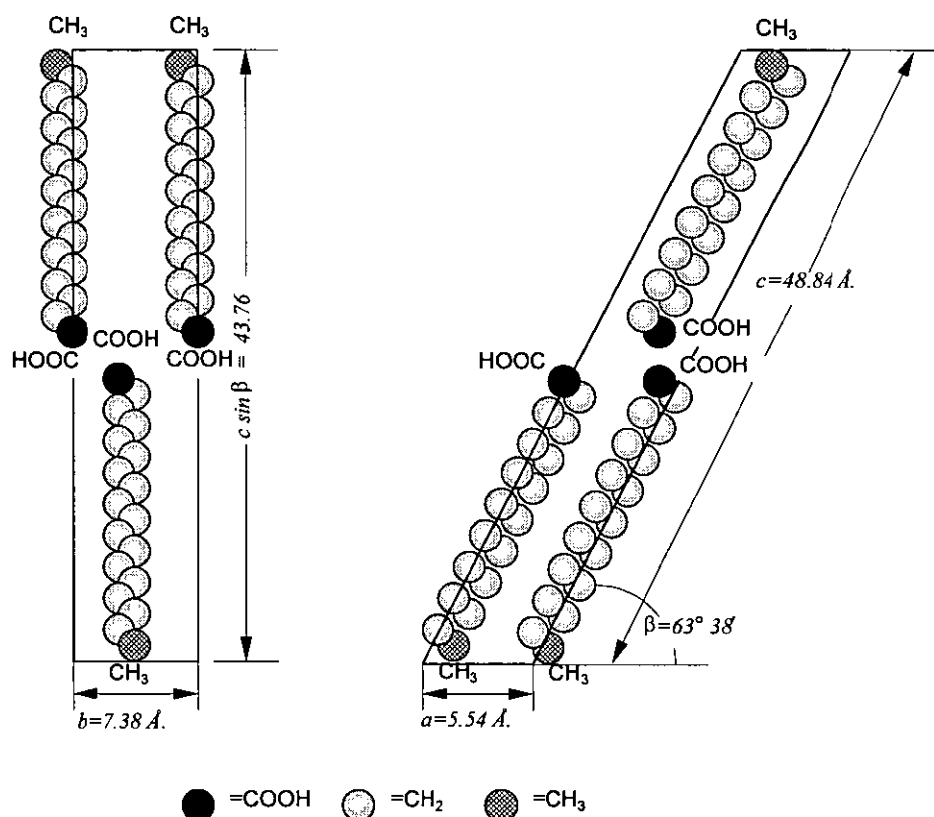


Figure 2.6: Diagrammatic representation of the unit cell of a stearic acid crystal [68].

2.5.5.2 Metal stearates. Metallic soaps are used for a variety of purposes in the rubber and plastics industries. In the former, metal stearates serve as softeners, vulcanisation accelerators, mould release agents, antiscorching agents and coating agents. Alkali metal soaps are used in the manufacture of protective and decorative coatings for many purposes including flattening, thickening and suspending agents in the paints industry. Properties of metal stearates used in this work are as follows:

- a) Magnesium stearate ($\text{Mg}(\text{C}_{18}\text{H}_{35}\text{O}_2)_2$) is a soft, white and light powder. It has a density of 1.028 g/cm^3 and a melting point of 132.0°C (technical grade). Magnesium stearate is tasteless, odourless, non flammable and insoluble in water and alcohol.
- b) Calcium stearate ($\text{Ca}(\text{C}_{18}\text{H}_{35}\text{O}_2)_2$) is a white powder, insoluble in water, slightly soluble in hot alcohol, decomposed by many acids and alkalis. Its melting point is $150.0\text{-}154.0^\circ\text{C}$.
- c) Zinc stearate ($\text{Zn}(\text{C}_{18}\text{H}_{35}\text{O}_2)_2$) is a combustible white powder, has a faint odour, is soluble in acids and common solvents such as toluene when hot, but insoluble in water. Its density is 1.095 g/cm^3 and melting point is 130.0°C [31].

Magnesium and zinc stearates are normally used as mould release agents in rubber forming and to reduce tackiness in uncured rubber. Zinc stearate has been used to soften rubber and improve its processing characteristics. Calcium and magnesium stearates are used as heat stabilisers in polyvinyl chloride. Furthermore, metal stearates act as plasticisers and internal lubricants in improving the processing characteristics of some types of plastics

2.5.5.3 Effects of fatty acid and their salt treatments on filled composite properties.

Many inorganic fillers manufactured for incorporation into plastics and rubbers are treated with organic reagents in order to modify the characteristics of the filler/matrix interface. This may lead to improved dispersion of the inorganic phase during compound preparation, to changes in the melt rheology of composite products and, in particular, improvement in the mechanical properties of filled polymer compositions. Hornsby and Watson [20] studied the effect of surface modification of filler on the mechanical behaviour of $\text{Mg}(\text{OH})_2$ filled polypropylene composites. They found that composites containing $\text{Mg}(\text{OH})_2$ modified with 6.0% w/w stearates (magnesium and

zinc) gave markedly higher impact strengths than with fatty acids, namely, stearic acid, azelaic acid and oleic acid. The surface treatment of magnesium hydroxide with several fatty acids and their derivatives showed a slight decline in flexural modulus and flexural strength of composites. Magnesium hydroxide coated with ammonium and sodium stearates improves the toughness of PP composites[69]. Calcium carbonate coated with stearic acid also reduces tensile strength and modulus, increases elongation at break and improves the impact properties of PP composites [70].

Rheological characterisation of PP filled with $Mg(OH)_2$ has been studied by Hornsby and Mthupha [19]. They found that $Mg(OH)_2$ particle morphology, size and applied surface coating affect the rheology of molten filled PP. These results were supported by Miyata's work [44] which showed that filled PP containing magnesium hydroxide coated with magnesium stearate gave substantially lower melt viscosity than PP containing uncoated magnesium hydroxide. It was believed that magnesium stearate enhanced compatibility between polymer and filler leading to a decrease in the degree of particle agglomeration. The melt viscosity, however, was not affected by stearic acid treatment of calcium carbonate and dolomite in PP [71].

2.6 CHARACTERISATION TECHNIQUES

Surface modification of filler particles is a common requirement in order to achieve desirable properties such as dispersability, filler-matrix bonding and even stability. Such modifications can range from the adsorption of less than one monomolecular layer of a surfactant to the precipitation of a coating many nanometres thick. Surface composition analysis therefore requires methods that possess sampling depths of order of 1-10 nm and which can characterise both inorganic and organic species, ideally in a fully quantitative manner. Sophisticated techniques have now been developed for characterising and quantifying the chemical nature of material surfaces. Several important techniques have been used to characterise the nature and extent of the coating and the coated surface, however, only Fourier transform infrared spectroscopy

(FTIR), X-ray diffraction (XRD), X-ray photoelectron spectroscopy (XPS), and contact angle measurement (surface energy analysis) are discussed in detail in this section.

2.6.1 FOURIER TRANSFORM INFRARED SPECTROSCOPY (FTIR)

Infrared (IR) spectroscopy is a technique that gives intimate structural details of the molecules under examination. The IR is absorbed causing changes in the vibrational state of a molecule, for example the bending or stretching of the molecular bonds. Consequently, the interpretation of the spectrum shows the presence of chemical groupings in the molecule, information about the environment of each grouping, and the structure of the molecule. As computers and computing techniques became more advanced, FTIR spectrometers have been developed and used for the identification and characterisation of materials. FTIR has had particularly wide application in the field of polymer analysis, not only because of the ability to look at intractable, thick, intensely absorbing materials, but also because of the ability to observe chemical and physical changes in the polymer structure. Therefore, this technique is an extremely useful tool for studying filler surfaces modified by coupling or coating agents, and has been used in a number of researches.

FTIR spectroscopy was used by Ishida and Koenig [72] to study the nature of the interface between silane coupling agents and porous silica on the molecular level. Fumed silica powder (Cab-O-Sil) was used as a fine porous glass powder and treated with 1 wt% vinyltriethoxysilane (VTES) coupling agent. Polyvinylsiloxane oligomer was also prepared and used to treat the glass powder for studying siloxane linkages through the coupling agent-bulk glass interface. The chemical reactions of the polymeric coupling agent on the glass surface could be detected in the spectral region 3800-450 cm^{-1} . In particular, the reduced intensity in the band at 893 cm^{-1} reflects the presence of few residual silanol (SiOH) groups of the coupling agent on the glass. The number of residual SiOH groups is a function of the drying conditions as

indicated by the spectra of the polyvinylsiloxane on the glass surface. The interaction between the polymer and the glass surface results in the reduction of intensity of bands at 970 and 893 cm^{-1} and the appearance of three new peaks at 1235, 1170, and 1080 cm^{-1} . The band at 970 cm^{-1} is assigned to the Si-O stretching mode of the surface hydroxyls and the band at 893 cm^{-1} is attributed to the Si-O stretching mode of silanols. In addition, the three new bands were assigned to the Si-O-Si antisymmetric stretching mode of the chemically reacted species at the interface. Consequently, it can be concluded that the surface hydroxyls and silanols of the coupling agent had reacted to form siloxane bonds at the interface (oligomer-Si-O-Si-glass).

The FTIR technique was also used to investigate silane coupling agents deposited on E-glass fibre [73]. The spectrum of the coupling agent on the E-glass fibre treated with 1 wt% VTES with that of untreated glass fibre subtracted was very similar to the highly crosslinked polyvinylsiloxane homopolymer in terms of band positions and relative intensities. Differences of spectra obtained after different drying times of the silane treated E-glass fibre showed decreases in the strong band at 880 cm^{-1} which was previously assigned to the Si-O stretching mode of SiOH groups in polyvinylsiloxanol. This indicated the formation of siloxane bonds at the glass fibre/coupling agent interface. The rate of condensation of polyvinylsiloxanol with and without fibre was obtained from the normalisation of the intensity of the Si-O stretching mode at 893 cm^{-1} by the vinyl band of polyvinylsiloxanol at 1411 cm^{-1} and plotted against time. The results showed that at room temperature the coupling agent on the glass fibre reacted much faster than that without glass. It was concluded that the coupling agent molecules near the glass fibre surface had molecular arrangements which enabled them to participate in the condensation reaction and that the thickness of the coupling agent layer on the glass fibre depended directly on the concentrations of the treating solution. Using the integrated absorbance ratios between the coupling agent and the filler the amount of coupling agent deposited on the filler surface can be evaluated. This method has been used by many workers with various coupling agents and fillers [74-76].

Recently, Diffuse Reflectance Fourier Transform infrared spectroscopy (DRIFT) has been used for surface analysis. The basic principle behind the DRIFT technique is that light incident upon a solid or powdered surface will be diffusely scattered in all directions. The scattered light is collected with a suitable optical setup and directed to the IR detector for analysis. This technique was designed to enable spectra of powders to be analysed without the need for grinding and elaborate preparation, which of course could modify the chemical nature of the material. This adaptation, together with the ability to subtract spectra and accumulate data from multiple scans, was ideal for analysing surface coatings on particulate fillers [77]. The spectrum of uncoated filler can be subtracted from that of the coated specimen, creating a difference spectrum of the surface coating.

Miller and Ishida [78-81] studied the quantitative monomolecular coverage of particulate inorganic minerals, clay and lead oxide, by γ -methacryloxypropyltrimethoxysilane (γ -MPS) using DRIFT spectroscopy. The DRIFT spectra results showed that there were structural differences between physisorbed and chemisorbed γ -MPS on particulate mineral filler substrates. The physisorbed silane coupling agent was defined as the multiple layers of coupling which were not interacting with the mineral surface and were easily removed by solvent washing. The chemisorbed silane was defined as two layers, one which was removed only by boiling water, and one that was found to be a monolayer or less and was not removed by exposure to hot water. The main difference between the physisorption and chemisorption was found to be hydrogen bonding between the carbonyl groups of γ -MPS and the surface of the mineral fillers in the chemisorbed γ -MPS. The γ -MPS structures on clay are represented in Figure 2.7 which showed a single band at 1700 cm^{-1} on the clay surface while additional bands appeared at 1720 and 1700 cm^{-1} resulting from free and hydrogen bonded carbonyl structures, respectively, in the multilayer coverage which contained the physisorbed silane.

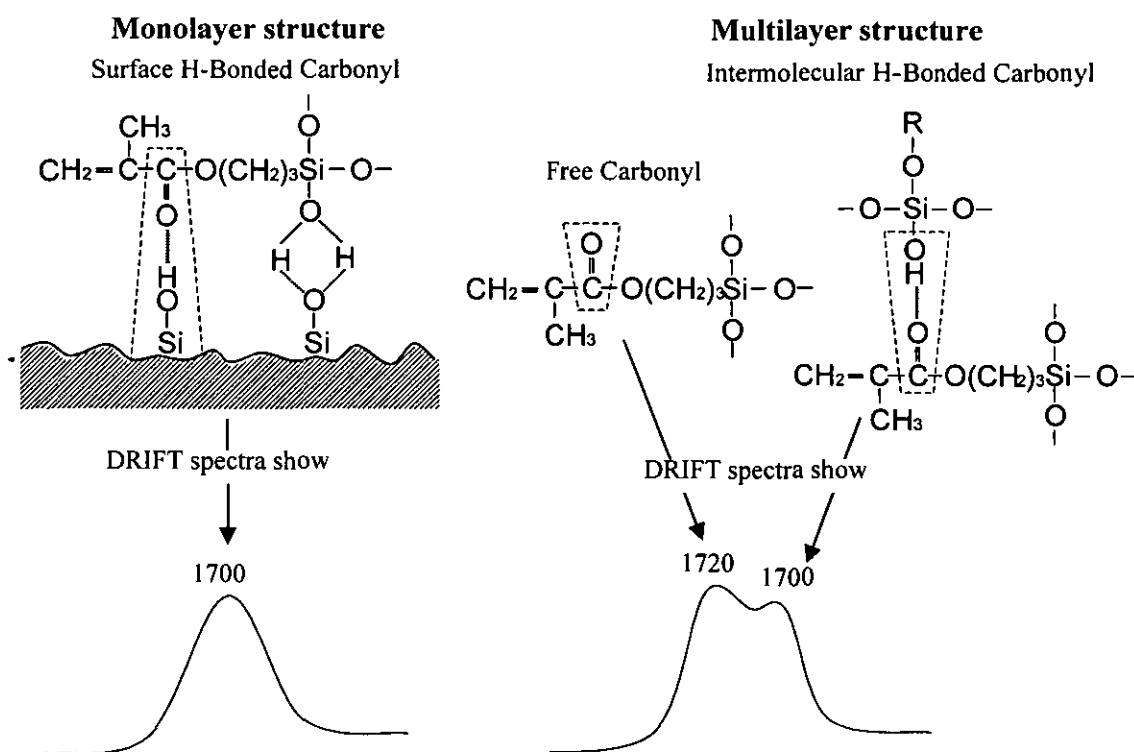


Figure 2.7: Illustrative molecular structure and the corresponding infrared carbonyl frequency of monolayer and multilayer γ -MPS molecules [78].

Similarly, the monomolecular coverage of the γ -MPS deposited on lead oxide was examined using the same method giving a silane concentration of 0.375 mg/g lead oxide. The monomolecular coverage was, moreover, confirmed by the illustration of a breakpoint (at silane concentrations of 9.0 and 0.375 mg/g) in the slope of lines plotted between integrated intensity of the individual carbonyl stretching frequencies on the clay and lead oxide surface against the adsorbate concentration. The spectroscopic characterisation of monomolecular coverage could also be used to calculate the area occupied per silane molecule on the substrate surface. The surface area of both clay and lead oxide substrates was experimentally measured using N_2 BET measurements giving surface areas of 13.1 and 0.5 m^2/g , respectively. Therefore, the calculated surface areas occupied per γ -MPS molecule were 60.0 \AA^2 on clay and 59.0 \AA^2 on lead oxide.

The molecular structure of γ -aminopropyltriethoxysilane (γ -APS) coupling agent deposited on silicon powder was studied by Culler, Ishida and Koenig using the DRIFT technique [82, 83]. The results revealed the formation of a chemical bond between the coupling agent and the surface of the reinforcement material. The DRIFT technique could be used to detect the differences between physisorbed and chemisorbed silane coupling agent, supporting the previous work [78]. These differences were as follows:

- the band positions of the Si-O-Si antisymmetric stretching mode changed for chemisorbed and physisorbed silane indicating that the chemisorbed silane was chemically bonded to the surface through Si-O-Si linkages, the physisorbed layers were not chemically bonded to the surface but were intermolecularly bonded through Si-O-Si bonds;
- the physisorbed layers were more condensed (less free Si-OH silanol band) than the chemisorbed layer(s);
- the amine groups of the coupling agent in the different layers were also different, in the chemisorbed layer the amine group formed a hydrogen-bonded structure to the surface and in the physisorbed layers the amine groups were free or formed an aminebicarbonate salt when dried in air.

Chemical bonding to the surface was detected through hydrogen bonding of the amine group and through Si-O-Si linkages which supported the chemical bonding theory of silane coupling agents.

The DRIFT technique has also been used successfully to study the adsorption of fatty acids, carboxylic acid anhydride derivatives and functionalised polymers on to $\text{Mg}(\text{OH})_2$, $\text{Al}(\text{OH})_3$, CaCO_3 and other fillers by many researchers [59, 61]. Gilbert and co-workers [84] studied filler/coating interactions in thermoplastics. $\text{Mg}(\text{OH})_2$ and CaCO_3 fillers were coated with various concentrations of stearic acid (0.5% to 4.5%). The DRIFT spectra of stearic acid coated $\text{Mg}(\text{OH})_2$ samples showed an alkyl CH stretching peak at 2900 cm^{-1} , a carbonyl band at 1700 cm^{-1} from stearic acid, and

the sharp band of the OH group from $\text{Mg}(\text{OH})_2$ at 3697 cm^{-1} . The intensity of the CH and carbonyl peaks increased with an increase of the acid concentrations, whereas the absence of a carbonyl stretching band at 1700 cm^{-1} from free stearic acid indicated that no unreacted stearic acid was detected in any samples. Similarly, no carbonyl peak was detectable when complete coating for modified CaCO_3 was achieved. It was indicated that the stearic acid had partially reacted with the CaCO_3 surface to liberate CO_2 and produced calcium stearate resulting in a peak at 1576 cm^{-1} . This observation was supported by Sutherland, Maton and Harrison [85]. They also used FTIR techniques for characterising stearic acid-coated calcium carbonate. Coating the surface of CaCO_3 with ammonium stearate gave rise to new bands at $2800\text{-}3000\text{ cm}^{-1}$, believed to be assigned to C-H vibrations in the alkyl chain of the stearate. No signals attributable to ammonium ions or the free carbonyl of stearic acid (1700 cm^{-1}) were detected at monolayer coverage indicating that no free acid remained in the system. The DRIFT spectrum of coated calcium carbonate had an absorption band at 1580 cm^{-1} showing that the coating reacted onto the surface to produce calcium stearate.

2.6.2 X-RAY DIFFRACTION (XRD)

X-ray diffraction has been routinely used for identification of polycrystalline materials since 1938 when the work of Hanawalt, Rinn, and Frevel was published [86]. The outstanding contribution of their scheme was a compilation of tested data on 1000 chemical compounds to form the basis of a reference pattern diffraction file. Over the last fifty year this diffraction file has been regularly enlarged and revised by the American Society for Testing and Materials (ASTM), and is now known as the Powder Diffraction File (PDF) and presently contains over 21500 numeric patterns of crystalline materials in the format of reference cards.

Some of the most important applications of X-ray diffraction are identification and quantitative analysis of elements, compounds and mixture as well as preferred orientation measurements, which can be applied for crystal structure determination of

filler/polymer, and orientation of filler particles/polymer chains in the bulk polymer under various conditions. Hatada and Nishii [87] used X-ray diffraction technique to investigate polymerisation of octadecyl methacrylate (ODM) in the form of a multilayer or monolayer. The polymerisation was induced with different doses of electron-beam irradiation in a nitrogen atmosphere or in air. X-ray diffraction patterns for the ODM Langmuir-Blodgett (LB) layers showed that the spacing of 31.10 Å decreased to 29.45 Å and its intensities increased when the irradiation dose increased. The decrease in spacing might be explained by the increasing tilt angle of the aliphatic chain to the normal to the LB layer during polymerisation. Since the increase of the tilt angle might result in the increase of molecular area of the monomer unit, the increase of intensity diffraction peaks with increasing dose might indicate that the layer structure of the LB layer became more regular as the polymerisation proceeded.

Naegele, Lando and Ringsdorf [88] investigated UV-initiated polymerisation of LB multilayers of cadmium octadecylfumarate using X-ray diffraction. The X-ray patterns of samples polymerised at $n = 3, 11, 19,$ and 61 multilayers of cadmium octadecylfumarate showed an increase of intensities, when the number of cadmium octadecylfumarate layers deposited increased.

Dismore and Statton [89] investigated the effects of annealing on oriented nylon 66 fibres using X-ray diffraction and tensile testing. Their results showed that on heating from 160 to 255 °C under zero tension, some of the molecules change from elongated to folded conformation. They also noted, on heating below the melting point, an increase in percent crystallinity and a larger proportion of fluid-like segments. They attributed the latter to an increase in defect concentration with annealing. The increased mobility might be attributed to disorientation of the amorphous phase. Annealing did not appreciably reduce crystal orientation but did lower the strength and elongation to break, likely to be due to fewer tie-molecules carrying the load. Unmelted, albeit annealed, intermolecular bonds appeared to prevent overall crystal orientation.

Another study of annealing effects of drawn nylon 66 was performed by Beresford and Beven [90]. The consequences of annealing were investigated by wide and small angle X-ray diffraction. Consistent with others [89, 91], they noted increases in both long period and small angle scattering intensity. As a result of their observations, a model for the structure of drawn polyamide fibres was proposed. This consists of chain-folded molecules aggregated into ordered states which vary between the extremes of discrete lamellar regions with a few tie-molecules and regions in which the molecules are so irregularly folded and arranged that individual lamellae are no longer distinguishable [90].

Structure and properties of self-reinforced polyethylene prepared by oscillating packing injection moulding under low pressure was studied by Guan and co-workers [92]. The preferred orientations of crystallographic planes of specimens were determined by X-ray diffraction. The reference axes in the sample, M, T, and N, were designated, respectively, as the machine (flow), transverse, and normal directions in the customary manner (Figure 2.8).

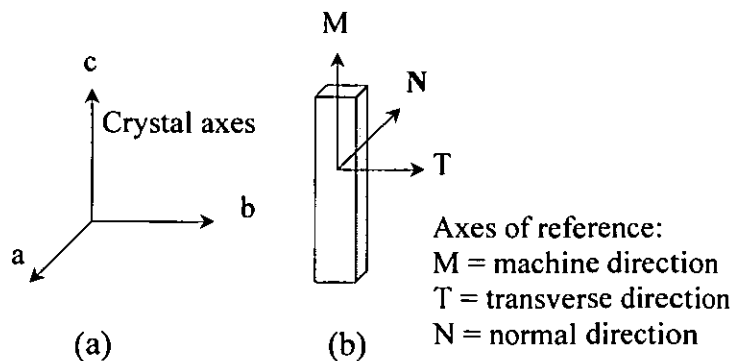


Figure 2.8: Diagrams of crystal axes and reference axes.

From the X-ray patterns it was revealed that the crystallographic planes (110), (200), and (020) were cylindrically distributed about M having an increase in probabilities particularly for plane (110) and (200). It was indicated that the probability of *c*-axis orienting parallel to M increased when samples were prepared by oscillating packing

injection moulding. The intensity of the planes (200) greatly increased resulting from the a -axis tending to orient parallel to T and lying in plane of MT. It was revealed that the macromolecular chains of the polyethylene prepared by oscillating packing tended to orient along the flow direction resulting in high modulus, high strength of HDPE.

The effect of mould temperature on the mechanical performance and microstructure of self-reinforced high density polyethylene prepared by melt deformation in an oscillating stress field was studied [93]. Wide angle X-ray diffraction (WAXD) showed that the diffraction intensities of crystallographic planes (110) and (200) of HDPE sample prepared using an oscillating stress field increased significantly compared with that of HDPE prepared in static stress field. The crystallographic planes (110), (200), and (020) were cylindrically distributed about M direction, so the c -axis was oriented parallel to the MT plane. The diffraction from (200) was much stronger in the plane of MT than that in the plane of MN. So crystallographic planes (200) mainly lay in the plane of MT. The a -axis oriented along the N direction. The orientation of molecular chains along the M direction was an aspect which contributed to the enhancement of mechanical behaviour of self-reinforced HDPE prepared in an oscillating stress field.

Many cases of polymorphic transformations during polyethylene deformation using X-ray diffraction have been reported. [94-97]. Seto *et al.* [94] first cold drew then laterally compressed samples of HDPE and noticed changes in texture of both the orthorhombic and monoclinic crystals formed. They attributed the textural changes to three possible deformations: (1) twinning and slip of crystal planes, (2) phase transformation (orthorhombic to monoclinic), and (3) slip at the grain boundaries (crystallite boundaries). Kiho *et al.* [95] reported that either twinning or a phase transformation occurred as a function of stretching. Earlier investigations had revealed stress-induced transformations from an orthorhombic to a pseudo-hexagonal [96], triclinic or monoclinic [97]. These authors noted that the monoclinic X-ray

reflections disappeared when deformed single crystals were allowed to relax [98].

2.6.3 X-RAY PHOTOELECTRON SPECTROSCOPY (XPS)

The XPS technique is one of a variety of techniques used for characterising modified surfaces. In XPS the sample, inside a high vacuum system (pressure $<10^{-5}$ Pa $\sim 10^{-7}$ torr), is irradiated with soft X-rays, usually Mg $K\alpha$ (1253.6 eV) or Al $K\alpha$ (1486.6 eV) radiation [99]. The primary event is photoemission of a core (atomic) electron, but relaxation processes lead also to emission of Auger electrons. The emitted electrons are collected by an electrostatic energy analyser and detected as a function of kinetic energy, producing a spectrum. The intense, narrow peaks, are emitted from core orbitals (e.g., carbon 1s) due to photoelectrons. The binding energies of these electrons are highly characteristic and can be used to identify all elements except hydrogen. Since the atomic structure of each element in the periodic table is distinct from all the others, a measurement of the positions of one or more of the electron lines allows the ready identification of an element present at a sample surface. The intensity of signal observed is also a function of the amount of material. Therefore, the observation of the intensities in XPS spectra can provide semi-quantitative and quantitative analysis of the materials' surface. The technique has a combination of high surface sensitivity and the ability to provide chemical information about species observed at surfaces.

A number of studies on treated surface filler with coupling and coating agents using XPS have been published over the last decade. Silane treated filler surfaces were studied. E-glass, alumina, and quartz were chosen as substrates, while the 3-methacryloxypropyltrimethoxy-silane was used as a coupling agent [100]. The results showed that the amount of silane coating on E-glass was greater than on alumina. This indicated that the E-glass surface had more hydroxyl groups that could promote the bonding of the silane than alumina. The binding energies of each component demonstrated that the silane organic side-chain was composed of one

carboxyl carbon (288.4-288.7 eV), one carbon singly bonded to oxygen (286.0-286.3 eV) and five carbons bonded to carbon, hydrogen, silicon (284.6 eV). The relative intensities of the components were approximately 5:1:1 in E-glass and alumina, but were 7:1:1 in quartz due to the different bonding of the silane in quartz with respect to alumina and E-glass. In alumina and E-glass, it was likely that the silane stood upright on the surface, therefore electrons coming from different functional groups had a similar probability of being detected. Whereas, in quartz a polymerisation occurred withdrawing the polar groups from the polymerised coating surface to maximise nonpolar groups at the surface. The adsorption of various silanes on E-glass was also studied by Pantano and Wittberg [101]. The XPS spectra showed that in each case of E-glass samples treated with silanes, the intensity of the C-O peak was much lower than those of the free silanes while the intensities of the C=O and C-H peaks were similar to untreated glass. The decreased intensity of C-O peak indicated that a hydrolysis reaction of an alkoxy group from the silane coupling agent occurred on the glass surface, which created siloxane bonds.

XPS has been used to study effects of flame treatment on polyethylene surfaces by Sheng and co-workers [102]. High-energy resolution XPS on the polymer surface showed chemically shifted C1s peaks which were attributed to C-O, C=O, and C(=O)-O. An angle-resolved XPS indicated that the oxidation depth induced by flame treatment was higher for PE than PP. XPS was also useful for characterising oxygen plasma treated polypropylene interfaces with air, water, and epoxy resins [103]. Zhong, Yu, Sun, and Zhang used the XPS technique to study radiation-induced structural changes in a copolymer of tetrafluoroethylene and ethylene [104]. Sutherland and co-workers indicated that XPS had some advantages in terms of identification of elements present on surfaces [85]. Detection limits were typically of the order of 0.2 atom percent and, where the coating was uniform, thickness was determined in the range of 0 to 8 nm. It was concluded that both FTIR and XPS techniques can be used quantitatively and the information obtained from the two techniques is complementary.

2.6.4 SURFACE ENERGY ANALYSIS

Some of most important and extensive applications of surface chemistry are concerned with solid-liquid interfaces, for example detergency, lubrication, precipitation and wetting of powders. The physical aspects of this interface are evident in the phenomena of wetting and spreading, which depend on the nature of materials and the effects of the forces that act at the interface. In order to understand this phenomenon, further measurements of contact angles can be performed to determine surface free energies of solid surfaces.

2.6.4.1 Contact angle measurement.

A drop of free liquid in space is drawn into a spherical shape by the tensile forces of its surface tension, and the magnitude of the surface free energy, which decreases in the order metals > hydrogen bonded compounds > polar compounds > nonpolar compounds [105]. When a drop of liquid is brought into contact with a flat solid surface, the final shape taken up by the drop depends on the relative magnitudes of the molecular forces that exist within the liquid (cohesive) and between liquid and solid (adhesive). The index of this effect is the contact angle (θ_1) which the liquid subtends with the solid. It is generally found that liquids with low surface tension easily wet most solid surfaces, giving a zero contact angle. This is because the molecular adhesion between solid and liquid is greater than the cohesion between the molecules of the liquid. Liquids with high surface tension mostly give a finite contact angle, and here cohesive forces become dominant [48].

Contact angle measurement, therefore, is an important tool for determining surface energy, and a number of techniques have been used with varying degrees of success. Contact angle is directly measured by dropping liquid on the flat solid surface and the three-phase line (interface between liquid, solid, and air) is observed. Reasonable

precision ($\pm 0.3^\circ$) is normally obtained. If a small volume of the liquid is added to a drop of the same liquid resting on a horizontal solid surface the drop gets taller but its base dimension does not change, hence the contact angle increases. Similarly, removal of liquid from the drop causes a reduction in contact angle. Addition of liquid gives advancing contact angles, and removal provides receding angles, and for each system there is a maximum value of the former before the three-phase line is broken and a minimum value of the latter before the drop contacts the solid surface.

2.6.4.2 Surface free energy determination.

In order to facilitate dispersion in the polymer matrix and to prevent loss of mechanical performance such as impact resistance, fillers are often surface treated with modifiers before incorporation into plastics. Therefore, the study of surface properties is of great interest to many workers in order to understand and to control surface coverage of fillers. The surface free energy of solids is a characteristic factor which affects the surface properties such as adsorption, wetting, adhesion, etc. However, a direct method for the measurement of the surface free energy of solids has not yet been established because of their restrained elasticity and the viscosity of the bulk phase, so surface free energy determination of solids is carried out using an indirect method.

Low surface energy solids. Indirect methods have been used to determine the surface free energy of solids using Young's equation [106-108]. In 1804 Thomas Young described the connection between the work of adhesion (W_{SL}) between the surface tension of a solid (γ_S) and a liquid (γ_L), and the interfacial tension between the solid and the liquid (γ_{SL}), in units of mJm^{-2} [47, 109]. The contact angle θ_1 was measured using a drop of liquid L deposited on a horizontal flat solid surface S at the triple point: solid/liquid/air (tangential to the drop) as shown in Figure 2.9.

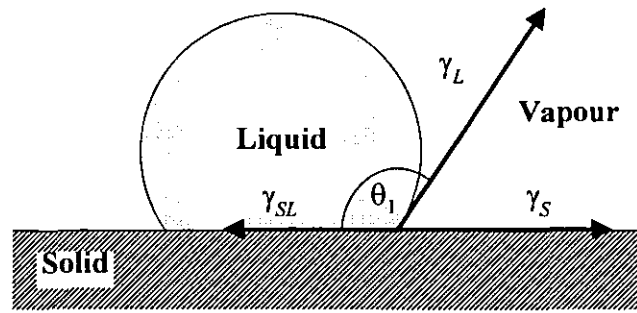


Figure 2.9: Diagrammatic of a drop liquid deposited on a horizontal flat solid surface.

From the diagram, Young's equation is usually expressed as:

$$\gamma_S - \gamma_{SL} = \gamma_L \cos \theta_1 \quad (2.19)$$

Dupre [109] expressed the relation between the work of adhesion between solid and liquids as:

$$W_{SL} = \gamma_S + \gamma_L - \gamma_{SL} \quad (2.20)$$

Inserting Equation (2.20) into the Young equation (Equation. 2.19) gives

$$W_{SL} = \gamma_L (1 + \cos \theta_1) \quad (2.21)$$

High surface energy solids. Wetting is generally complete and determination of surface energy from simple contact angle measurements becomes impossible. Therefore, an indirect determination of the surface energy is obtained in terms of several kinds of forces which exist between the molecules of two phases in contact. According to Fowkes [110] these forces can be expressed as the sum of work of adhesion terms for the different kinds of interactions giving the total reversible work of adhesion for the solid/liquid interface as:

$$W_{SL} = W_{SL}^D + W_{SL}^H + W_{SL}^{\pi} + W_{SL}^P + W_{SL}^E \quad (2.22)$$

where the superscripts refer to the types of interaction; D = dispersion, H = hydrogen

bond, $\pi = \pi$ -bond, $P =$ other polar interactions, and $E =$ electrical double layer or electrostatic interaction. The dispersion (W_{SL}^D) and polar interaction (W_{SL}^P) are usually dominant terms for high surface energy surfaces, and in the case of the materials which do not have hydrogen and π -bonds, or electrostatic interaction at interface, Equation (2.22) becomes:

$$W_{SL} = W_{SL}^D + W_{SL}^P \quad (2.23)$$

Dupre presented an equation of the dispersive energy between the solid S and liquid L for completely apolar materials [109], which is known as the Dupre equation, given by:

$$W_{SL}^D = \gamma_S^D + \gamma_L^D - \gamma_{SL}^D \quad (2.24)$$

For dispersive components, Fowkes [110] defined the work of adhesion as:

$$W_{SL}^D = 2\sqrt{\gamma_S^D \gamma_L^D} \quad (2.25)$$

where (γ_S^D) and (γ_L^D) are the surface energy of the solid and liquid phase, respectively.

Lewis acid-base or polar interaction can be presented in terms of the electron acceptor-electron donor interactions. Electron acceptor and electron donor parameters of most substances are not equal to each other, and electron acceptors of liquid will react with electron donors of a solid, thus, the polar interactions can be expressed as:

$$W_{SL}^P = 2\sqrt{\gamma_S^+ \gamma_L^-} + 2\sqrt{\gamma_S^- \gamma_L^+} \quad (2.26)$$

where γ^+ stands for the electron acceptor parameter and γ^- for the electron donor parameter of the surface tension of solid S and liquid L. Taking both W_{SL}^D and W_{SL}^P into account (Equation (2.21) and (2.23)), the Young-Dupre equation can be more precisely given by:

$$W_{SL}^D + W_{SL}^P = \gamma_L(1 + \cos\theta_1) \quad (2.27)$$

Upon combination with Equations (2.25), (2.26), and (2.27) the complete Young-Dupre equation then becomes:

$$(1 + \cos\theta_1)\gamma_L = 2(\sqrt{\gamma_S^D\gamma_L^D} + \sqrt{\gamma_S^+\gamma_L^-} + \sqrt{\gamma_S^-\gamma_L^+}) \quad (2.28)$$

For non-dispersive components of surface free energy, Schultz and co-workers [111] also suggested that all non-dispersive interactions such as dipole-dipole, dipole-induced dipole, π -bond, hydrogen bond, and interactions might be considered together and unified as a polar interaction. According to Owens and Wendt, the polar interaction may be represented as a geometric mean of the polar part of the surface free energy of liquid and solid by a method/equation analogous to that used for W_{SL}^P [109] so that:

$$W_{SL}^P = 2(\sqrt{\gamma_S^+\gamma_L^-} + \sqrt{\gamma_S^-\gamma_L^+}) = 2\sqrt{\gamma_S^P\gamma_L^P} \quad (2.29)$$

where γ_S^P and γ_L^P are the polar part of the surface free energy of solid and liquid phases, respectively. The values of relative parameters used are shown in Table 2.1. It should be pointed out that if the geometric mean, γ^P -approach, is followed, Young's equation for polar materials becomes (instead of Equation (2.28)):

$$(1 + \cos\theta_1)\gamma_L = 2(\sqrt{\gamma_S^D\gamma_L^D} + \sqrt{\gamma_S^P\gamma_L^P}) \quad (2.30)$$

Dividing by a term of $\sqrt{\gamma_L^D}$, Equation (2.30) can also be written as:

$$\frac{(1 + \cos\theta_1)\gamma_L}{2\sqrt{\gamma_L^D}} = \sqrt{\gamma_S^D} + \sqrt{\gamma_S^P} \left(\sqrt{\frac{\gamma_L^P}{\gamma_L^D}} \right) \quad (2.31)$$

A plot of $\frac{(1 + \cos\theta_1)\gamma_L}{2\sqrt{\gamma_L^D}}$ versus $\sqrt{\frac{\gamma_L^P}{\gamma_L^D}}$ should be linear with a slope of $\sqrt{\gamma_S^P}$ and an intercept of $\sqrt{\gamma_S^D}$. Therefore the total surface free energy of the solid is obtained from:

$$\gamma_S = \gamma_S^D + \gamma_S^P \quad (2.32)$$

Table: 2.1: Surface tension components and parameters of a number of liquids used in contact angle determination, at 20 °C, in mJ/m² [109].

Liquids	Surface tension, γ_L	Dispersive energy, γ_L^D	Polar interaction, γ_L^P	γ_L^+	γ_L^-
Polar					
Water	72.8	21.8	51.0	25.5	25.5
Glycerol	64.0	34.0	30.0	3.92	57.4
Apolar					
DIM (Diiodomethane)	50.8	50.8	0	≈ 0	0
BNL (1-bromonaphthalene)	44.4	44.4	≈ 0	≈ 0	≈ 0

The surface energy of silica grafted with alkyl chains was determined using contact angle measurements by Kessaissia *et al.* [112]. They found that the original silica adsorbed more water than compacted silica resulting from kinetic effects since powdered silica can readily accept water vapour whereas diffusion processes control the adsorption in the compacted silica disc. It appeared, moreover, that the surface polarity of silica decreased with increasing surface coverage and the chain length of the grafts. It was seen that the chemical surface modification caused a significant decrease of the polar components of the surface free energy.

2.7 MODIFICATION OF MECHANICAL PROPERTIES

Incorporation of fillers into thermoplastics modifies many properties of the resulting materials. Some changes will be beneficial and enhance the use of plastics, while

some cause deterioration of the composite properties. This section discusses the effects of filler incorporation on tensile, flexural, and impact properties as well as on crystallisation.

2.7.1 EFFECT ON TENSILE AND FLEXURAL PROPERTIES

The main reason why mineral fillers are used in thermoplastics is to increase rigidity or stiffness, especially at elevated temperatures. Stiffness is usually measured in terms of tensile modulus and strength. A number of models have been built to predict the tensile strength of particulate composites. Power law models are the most frequently used:

$$\sigma_c = \sigma_m(1 - V_p^{2/3})K \quad (2.33)$$

$$\sigma_c = \sigma_m(1 - 1.21V_p^{2/3}) \quad (2.34)$$

$$\sigma_c = \sigma_m(1 - V_p) - kV_p d \quad (2.35)$$

$$\sigma_c = \sigma_m + kd^{-1/2} \quad (2.36)$$

where σ_c is the composite tensile strength, σ_m is the matrix tensile strength, V_p is the volume fraction of filler, K is the stress concentration factor, k is the slope of plot of tensile strength and d is the average particle diameter.

The above equations are known as the Nielsen, Nicolais-Narkis, Landon, and Leidner-Woodhams equations, respectively [26]. As in the case of modulus, the equations predict that the tensile strength increases with an increase in the filler fraction. Additionally, Equations (2.35) and (2.36) predict that as particle size increases tensile strength decreases. Miyata [44] compared these models with experimental data and showed that the tensile yield strength of polypropylene decreased with an increase in the amount of $\text{Mg}(\text{OH})_2$ incorporated. It was evident that the tensile yield strength of $\text{Mg}(\text{OH})_2$ filled PP was proportional to the effective volume of PP excluding the volume occupied by $\text{Mg}(\text{OH})_2$, because no chemical bonding existed between $\text{Mg}(\text{OH})_2$ and polypropylene.

Stiffness of composites related to loading, particle size, and aspect ratio of filler has been considered. The aspect ratio is defined as the ratio of the length to diameter of a filler particle. An increase of tensile and flexural modulus of composites resulted from an increase in the filler loading and the aspect ratio [71, 113-116] and a decrease in the particle size of the fillers [117-121]. For example, mica additives with a plate like geometry were twice as efficient as CaCO_3 (pseudo-sphere) in enhancing the modulus at similar loading levels. In addition, the filler geometry gives rise to orientation during moulding and hence has a substantial influence on the stiffness properties of composites. However, an increase of modulus reflects a reduction of ductility and toughness of composites. These poorer properties may, however, be improved by treating the filler surface with a modifier.

The effect of surface modification of filler on tensile/flexural properties of composites has been studied in recent years. Ramos and Bajaa *et.al.* [56, 57] reported that talc modified by titanate coupling agent gave a stiffer PP composite showing improved flexural properties with increasing talc content. It was indicated that stronger adhesive bonds were formed between filler and polymer. Moreover, fatty acids and their derivatives were selected to modify the surface of basic fillers such as calcium carbonate and magnesium hydroxide. Tensile strength of LDPE composites containing calcium carbonate coated with stearic acid decreased while their deformability increased with increasing surface coverage [122]. This indicated that surface modification of filler results in a reduction of surface free energy leading to an increase in dispersion of filler in the matrix [123]. It was also found that several fatty acid and fatty acid derivative treatments for $\text{Mg}(\text{OH})_2$ filler in PP caused a slight decline in tensile/flexural modulus and tensile/flexural strength [69, 124] due to increased lubrication between filler and matrix. It is evident that both modulus and ductility responded significantly to the filler surface treatment, thereby underlining the importance of the filler/polymer interface to properties.

2.7.2 EFFECT ON IMPACT PROPERTIES

It is widely known that addition of a mineral filler to a thermoplastic results in a decrease in the plastic toughness that is often measured in terms of impact strength. The higher impact strengths of the composite in comparison to its component parts have been explained in terms of the energy required to cause debonding and work done against friction in pulling the fibres out of the matrix. Impact strengths are higher if the bond between the fibre and the matrix is relatively weak because if the bond is so strong that it cannot be broken, then cracks propagate across the matrix and fibres, with very little energy being absorbed. Impact strengths are also affected by particle size, shape, loading, and surface modification of filler.

Mitsuish, Ueno, Kodama, and Kawasaki [62] showed that fine particle fillers tend to give low impact strengths resulting in brittle compounds (high crystallinity). Three possibilities were used to explain this result:

- poor dispersion obtained with fine filler particles acting as flaws which can initiate cracks [70, 113, 125];
- the high degree of crystallinity as fine particles have high surface area in contact with the matrix;
- the surface of the filler might act as a nucleating agent for a semi-crystalline polymer, so that crystallisation is rapidly induced.

An increase of filler loading causes a decrease in impact strength or toughness of composites. Composite fracture occurs in a ductile mode at low filler loadings but in a brittle manner at high filler loadings [116, 126]. Jancar and co-workers [127] studied notched charpy impact strength of CaCO₃-filled polypropylene. In the case of no adhesion between two components, the size of the crack tip plastic zone increased with increasing filler volume fraction because of a reduction of the amount of polymer between filler particles. This results in decreasing yield strength and resistance to crack propagation giving a brittle characteristic to the composites.

Pukanszky, Belina and Volk [128] showed that surface modification of fillers improved impact properties of modified filled PP composites. Impact strengths of a compound with modified filler increased with an increase of coating level [71]. Titanate coupling agent was found to improve the impact strength of mica-filled polypropylene and further improvement was shown with increased coupling agent concentration. The increase in impact strength was because of the effective wetting of filler in the matrix and more adhesion at the filler/polymer interface hence more energy was absorbed before fracture [57]. Silane coupling agents, fatty acids and their derivatives also gave some improvements in the impact and tensile strengths of composites [125]. Riley and co-workers [113] also emphasised that good dispersion resulting from surface modification of filler was important. Their results showed that a filler such as CaCO_3 enhanced impact strength when well dispersed. Surface treatment of filler, particularly when the surface was rendered hydrophobic, reduces the tendency of the particles to accumulate at grain boundaries and thereby also enhances impact strength.

2.7.3 EFFECT ON CRYSTALLISATION

For an unfilled polymer system, when a polymer melt is cooled below its melting temperature, T_m , crystallisation is initiated at nuclei at different points in the melt. The crystallisation proceeds by the growth of the spherulites, which at this stage are spherical, each spherulite having a nucleus at its centre. The spherulite expands at a constant rate if the temperature is held constant. This stage of crystallisation is known as primary crystallisation and is complete when the spherulites completely fill the space. For a filled polymer system, fillers can initiate crystallisation inducing a changed morphology of the matrix resulting in significant property changes. The addition of filler to polymer results in an increase of modulus and usually in a decrease of impact strength or toughness of composites. Chen *et. al.* [129] and Kowalewski [130] suggested that because a filler acts as a nucleating agent to induce

crystallisation in the matrix, the number of spherulites in a filled polymer is greater while the crystallite size is smaller than in an unfilled polymer. Hutley and Darlington [125] found that the addition of nucleating agents also increases the rate of crystallisation resulting in a reduction of the impact strength of filled composites.

Mitsubishi and co-workers [62] studied crystallisation behaviour of PP filled with surface-modified CaCO_3 using alkyl dihydrogen phosphate as a surface modifier. They found that the crystallisation temperature in nonisothermal crystallisation increased with increasing CaCO_3 content and decreasing CaCO_3 particle size resulting in the higher modulus of the smaller-particle-filled PP composites. This was because the crystallisation rate of the PP matrix had been changed by the interactive motion of the PP matrix layer at the particle surface, which increased with an increase in filler content and a decrease in particle size. The crystallisation of the unmodified CaCO_3 system increased, while that of the modified CaCO_3 -PP composites decreased with increasing concentration of the same filler in comparison with unfilled PP. Resistance to relaxation of the polymer chain movement at the PP- CaCO_3 interface occurred and restriction of rapid crystallisation took place when the filler surface was modified by coating agent.

Nucleating characteristics of unmodified and modified mineral fillers in semi-crystalline thermoplastics have been discussed further. Surface modification of fillers is often carried out using various additives. The aim of such surface modification is to reinforce the bond between polymer and filler. Modifiers serve to overcome the low compatibility of blend components, forming a monomolecular layer on the filler surface, oriented with the polar part of the molecule toward the filler surface, and the non polar part toward the non polar polymer. Surface modification of these fillers has been shown both to enhance and inhibit the nucleation ability of the polymer depending on the nature of surface treatment. Rybnikar [16] investigated the crystallisation of CaCO_3 filled and unfilled linear polypropylene and found that CaCO_3 particles evidently increased the number of heterogeneous crystallisation

nuclei resulting in a higher crystallisation rate. The surface modification of CaCO_3 with phthalic and benzoic acids increased nucleation ability in the composites. Phthalic acid acted as a primary nucleation agent by introducing new solid nucleation centres. Benzoic acid acted as a secondary nucleation agent and its nucleation activity was attributed to it being liquid at crystallisation conditions, which enabled better wetting of the filler or otherwise inactive heterogeneity in the polymer inducing an increase of crystallisation of the PP in the composite. On the other hand, stearic acid and some coating agents blocked or destroyed nucleation centres in PP and/or in the filler producing a decrease of crystallinity of the composites. As the original nucleation centres in PP were mainly polymerisation catalyst residues, it was possible to considerably reduce their number by alkaline reagents. Cook and Harper [69] also showed that the coating of filler caused a decrease in crystallisation onset temperature which continued to decline slowly with increased coating level. It was revealed that stearate coating reduces the polar forces on the $\text{Mg}(\text{OH})_2$ surface which were partially responsible for nucleation.

Furthermore, a nucleation blocking effect has been suggested to arise from coverage of the filler with fatty acid alkyl chains, which then prevent the matrix polymer chains getting close enough to the filler surface to allow adsorption and nucleation. In addition, this effect of blocking of filler surface nucleation sites is probably one of the causes of the reduced filler-matrix adhesion that is often encountered with fatty acid treated fillers. Kowalewski and Galeski [130] also reported that chalk influenced the crystallisation of PP, showing nucleating ability. They found that the number of spherulites in chalk filled PP was greater than in pure polymer. Some small fractions of chalk particles were found to act as spherulite nuclei. It was indicated that a much larger fraction of chalk particles caused the formation around them of a thin epitaxial layer of polypropylene. Thus PP/chalk interface morphology was determined to some extent by the nucleating activity of the filler. Surface modification of chalk with liquid (an oligomer of ethylene oxide) also led to a decrease in the nucleating activity of chalk due to changes in the interface morphology.

Investigation of the crystallisation of linear polyethylene and its composites with talc and kaolin have revealed the nucleation activity of the solid fillers [131]. Morphological examination demonstrated that polyethylene tended to crystallise on the basal planes of sheet silicates epitaxially, in such a way that a system of parallel lamellae, oriented perpendicular to the basal plane of the substrate, grew out from the filler surface [132]. Epitaxial lamellae tended to be aligned in a pseudo-hexagonal array, suggesting that polyethylene lamellae nucleated along rows of equally charged ions in the basal plane of sheet silicates. Polyethylene molecular segments were oriented due to the electrostatic forces of the ionic substrate lattice in an extended zigzag conformation.

Surface modification of inert fillers was also studied by Rybnikar [131]. A PE composite with glass spheres crystallised equally fast as polyethylene alone, therefore glass spheres were not nucleation-active. Fracture surfaces proved poor adhesion of polyethylene to the glass surface. On improving the wetting of the glass surface by sodium benzoate, the initially inert filler changed into a nucleation-active one, characterised by a higher crystallisation rate of PE in the composite with modified glass spheres, compared with unfilled polyethylene or polyethylene with unmodified glass spheres. Fracture surfaces of the PE-modified glass spheres composite showed evidence of a strong interaction between polymer and filler. Detailed inspection revealed that lamellae polyethylene crystals were oriented with their basal planes perpendicular to the glass surfaces.

To clarify further the crystallisation of polymers and composites, three types of nucleation mechanism were proposed by Mercier [133]. In the first case the nucleation mechanism was self-nucleation (homogeneous), which related to the nucleation of a polymer melt by fragments of its own crystals previously present in melt. The second mechanism was heterogeneous nucleation represented by epitaxial nucleation of polymers on inorganic and organic substrates. In the third case it was

shown that finely divided organic salts added to reactive polymers did not behave as inert heterogeneous substrates. Rather, these organic salts dissolved and split molten macromolecules producing ionic chain ends which precipitated into the melt and formed organised aggregates which were the true nucleating species. Therefore, mechanisms of physical and chemical origin were involved in heterogeneous primary nucleation of polymer crystallisation.

CHAPTER 3

EXPERIMENTAL

3.1 GENERAL

This thesis describes two separate studies: first, the effects of various amounts of magnesium and calcium stearate coated $\text{Mg}(\text{OH})_2$ on the mechanical properties of filled HDPE composites (Series I, Tables 3.3, 3.4, 3.8, and 3.9); second, an examination of the properties of various types of coating agent together with their effects as coating agents on $\text{Mg}(\text{OH})_2$ and CaCO_3 fillers (Series II as shown in Tables 3.5, 3.6, 3.10, and 3.11). The effect of the coating agent alone on the mechanical properties of HDPE compounds was also investigated (Series II, Table 3.12). Magnesium, calcium, and zinc stearates, and stearic acid were used as coating agents. The same experimental methods were used to prepare and characterise the samples for both series and these are described below.

3.2 MATERIALS

3.2.1 POLYMER

A Rigidex high density polyethylene supplied in the form of granules by BP Chemicals Ltd was used as the polymer matrix. This HDPE is an injection-moulding grade copolymer (HD5211EA) with a narrow molecular weight distribution, a Melt Flow Index (MFI) of 11 g/10 min and a density of 0.951 g/cm^3 .

3.2.2 FILLERS

Two main fillers were used in this thesis. One was a magnesium hydroxide ($\text{Mg}(\text{OH})_2$), grade number DP393, and batch number ST-109 produced by Premier Periclase, Ireland and supplied by ICI. The other was an experimental grade of calcium

carbonate (CaCO_3) supplied by ECC (grade number of RLO6083). The technical specifications for both fillers, supplied without coating are shown in Table 3.1.

Table 3.1: Technical specification of fillers.

Properties	Magnesium hydroxide	Calcium carbonate
Molecular weight (g/mole)	58.3	100.0
Average particle size (μm)	0.80 [134]	0.55 [175]
Specific gravity	2.36 [8]	2.70 [30]
Surface area (m^2/g)	13.00 [134]	17.33 [175]
Particle morphology*	plate-like [69]	Pseudo-sphere [175]

*Particle morphology and size distribution of magnesium hydroxide were shown in previous work [69, 134].

3.2.3 COATING AGENTS

One kind of fatty acid and three derivatives were used as coating agents. Stearic acid, magnesium stearate and zinc stearate were obtained from Fisons. Calcium stearate was supplied by Harochem Chemical. The technical data are shown in Table 3.2.

Table 3.2: Technical data of coating agents.

Properties	Stearic acid	Mg stearate	Ca stearate	Zn stearate
Formula	$\text{CH}_3(\text{CH}_2)_{16}\text{COOH}$	$[\text{CH}_3(\text{CH}_2)_{16}\text{CO}_2]_2\text{Mg}$	$[\text{CH}_3(\text{CH}_2)_{16}\text{CO}_2]_2\text{Ca}$	$[\text{CH}_3(\text{CH}_2)_{16}\text{CO}_2]_2\text{Zn}$
Molecular weight (g/mole)	284.0	590.3	606.1	631.4
Melting point ($^\circ\text{C}$)	69.6 [64]	132 [135]	150 to 154 [135]	130 [135]

3.3 SAMPLE PREPARATION

There were three stages of sample preparation. The first stage was surface modification of the fillers. The second stage was compounding to produce granules of formulated composites. The last stage, injection moulding, was used to produce specimens for physical and mechanical property measurements.

3.3.1 SURFACE MODIFICATION OF FILLERS

Small scale mixing to determination the optimum filler coating conditions was carried out using a Waring blender and large scale coating using a Fielder mixer.

3.3.1.1 Waring blender

A Waring blender was used for small scale coating of magnesium hydroxide with magnesium and calcium stearates to establish the appropriate coating procedure for the Fielder mixer. 80 g of magnesium hydroxide was coated with coating agent in the approximately 1 litre capacity Waring blender. The temperature inside the Waring blender was controlled by altering voltage across a heater coil. This could be adjusted from 0 to 80 volts, and temperature was recorded every 2 minutes using a thermocouple. A sample was taken every 5 minutes for analysis using FTIR. The coating of this filler was previously studied by Raymond [134] and it was found that 6.0%w/w stearic acid was the optimum coating to achieve monolayer coverage of DP393 magnesium hydroxide. Consequently, 6.2%w/w magnesium stearate and 6.4%w/w calcium stearate were selected for magnesium hydroxide coating to be equivalent to the monolayer coverage of stearic acid (see calculations in Appendix D.2). The calculation of monolayer coverage is shown in Appendix D.1.

3.3.1.2 Fielder mixer

After the optimum temperature and time for complete coating was obtained using the Waring blender, a Fielder mixer was used for coating approximately 2 kg magnesium hydroxide. The Fielder mixer is a high speed mixer which is a more sophisticated and rapid machine for large scale blending. The principle of this mixer is to use fast rotating blades in a bed of particles in a compact container. The path of these particles can be seen as a spiral around the container axis superimposed with gravitational force creating the well-known vortex movement in a fluid bed. The material moves rapidly in both horizontal and vertical directions. Particles impact each other, the walls of the container, and the mixer blades. The container is usually equipped with a jacket for additional heat input. Discharge is through a port at the bottom of the container. This machine runs at several thousand rpm and forms a circulating vortex of powder which becomes heated by friction, up to 150-200°C. The temperature of the mixer is controlled by a water jacket for mixing heat-sensitive materials. The Fielder mixer is

widely used for drying, incorporating pigments, and coating fillers. A typical design is shown in Figure 3.1.

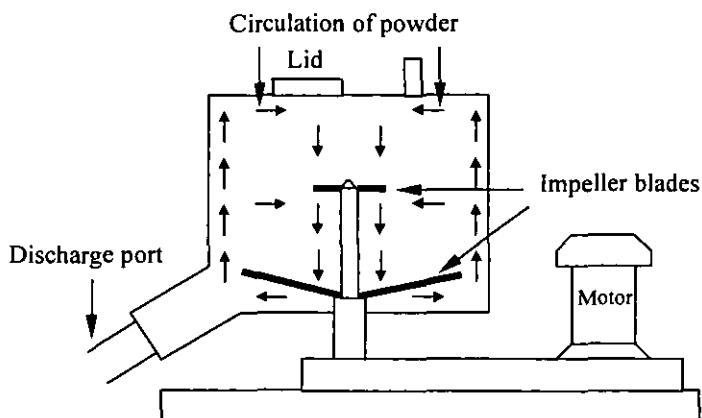


Figure 3.1: Fielder mixer.

For Series I samples, the amount of magnesium and calcium stearates used for coating magnesium hydroxide corresponded to 0.5, 1.0, and 1.5 monolayer coverage. Consequently, mixes containing 3.1%, 6.2%, and 9.3% w/w magnesium stearate on magnesium hydroxide were prepared together with a 6.0% w/w stearic acid mix, used for comparison. A coating time of 40 minutes was used for all samples. A coating time of 10 minutes was also used for the sample with 6.2% w/w magnesium stearate to investigate the effect of coating time on the mechanical properties of filled HDPE. Samples with, 3.2%, 6.4% and 9.6% w/w calcium stearate coating on magnesium hydroxide were also prepared.

In Series II, magnesium hydroxide and calcium carbonate were both used. They were coated with various coating agents such as magnesium stearate, calcium stearate, zinc stearate, and stearic acid. The coating of the same grade of calcium carbonate with stearic acid had previously been studied by Raymond [134]. It had been found that 4.0%w/w stearic acid was the optimum coating to achieve monolayer coverage of the calcium carbonate. Hence, the amount of coating agents for calcium carbonate was calculated to be equivalent to 4.0%w/w of stearic acid, calculation details are illustrated in Appendix D.2. To correspond to a monolayer coverage of each coating agent, magnesium hydroxide was coated with 6.2%w/w magnesium stearate,

6.4%w/w calcium stearate, 6.7%w/w zinc stearate, and 6.0%w/w stearic acid. Similarly, calcium carbonate was coated with 4.2%w/w magnesium stearate, 4.3%w/w calcium stearate, 4.5%w/w zinc stearate, and 4.0%w/w stearic acid. Furthermore, 6.2%w/w Mg stearate and 4.3%w/w Ca stearate were mixed with $\text{Mg}(\text{OH})_2$ and CaCO_3 , respectively, using low speed of mixing at room temperature to compare the effect of mixing conditions.

Before mixing, filler was put into an air-circulating oven for at least 12 hours at 60°C to remove moisture from the particle surfaces. For the coating of filler, the blender temperature set to obtain the temperature of filler sample was 140°C. The rotor speed was fixed at 1,000 rpm while preheating the filler for 5 minutes. The filler was added when the temperature reached 60°C. The measured time started when the coating agent was added through the port on the lid of the chamber. The rotor speed was gradually increased to 3,000 rpm and mixing continued for a total time of 40 minutes. For the “added” filler sample, filler and coating agent were mixed together using 100 rpm rotor speed at room temperature for 40 minutes. Time and temperature data were collected and a sample was taken every 5 minutes for FTIR (DRIFT), DSC, and X-ray diffraction analysis. Samples taken from the Fielder mixer after 40 minutes of coating were extracted using toluene as solvent and then the extract were analysed using transmission FTIR spectroscopy. Lists of uncoated and coated fillers produced are shown in Tables 3.3-3.6.

Table 3.3: Filler formulations used for Series I-a.

FILLERS		
No.	Sample Details for Series I-a	Code
1	100% $\text{Mg}(\text{OH})_2$ Uncoated	MHUC
2	$\text{Mg}(\text{OH})_2$ +3.1%Mg stearate (40 min coating)	MMSC31
3	$\text{Mg}(\text{OH})_2$ +6.2%Mg stearate (10 min coating)	MMSC61
4	$\text{Mg}(\text{OH})_2$ +6.2%Mg stearate (40 min coating)	MMSC62
5	$\text{Mg}(\text{OH})_2$ +9.3%Mg stearate (40 min coating)	MMSC93
6	$\text{Mg}(\text{OH})_2$ +6.0%stearic acid (40 min coating)	MSAC60

Table 3.4: Filler formulations used for Series I-b.

FILLERS		
No.	Sample Details for Series I-b	Code
1	100% Mg(OH) ₂ Uncoated	MHUC
2	Mg(OH) ₂ +3.2%Ca stearate (40 min coating)	MCSC32
3	Mg(OH) ₂ +6.4%Ca stearate (40 min coating)	MCSC64
4	Mg(OH) ₂ +9.6%Ca stearate (40 min coating)	MCSC96

Table 3.5: Filler formulations used for Series II-a.

FILLERS		
	Sample Details for series II-a	Code
1	100% Mg(OH) ₂ Uncoated	MHUC
2	Mg(OH) ₂ +6.2%Mg stearate (added)	MMSA62
3	Mg(OH) ₂ +6.2%Mg stearate (coated)	MMSC62
4	Mg(OH) ₂ +6.4%Ca stearate (coated)	MCSC64
5	Mg(OH) ₂ +6.7%Zn stearate (coated)	MZSC67
6	Mg(OH) ₂ +6.0%stearic acid (coated)	MSAC60

Table 3.6: Filler formulations used for Series II-b.

FILLERS		
	Sample Details for series II-b	Code
1	100% CaCO ₃ Uncoated	CCUC
2	CaCO ₃ +4.2%Mg stearate (coated)	CMSC42
3	CaCO ₃ +4.3%Ca stearate (added)	CCSA43
4	CaCO ₃ +4.3%Ca stearate (coated)	CCSC43
5	CaCO ₃ +4.5%Zn stearate (coated)	CZSC45
6	CaCO ₃ +4.0%stearic acid (coated)	CSAC40

3.3.2 COMPOUNDING

An APV type MP30TC was used to convert polymer formulations and additives into granules which are more convenient for use in other processing methods, such as injection moulding. This machine consists of a co-rotating twin screw extruder which has a screw diameter of 30 mm and a L/D ratio of 30:1. Screw configuration is shown

in Appendix A.4. The extruder is equipped with two K-Tron volumetric screw feeders, type T-20. Each uncoated/coated filler and high density polyethylene was separately fed into their hopper. Before compounding, calibration curves as shown in Appendix D.3 were obtained for each filler and polymer to determine the appropriate speed of the feeder. In the extruder the feedstock was melted, and homogenised in the barrel which was set at temperatures shown in Table 3.7. The screw speed was maintained at 350 rpm usually producing a torque of 50-60% of the machine maximum. The extrudate was forced through a multi-hole die and emerged as a continuous lace which was cooled in a long water bath and then chopped into short granules and packed into sacks. The production rate was fixed at approximately 15 kg/hr and the aim was to produce 40% w/w filler content in all compounds. The compound granules were dried at 60°C for at least 12 hours in a circulating air oven before injection moulding. Details of the extruder parameters and screw design are shown in Appendix A.1 and A.4, respectively. Specific energy calculations are shown in Appendix D.9. The typical apparatus is shown in Figure 3.2. After compounding, compounds produced are listed in Tables 3.8-3.12.

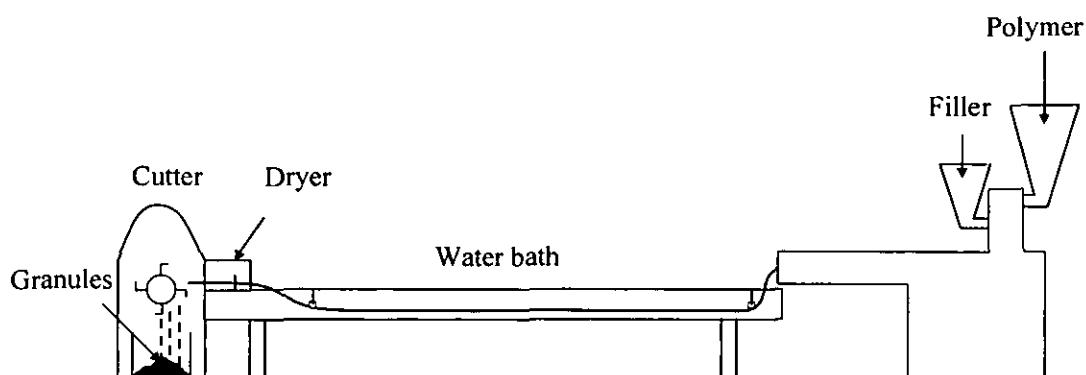


Figure 3.2: Typical compounding equipment.

Table 3.7: Setting temperatures of the barrel.

Die	Zone 4	Zone 3	Zone 2	Zone 1	Feed
160°C	160°C	160°C	160°C	155°C	125°C

Table 3.8: Compound formulations used for Series I-a.

COMPOUNDS		
No.	Sample Details for series I-a	Code
1	100% HDPE	HDUF
2	HDPE+40%Mg(OH) ₂ Uncoated	HMUC
3	HDPE+40%[Mg(OH) ₂ +3.1%Mg stearate] (40 min coating)	HMMSC31
4	HDPE+40%[Mg(OH) ₂ +6.2%Mg stearate] (10 min coating)	HMMSC61
5	HDPE+40%[Mg(OH) ₂ +6.2%Mg stearate] (40 min coating)	HMMSC62
6	HDPE+40%[Mg(OH) ₂ +9.3%Mg stearate] (40 min coating)	HMMSC93
7	HDPE+40%[Mg(OH) ₂ +6.0%stearic acid] (40 min coating)	HMSAC60

Table 3.9: Compound formulations used for Series I-b.

COMPOUNDS		
No.	Sample Details for Series I-b	Code
1	100% HDPE	HDUF
2	HDPE+40%Mg(OH) ₂ Uncoated	HMUC
3	HDPE+40%[Mg(OH) ₂ +3.2%Ca stearate] (40 min coating)	HMCSC32
4	HDPE+40%[Mg(OH) ₂ +6.4%Ca stearate] (40 min coating)	HMCSC64
5	HDPE+40%[Mg(OH) ₂ +9.6%Ca stearate] (40 min coating)	HMCSC96

Table 3.10: Compound formulations used for Series II-a.

COMPOUNDS		
No.	Sample Details for series II-a	Code
1	100%HDPE	HDUF
2	HDPE+40%Mg(OH) ₂ Uncoated	HMUC
3	HDPE+40%[Mg(OH) ₂ +6.2%Mg stearate] (added)	HMMSA62
4	HDPE+40%[Mg(OH) ₂ +6.2%Mg stearate] (coated)	HMMSC62
5	HDPE+40%[Mg(OH) ₂ +6.4%Ca stearate] (coated)	HMCSC64
6	HDPE+40%[Mg(OH) ₂ +6.7%Zn stearate] (coated)	HMZSC67
7	HDPE+40%[Mg(OH) ₂ +6.0% stearic acid] (coated)	HMSAC60

Table 3.11: Compound formulations used for Series II-b.

COMPOUNDS		
No.	Sample Details for series II-b	Code
1	100%HDPE	HDEF
2	HDPE+40%CaCO ₃ Uncoated	HCUC
3	HDPE+40%[CaCO ₃ +4.2%Mg stearate] (coated)	HCMSC42
4	HDPE+40%[CaCO ₃ +4.3%Ca stearate] (added)	HCCSA43
5	HDPE+40%[CaCO ₃ +4.3%Ca stearate] (coated)	HCCSC43
6	HDPE+40%[CaCO ₃ +4.5%Zn stearate] (coated)	HCZSC45
7	HDPE+40%[CaCO ₃ +4.0%stearic acid] (coated)	HCSAC40

Table 3.12: Compound formulations used for Series II-c.

COMPOUNDS		
No.	Sample Details for series II-c	Code
1	100%HDPE	HDEF
2	HDPE+4.0%Mg stearate	HDMS
3	HDPE+4.1%Ca stearate	HDCS
4	HDPE+4.3%Zn stearate	HDZS
5	HDPE+3.9%stearic acid	HDSA

3.3.3 INJECTION MOULDING

The basic principle of injection moulding is to inject molten polymer into a closed and cooled mould, where the product is produced by solidifying of the molten polymer. The mould then opens to release the moulding. A Negri Bossi NB55 injection moulding machine was used. It consists of an injection unit and a clamp unit. Each formulated compound granule is fed by a hopper into the single screw extruder which contained a heated jacket. The melted plastic is continuously pushed by the screw through a nozzle into the mould until the mould is filled. The melted plastic is held under pressure by the screw for a period of time, compound flows into the mould, and then the screw returns to begin a new cycle. The clamp unit consists of a fixed and a moveable platen. When the mould is closed, the polymer melt is injected into a cavity between the two platens held together. Upon completion of the injection cycle and

cooling, the mould is opened and the moulding ejected. Various specimen shapes were produced from two different moulds as shown in Figure 3.3; a four part mould (a) and a four piece tensile mould (b). A circular sheet specimen taken from a four part mould was used for impact testing. A square sheet specimen was used for contact angle measurements. The dumbbell rod specimens taken from both moulds were used for tensile, flexural, reversion, crystallinity, and filler/polymer orientation testing. Details of the injection-machine settings are shown in Appendices A.2 and A.3.

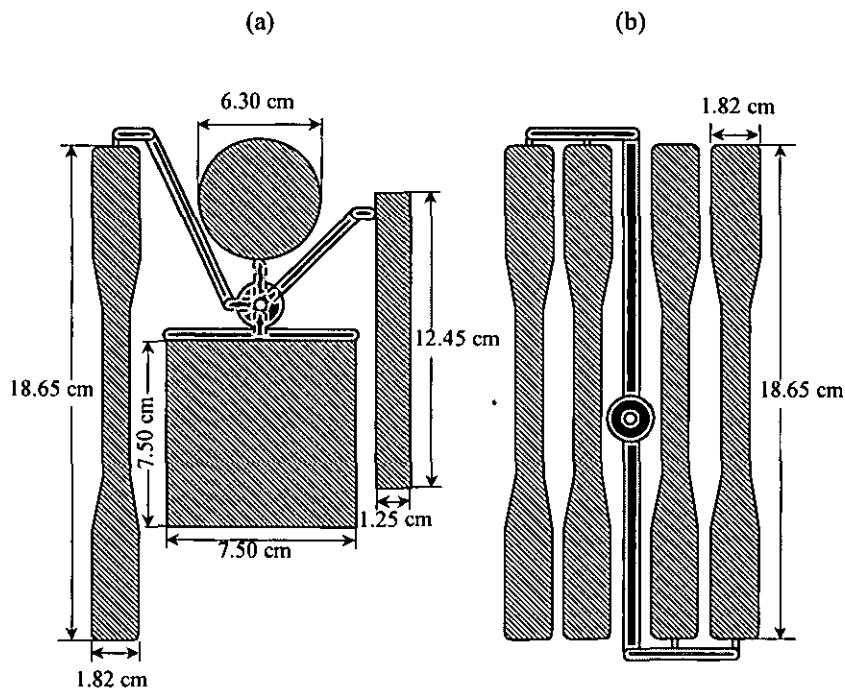


Figure 3.3: Injected specimen obtained from a) a four part mould, b) a four piece tensile mould.

3.4 PHYSICAL PROPERTY CHARACTERISATION

In general, the incorporation of fillers into thermoplastics decreases the mechanical properties of composites, particularly compound toughness. The composite properties can be improved by surface modification of fillers. To further understand the effects

of uncoated and coated fillers on composite properties, methods to characterise physical properties of materials were used as follows:

3.4.1 FOURIER TRANSFORM INFRARED SPECTROMETRY (FTIR)

3.4.1.1 Fundamentals

The basic construction of an FTIR instrument is illustrated in Figure 3.4(a). The emission of an approximately continuous spectrum is produced from a high intensity mercury lamp or heated wire as the light source. The beam of IR radiation passes into a Michelson interferometer which is at the core of the spectrometer (Figure 3.4(b)). The essential components of the interferometer consist of two mirrors, one fixed and the other moveable. The beam splitter is set at an angle of 45° to the path of the collimated beam. The incoming light is divided at the beam splitter and reflected from the two mirrors. Upon recombination at the beam splitter, constructive and destructive interference occurs. These effects depend on the path-length difference of the light and its wavelength. The beam then passes through the sample and it is collected by the detector. If the locations of the mirrors are precisely equivalent to the distance from the beam splitter or if the optical path difference is an integral number of wavelengths, the reflected beams are in phase and so constructive interference is produced. Conversely, when the optical path difference is a fraction of a wavelength, destructive interference will occur. The movement of the moveable mirror creates relative phase displacement resulting in an oscillatory interferogram. This interferogram is represented in the form of the spectral distribution and displayed as an absorption signal on the detector.

Diffuse Reflectance Fourier Transform Spectroscopy (DRIFT) is a technique used for rough surfaces such as powders by collecting the infrared radiation scattered from the surface. A simplified diagram of a cell is shown in Figure 3.4(c). The essential features of the cell are mirrors and optics to focus the incident IR beam on to the

surface of the powdered sample, which is mounted on the sample holder. Since the surface of powder particle is at random orientation, the scattered radiation is reflected across a wide angle and captured by the elliptical output mirror. The radiation is refocused back into a beam by the mirror and corrected by the output optics then passed through to the detector.

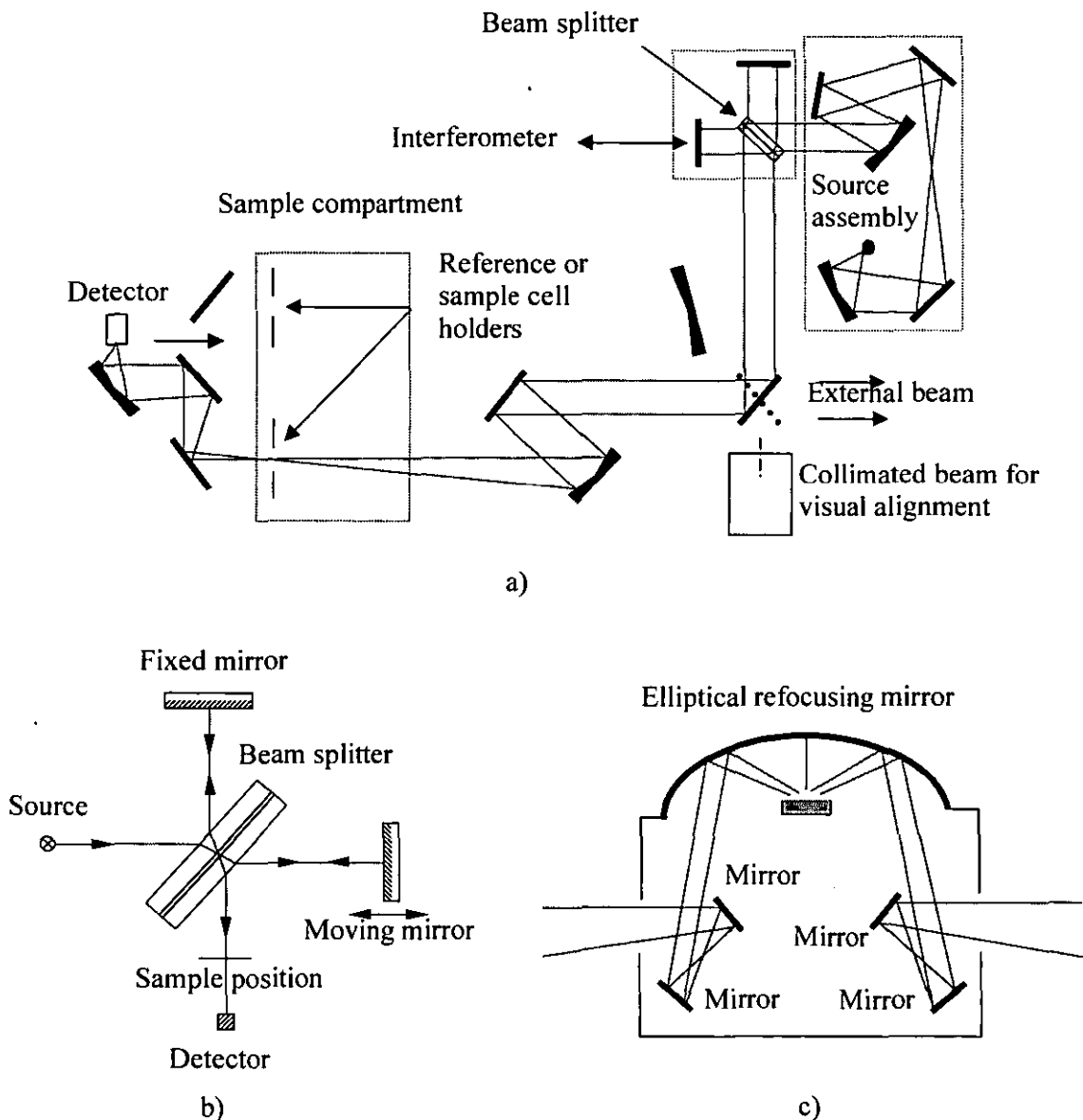


Figure 3.4: Schematic diagrams of a) an optical bench of FTIR [136] spectrometer, b) a Michelson Interferometer [137], c) DRIFT cell.

3.4.1.2 Analytical procedures

DRIFT Technique

The characteristics of the surface coatings were analysed by the DRIFT technique. The DRIFT facility was installed on a Unicam Mattson 3000 spectrometer. Since the DRIFT signal response will be linear only when the absorbance is less than one, the sample needs to be diluted with KBr. Spectroscopic grade KBr supplied from Fisons was ground in a Braun coffee grinder for 20 one minute intervals to obtain a fine particle size and then to produce 2.5%w/w samples, the uncoated/coated fillers were dispersed in the ground spectroscopic grade KBr. To ensure an even distribution of the sample, the mixture was ground again with a small mortar and then shaken using a high speed shaker for 1 minute. The same batch of ground KBr was used for all samples to keep particle size consistent. The FTIR machine was initialised with no sample in, to take account of the air and then with a pure KBr sample to provide a background reading. KBr was placed in a stainless steel cup and the surface smoothed with a clean spatula before being placed in the machine. KBr was scanned as a background with single beam from 4000 to 400 cm^{-1} . 400 scans were carried out at 4.00 cm^{-1} resolution and a speed of 0.6 $\text{cm}^{-1}\text{s}^{-1}$. Similarly, prepared samples were also placed in the machine and scanned under the same conditions. The next sample was then mounted within the IR beam until all of the samples were scanned. The O-H stretching vibration of the magnesium hydroxide filler was observed from 3751 to 3605 cm^{-1} . Calcium carbonate filler gave a CO stretching vibration at 1440-1395 cm^{-1} and CO bending vibration at 2700-2395 cm^{-1} . The coating agent containing carboxylate group gave a COO^- band at 1637-1278 cm^{-1} and C-H stretching vibrations at 3001-2785 cm^{-1} . The CH/OH, COO/OH, and CH/CO ratios of the integrated peak areas under the bands were determined for coated magnesium hydroxide and calcium carbonate, respectively. The spectrum of $\text{Mg}(\text{OH})_2$ coated with 6.2%w/w magnesium stearate is shown in Figure 3.5.

A spectral subtraction technique is an alternative approach used to reduce the interference of an unwanted spectrum. A particular band due to the filler alone, e.g. an OH peak for $\text{Mg}(\text{OH})_2$ or CO peak for CaCO_3 , can be subtracted from the total complex spectrum of the coated filler leaving the spectrum of coating agent. Hence, the OH peak at 3695 cm^{-1} of coated magnesium hydroxide or the CO peak at 1448 cm^{-1} of coated calcium carbonate could be subtracted so that coating could be investigated at greater sensitivity.

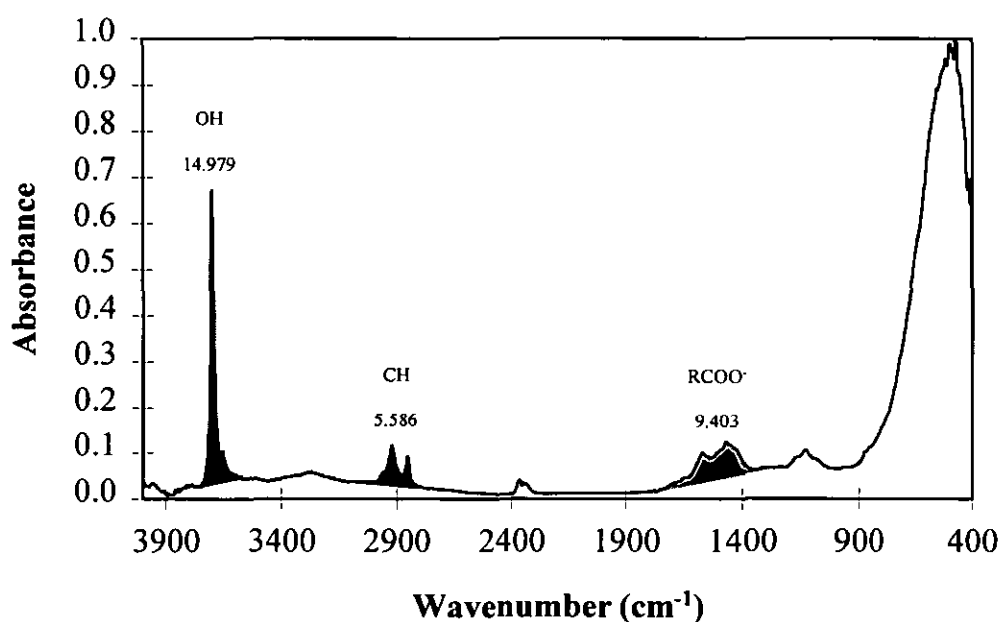


Figure 3.5: FTIR spectrum of magnesium hydroxide coated with 6.2%w/w magnesium stearate.

Transmission Technique

To further understand the filler-coating area, the continuous extraction of solid by a hot solvent was used to extract coating agents from final coated fillers (taken from the Fielder mixer after 40 minutes of coating). 2 grams of coated filler were placed in a porous thimble made of tough filter-paper and covered with glass wool and the latter was placed in the inner tube of a Soxhlet apparatus as shown in Figure 3.6. The apparatus was then fitted to a round-bottomed flask of appropriate size containing 100 ml toluene (as solvent) and boiling chips, and to a reflux condenser. The solvent was

boiled gently. The vapour passed up through an adjacent tube of the apparatus and condensed by the condenser and then the condensed solvent fell into the thimble and slowly filled the body of the Soxhlet. When the solvent reached the top of a double tube, it siphoned over into the flask so that the portion of soluble coating agent was extracted from the coated filler. The process was repeated automatically until complete extraction was effected which required 20 hr. The extracted compound was dropped on a sodium chloride disc, which is transparent in IR region, and was placed under an infrared lamp to evaporate solvent. The dried disc was scanned using a transmission technique with a single beam obtaining 64 scans at 4.00 cm^{-1} resolution from the wavelength of $4000\text{ to }400\text{ cm}^{-1}$. The observed spectra of extracted samples are shown in Appendices F.2 and F.3.

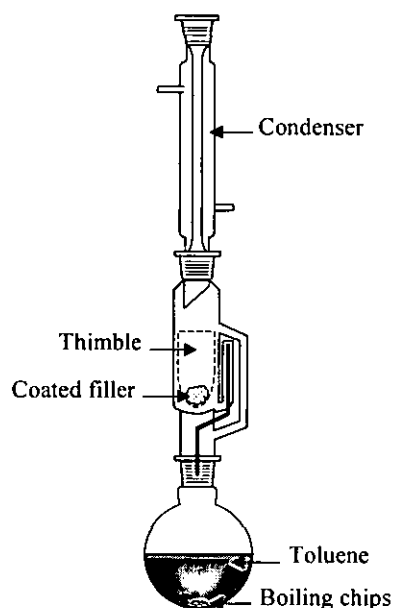


Figure 3.6: A Soxhlet extraction apparatus.

3.4.2 THERMAL ANALYSIS

3.4.2.1 Differential scanning calorimetry (DSC) technique

This technique involves the measurement of heat flow (dQ/dt) to or from a sample chamber compared with that to a reference chamber as a function of time or

temperature. The temperature inside the furnace was controlled by a temperature programmer (Figure 3.7). Practically all physical and chemical processes result in enthalpy changes which can be detected by DSC. A DSC measurement is a quantitative process and gives the rate of change of enthalpy.

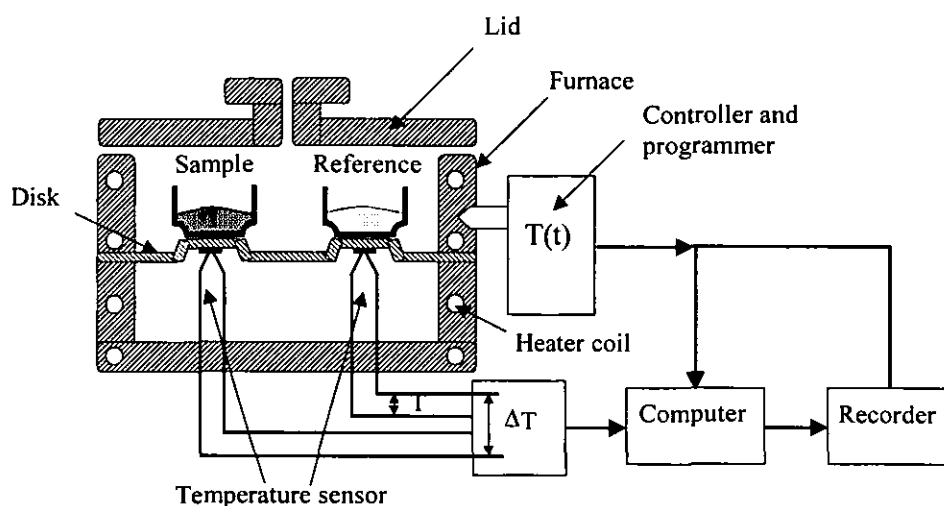


Figure 3.7: DSC apparatus [138].

3.4.2.2 Analytical procedures

The DSC was used to follow the process of coating the filler with stearates. Fillers and coating agents were loaded into the Fielder mixer and samples were taken every 10 minutes during the mixing process. These samples and samples of various coating agents, i.e. metal stearates and stearic acid, were weighed and placed in the DSC cell. Samples were heated from 30°C to 180°C with a heating rate of 10°C/min using a Dupont Thermal Analyser Model 2000 fitted with a DSC cell. Data concerning enthalpy of fusion was extracted from the curve.

For the determination of crystallinity properties of formulated polymer compounds, a specimen was cut from the centre of a tensile bar to avoid the more rapidly cooled skin part of the moulding. The specimen, of accurately known weight, was placed in the DSC cell and heated with a heating rate of 10°C/min from 30°C to 180°C. The sample was held isothermally at the upper temperature for 2 minutes before cooling to

30°C with a cooling rate of 10°C/min. The melting temperature (T_m), recrystallisation temperature (T_c), onset of melting temperature (T_{sm}), onset of recrystallisation temperature (T_{sc}), heat of fusion (ΔH_m), and heat of recrystallisation (ΔH_c) were obtained from the thermograms for all samples. An example of a thermogram of high density polyethylene is shown in Figure 3.8. The percentage of crystallinity reported was corrected using the actual polymer fraction obtained from ash determinations (see section 3.4.7). The percentage of crystallinity (f_c) is given by:

$$f_c = \frac{\Delta H_m}{\Delta H_{mc}} \times \frac{1}{\text{Polymer fraction}} \times 100 \quad (3.1)$$

where ΔH_m is the enthalpy of fusion of semi-crystalline polymer, and ΔH_{mc} is the enthalpy of fusion of a completely crystalline sample of the same polymer. The enthalpy of fusion of pure polyethylene is 293 J/g [139]. The calculation details are presented in an Appendix D.4.

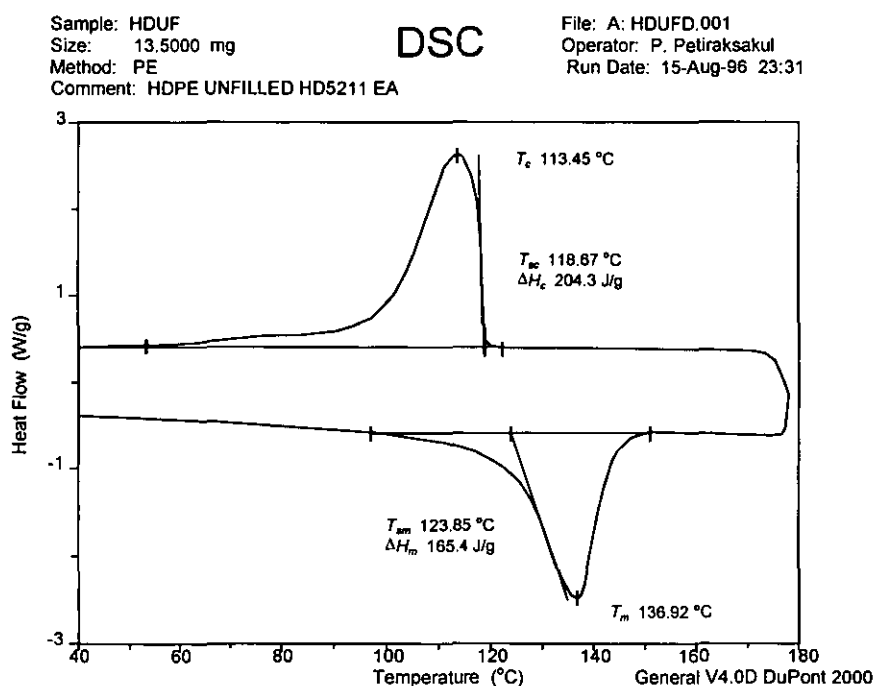


Figure 3.8: The thermogram of high density polyethylene.

3.4.3 X-RAY DIFFRACTION

3.4.3.1 Fundamentals

The X-rays of importance in diffraction studies are generated when high-energy electrons impinge on a metal target, such as iron, copper or molybdenum. At a sufficiently high X-ray-tube voltage an X-ray beam is produced. A divergent X-ray beam impinges on a sample which is carefully mounted on a sample mount assembly. The sample surface is adjusted to be parallel to the mount bed. When the Bragg conditions are satisfied reflections from crystalline components in the sample are produced and the X-ray beam then passes into a counter to be recorded. Since the diffraction is collected only when the lattice planes are parallel to the sample surface, the counter must be mounted on the circular track which is located in synchronisation with the sample. This condition requires the counter axis to be always directed towards the sample and rotated through twice the angle through which the sample moves. Bragg's law states that:

$$2d_{hkl} \sin \theta_{hkl} = n\lambda \quad (3.2)$$

where d is interplanar spacing for (hkl) planes, $2\theta_{hkl}$ is the angle of deviation of the diffracted rays from the incident X-rays, and λ is the X-ray wavelength (Å). Since λ is known, i.e. using copper as X-ray source λ is 1.542 Å, and $2\theta_{hkl}$ can be read directly from the counter setting, hence d_{hkl} can be determined. The sample and the counter are practically rotated very slowly at a constant rate using a common motor and appropriate gearing. The counter has a very fast response and gives a signal proportional to the X-ray intensity. The signal is amplified and displayed on a meter, and is normally fed to computer to produce a continuous trace of intensity versus degree 2θ . The peak positions can be determined quite accurately. The basic layout of a diffractometer and block diagram of detector circuits for a diffractometer are shown in Figure 3.9.

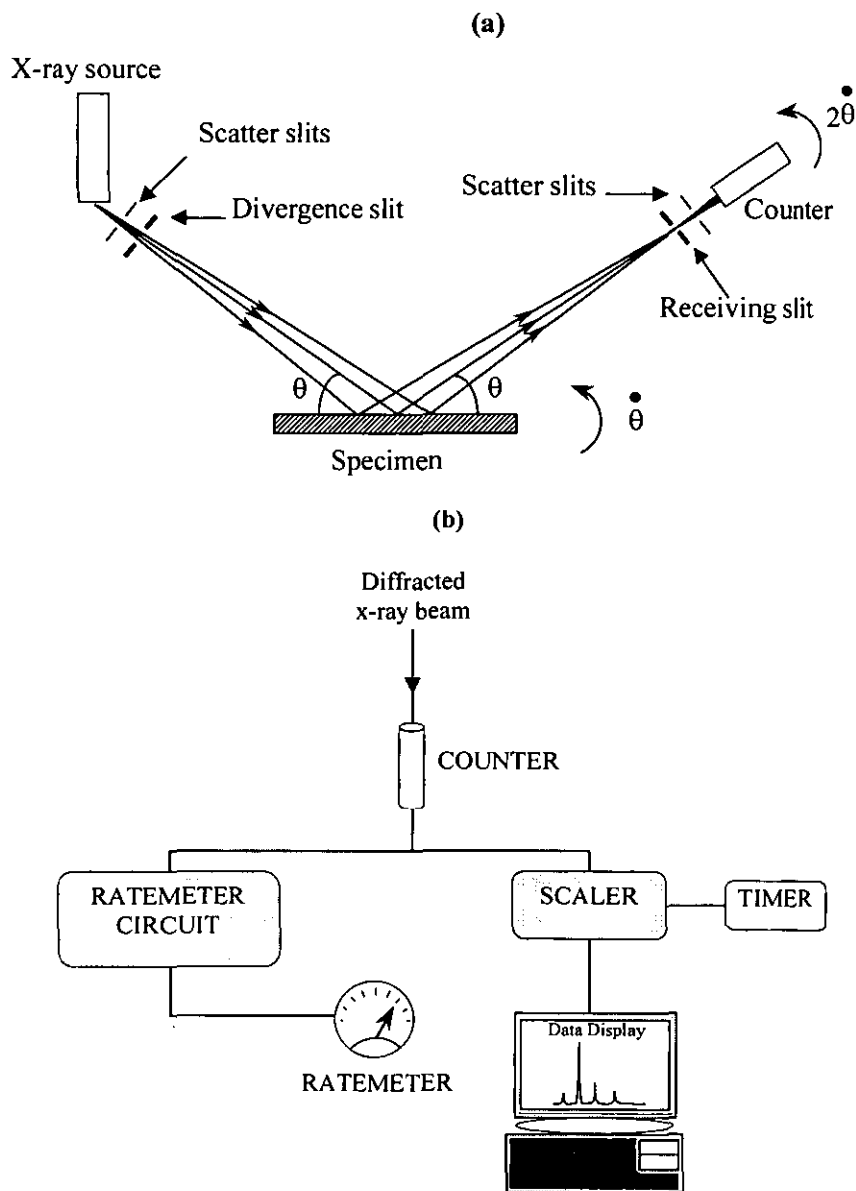


Figure 3.9: Basic layout of a diffractometer (a) and block diagram of detector circuits for a diffractometer (b).

3.4.3.2 Analytical procedures

Samples were individually scanned using a Philips type PW 1050 diffractometer with a graphite monochromator to remove the $K\beta$ radiation. X-rays were produced from an X-ray tube with a copper target ($\lambda = 1.542 \text{ \AA}$) run at 40 kV and 30 mA from a Hilton Brooks power supply model DG3. Data was collected by computer using a single

programme provide by Hilton Brooks. For filler characterisation, uncoated/coated fillers and coating agents were scanned at diffraction angle from 19 to 24 degree 2θ , step size of 0.02 degree 2θ , dwell time of 15 sec/step using divergence, receiving and scatter slit size of 1.0, 0.2, 1.0 (degree, mm, degree) respectively. Using the XRD software programme, the interplanar spacing can be calculated. The d spacing and the intensity of peaks were needed to identify the coating agents and to compare the filler coating by matching both values to those in the powder diffraction file of materials (PDF) [140] which contains the d spacing for every line for each material and the relative intensities of the lines based on the strongest line as 100 [86]. X-ray diffraction pattern of fillers and coating agents are shown in Appendices G.3 and G.4.

As a compound was produced using injection moulding, typically the polymer molecules and filler lost their isotropic structure and tended to become oriented in the machine direction affecting mechanical properties. In order to understand more about the effect of processing on the mechanical properties of the compounds, the X-ray diffraction method was also used to investigate the polymer and filler orientations. Each specimen was cut from the same side of a tensile specimen and scanned from 2 to 50 degree 2θ , step size of 0.05 degree 2θ , dwell time 59 sec/step, and slit size of 1.0, 0.2, 1.0 (degree, mm, degree). The polymer orientation can be examined by calculating the peak intensity ratios of the PE200 and PE110 lines. Similarly, the peak intensity ratios of MH001/101 and CC104/110 were also calculated to determine the filler orientation for magnesium hydroxide (MH) and calcium carbonate (CC), respectively. The X-ray pattern of intensity versus angle for high density polyethylene filled with uncoated $\text{Mg}(\text{OH})_2$ is shown in Figure 3.10.

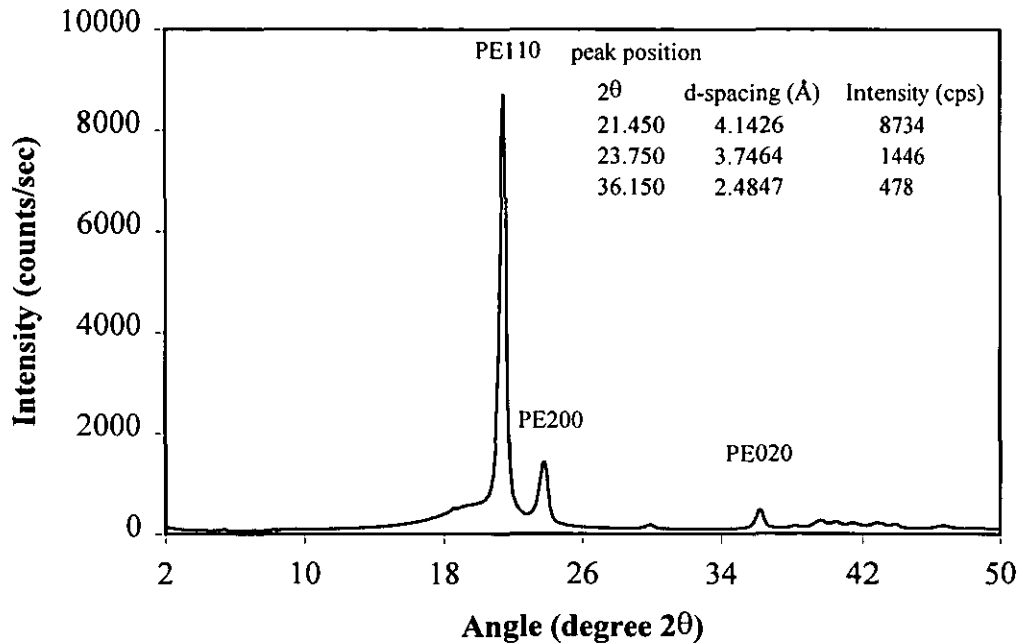


Figure 3.10: The X-ray diffraction pattern of $\text{Mg}(\text{OH})_2$ filled HDPE.

3.4.4 CONTACT ANGLE MEASUREMENT

Mechanical properties of filled polymers depend, among other things, on the uniformity of filler dispersion in the polymer matrix and the adherence between filler surface and polymer which, in turn, greatly depends on their surface free energies. The surface free energy of solids is usually obtained using a determination of the contact angle of a liquid of known surface tension on the surface of a solid. To determine the surface free energies of the polymer, fillers, and coating agents, the contact angle of polar and nonpolar liquids on a variety of flat surfaces were measured by a technique using a sessile drop of the liquids. The contact angles (θ_1) on the flat surfaces were measured using a model G40 apparatus made by Kruss of Hamburg, Germany. Two hydrophilic liquids, deionised water and glycerol ($\text{C}_3\text{H}_8\text{O}_3$), and two hydrophobic liquids, diiodomethane (CH_2I_2) and 1-bromonaphthalene ($\text{C}_{10}\text{H}_7\text{Br}$), were used. The last three chemicals were obtained as analytical grade liquids from Acros, Geel, Belgium. The surface tension of the four liquids is shown in Table 3.13.

Table 3.13 The surface tension of four liquids [109].

No.	Liquid	Surface tension, γ_L , (mJ/m ²)
1	deionised water	72.8
2	glycerol (C ₃ H ₈ O ₃)	64.0
3	diiodomethane (CH ₂ I ₂)	50.8
4	1-bromonaphthalene (C ₁₀ H ₇ Br)	44.4

The uncoated and coated fillers (the end product) were ground in a mortar and pressed under a 10 ton load using an evacuated die to produce a disc specimen. For the polymer formulations, a rectangular specimen of each compound was cut from the square sheet of the four part mould produced by injection moulding. A drop of liquid was injected using a microsyringe onto the surface of the specimen and the advancing contact angle was measured visually through a microscope objective (Figure 3.11).

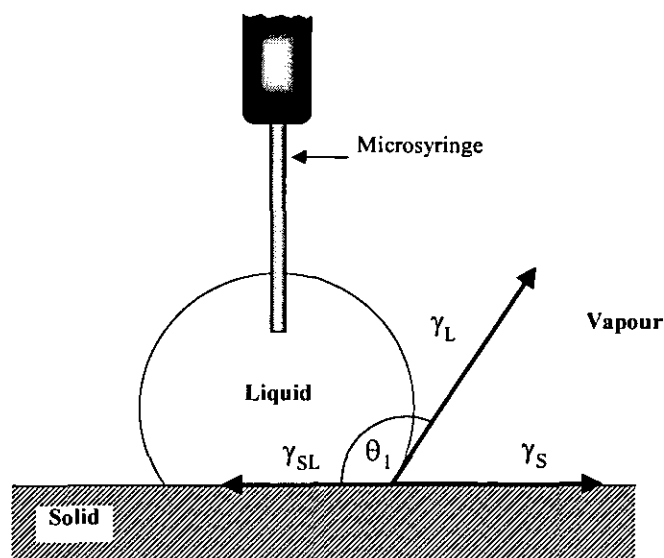


Figure 3.11: Diagram of a contact angle measurement where γ_{SL} = solid-liquid surface tension or interfacial tension between solid and liquid, γ_S = surface free energy or surface tension of solid S, and γ_L = surface tension of liquid L, and θ_1 = contact angle.

The microsyringe needle was fixed above the test surface and the drop of liquid was enlarged by injecting more liquid during measurement. The contact angle

measurement was repeated at least five times for each liquid. The reproducibility was ± 2 degrees. The contact angles of specimens are later used to calculate surface free energy. The calculation of surface energy is shown in Appendix D.6.

3.4.5 X-RAY PHOTOELECTRON SPECTROSCOPY (XPS)

3.4.5.1 Fundamentals

This technique is sometimes known as electron spectroscopy for chemical analysis (ESCA) and is based on the observation that electrons are emitted by atoms under X-ray bombardment as shown in Figure 3.12. X-ray photons, $h\nu$, from a nearly monoenergetic beam impinge on the sample. The photons are absorbed by sample atoms then electrons from the orbitals with a binding energy, E_b , less than the X-ray energy are excited resulting in the emission of electrons. The emitted electrons are collected by an electrostatic energy analyser and detected as a function of their kinetic energy, KE . The binding energy of the electron in the atomic orbital can be obtained from the Einstein relation

$$E_b = h\nu - KE + \phi_s \quad (3.3)$$

where ϕ_s is a correction factor for the spectrometer work function, normally applied as part of the spectrometer calibration procedure. It is capable of detecting all elements in the periodic table which have atomic number greater than hydrogen.

3.4.5.2 Experimental procedures

Samples of magnesium hydroxide and calcium carbonate coated with metal stearates were analysed using an XPS model VG ESCALAB mark 1 and carried out with help of personnel of the Institute of Surface Science and Technology (ISST) at Loughborough University.

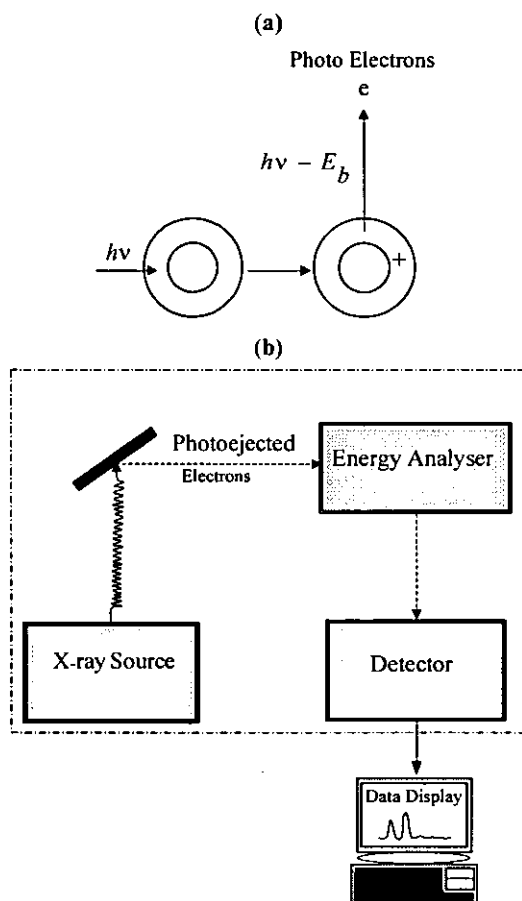


Figure 3.12: The basic elements of X-ray photoelectron spectroscopy a) X-ray bombardment, b) instrumentation.

The coated filler was mounted on a sample holder stub and placed in the vacuum chamber of the equipment. The sample was then irradiated with X-rays from an Al $K\alpha$ source with energy 1486.6 eV. The X-ray photons were absorbed by the sample surface; the electrons were then emitted and detected. The detector displayed the signal as a spectrum of electron intensity against binding energy. Since the atomic structure of each element in the periodic table is distinct from all the others, measurement of the positions of the electron lines allows the ready identification of an element present at a surface sample. Only electrons close to the sample surface have enough energy to escape and the elements present in the surfaces were carbon, oxygen, magnesium, calcium, and zinc, therefore, the peaks of C1s, O1s, Mg2p,

Ca2p, and Zn2p were measured. The XPS spectra of uncoated/coated fillers are shown in Appendix F.5.

3.4.6 SCANNING ELECTRON MICROSCOPY (SEM)

3.4.6.1 The basis of instrument

A monoenergetic beam of electrons is generated from a heated tungsten filament. This beam is accelerated with a potential difference between the filament and an anode (and the specimen) at earth potential. The beam passes through a hole in the anode and is focused on to the specimen using an electromagnetic lens system. As soon as the electron beam impinges on the specimen surface, a number of interactions occur which can be used to generate information. Various detectors are arranged in the specimen chamber for the measurement of the several signals which are characteristic of the region of the specimen under bombardment. The electron beam can be moved over the specimen surface using a variable magnetic field provided by a current-carrying 'scan coil' (see Figure 3.13).

When the beam moves to a different site the characteristic signal measured by any of the detectors may change, and this is exploited to form "image contrast". In the SEM the electron beam is made to move across the specimen surface in a regular TV-like raster, tracing out a rectangle line-by-line under the command of the scan coils which are fed by a "scan generator". The signal change is continuously measured using detectors. This phenomenon is in correspondence with the characteristics of the surface probed by the electron beam. The amplified signal is used to control the brightness of the spot on a cathode ray tube (CRT) and the CRT scan is controlled by the same scan generator that controls the beam position. Hence an image can be built up representative of the sample surface.

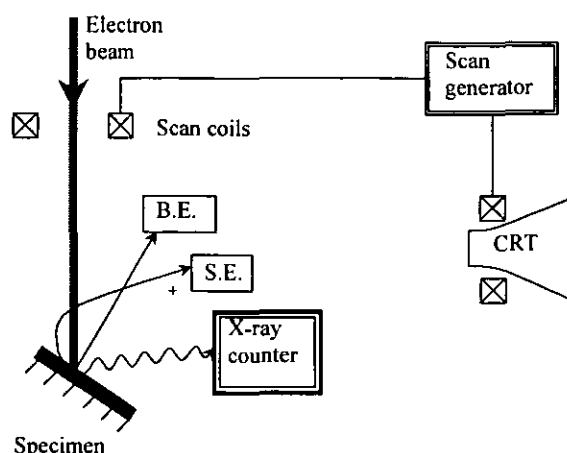


Figure 3.13: Layout of the SEM [139], BE = backscattered electron detector; SE = secondary electron detector; CRT = cathode ray tube display.

3.4.6.2 Specimen preparation

The use of scanning electron microscopy presented here is to examine fracture surfaces to investigate failure modes. As polymer is an electrical insulator fractured impact samples were mounted on individual aluminium stubs and sputtered with a conductive coating layer such as gold and carbon. It was found that carbon coating gave better images than gold coating, therefore carbon was used to obtain appropriate coating in this work. The specimen details were viewed on a vdu screen using a Cambridge Stereoscan 360 SEM instrument at 10 kV. Several magnifications were used for coarse prospecting, however, only 50 K magnification was represented in the photomicrographs. The wavelength dispersive X-ray mapping (WDXM) technique is capable of detecting elements heavier than boron. This technique was also used in this study to examine the different metal elements in composites. Examples of micrographs are shown in Figures 5.32 and 5.33.

3.4.7 ASH DETERMINATION

3.4.7.1 Method

The determination of ash according to British Standard BS 2782: Part 4: Method 454A [141] was used for analysing the weight percent of filler and coating in each

compound. All samples, including coating agents, uncoated/uncoated fillers, and unfilled/filled HDPE, were burned in a furnace until the weight of their ash was constant. To determine filler/polymer content, the weight percent ash contents of 100% HDPE (a) and each value of 100% uncoated/coated fillers (b) were plotted on the axes of the graph shown in Figure 3.14(a). These points were joined by a straight line, and the percent ash content of the filled compound (y_1) is then related to the percent of polymer in the compound as follows:

$$\text{Percent ash content of the compound } (y_1) = m_1x_1 + b \quad (3.4)$$

where m_1 = slope of line ab . The weight percent of the polymer in compound (x_1) can be calculated using the above equation. Finally, the final filler content of each compound is given by:

$$\text{Final filler content} = 100 - \text{weight percent of the polymer in that compound } (x_1) \quad (3.5)$$

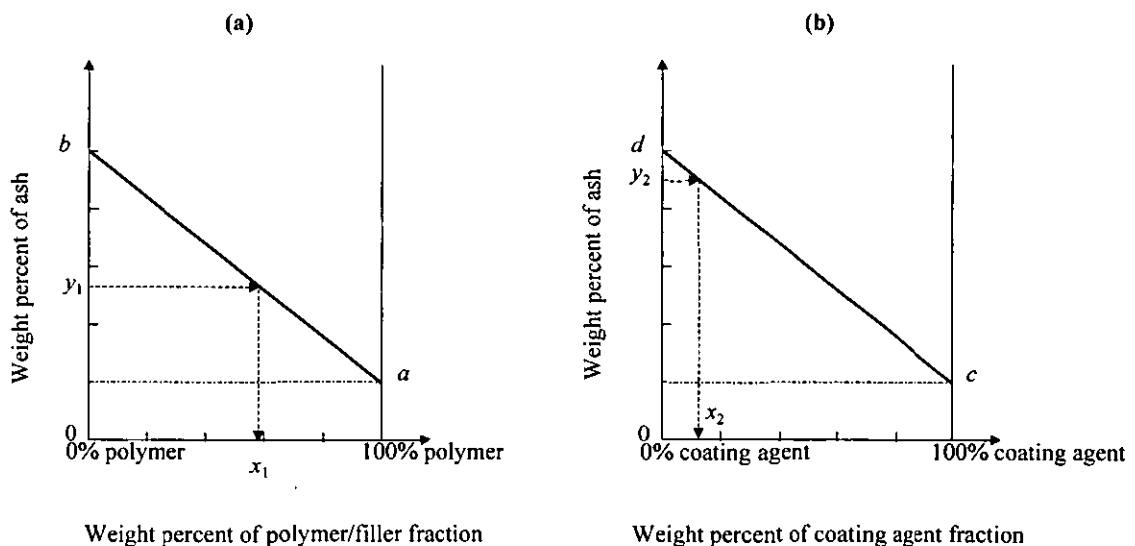


Figure 3.14: Polymer, filler, and coating agent content determination of a) compounds, b) coated fillers.

Similarly, the final coating content can be calculated using Equation (3.6). The weight percent ash content for 100% coating agent (c) and for 100% uncoated filler (d) were plotted on the axes of the graph shown in Figure 3.14(b). These points were joined by a straight line, and the percent ash content of the coated fillers (y_2) is then related to the percent of coating agent in the filler by:

$$\text{Percent ash content of the coated filler } (y_2) = m_2x_2 + d \quad (3.6)$$

where m_2 = slope of line cd. The percent of coating content in the filler (x_2) can be calculated.

3.4.7.2 Analysis procedures

The ashing determination technique was used to determine the filler and coating content of each compound. After compounding, the compound granules were dried overnight in an air circulating oven at 60°C. To determine the amount of inorganic residue remains, unfilled and filled polymer, uncoated and coated fillers and coating agents were ashed. Approximately 2 grams of each sample was exactly weighed (accuracy of ± 0.001 g) into each silica crucible and ashed in a furnace set at 850°C for 3 hours. After removing from the oven, the crucible with sample was placed in a desiccator for at least 1 hour to cool and then re-weighed. These operations were repeated until a constant mass was obtained, that is, until two successive weights did not differ by more than 0.005 grams. Two determinations were carried out on each sample with an average value recorded. The weight of ash in the crucible was recorded. Percent ash is calculated from the percent fraction of ash weight to total weight of the sample. The calculations of %polymer, %filler, and % coating agent contents are shown in Appendix D.7.

3.5 MECHANICAL PROPERTY CHARACTERISATION

There are a variety of methods to characterise mechanical properties of compounds. Three of the most commonly used techniques are tensile property determination,

flexural property determination, and impact property determination. Other relevant tests are reversion measurement and melt flow index determination.

3.5.1 REVERSION MEASUREMENT

Specimens of all compounds were produced from injection moulding. During injection moulding the material in the melt front is stretched as it advances, and is then cooled rapidly when in contact with the mould wall, with the result that molecular orientation is retained. Fresh material then flows between the frozen surface layers to create a new melt front. This cycle continues until the mould is full. Relaxation takes place rapidly in the melt if it has a low viscosity, and orientation is therefore highest when the melt temperature is relatively low. In order to investigate molecular orientation a reversion test was used. The amount of orientation can be estimated by measuring the maximum reversion of the specimens. The maximum reversion of the mouldings according to the British Standard BS 2782: Part 9: Method 941 [142] were determined for compounds containing different types of fillers coated with various levels and types of coating agents. The percentage change in length of each sample was calculated as the maximum reversion value (R_m) by:

$$R_m = \left(\frac{L_0 - L_1}{L_0} \right) \times 100 \quad (3.7)$$

Sample preparation was carried out as follows. The middle portion of a tensile bar was cut to an approximate length of 40 mm and accurately measured using a vernier caliper to give the initial length (L_0). The samples were coated with a slip agent to enable shrinkage without hindrance and were then placed on an aluminium sheet. The slip agent used consisted of 80 parts by weight silicone oil and 20 parts talc. The aluminium sheet was placed in an air-circulating oven at $132 \pm 1^\circ\text{C}$ (melting temperature of HDPE) for 30 minutes. After this heat treatment, the sheet with the samples was removed and allowed to cool to room temperature. Each sample was re-

measured and the length recorded as the final length (L_1). Five sets of samples were used for each formulated compound and the average value recorded.

3.5.2 MELT FLOW INDEX DETERMINATION (MFI)

The MFI testing is a method used to characterise polymer melts. It is a single point ram extruder test using the British Standard testing conditions (BS2782: Methods 720A [143]) as illustrated in Figure 3.15. The polymer sample was heated to 190°C in the barrel with a standard weight of 2.16 kg on the top of a piston and then was extruded through a standard die of 2.096 mm diameter. The weight (in grams) of polymer extruded in 10 minutes is quoted as the melt flow index (MFI) of the polymer. Virgin, processed HDPE, and HDPE containing coating agent were tested with the MFI tester to study the effect of coating agent on the polymer processing.

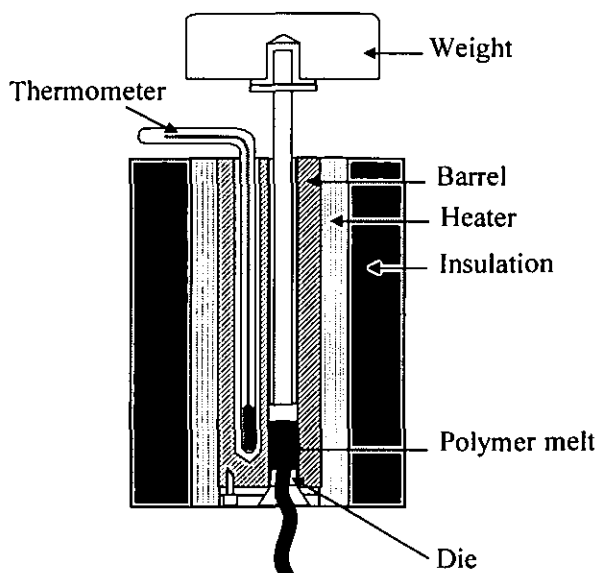


Figure 3.15: Diagram of apparatus for measuring Melt Flow Index.

3.5.3 TENSILE PROPERTY DETERMINATION

The tensile properties were determined according to British Standard BS 2782: Part 3: Method 320A [144] using a Lloyd Tensile Testing Machine, Type L2000R (J.J. Lloyd

Instruments Limited) fitted with a 10.0 kN load cell. The width and thickness of samples of specified shape, typically a dumbbell were measured using a micrometer. The ends were clamped and pulled at a constant grip separation speed of 5 mm/min at room temperature. The small change in length during the test was detected by a clip-on extensometer connected to the tensile testing machine and attached to the specimen. The length of the centre section, 50 mm long, is called the initial gauge length, L_0 . The grips of the extensometer are connected to an induction coil, which moves with the specimen during the test, and feeds an electrical signal to a computer, which displays the signal as an extension of the specimen. The force F applied to specimen was measured at the fixed end as a function of elongation. Since the specimen increases in length and decreases in area during the test, the specimen dimensions are constantly changing. The stress (σ) can easily be computed from the ratio of the applied force to the original area of specimen (A_0) which is given by:

$$\sigma = \frac{F}{A_0} \quad (3.8)$$

The strain (ϵ) was measured by the change in the length per unit length. If L_0 is the original length and L is the length of interest during the test, the strain is expressed by the following equations:

$$\epsilon = \frac{L - L_0}{L_0} = \frac{\Delta L}{L_0} \quad (3.9)$$

The initial stress-strain relation in polymers is approximately linear and can be described in term of Hooke's law [13, 14]. Young's modulus, typically defined as the slope of the stress-strain plot is given by:

$$E = \frac{\Delta\sigma}{\Delta\epsilon} \quad (3.10)$$

where $\Delta\sigma$ is the difference in stress between two points on the straight line and $\Delta\varepsilon$ is the difference in strain between the same two points.

Using the Dapmat software programme, the maximum load, extension, tensile modulus, and work done were automatically calculated and recorded, together with standard deviation. The load-extension curve was plotted as the test took place (as shown in Appendix B.8). This programme can convert extension to strain automatically. Young's modulus was obtained by fixing loads between 100 and 250 N where the initial straight portion of load against extension curve was observed for all compounds.

3.5.4 FLEXURAL PROPERTY DETERMINATION

Flexural testing of plastics is the most commonly used standard test for small deflections during bending of a rectangular beam supported at the mid-point and normally the span-depth ratio should be about 16:1.

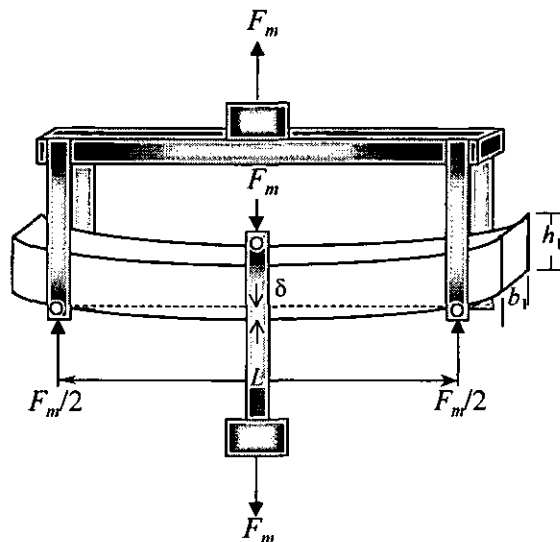


Figure 3.16: Flexural test in tensile machine.

The flexural stress (σ_F) is given by:

$$\sigma_F = \frac{3F_m L}{2b_1 h_1^2} \quad (3.11)$$

where F_m is the force at the mid-point and b_1 , h_1 , and L are the specimen dimensions as shown in Figure 3.14. The flexural modulus (E_F) is given by

$$E_F = \frac{L^3}{4b_1 h_1^3} \times \frac{F_m}{\delta} \quad (3.12)$$

where δ is the central deflection and F_m/δ is the slope of the initial linear force-deflection curve.

Flexural testing was carried out to obtain flexural properties, according to the British Standard: BS 2782: Part 3: Method 335A [145]. A tensile bar specimen was used, with the span of the flexural testing apparatus set to 50 mm. The same J.J. Lloyd tensile test machine was used as for the tensile tests, but with a different load cell and with different grips (Figure 3.16). Since the loads measured in this mode are considerably lower than those involved in conventional tensile testing, a more sensitive load cell of 2.5 kN was used with a crosshead speed of 5 mm/min. All flexural properties were calculated automatically by the Dapmat computer programme software. The initial linear portion of load against extension curve was used for calculating the flexural modulus and loads between 5 and 15 N were used for all compounds. The load-extension curves of compounds are shown in Appendix B.9.

3.5.5 FALLING WEIGHT IMPACT PROPERTIES

A Rosand Impact Falling-Weight Instrument (IFWI), type 5A was used to evaluate the impact properties at room temperature. A circular sheet specimen approximately 1.3 mm thick produced from the four part mould by injection moulding was mounted on the sample holder. The weight of 25 kg was raised to a height of 461.0 mm and

was allowed to fall almost freely under the effect of gravity along a set of guide rails. A hemispherical striker was mounted under the weight and set to give the terminal velocity of 3.0 m/s, which depends on the square root of the drop height assuming free fall. A diagram of the instrument is shown in Figure 3.17. Since the velocity used in this machine is high, it results in interference from vibration and an inertial effect on the recording of the load signal. Consequently, the velocity is measured directly by a linear array of sensors positioned near the end of the fall. An accelerometer attached to the falling weight measures force and velocity separately. The electrical signal from the accelerometer was digitally recorded. The absorbed energy and the force were calculated from the change in velocity caused by impact. The Rosand impact instrument is equipped with a microprocessor system to measure and store the force and deflection readings throughout impact, thus calculations of energy can be carried out. The force-deflection curves of compounds are shown in Appendix B.10.

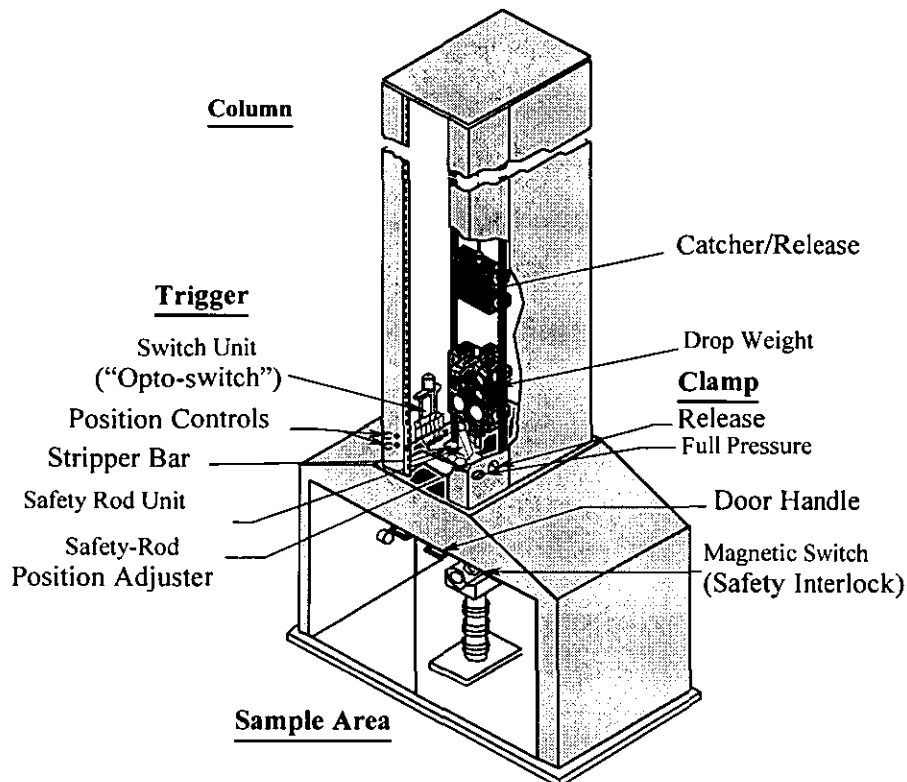


Figure 3.17: Impact Falling Weight equipment.

CHAPTER 4

RESULTS AND DISCUSSION: SERIES I

4.1 GENERAL

In order to gain overall understanding in this work, melting points of coating agents, chemical reactions between magnesium hydroxide or calcium carbonate and each coating agent are summarised in this section. It is known that metal stearates and fatty acids are polymorphic materials which have several transitions up to their melting points [146]. Polymorphic forms are defined as solid phases of the same chemical composition, differing among themselves in crystalline form, free energy, and other physical and chemical properties [64]. However, some transitions are difficult to detect because they are unstable forms. From DSC examination, the melting point and heats of fusion for metal stearates and stearic acid are shown in Table 4.1 and the DSC traces are shown in Appendix E.1.

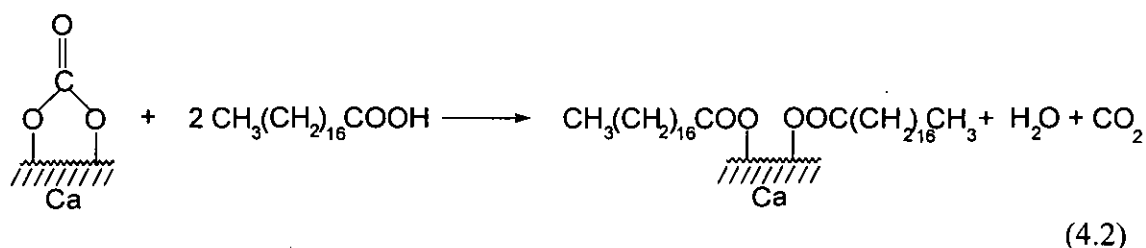
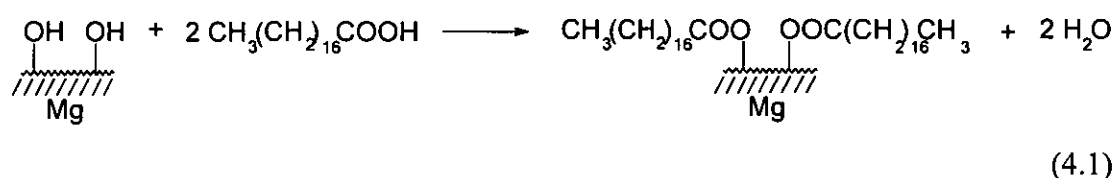
Table 4.1: Melting properties of coating agents.

Coating agents	Melting temperature (°C)		Heat of fusion (J/g)
	Literature	DSC analysis	
magnesium stearate	132.0 [135]	124.9	140.1
calcium stearate	150.0-154.0 [135]	136.9	144.3
zinc stearate	130.0 [135]	130.8	182.5
stearic acid	69.6 [64]	66.7	197.8

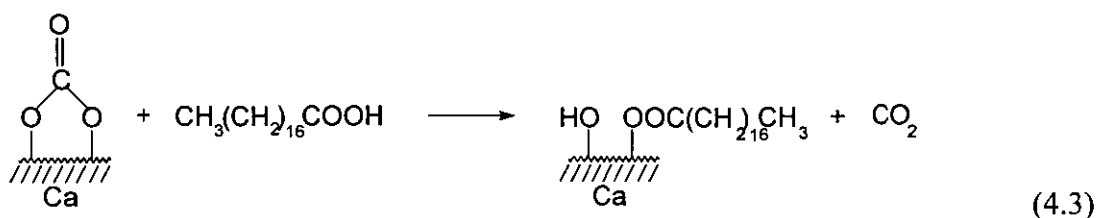
It is apparent that the melting point values of these coating agents obtained from DSC analysis are different from those in the literature. This may be caused by the differences in the raw materials due to production processes, precise composition, and the amount of impurity. Fatty acid soaps are prepared from mixtures of natural fatty acids and consist of a large number of components. Hence it is not unnatural to expect variations in commercial products.

In the current work, when magnesium stearate, zinc stearate, and stearic acid, were coated on magnesium hydroxide and calcium carbonate fillers, they showed double or triple polymorphic transitions up to their melting point. Calcium stearate is the only coating agent that gave a single melting transition when it was coated on either filler. This result is in agreement with Rek [146] who reported that the polymorphism of fatty acid soaps shows 5 or 6 polymorphic transformations which are reversible and which differ in the rate of transition. The polymorphism becomes simpler with increasing atomic weight of the metal. Each soap has its own characteristic thermal behaviour. Therefore, in this study the melting point values of coating agents are those obtained from the DSC analysis as shown in Table 4.1.

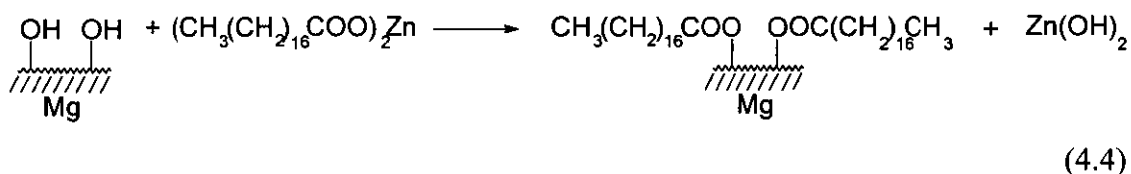
Reactions/interactions between the coating agent and a filler, such as magnesium hydroxide and calcium carbonate, are also considered. Stearic acid can react with magnesium hydroxide and produce magnesium stearate [84]; in similar circumstances, calcium stearate may be produced when stearic acid reacts with calcium carbonate according to the following equations:



However, Fekete and co-workers [122] reported that calcium carbonate/stearic acid interaction can not be explained either by a simple adsorption process or by a reaction leading to calcium stearate as a final product. The mechanism might be as follows:



The current work found no reaction between the following pairs: magnesium stearate/magnesium hydroxide, magnesium stearate/calcium carbonate, calcium stearate/magnesium hydroxide, or calcium stearate/calcium carbonate. As a filler, magnesium hydroxide is more reactive than calcium carbonate. Comparing the metal stearates, zinc stearate is more reactive than magnesium stearate, which in turn is more reactive than calcium stearate, therefore zinc stearate may react with magnesium hydroxide in toluene and produce magnesium stearate (shown FTIR spectrum in Appendix F.2(c)). The proposed reaction may be represented as follows:



The results and discussion in this thesis are divided into two series. The first series of study is the effect of various magnesium and calcium stearate concentrations on mechanical properties of $\text{Mg}(\text{OH})_2$ filled HDPE. The second series of study focuses on the effects of various coating agent types on mechanical properties of $\text{Mg}(\text{OH})_2$ and CaCO_3 filled HDPE.

THE EFFECT OF VARIOUS MAGNESIUM AND CALCIUM STEARATE CONCENTRATIONS ON MECHANICAL PROPERTIES OF $\text{Mg}(\text{OH})_2$ FILLED HDPE : SERIES I

Series I, results are divided into three main parts, the first is a study of the coating process, the second is a characterisation of the coated fillers, and the last concerns the physical and mechanical properties of the composites.

4.2 CHARACTERISATION OF THE COATING PROCESS

4.2.1 EFFECT OF TEMPERATURE

To characterise the coating process, the Waring blender was used for coating magnesium hydroxide with two types of coating agents, i.e. magnesium stearate and calcium stearate. Previous work was carried out by Raymond [134], who reported that in practice the amount of 6.0% w/w stearic acid as twice the value of a theoretical coating (3.0% w/w), achieves one monolayer coating of magnesium hydroxide. In current work, therefore magnesium hydroxide was coated with one monolayer of magnesium stearate (equivalent to 6.2% w/w) and calcium stearate (equivalent to 6.4%w/w) in the blender for 60 minutes with varying heater voltages from 0 to 80 volts. Results are shown in Figure 4.1 and 4.2, respectively.

It can be seen from Figure 4.1 that at low voltages the temperature of magnesium hydroxide coated with 6.2% w/w magnesium stearate increased gradually with increased coating time until 30 minutes. At medium and high voltages (40-80 volts) the coating temperature increased rapidly with an increase in coating period and reached a maximum temperature after about 20 minutes.

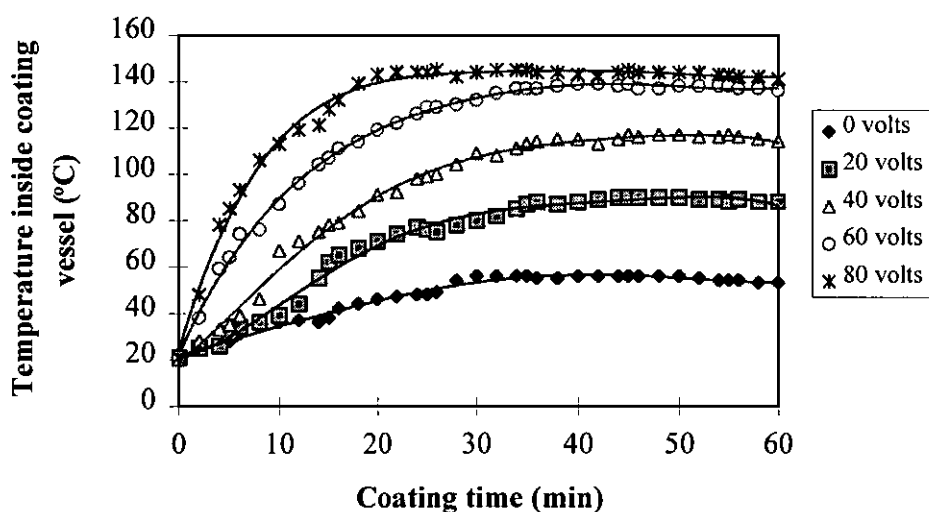


Figure 4.1: Temperature against time for $Mg(OH)_2$ coated with 6.2% magnesium stearate in the Waring blender.

Similarly, magnesium hydroxide coated with 6.4% calcium stearate showed an increase in temperature with increasing time, reaching to a plateau region after about 30 minutes (Figure 4.2). The coating curves show a greater temperature increase with higher voltages applied. Comparison of Figures 4.1 and 4.2, the slope for each voltage for samples coated with magnesium stearate is lower than that coated with calcium stearate. The temperature rapidly increased with increased coating time up to about 20 minutes when magnesium stearate was used while the rapid increase took up to about 30 minutes for the coating with calcium stearate. This may be because both experiments were done at different room temperatures leading to a difference in temperature gap between inside and outside the Waring blender, hence temperature dropping during taking the samples should be taken into account. Another possibility is that these are differences in the heat capacity and thermal conductivity of the two coating agents.

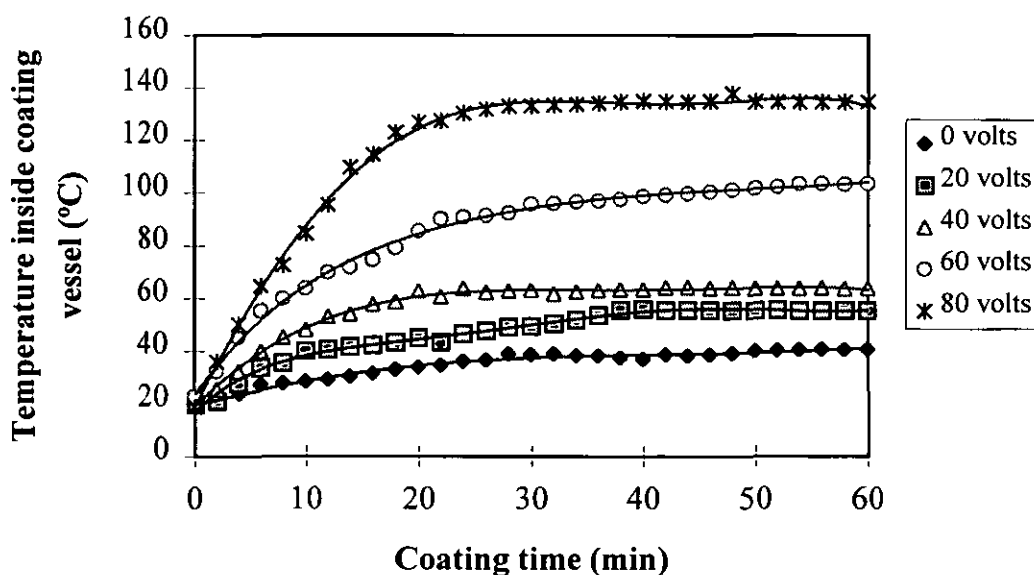


Figure 4.2: Temperature against time for $\text{Mg}(\text{OH})_2$ coated with 6.4% calcium stearate in the Waring blender.

The samples coated with magnesium and calcium stearates were taken from the Waring blender at 5 minute intervals, and analysed by FTIR using the DRIFT

technique. Typical spectra which represent coating of $\text{Mg}(\text{OH})_2$, after 5 minutes with no applied voltage to a heater (denoted as 0005) and that at 40 minutes with 80 volts (8040), for 6.2% w/w magnesium stearate and 6.4% calcium stearate are shown in Figures 4.3 and 4.4, respectively.

It appears from Figure 4.3 that the spectral characteristics change with temperature and coating time. From observation, the spectral features in the CH stretching region show strong intensities of asymmetric (2963 cm^{-1}) and symmetric (2876 cm^{-1}) methylene stretching bands [147]. The broad band at $1700\text{--}1300\text{ cm}^{-1}$ relates to RCOO^- from the coating agents, and the sharp peak at 3697 cm^{-1} is due to the OH group in the magnesium hydroxide [84].

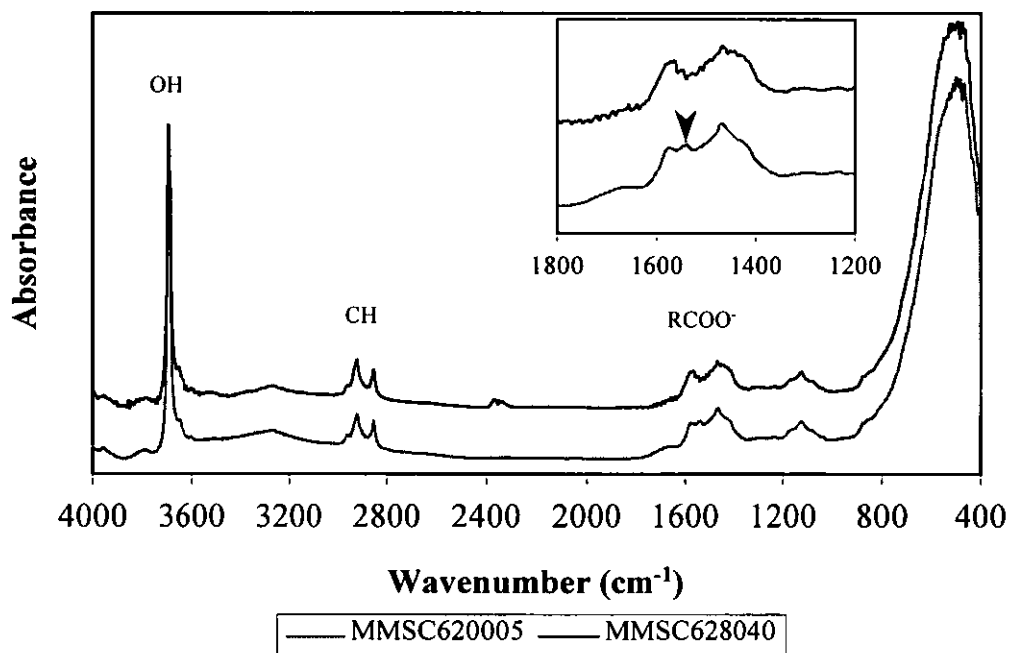


Figure 4.3: FTIR spectra of $\text{Mg}(\text{OH})_2$ coated with 6.2% w/w magnesium stearate taken from the Waring blender after 5 and 40 minutes.

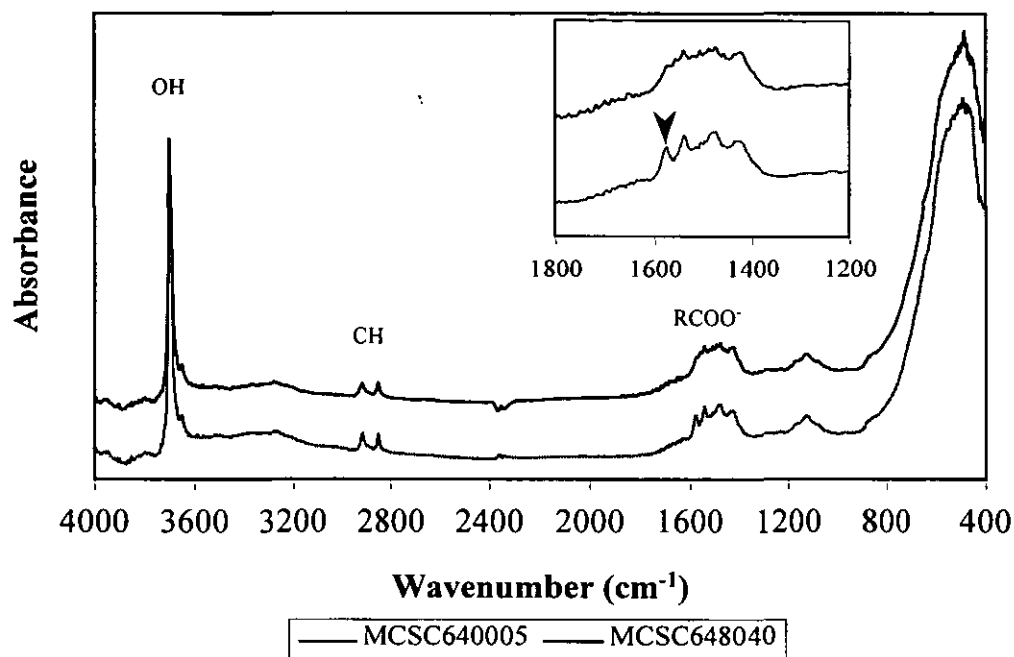


Figure 4.4: FTIR spectra of $\text{Mg}(\text{OH})_2$ coated with 6.4% w/w calcium stearate taken from the Waring blender after 5 and 40 minutes.

The coated filler removed after 5 minutes from the blender without heating (MMSC620005) has not reached a temperature above room temperature, while that 40 minutes in the blender with heat applied (MMSC628040) has increased to about 140°C (Figure. 4.1). This temperature is well above the melting point of the magnesium stearate. No chemical reaction between the coating and filler is expected. However, the differences between unmelted and melted magnesium stearate, which are deposited/coated on magnesium hydroxide surfaces, can be observed from an absence of the middle peak in RCOO^- band from FTIR spectra examined at room temperature (indicated on Figure 4.3 with an arrow). This may be caused by the destruction of the magnesium stearate crystals by heat and these crystals may not be able to recrystallise back to the former structure. Stearate would also be in a position to coat the filler more effectively after melting. Close observation of the RCOO^- absorbance shows that the middle peak has gradually disappeared at the higher temperature.

For the filler coating with calcium stearate (Figure 4.4), the FTIR spectra examined at room temperature also show differences in shape between MCSC64005 and MCSC648040. MCSC64005 refers to a coated sample removed after 5 minutes from the blender without heating. MCSC648040 is in respect of a coated sample removed after 40 minutes from the blender with 80 volt applied (140°C). Careful observation shows that the RCOO⁻ band differs in shape between unmelted and melted calcium stearate coated on Mg(OH)₂. The first peak at 1577 cm⁻¹ of the RCOO⁻ band (indicated with an arrow) from the stearate group is absent for the sample heated to a higher temperature implying that the molecules of calcium stearate might have undergone a phase transformation. This result is in agreement with Umemura *et al.* [147] who studied Langmuir-Blodgett (LB) films of calcium stearate with 1, 3, 9, and 21 monolayers fabricated on silver-coated glass slides at different temperatures and found the absence of some peaks as phase transformation occurred. Therefore, a mixing temperature of 140°C is the optimum temperature for the filler coating to obtain complete melting of the coating agents coated on the filler in this study.

Integrated areas due to CH, OH and RCOO⁻ absorbances obtained from DRIFT spectra were examined. The CH/OH and RCOO⁻/OH ratios were graphically plotted as a function of coating time. The results are demonstrated in Figures 4.5 and 4.6 for the coating of magnesium hydroxide with 6.2% w/w magnesium stearate and Figures 4.7 and 4.8 for that with 6.4% w/w calcium stearate.

Figures 4.5 and 4.6 show that the ratios of CH/OH and RCOO⁻/OH change very little with changes in heater voltage and coating time. The results indicate that blending conditions appear to have little effect on the results. It appears, moreover, that magnesium stearate melts and deposits upon magnesium hydroxide without reaction. This result can also be confirmed from the characterisation of magnesium stearate. This is obtained by extracting magnesium hydroxide coated with 6.2% w/w magnesium stearate sample taken from the Fielder mixer after 40 minutes with toluene and analysing using FTIR transmission (see FTIR spectra in Appendix F.2(a)). The full details will be discussed in chapter 5.

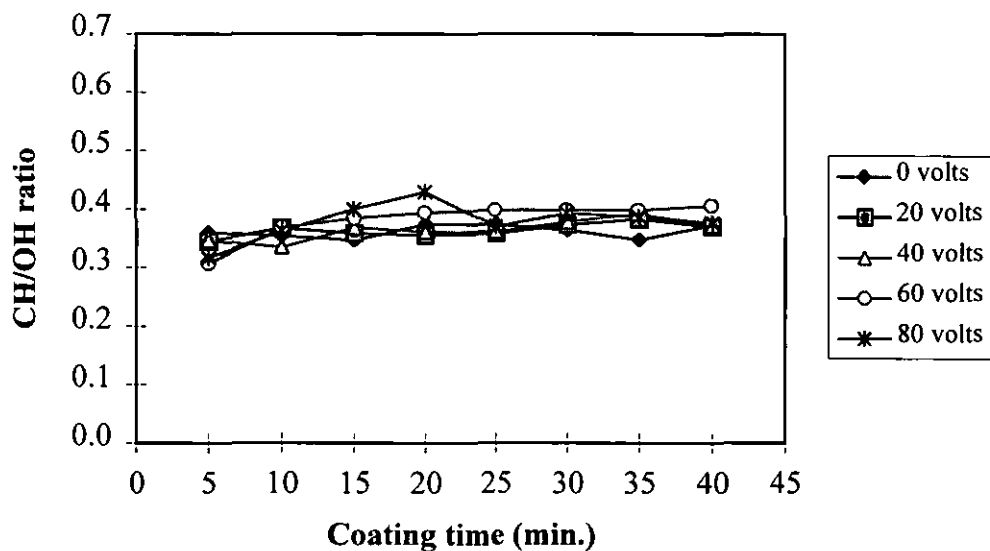


Figure 4.5: Plot of CH/OH ratio versus coating time for $\text{Mg}(\text{OH})_2$ coated with 6.2% w/w magnesium stearate at various voltages in the Waring blender.

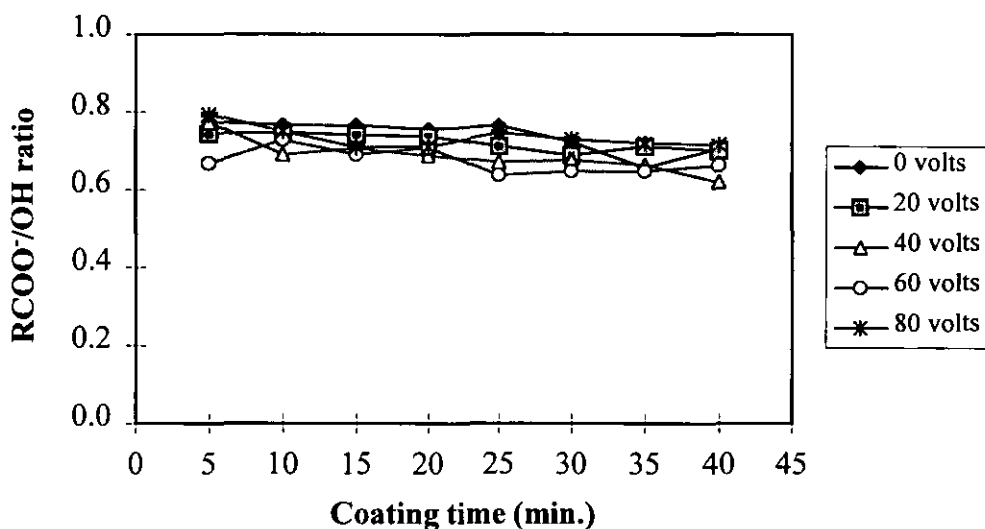


Figure 4.6: Plot of RCOO-/OH ratio versus coating time for $\text{Mg}(\text{OH})_2$ coated with 6.2% w/w magnesium stearate at various voltages in the Waring blender.

Figures 4.7 and 4.8 show that the integrated peak ratios of CH/OH and RCOO-/OH for calcium stearate coated $\text{Mg}(\text{OH})_2$ are also independent of changes in voltage and coating time. This implies little effect of blending conditions on the filler coating as the amount of calcium stearate is constant for each experiment. It suggested,

moreover, that like magnesium stearate, calcium stearate deposits and coats upon magnesium hydroxide without reaction.

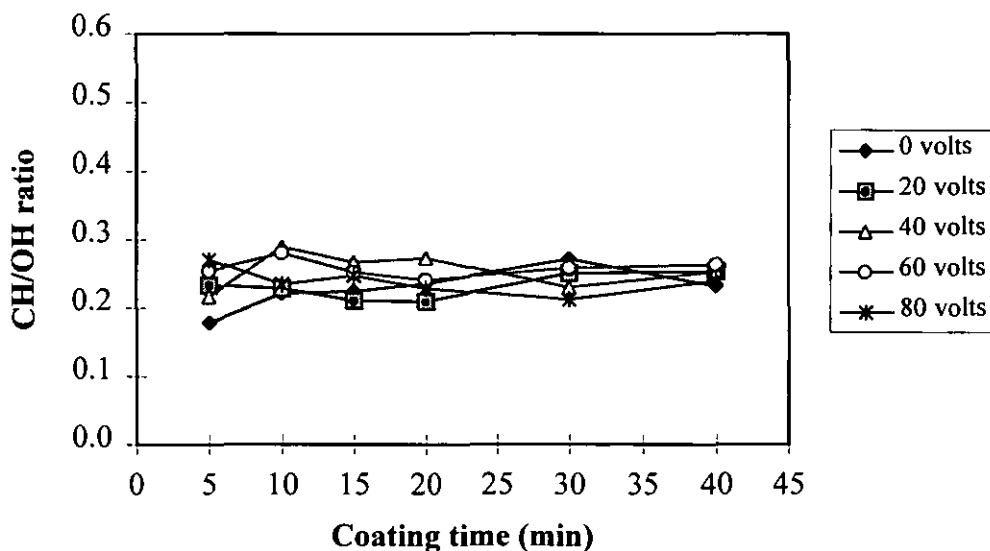


Figure 4.7: Plot of CH/OH ratio versus coating time for $\text{Mg}(\text{OH})_2$ coated with 6.4% w/w calcium stearate at various voltages in the Waring blender.

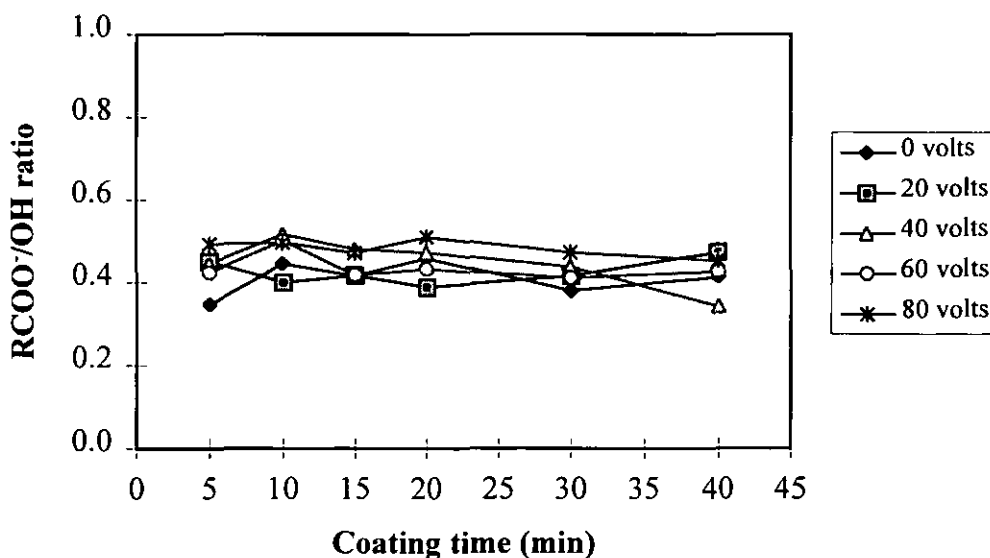


Figure 4.8: Plot of RCOO⁻/OH ratio versus coating time for $\text{Mg}(\text{OH})_2$ coated with 6.4% w/w calcium stearate at various voltages in the Waring blender.

4.2.2 EFFECT OF VARIOUS CONCENTRATIONS OF COATING AGENTS ON COATING PROCESS

In the current work, magnesium hydroxide was coated with various concentrations of magnesium stearate, (3.1%, 6.2%, and 9.3%w/w) together with 6.0% w/w stearic acid for comparison. To produce coated samples on a larger scale, a Fielder mixer was used. Heating characteristics of the Waring and Fielder mixer were considered. It was known from previous section that the optimum temperature for the filler coating is 140°C, therefore the temperature inside the Fielder mixer was set to obtain a filler temperature of 140°C and mixing for 40 minutes. A sample of magnesium hydroxide coated with 6.2% w/w magnesium stearate for 10 minutes was also prepared to observe the effect of coating time. The coating agent was added to the filler when the temperature of the filler inside the Fielder mixer reached 60 °C and time was recorded. Magnesium hydroxide was also coated with different concentrations of calcium stearate (3.2%, 6.4%, and 9.6% w/w) using the same mixing conditions (140°C for 40 minutes). The heating characteristics using the Fielder mixer are shown in Figure 4.9. FTIR spectra for Mg(OH)₂ coated with various magnesium and calcium stearate concentrations after a coating time of 40 minutes are shown in Figures 4.10 and 4.11.

The results shows that the temperature of sample powder in the Fielder mixer increases rapidly from 60°C to about 118°C ($\pm 2^\circ\text{C}$) after 5 minutes and reaches to a plateau region after about 10 minutes. After 10 minutes, the temperature of powder is about 137°C ($\pm 1^\circ\text{C}$), which is higher than the melting point of coating agents. This implies that after 10 minutes all coating agents in each sample are melted and coated on magnesium hydroxide surfaces. At the same coating time, the temperature of filler inside the Fielder mixer increases more rapidly than in the Waring blender with 80 volts heat applied. Since, the temperature profile inside the Fielder mixer at various coating time gives approximately similar values ($\pm 2^\circ\text{C}$) for all coated filler samples, only

Figure 4.9 is shown and used to indicate the heat characteristics of the Fielder mixer for all coated filler in this study.

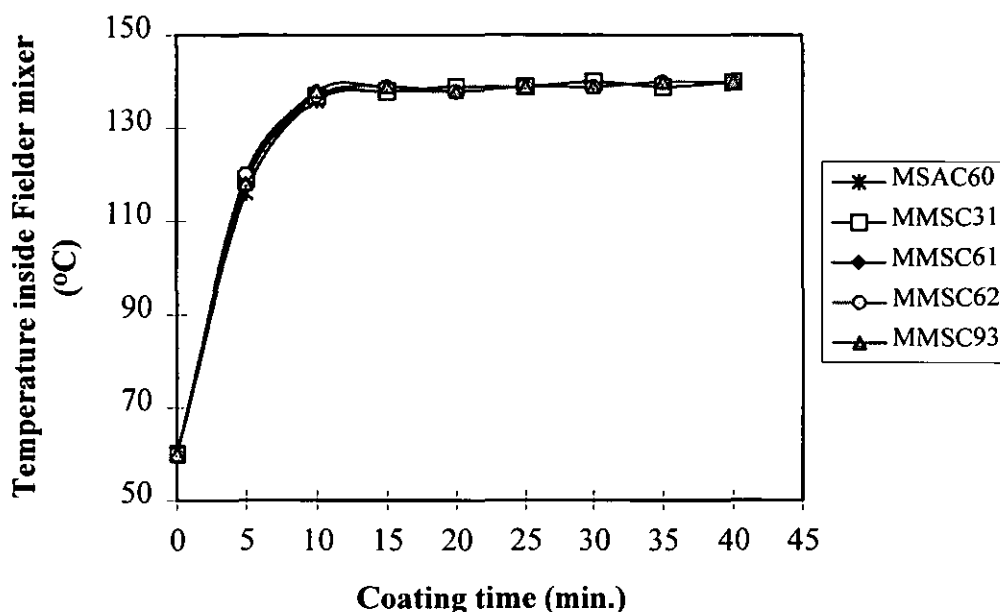


Figure 4.9: Temperature against time for $\text{Mg}(\text{OH})_2$ coated with various concentrations of magnesium stearate and stearic acid in the Fielder mixer.

The results obtained from thermal analysis and X-ray diffraction (later sections) also show that the amount of free particles of coating agent decrease, relating to an increase in the degree of coating as time increases. After 40 minutes of coating no free coating agent particles have remain for one monolayer coverage of magnesium hydroxide. Therefore, 40 minutes is the optimum of coating time to achieve a complete coating of filler. In order to achieve comparable results in mechanical properties, the operating conditions of the Fielder mixer for the coating of filler are set to give a mixing temperature of 140°C for 40 minutes for all coated samples.

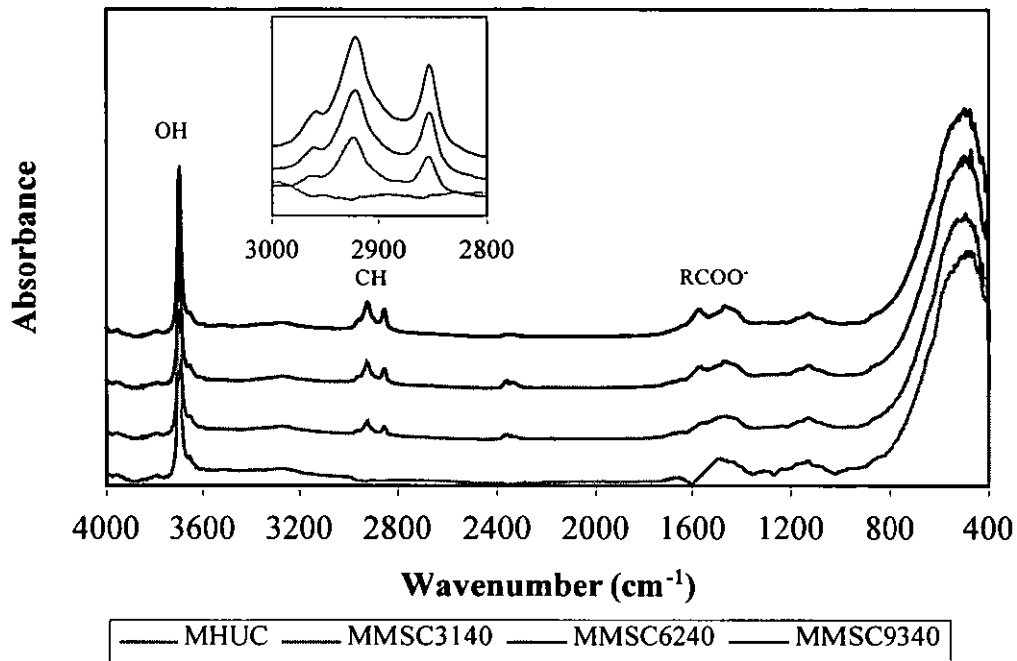


Figure 4.10: FTIR spectra of $\text{Mg}(\text{OH})_2$ uncoated and coated with 3.1%, 6.2%, and 9.3% magnesium stearate after coating 40 minutes in the Fielder mixer.

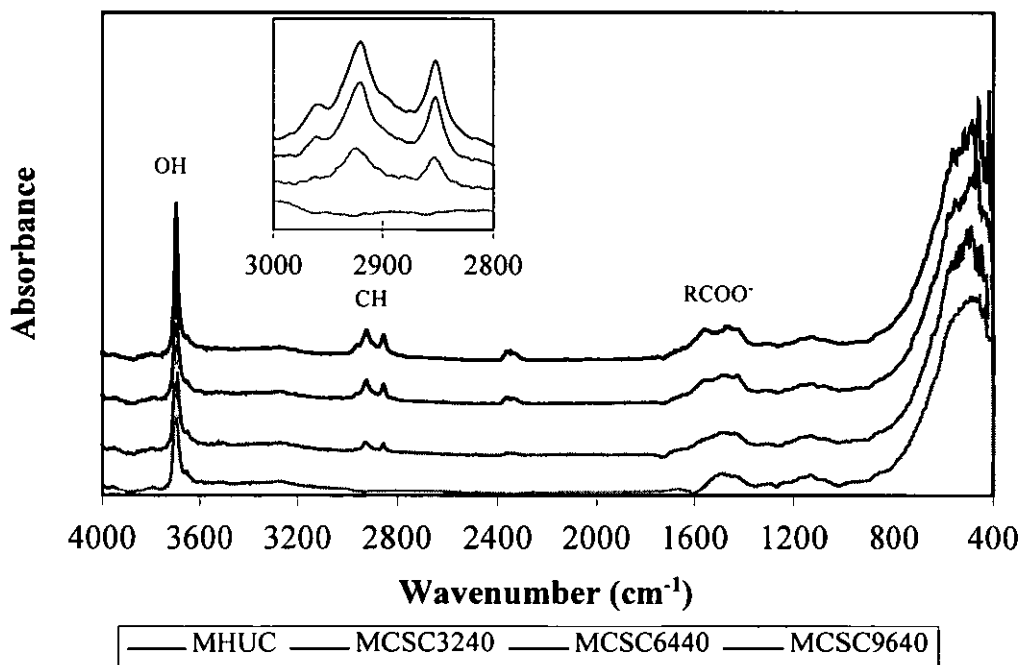


Figure 4.11: FTIR spectra of $\text{Mg}(\text{OH})_2$ uncoated and coated with 3.2%, 6.4%, and 9.6% calcium stearate after coating 40 minutes in the Fielder mixer.

The average amounts of the stearates described here correspond approximately to 0.5, 1.0 and 1.5 monomolecular layers. Figures 4.10 and 4.11 show that, by comparison with FTIR spectra of samples taken from the Waring blender (Figures 4.3 and 4.4), melting of magnesium/calcium stearate has occurred in all cases for samples taken from the Fielder mixer by showing the absence of the middle peak in the RCOO^- bands. After magnesium hydroxide subtraction, the area under CH and RCOO^- bands was found to increase with an increase in coating agent concentration. These areas show the amount of coating agent on magnesium hydroxide, therefore, DRIFT can be a powerful technique for quantitative analysis of surface species as it seems to have a surface sensitivity. Detection of surface species is much easier with the DRIFT technique than with the transmission technique. It is also a technique where no optical elements are in contact with the sample [78].

During the coating process, samples were taken from the Fielder mixer at 10 minute intervals for DRIFT analysis. The integrated absorbance of the CH and RCOO^- bands against the integrated absorbance of the OH peaks was ratioed to obtain a value for the relative amount of coating agent. These integrated intensity ratios are plotted as a function of coating time as shown in Figures 4.12 and 4.13 for magnesium stearate coating and Figures 4.14 and 4.15 for calcium stearate coating, respectively.

A number of features can be observed from Figures 4.12 and 4.13. For magnesium stearate coating, absorbance intensities of CH and RCOO^- corresponding to CH/OH and RCOO^-/OH ratios increase with increasing coating concentration while these ratios are almost constant after longer coating times. It is believed that no reaction between magnesium stearate and magnesium hydroxide occurs during the coating process. For samples with 9.3% magnesium stearate coating, time for full development of the CH/OH peak absorbance was rather longer. It is anticipated that the amount of coating was more than that required producing a monolayer. For stearic acid coating, the CH/OH ratio gradually rises with increased coating time

because there is reaction between stearic acid and magnesium hydroxide producing magnesium stearate as reported by Hornsby and Watson [124]. FTIR transmission also shows a spectrum corresponding to magnesium stearate when the sample of magnesium hydroxide coated with stearic acid for 40 minutes was extracted by toluene. The results are shown in Appendix F.2 (d). The details are discussed in chapter 5.

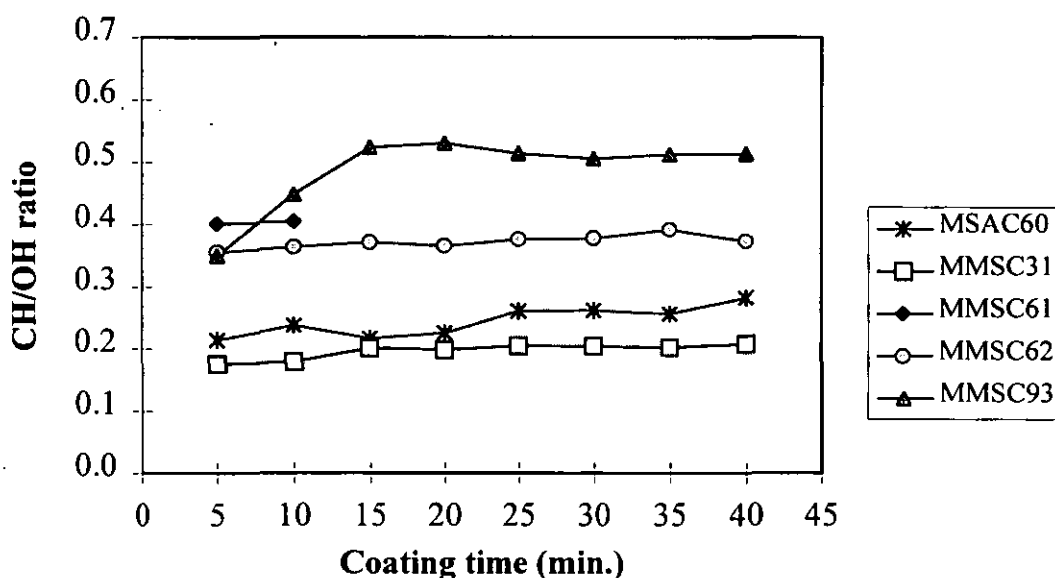


Figure 4.12: Plot of CH/OH ratio versus coating time for $\text{Mg}(\text{OH})_2$ coated with various concentrations of magnesium stearate and stearic acid in the Fielder mixer.

From Figures 4.14 and 4.15, the ratios of integrated peak absorbances of CH and RCOO^- against the peak absorbance of OH increase with an increase in calcium stearate concentration. These ratios are again found to be almost constant with changing coating time. This may be because there is no reaction between calcium stearate and magnesium hydroxide.

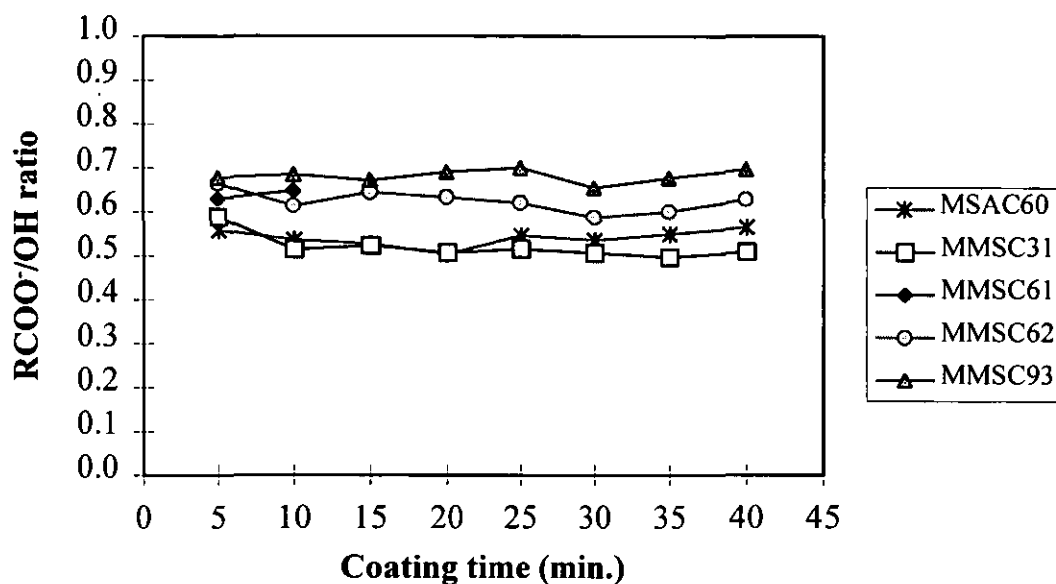


Figure 4.13: Plot of RCOO⁻/OH ratio versus coating time for Mg(OH)₂ coated with various concentrations of magnesium stearate and stearic acid in the Fielder mixer.

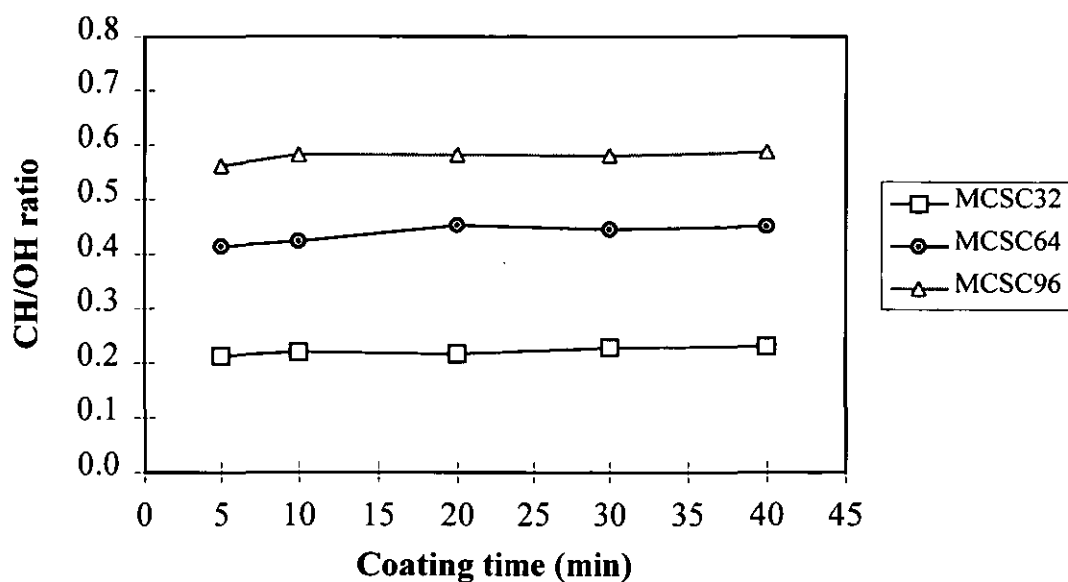


Figure 4.14: Plot of CH/OH ratio versus coating time for Mg(OH)₂ coated with various concentrations of calcium stearate in the Fielder mixer.

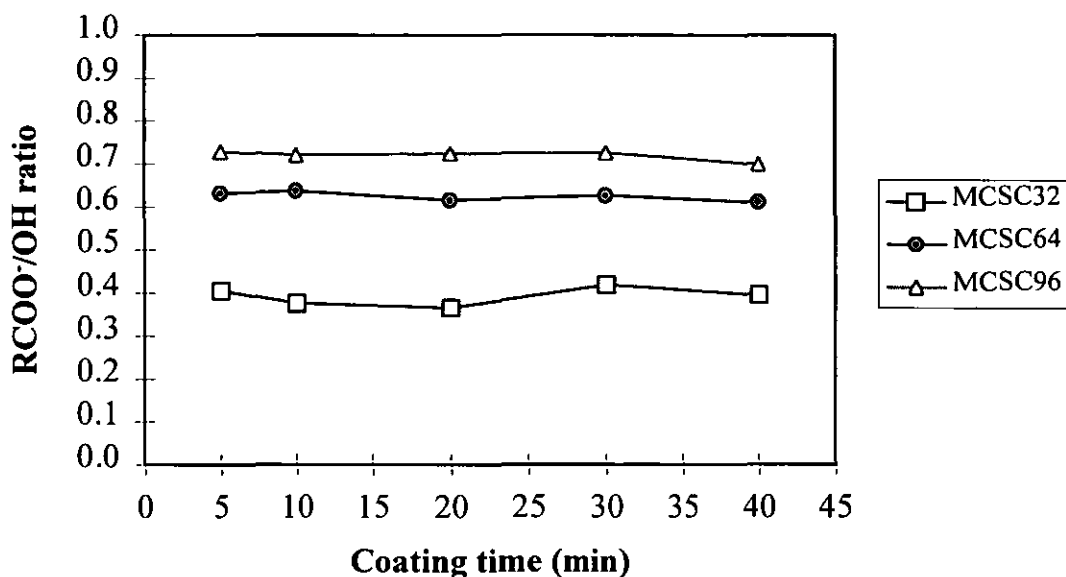


Figure 4.15: Plot of RCOO/OH ratio versus coating time for $\text{Mg}(\text{OH})_2$ coated with various concentrations of calcium stearate in the Fielder mixer.

4.3. CHARACTERISATION OF COATED FILLERS

In order to understand how filler coating affects the mechanical properties of compounds it is essential to characterise coating agents, fillers, and coated fillers. In addition to Fourier transform infrared spectroscopy, differential scanning calorimetry, X-ray diffraction, and contact angle measurement were also used to analyse coated filler surfaces, and are discussed in this section

4.3.1 DIFFERENTIAL SCANNING CALORIMETRY (DSC)

DSC is especially useful for studying organic solids. The small sample involved and the high sensitivity make DSC a particularly useful research tool for the characterisation of new materials. The high thermal resolution is very useful in studying closely spaced transitions and recrystallisations [148]. From a DSC trace (Appendix E) the area under the melting curve can be used to obtain the heat of fusion of substances at their melting temperature. In the current work, individual coated

samples taken from the Fielder mixer at various coating times were examined using thermal analysis. Magnesium stearate, zinc stearate, and stearic acid coated on magnesium hydroxide have polymorphic structures which show multiple transition stages up to the melting point when they are heated. It suggests that for stearic acid coated filler the appearance of several transitions may be the polymorphic form of metal stearate produced from the chemical reaction rather than that of stearic acid on its own. Each transition corresponds to a change from one crystal form to another at a given temperature. The transitions were detected at three different temperatures for coated fillers. The first transition, detected at a temperature of about 60-81°C will be designated A-form (see Appendix E.2(a): at 30 and 40 min of coating). The second transition was found at a temperature of about 82-110°C and designated as mesomorphic B-form (Appendix E.2(a): at 20 min of coating). The last transition (C-form) occurred between 111 to 140°C (depending on metal stearate type) and relates to the melting point of free stearates (Appendix E.2(a): at 5 min of coating). From DSC traces, the mesomorphic C-form shows the largest while that of A- and B-form give very small peaks indicating insignificance or instability of A- and B-form. Vold and Hatsubgi [149] reported that calcium stearate has several transitions but in the current work only one transition (C-form) was found. This may be because some transitions of calcium stearate are unstable. Moreover, the DSC heating rate in the current work (10°C/min) is much higher than that in the literature (1°C/min), which may be fast enough to pass the transitions without detecting results.

Using the heat of fusion value, the proportion of free components for coated magnesium hydroxide at various coating times can be obtained from the fractional enthalpy of coated filler to coating agent and then multiplied by the percentage of coating. For example, the heat of fusion of magnesium stearate is 140.1 J/g and that of 6.2% w/w magnesium stearate coated magnesium hydroxide after coating for 5 minutes is 4.31 J/g. This peak occurs at a temperature of 120.9°C relating to mesomorphic C-form. Therefore, the free component of C-form can be expressed as a fraction of the total present as below:

$$\frac{4.31 \times 100}{140.1 \times 6.2} = \frac{1}{2.015} = 0.496$$

From observation, it is found that after longer periods of coating the proportion of free component (C-form) progressively decreases indicating an increase in degree of coverage on the filler surface. The results are shown in the Appendix B.6 and the plots of free polymorphic components against coating time are shown in sections 4.3.1.1 and 4.3.1.2.

4.3.1.1 Mg(OH)_2 coated with magnesium stearate.

The results for 3.1% magnesium stearate coating on magnesium hydroxide are shown in Figure 4.16 (a). It appears that at 5 minutes of coating free magnesium stearate still remains in the mixture (temperature inside the Fielder mixer is about 118°C ($\pm 2^\circ\text{C}$)). The amount of free stearate (C-form) rapidly decreases and disappears from the system while a small amount of free stearate (A-form) is detected. It indicates that after 5 minutes of coating some magnesium stearate particles deposit and coat on the filler while other particles have not coated. At longer coating times most magnesium stearate has melted and coated on the magnesium hydroxide surface no free magnesium stearate particles remain in the surroundings at the end of these coating process. This mechanism presumes that magnesium stearate smears onto the magnesium hydroxide surfaces as a result of vigorous mixing as magnesium stearate powder is soft and easy to break to very fine particles. This smear becomes gradually thinner after longer periods of mixing, and melts during with increasing temperature up to the melting point of coating agent.

A change in form between A- and B-form is observed after 20 minutes of coating. A small amount of the mesomorphic A-form is left at the end of coating. The DSC trace shows characteristic double transitions as magnesium stearate is a polymorphic material which consists of more than one crystal structure. However, most of these

transition peaks are very small in comparison with the melting point peak. This result is in agreement with the results from many others [146, 148-150]. According to Barrall and Johnson [148], Vold and Vold recorded a DTA curve for pure sodium palmitate. This curve appeared to be entirely reproducible and it was obvious that transitions at 119°C, 138°C, 203°C, and 253°C could be distinguished. Matsubara [150] reported that the DSC trace of magnesium stearate contained several transitions, suggesting that there were several transformations during increasing temperature [147].

Figure 4.16(b) shows a similar result to (a) but gives greater values of free components (C-form) due to an increase in magnesium stearate coating concentration. The end product also shows the formation of a small amount of A-form.

Figure 4.16 (c) illustrates the reduction of free magnesium stearate component (C-form) with increased coating time indicating an increased amount of magnesium stearate depositing on the filler. Mesomorphic A- and B-form were also produced during the coating process. The DSC trace for the final product shows that some free magnesium stearate (C-form) has remained. A small amount of A-form has also been produced. This indicates that 9.3% magnesium stearate is in excess of the amount required to produce a monolayer coating of magnesium hydroxide. This implies that the cohesion force between each stearate molecule is less than the adhesion force between stearate molecules and the surface of a magnesium hydroxide particle. When the surface of magnesium hydroxide is fully covered with magnesium stearate molecules, therefore the excess stearate molecules do not deposit on their own kind but they remain free. The re-transform between an A- and B-form also occurs.

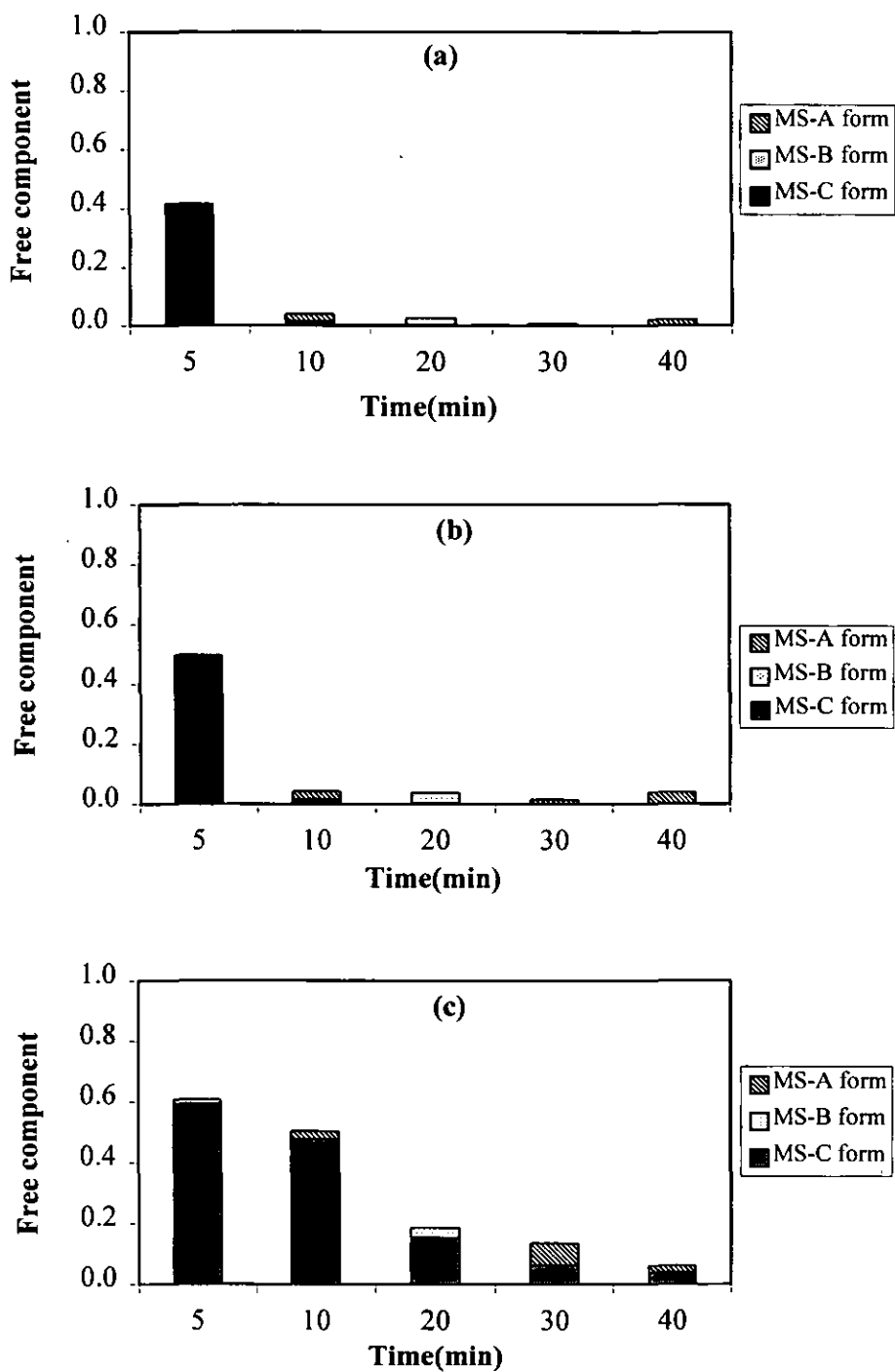


Figure 4.16: Plots of free components against coating time for magnesium hydroxide coated with magnesium stearate, results normalised to nominal amount of magnesium stearate: a: 3.1% w/w, b: 6.2% w/w, and c: 9.3% w/w.

4.3.1.2 Mg(OH)₂ coated with calcium stearate

DSC traces of magnesium hydroxide coated with calcium stearate were obtained. The free component for coated samples taken every 10 minutes with various voltages from the Waring blender against recorded temperature are shown in Figure 4.17.

Figure 4.17 shows the decrease in free calcium stearate (C-form) with increasing temperature. The higher the temperature, the less the free calcium stearate in the system. It is possible that calcium stearate (C-form) melts and deposits on magnesium hydroxide surface.

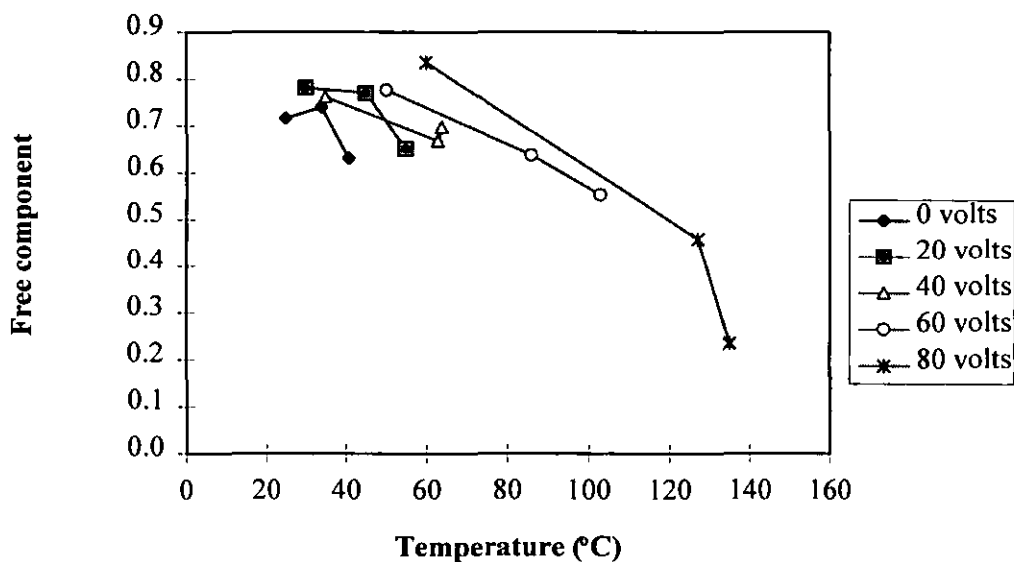
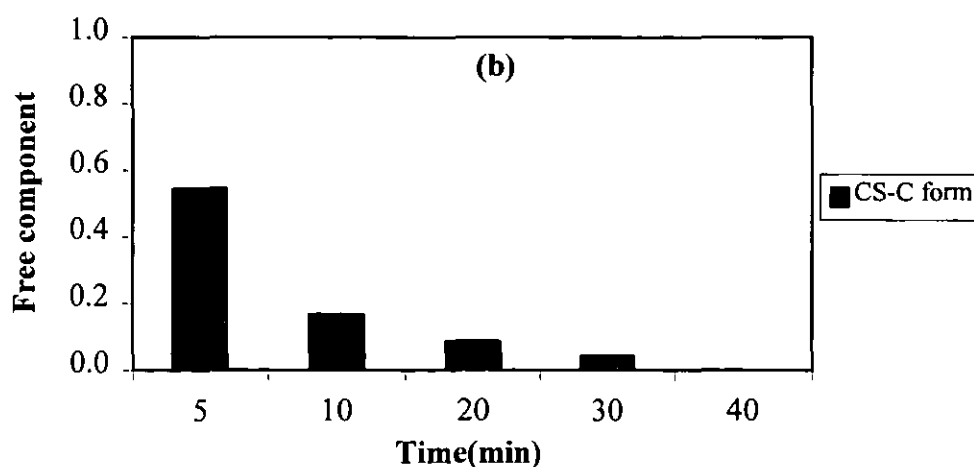
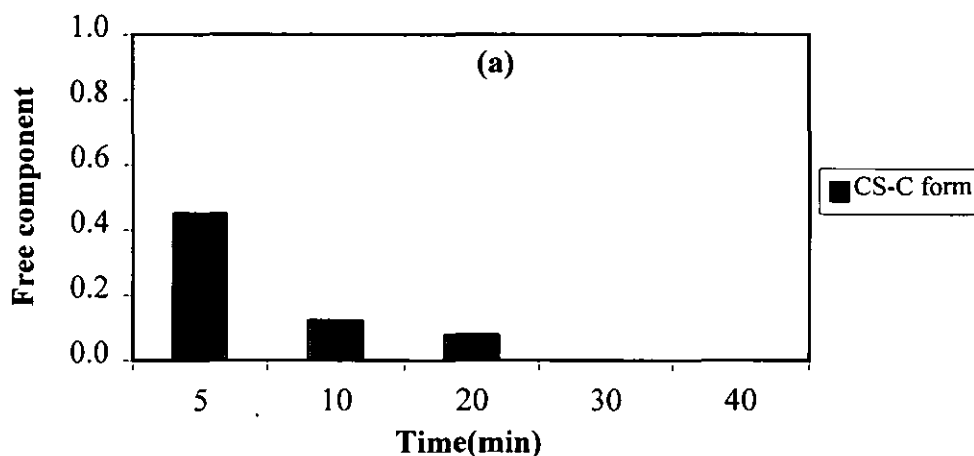


Figure 4.17: Plot of free component normalised with respect to calcium stearate against temperature for magnesium hydroxide coated with 6.4% w/w calcium stearate at different voltages supplied in the Waring blender.

For large scale of coating (the Fielder mixer) the proportion of free calcium stearate (C-form) was also examined and the results are shown in Figure 4.18. DSC traces showed only one peak at about 120°C ($\pm 2^\circ\text{C}$) indicating C-form was detected. Examples of DSC traces for 6.4% calcium stearate coated magnesium hydroxide taken from the Fielder mixer at 5 and 40 minutes are shown in Appendix E.2 (b).

DSC traces are similar for intermediate coating time. Neither A- nor B-form is produced for calcium stearate coating. It suggests that calcium stearate is more stable than magnesium stearate. This result is in agreement with Markley [64] who reported that the polymorphic forms of fatty acid salts are more stable with a higher atomic weight of cation in their salt molecules. According to Rek [146], Hattiangdi *et al.* also produced DTA curves for stearates and palmitates of alkaline-earth metals and some heavy metals. The curves obtained during the heating cycle were revealed that the alkaline-earth stearates and palmitates display a series of polymorphic transitions similar to those of the sodium and potassium soaps but that the polymorphism of the other salts is much simpler.



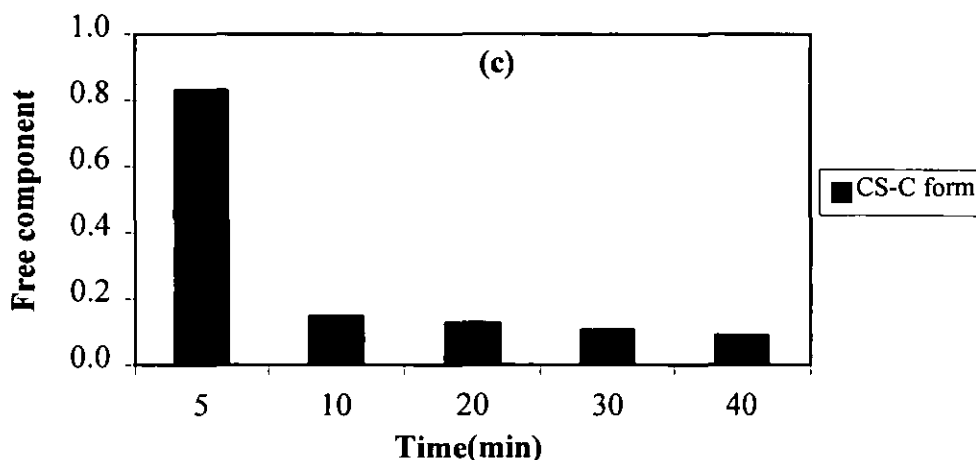


Figure 4.18: Plots of free components against coating time for magnesium hydroxide coated with calcium stearate, results normalised to nominal amount of calcium stearate: a: 3.2% w/w, b: 6.4% w/w, and c: 9.6% w/w.

Figure 4.18 reveals that free calcium stearate (C-form) decreases with increased coating time. The results for coating magnesium hydroxide with 3.2%w/w calcium stearate (Figure 4.18(a)) shows that the free calcium stearate component disappears after 20 minutes. This is explained by the fact that the amount of calcium stearate added is not enough for monolayer coverage.

For 6.4% calcium stearate coating (Figure 4.18 (b)), free stearate has disappeared after 30 minutes and no stearate is detectable at the end of coating indicating monolayer coverage. Since the coating is one monomolecular layer which is not thick enough to produce a crystalline structure, a DSC trace does not show the melting endotherm for one monolayer calcium stearate. Figure 4.18 (c) for the 9.6% calcium stearate coated sample reveals remaining free stearate (C-form) in the final product due to the excess of stearate for coating the filler.

4.3.2 X-RAY DIFFRACTION

X-ray diffraction is a powerful tool for investigating the crystalline materials. The diffraction patterns are characteristic of a substance, so that they can be used as

“fingerprints”. Moreover, this technique can estimate proportions of components in a mixture. The diffraction pattern of a mixture is the superposition of the diffraction patterns of its components [151]. To investigate the filler coating process, all coated and uncoated fillers and coating agents were examined using this technique. The X-ray patterns of materials studied are shown in Appendix G. The coated magnesium hydroxide samples removed from the Fielder mixer after 5 and 40 minutes were examined using X-ray diffraction, as well as uncoated magnesium hydroxide for comparison. Samples were scanned from 19.0 to 24.0 degree 2θ where uncoated magnesium hydroxide shows a flat background diffraction while metal stearates and stearic acid give a variety of peaks. It is expected that certain peaks of the coating agents will vanish because of the monolayer coverage of coating agent on magnesium hydroxide surfaces. The X-ray patterns are shown in Figures 4.20 and 4.21 for magnesium stearate coated for 5 and 40 minutes and Figures 4.22 and 4.23 correspond to calcium stearate coating. Before discussion it is useful to understand the characteristics of peaks which can provide information as follows [152]:

1. **Position.** The position of peak, measured as the angle θ , gives information of size, shape and orientation of the unit cell.

2. **Intensity.** The relative intensity of the peaks, measured either as peak height or, more correctly, as the area under its profile, provides the data for determining the position of the atoms in the unit cell.

3. **Shape.** The shape of peak, of which its breadth is a useful guide, provides information regarding crystallite size and lattice imperfections, including strain.

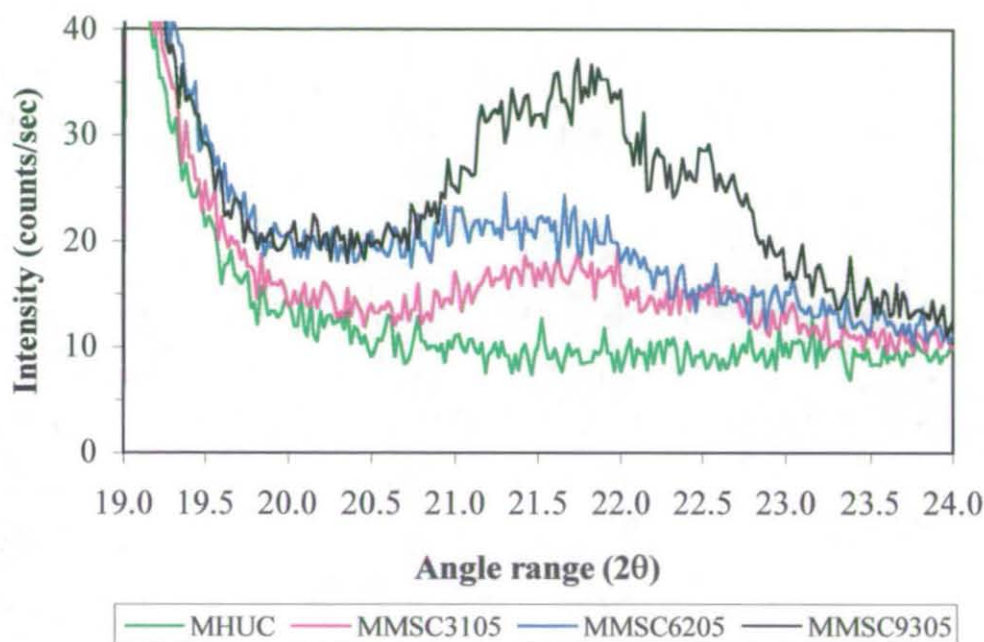


Figure 4.19: X-ray patterns of magnesium hydroxide coated with various magnesium stearate concentrations at coating time of 5 minutes in the Fielder mixer.

Figure 4.19 shows that increased coating concentration gives an increase in peak intensity. All samples taken from the Fielder mixer after 5 minutes of coating show the characteristic shape of magnesium stearate (see Appendix G.4 for X-ray diffraction pattern of coating agents). It indicates that magnesium stearate has neither melted completely nor perfectly coated the magnesium hydroxide in all samples. Some of the coating agent particles are still free as powder in the system resulting in two peaks at 21.78 and 22.45 degree 2θ corresponding to free magnesium stearate crystals. This result can also be observed from DSC (see Figure 4.16(a-c)) which showed the remaining free stearate particles in the mixture for all coated samples removed from the Fielder mixer after 5 minutes of coating. Intensity of peaks is also affected by the amount of coating agent present. For example, the coated magnesium hydroxide containing 9.3% magnesium stearate gave a higher stearate fraction than that containing 6.2% magnesium stearate and, in order, than that containing 3.1% magnesium stearate. It is apparent that polar long-chain compounds such as soaps, fatty acids and their derivatives are almost always highly complex mixtures containing a wide range of

chain lengths. Their crystals, however, consist of the chains which are usually arranged parallel to each other and associated together in pairs (head-to-head and tail-to-tail) and form double layers [153] (see a crystalline structure of stearic acid in Figure 2.6).

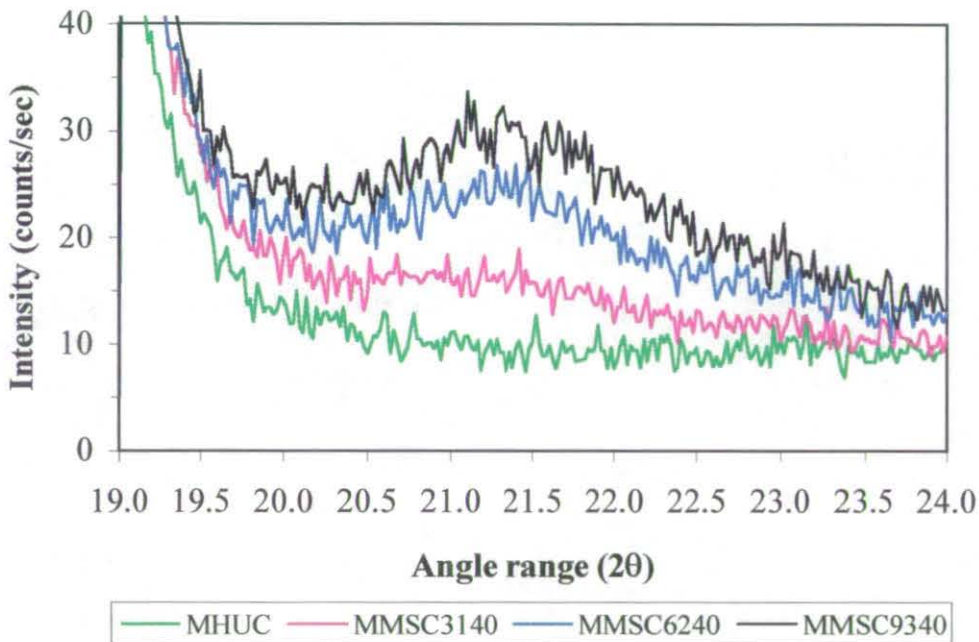


Figure 4.20: X-ray patterns of magnesium hydroxide coated with various magnesium stearate concentrations at coating time of 40 minutes in the Fielder mixer.

X-ray patterns in Figure 4.20 show that when coating time for magnesium hydroxide coated with magnesium stearate is increased to 40 minutes the peaks which have been detected at 5 minutes are less pronounced. It is explained that magnesium stearate gradually melts and deposits as a thin layer upon the magnesium hydroxide surface during coating. The coating layer is very thin (maximum 1.5 monolayer thick). The crystal structure of magnesium stearate may also transform as a result of heat and then it cannot reform as a single crystal in the thin layer. Therefore X-ray diffraction does not detect a monomolecular layer coverage of magnesium stearate on magnesium hydroxide. Normally a unit cell of magnesium stearate is composed of a bimolecular layer of magnesium stearate [64]. Therefore, a monolayer of magnesium stearate on coated samples does not produce a typical X-ray diffraction pattern. According to

Rek [146], Thiessen and Spsychalski have shown by X-ray diffraction that a characteristic reflection of fatty acid soaps disappears at the temperature at which the pure fatty acid would melt. The absence of diffraction peaks after heating a sample has also been reported by Baxter and co-worker [153]. They suggested that when the sample was heated the sample transformed into a different solid phase and then produced an isotropic liquid on further heating. However, X-ray diffraction can differentiate between three levels of coating concentration. It can, therefore, be used for semi-quantitative analysis.

The samples of the magnesium hydroxide coated with various calcium stearate concentrations after 5 minutes in the Fielder mixer were also investigated using the X-ray diffraction technique (Figure 4.21). The results show that the peak intensity increases with an increase in coating concentration. MCSC9605 shows a distinct pattern of calcium stearate containing three peaks at 20.4, 22.0, 22.8 degree 2θ . It indicates that after 5 minutes of coating most calcium stearate is free in the system. Calcium stearate has not been melted as temperature inside the Fielder mixer has not been high enough ($118\text{ }^{\circ}\text{C} (\pm 2^{\circ}\text{C})$).

Comparison between Figure 4.21 and 4.22, shows that three peaks in Figure 4.21 become one broad peak in Figure 4.22 relating to the transforming of calcium stearate crystal structure by rising temperature. After 40 minutes of coating, the recorded temperature inside the Fielder mixer is about $140^{\circ}\text{C} (\pm 2^{\circ}\text{C})$ which is higher than the melting point of calcium stearate (136.9°C), hence the calcium stearate can be melted and deposited on the magnesium hydroxide surfaces. The X-ray diffraction technique is not able to detect the thin layer of calcium stearate, however, this technique can differentiate the amount of coating agent coated on magnesium hydroxide.

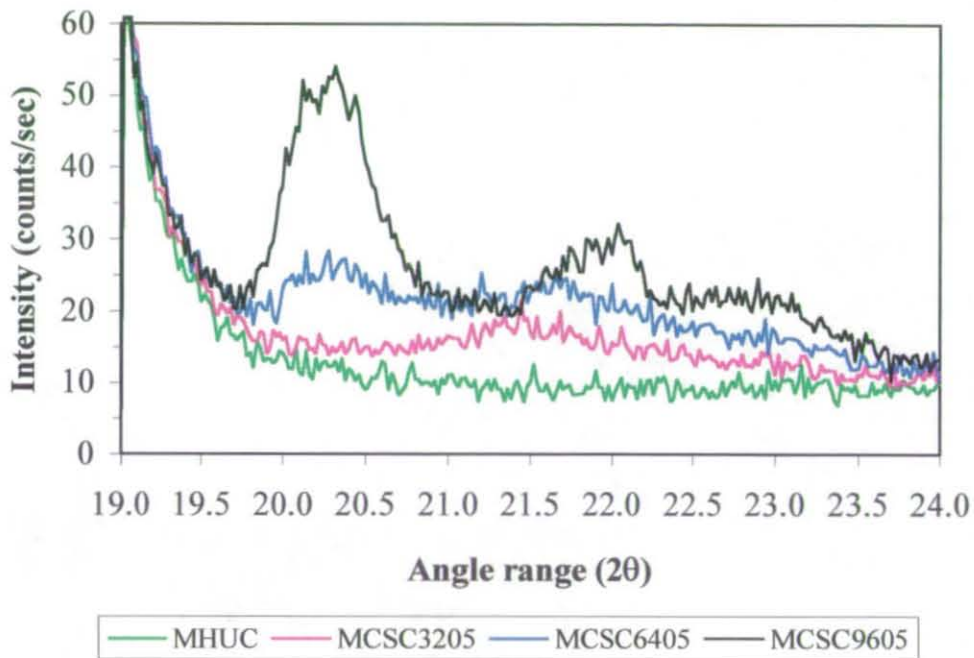


Figure 4.21: X-ray patterns of magnesium hydroxide coated with various calcium stearate concentrations at coating time of 5 minutes in the Fielder mixer.

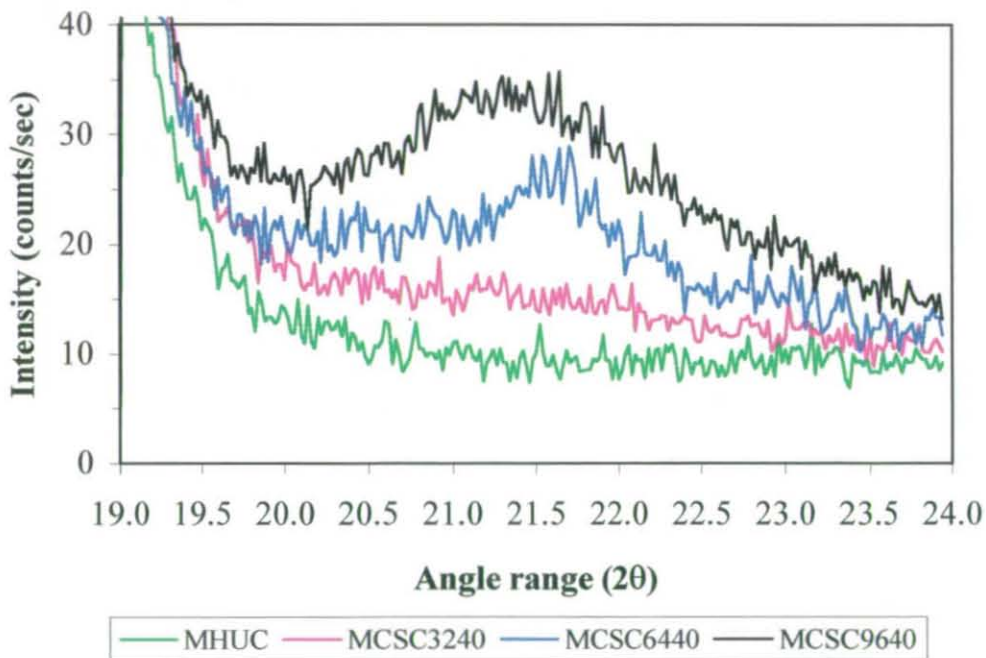


Figure 4.22: X-ray patterns of magnesium hydroxide coated with various calcium stearate concentrations at coating time of 40 minutes in the Fielder mixer.

4.3.3 CONTACT ANGLE MEASUREMENT

For highly filled polymer systems, it is important to reduce the degree of filler agglomeration to a minimum level, in order to decrease the system viscosity for easier processing and to increase the extent of filler loading [154]. One effective method of reducing the number of filler agglomerates in a filled polymer system is by the use of surface modifiers. Surface modifiers are generally bifunctional molecules with one end capable of adhering to the filler and the other end compatible with the polymer, and at times even capable of reacting with it [155]. Surface treatment basically helps the polymer to wet the filler better and disperse it, thereby reducing agglomeration because of promotion of filler-polymer contact as against filler-filler contact [155]. The interfacial forces between filler particles can be determined from the surface free energy obtained from contact angle measurement. After 40 minutes of mixing at 140°C in the Fielder mixer the contact angles for the coated filler samples were measured with four different kinds of liquids, water and glycerol (polar liquids) and 1-bromonaphthalene (BNL) and diiodomethane (DIM) (nonpolar liquids). A drop of each liquid was placed on the solid surface. The calculation of surface free energy is shown in Appendix D.6. The results of the various calcium stearate coated magnesium hydroxides together with calcium stearate are shown in Table 4.2.

Table 4.2: Contact angle and surface energy of coating agent, uncoated filler, and coated filler with various calcium stearate concentrations (average of 5 results).

Code	Contact angle (degree)				Surface energy (mJm ⁻²)
	Water	Glycerol	DIM	BNL	
MHUC	35.6	39.6	28.0	26.4	62.02
MCSC32	98.2	78.0	52.6	44.2	33.71
MCSC64	106.2	89.6	57.4	49.4	30.09
MCSC96	106.2	91.0	61.6	56.8	27.07
CaSt	106.5	92.4	76.0	66.0	21.29

A high surface free energy would signify a high polarity or hydrophilicity of solid surfaces. The results show that uncoated magnesium hydroxide gives the highest surface free energy while calcium stearate shows the lowest value as magnesium hydroxide has high polarity (hydrophilic) surfaces while calcium stearate is a nonpolar substance (hydrophobic). Coating of filler with 0.5 monolayer calcium stearate decreases the polarity of the magnesium hydroxide, however some polar part of the filler surfaces has remained. At 1.0 monolayer coverage of magnesium hydroxide, the sample shows greater reduction of surface free energy as polar surfaces of magnesium hydroxide are coated with one molecular layer of coating agent. With 1.5 monolayer coverage of magnesium hydroxide results in a lower surface free energy compared to one monolayer coating. It suggests that surface treatment of magnesium hydroxide with one monolayer coverage can improve wetting and dispersion of the filler in polymer matrix thereby reducing agglomeration of the filler leading to better mechanical properties of composites. Moreover, at one monolayer coverage the interfacial force at filler/coating interphase is higher than at other monolayer coatings. It is known from DSC and X-ray diffraction results that at 1.5 monolayer (9.6% calcium stearate) coverage of magnesium hydroxide some free calcium stearate particles have remained in the mixture leading to the further reduction of surface free energy compared with one monolayer coating. Although the coating of filler decreases the surface free energy, the coating of filler with more than one monolayer gives inferior properties of compounds which is discussed in the next section.

4.4 EFFECT OF FILLER COATING ON COMPOUND PROPERTIES

Inorganic particulate fillers are routinely compounded into thermoplastic materials. The aims of adding the fillers are to improve mouldability by reducing shrinkage, to decrease the cost of products, and to enhance certain mechanical properties such as the tensile modulus of the composite. However, at high filler loading the filled compounds become brittle and deterioration in such properties as impact strength, elongation at yield, extension at maximum load, and fracture toughness can occur.

Therefore, modification of filler has been used in the plastics industry to mitigate these effects. However, the coating of filler with excess coating agents also leads to a reduction of mechanical properties of composites. The end point of aiming for the optimum mechanical performance of modified filled-composites is, therefore, to improve toughness of unmodified filled-compounds without or with having little effects on tensile and flexural strength. The improvement in the toughness of the coated filled-composites can be obtained from a variety of indications such as reductions in tensile/flexural modulus, increase in elongation at yield/extension at maximum load, higher impact properties, and higher filler/polymer orientations, in comparison with uncoated filled-composites.

Typically, polymer chains contain nonpolar parts (hydrophobic), while fillers have polar (hydrophilic) surfaces. It is difficult to form a strong bond between the filler and the matrix due to poor wettability of the filler, and due to the presence of contaminants or moisture on the filler surfaces, which prevents physical or chemical adsorption of the polymer molecules. The wettability of filler can be increased by the surface treatment. The coating of filler with coating agents containing both nonpolar and polar parts in the molecule can modify the interfacial force at the polymer/filler interphase leading to property changes of its composite.

To understand the effect of filler coating on compound properties, filler content, tensile, flexural and impact properties have been determined. Crystallinity, reversion, and filler/polymer orientation of compounds have also been investigated. These results are discussed below.

4.4.1 FILLER CONTENT

The formulated compound granules, coating agents, and uncoated/coated fillers taken after 40 minutes from the Fielder mixer were burned in a furnace for 3 hours at 850°C to produce ash. Ashing results are shown in Appendix B.7. The polymer/filler

contents were determined using an ashing test. Calculations are shown in Appendix D.7 and the results are given in Tables 4.3 and 4.4.

Table 4.3: Polymer, filler, and coating contents for unfilled HDPE and compounds containing $Mg(OH)_2$ coated with various concentrations of magnesium stearate and stearic acid (average of 2 results).

Code	DETAILS	%Polymer Content	%Filler Content	%Coating Content*
HDPE	100% HDPE	100	0.00	(0.00)
HMUC	HDPE+40% $Mg(OH)_2$ UNCOATED	56.83	43.17	(0.00)
HMMSC31	HDPE+40% $[Mg(OH)_2+3.1\%MgSTEARATE]$ 40min coating time	56.47	43.53	(3.50)
HMMSC61	HDPE+40% $[Mg(OH)_2+6.2\%MgSTEARATE]$ 10min coating time	56.59	43.41	(6.71)
HMMSC62	HDPE+40% $[Mg(OH)_2+6.2\%MgSTEARATE]$ 40min coating time	57.77	42.23	(6.68)
HMMSC93	HDPE+40% $[Mg(OH)_2+9.3\%MgSTEARATE]$ 40min coating time	62.30	37.70	(9.62)
HMSAC60	HDPE+40% $[Mg(OH)_2+6.0\%STEARIC ACID]$ 40min coating time	62.28	37.72	(6.16)

* : % coating agent in the filler

The results from Table 4.3 illustrate that in all cases the coating contents are higher than the intended values. This is attributed to the fact that during initial period (1-10 minutes) of mixing the temperature inside the Fielder vessel increases rapidly before mixing has been completely achieved. The pressure builds up due to the evaporation of moisture probably produced from chemical reactions or adsorbed on magnesium hydroxide surfaces, therefore some filler and coating agent leak from the system. This may affect the actual amount of filler and coating agent in the mixture.

The results also show differences between intended and actual filler contents. The filler contents are difficult to control because the amount of filler fed depends not only on environment (temperature and humidity) but also on characteristics of the compounder, fillers, and coating agents. The filler contents of coated $Mg(OH)_2$ samples containing 3.1% and 6.2% magnesium stearate with both 10 and 40 minutes

coating time are higher than that containing 9.3% magnesium stearate and 6.0% stearic acid. These results may affect mechanical properties of the composites.

Table 4.4: Polymer, filler, and coating contents for unfilled HDPE and compounds containing $Mg(OH)_2$ coated with various concentrations of calcium stearate (average of 2 results).

Code	DETAILS	%Polymer Content	%Filler Content	%Coating Content*
HDPE	100% HDPE	99.95	0.00	(0.00)
HMUC	HDPE+40% $Mg(OH)_2$ UNCOATED	60.77	39.23	(0.00)
HMCS32	HDPE+40% $[Mg(OH)_2+3.2\%CaSTEARATE]$ 40min coating time	60.62	39.38	(3.16)
HMCS64	HDPE+40% $[Mg(OH)_2+6.4\%CaSTEARATE]$ 40min coating time	60.09	39.91	(6.35)
HMCS96	HDPE+40% $[Mg(OH)_2+9.6\%CaSTEARATE]$ 40min coating time	60.25	39.75	(9.46)

* : % coating agent in the filler

The ashing results from Table 4.4 show that in all cases the coating levels of filler are close to the planned values. The %filler contents are slightly lower than the intended values. This may be because these compounds were produced in conditions of high humidity. The humidity affects the polymer and filler feeding. However, the results are reasonable and there is no significant difference between the actual and intended filler levels.

4.4.2 TENSILE PROPERTIES

One of the most informative mechanical experiments for any material is the determination of its stress-strain curve in tension. This is usually done by measuring continuously the force developed as the sample is elongated at a constant rate of extension. The generalised stress-strain curve for high density polyethylene is shown in Appendix B.8. This curve can be used to define several useful quantities, including tensile modulus (the slope of the curve), tensile yield strength or maximum yield

stress, and elongation at yield. In order to study the effects of coating agent concentration on the mechanical properties of its composite, tensile bar specimens were produced using a Negri Bossi NB55 injection moulder. The tensile properties were determined using a Lloyd tensile testing machine, type L200R. Tensile properties are summarised in two subsections as below.

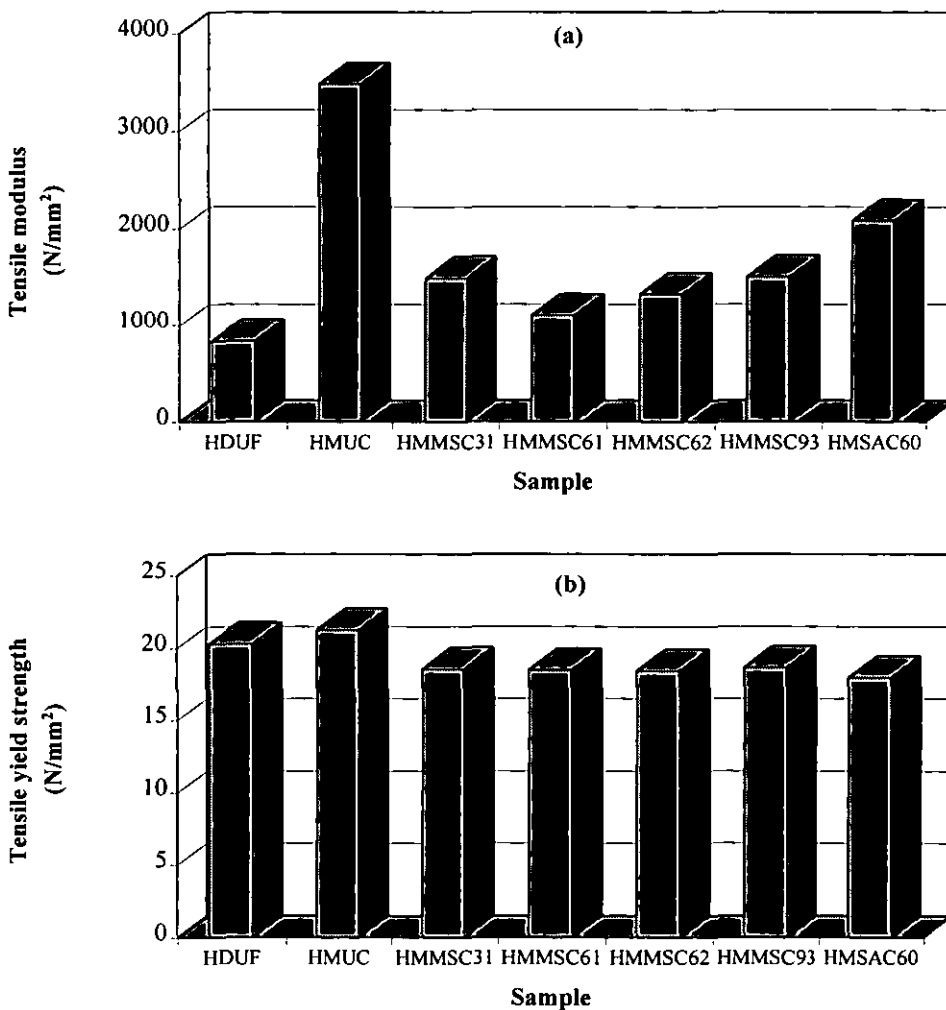
4.4.2.1 Magnesium hydroxide modified with magnesium stearate and stearic acid.

It is seen from Figure 4.23 that all filled composites have a higher tensile modulus and lower elongation at yield than unfilled composite. The composite containing uncoated magnesium hydroxide has the highest tensile modulus and the lowest elongation at yield. The addition of 40% magnesium hydroxide increases tensile modulus of composite by 300%. However, with these values the composite displays brittle failure under tension. Magnesium hydroxide is an inert filler (not a reinforcing filler), hence it has no bonds present between the filler and the matrix. It is, moreover, due to the fact that the individual filler particles are not separated from one another, and wetted individually by the matrix phase, instead, the filler particles are often agglomerates made up of many small particles. The increase in tensile modulus of composite due to an incorporation of filler into the polymer may come from an increase in crystallinity of composites. The filler particles also restrict the mobility and deformability of the matrix by introducing a mechanical restraint, the degree of which depends on the particulate spacing and the properties of the particle and the matrix. However, an increase of tensile modulus reflects a reduction of ductility and toughness of a composite. This result is consistent with results reported by many others [156, 157], where the addition of filler increases tensile modulus in composites. It is believed that if the filler is rigid with a tensile modulus greater than the modulus of the polymer, the modulus of the mixture increases with filler content. If fillers in the form of fine powders are added to most polymers, especially brittle polymers, the elongation to fracture and the ultimate strength both generally decrease as the amount of filler in the polymer increases.

On surface modification of the filler, the results show a decrease in modulus (by 43-69% depending on the coating concentrations) and increase in elongation at yield in comparison with uncoated filled-composite. This phenomenon may be explained by the lubricating effect of coating agents produced at the filler/polymer interphase, which facilitates the wetting of the filler particle and consequently decreases tensile modulus. These additives also assist in removal of traces of residual water from the filler facilitating dispersion [124, 158, 159]. However, there is no strong chemical bonding between polymer/coating/filler interface (known as polymer/filler interphase). A monolayer coverage of magnesium hydroxide with magnesium stearate give a lower tensile modulus (and usually higher toughness) compared to that with stearic acid. This indicates that when magnesium stearate is applied the interfacial adhesion between polymer and filler is decreased greater than when stearic acid is used. Magnesium stearate reduces hydrophilicity of magnesium hydroxide more than stearic acid does, since magnesium stearate has lower surface free energy than stearic acid as shown in Table 4.2. However, this result may relate to the lower coating content of the sample containing stearic acid compared to samples containing magnesium stearate.

To better evaluate the effect of magnesium stearate treatment, magnesium hydroxide was coated with different concentrations of the stearate (0.5, 1.0, 1.5 monolayer) for 40 minutes and coated with one monolayer for 10 minutes for comparison. It appears that the composites containing $Mg(OH)_2$ coated with a monolayer coverage of magnesium stearate after both coating times (10 and 40 minutes) give lower tensile modulus and higher elongation at yield than that with other levels of magnesium stearate. The lowest interfacial force between the filler and the polymer matrix occurs at a monolayer coverage, leading to a marked reduction in modulus [154]. No significant differences in tensile properties was obtained from a variation of coating time after the temperature in the Fielder mixer reached to the melting point of the coating agent (see section 4.2.2). However, it is evident that the surface coating can

improve ductility of the composite. The various types and levels of coating have little effect on tensile yield strength. This result is consistent with results reported by Hornsby and Watson [124]. They studied the mechanical properties of 50% magnesium hydroxide filled polypropylene and found that tensile yield strength was little influenced by uncoated magnesium hydroxide filler. They also suggested that there was some degree of filler-matrix interaction, capable of resisting the imposition of a tensile force, although there was unlikely to be any chemical interaction occurring between the magnesium hydroxide particles and the polymer.



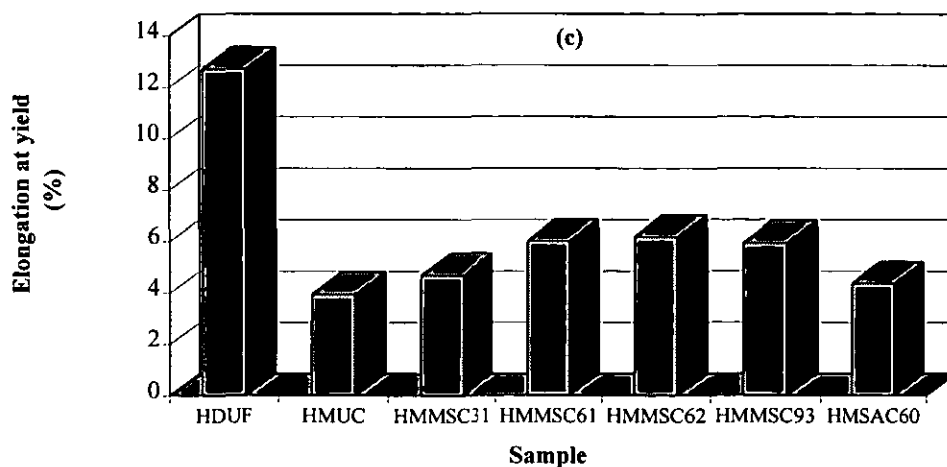


Figure 4.23: Tensile properties of unfilled HDPE and HDPE compounds containing $\text{Mg}(\text{OH})_2$ coated with various magnesium stearate levels and one monolayer stearic acid; (a) tensile modulus, (b) yield strength, (c) elongation at yield (average of 8 tests).

4.4.2.2 Magnesium hydroxide modified with calcium stearate.

Figure 4.24 shows that filled composites again give higher tensile modulus and lower elongation at yield (more brittle) than unfilled HDPE. Surface modification of filler causes a distinct reduction in tensile modulus (increase in toughness), there is smaller effect of decrease of tensile yield strength and an increase of elongation at yield. A $\text{Mg}(\text{OH})_2$ sample with 1.0 monolayer coverage of calcium stearate again gave the lowest tensile modulus and slightly higher elongation at yield in comparison with 0.5 and 1.5 monolayer equivalent. This is because the high wettability and dispersibility of filler particles occurs leading to yielding when one monolayer coverage is produced (as seen in SEM micrographs Figure 5.30 (d)). The various levels of calcium stearate coating have little effect on tensile yield strength and elongation at yield.

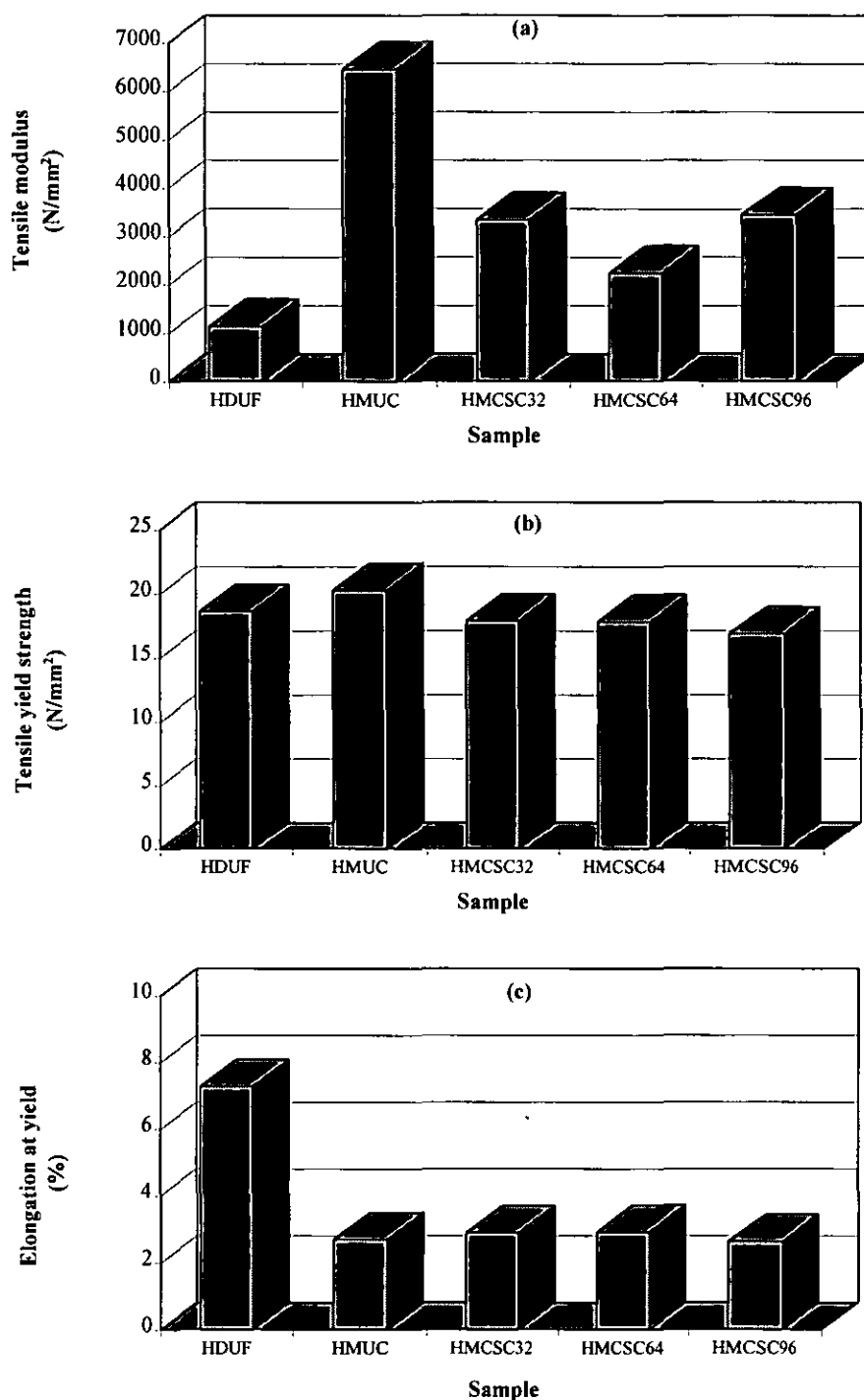


Figure 4.24: Tensile properties of unfilled HDPE and HDPE compounds containing $Mg(OH)_2$ coated with various calcium stearate levels; (a) tensile modulus, (b) yield strength, (c) elongation at yield (average of 8 tests).

As with other mechanical tests, the tensile properties of polymers are sensitive to temperature [160]. The tensile modulus and yield strength generally increase as the temperature decreases; the elongation usually decreases as the temperature is lowered for plastic materials. To avoid the temperature effects, each group of samples was tested in a short spaced period to try to maintain the same conditions. Therefore, the differences in values of tensile modulus and elongation at yield for unfilled HDPE and compounds containing uncoated magnesium hydroxide as shown in Figures 4.24 and 4.25 are insignificant.

4.4.3 FLEXURAL PROPERTIES

Flexural properties of filled HDPE containing surface treated magnesium hydroxide with different levels of magnesium stearate, stearic acid, and calcium stearate were determined using the same tensile testing machine in three point flexural mode. The flexural stress-strain curve for high density polyethylene is shown in Appendix B.9. The results are summarised in two subsections.

4.4.3.1 Magnesium hydroxide modified with magnesium stearate and stearic acid.

Figure 4.25 shows the comparison between the flexural modulus of the systems containing varying levels of magnesium stearate coating together with stearic acid coating. It reveals that by adding of 40%w/w the filler to the polymer, flexural modulus of composites increase by 100%. As expected, the unmodified filled-composite has a higher flexural modulus than the modified filled- and unfilled composites. The presence of coating agents leads to an obvious decline in flexural modulus compared to uncoated filled-composite. In comparison with the stearic acid coating, the magnesium stearate coating gave a greater reduction in the modulus and increase in extension at maximum load, while the effects of coating type on flexural yield strength are small. It appears that when magnesium stearate is applied the interfacial force at the polymer/filler interface is lower than when stearic acid is used (as explained above). This result is consistent with the assertion of Hornsby and

Watson [124]. They found that the treatment of magnesium hydroxide with fatty acids and fatty acid derivatives caused a slight decrease in flexural modulus and flexural strength relative to the equivalent composition containing untreated filler.

Like tensile properties, significantly decreased flexural modulus is observed in composites containing a monolayer coverage of magnesium stearate compared to other filled composites. The presence of a monolayer coverage of magnesium hydroxide decreases the interfacial force at the filler/polymer interphase more than that of 0.5 and 1.5 monolayer coverage samples. Magnesium hydroxide has hydrophilic or polar surfaces, when it was coated with nonpolar substance, such as magnesium stearate, its surfaces become less polar (more hydrophobicity). Surface free energy appears to decrease with an increase amount of coating agents. At 0.5 monolayer of coating some area on magnesium hydroxide surfaces have not been coated with the coating agent, therefore polarity of the sample decreases slightly compared with uncoated magnesium hydroxide (but remaining at a high value compared with other coating levels as shown in section 4.3.3). This leads to an increase in wettability and dispersibility of filler compared with the uncoated filler. Moreover, this results in a decrease in flexural modulus of the composite in comparison with uncoated filled-compound, because of the lubricating effect of magnesium stearate. Compared with 0.5 monolayer coverage, with 1.0 monolayer coverage the polar surfaces of $Mg(OH)_2$ were perfectly covered by magnesium stearate leading to a low value of surface free energy. Therefore, the decreased interfacial force is enhanced leading to a further reduction of flexural modulus of the composite caused by yielding. Although 1.5 monolayer coverage of magnesium hydroxide shows the lowest value of surface free energy in comparison with 0.5 and 1.0 monolayers, excess coating agent has remained on the magnesium hydroxide surfaces. This excess stearate leads to a slippage of polymer molecules at the interface during processing and the distance between polymer chains and filler particles is increased. Therefore the interfacial force between filler and polymer is increased resulting in a higher flexural modulus of the composite compared to compounds containing magnesium hydroxide coated with 0.5 and 1.0 monolayer of magnesium stearate.

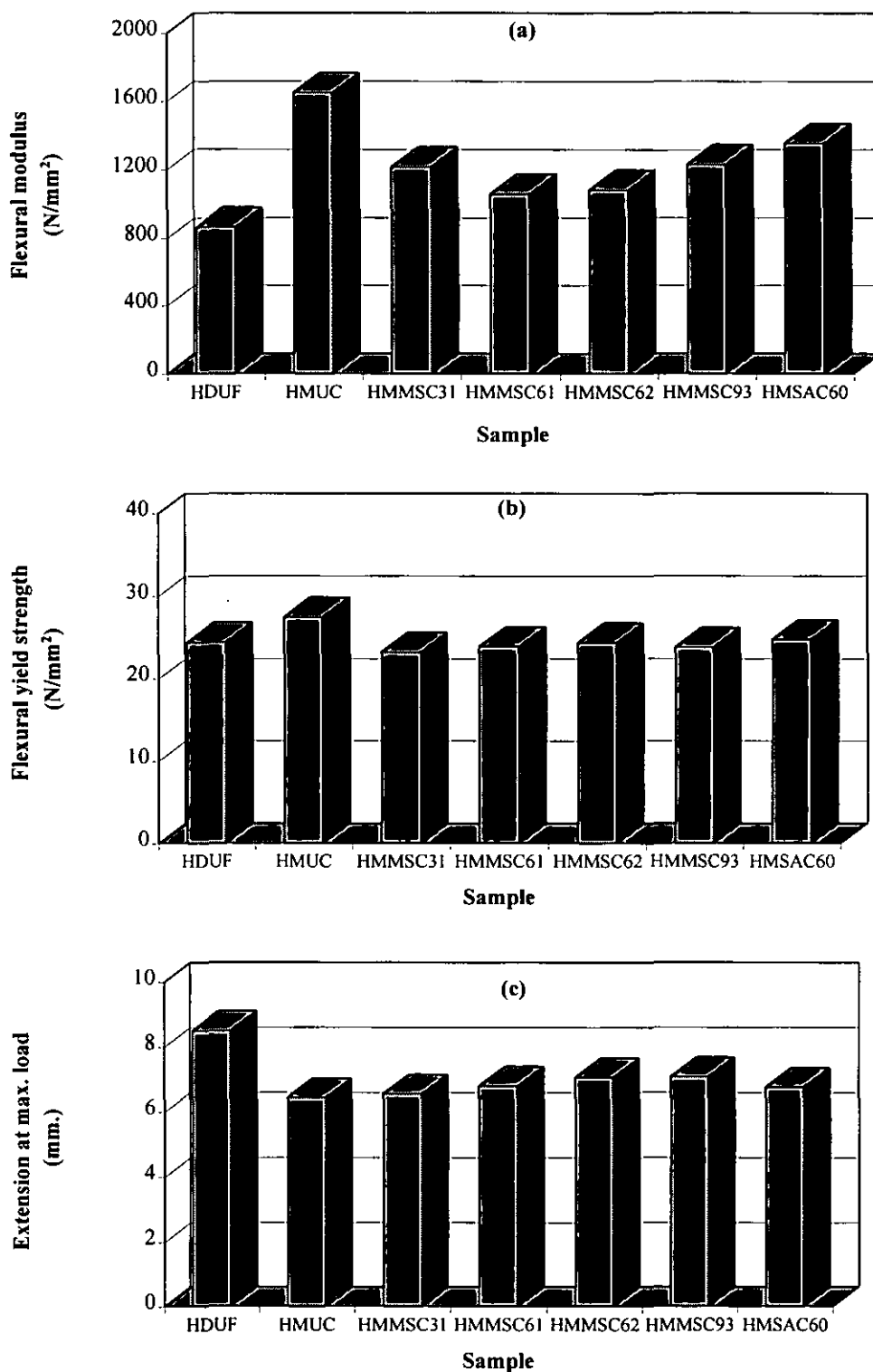


Figure 4.25: Flexural properties of unfilled HDPE and HDPE compounds containing $\text{Mg}(\text{OH})_2$ coated with various Mg stearate concentrations and stearic acid; (a) flexural modulus, (b) flexural yield strength and (c) extension at maximum load (average of 8 tests).

4.4.3.2 Magnesium hydroxide modified with calcium stearate.

The effect of surface modification of magnesium hydroxide with calcium stearate on flexural properties of filled HDPE is shown in Figure 4.26. The addition of filler results in an increase of flexural modulus and yield strength of the composite. The composite containing uncoated filler shows the highest flexural modulus and yield strength as magnesium hydroxide is stronger and more rigid than HDPE. However, filler addition produces a brittle compound, demonstrated by the lowest value of extension at maximum load. It suggests that the primary particles of uncoated filler have some degree of agglomeration (as seen in SEM micrographs Figure 5.31(a)). It is evident that the modification of magnesium hydroxide with calcium stearate results in considerable reduction in flexural modulus and a slight decline in flexural yield strength compared with unmodified filled-compounds. Extension at maximum load of the composite decreases with the addition of filler but increases slightly with the modification of filler. The flexural modulus was also found to be at a minimum value while the extension at maximum load shows the greatest value at a monolayer coverage of calcium stearate. The calcium stearate treatment provides some improvement in dispersing and lubricating the magnesium hydroxide particles in the polymer matrix causing the observed increase of flexural properties of composites as suggested by McKane [159].

It should be noticed that there are differences in the moulds used for producing specimens. In section 4.4.2.1 and 4.4.3.1 the specimens were produced from a mould with four part specimens while the specimens in section 4.4.2.2 and 4.4.3.2 were produced from a mould designed to produce four tensile bars (see the characteristics of both moulds in Figure 3.3). Therefore, the tensile and flexural results in each section may give slightly different values.

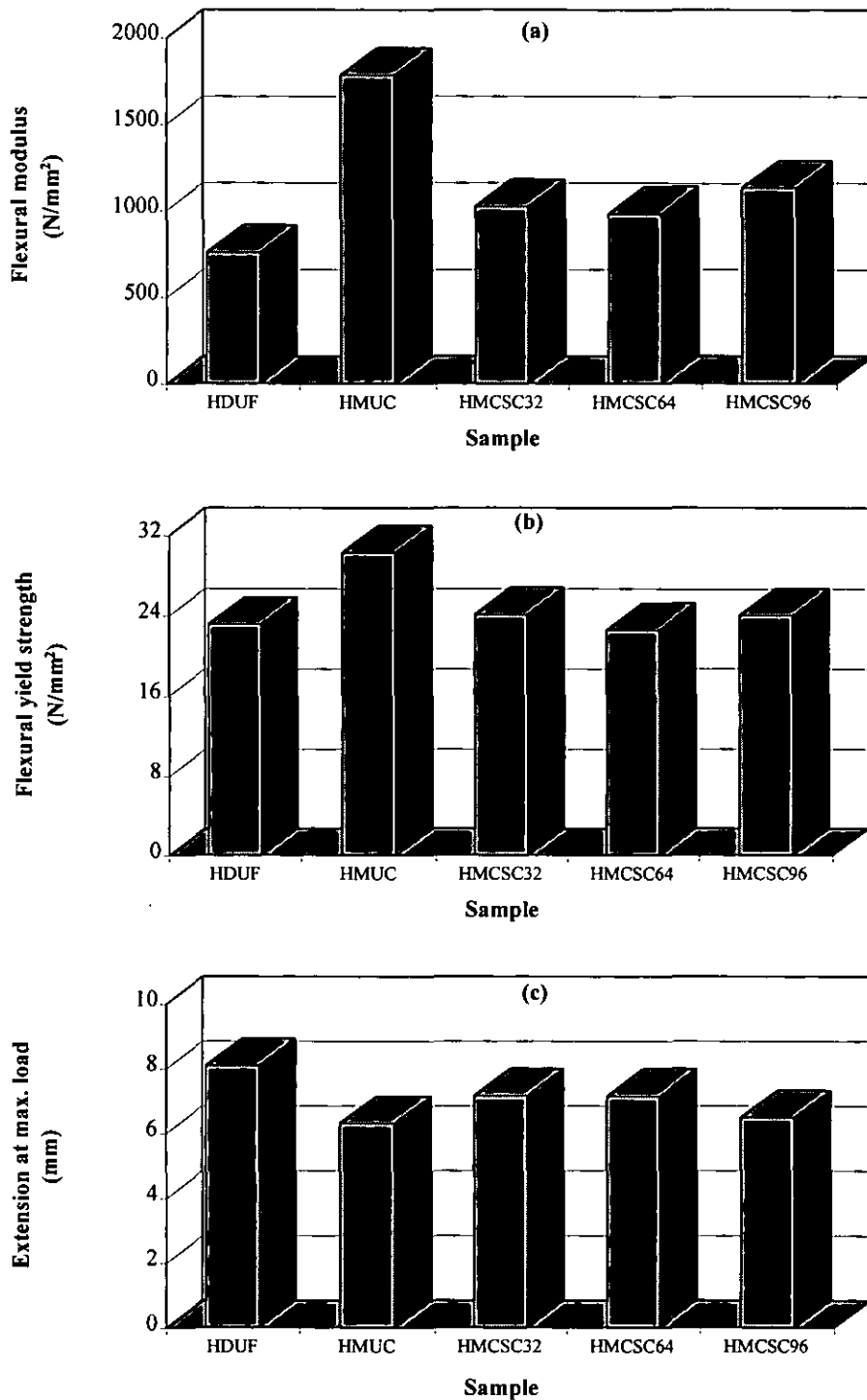


Figure 4.26: Flexural properties of unfilled HDPE and HDPE compounds containing Mg(OH)₂ coated with various calcium stearate concentrations; (a) flexural modulus, (b) flexural yield strength and (c) extension at maximum load (average of 8 tests).

4.4.4 IMPACT PROPERTIES

The resistance to impact is one of the important properties of materials, and is defined as the ability of material to absorb energy before its failure. The circular disks produced by injection moulding were used for impact testing. Impact strength was measured using a Rosand Falling Weight Impact tester with a dropping height of 461 mm and impact velocity of 3 m/s. An example of an impact trace is shown in Appendix B.10. Impact properties are summarised in Figures 4.27 and 4.28.

4.4.4.1 Magnesium hydroxide modified with magnesium stearate and stearic acid.

Figure 4.27 shows that the peak force, peak energy and failure energy decrease with addition of filler. The addition of 40% w/w magnesium hydroxide reduces the impact strength of the composite by 62%. The uncoated filled-compound shows a brittle fracture while coated filled-compounds fail in a ductile manner. This may be attributed to poor filler dispersion for the uncoated filled-composite causing a lower ability to resist the propagation of cracks. The impact properties increase with the modification of filler surface. It is because of the effective wetting and dispersion of filler in the matrix hence more energy is absorbed before fracture. A monolayer coverage of magnesium stearate using coating times of 10 and 40 minutes gives the highest impact resistance in comparison with all modified filled-composites, improving the impact properties by 100-110% compared with uncoated filled-composites. The coating for different times has little effect on impact properties as well as on tensile and flexural properties. This observation is consistent with results reported for many other polymer composites, where the presence of inorganic fillers (such as talc and mica) is detrimental to toughness properties [57, 113]. Riley and co-workers [113] also emphasised that good dispersion resulting from surface modification of filler can enhance impact strength of the composite.

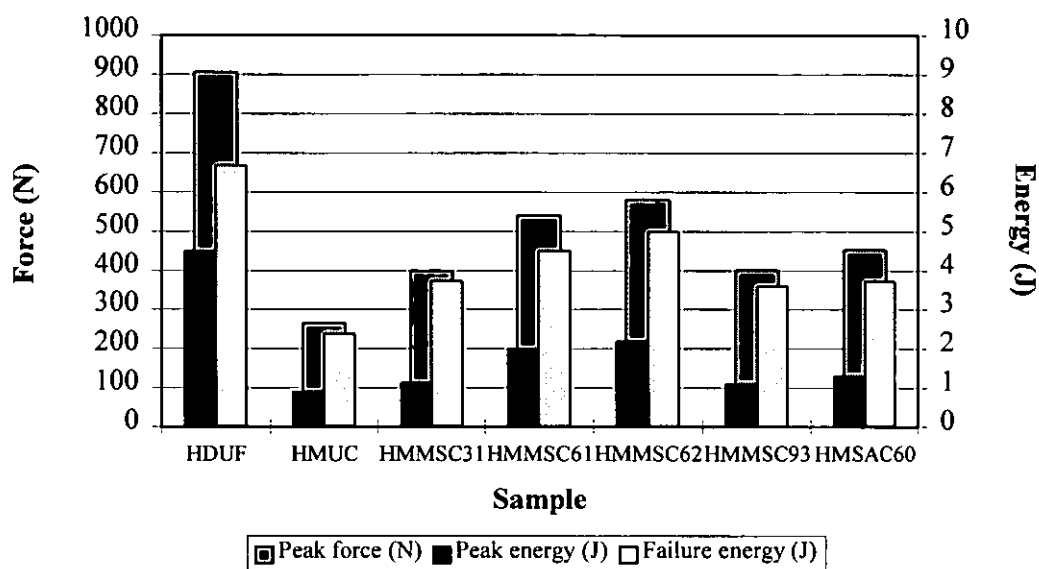


Figure 4.27: Falling Weight Impact properties of unfilled HDPE and compounds containing $\text{Mg}(\text{OH})_2$ coated with different levels of magnesium stearate and stearic acid (average of 10 tests).

The impact properties of filled composites containing one monolayer coverage with magnesium stearate give greater values than that containing stearic acid. Magnesium stearate is a more effective coating agent and modifies interfacial adhesion between polymer and filler, since it has a lower surface free energy than stearic acid (section 4.3.3). This result is in agreement with Hornsby and Watson [124] who found that at treatment levels of 6% stearate (magnesium and zinc stearate) gave markedly higher impact strengths than fatty acids (stearic acid, azelaic acid and oleic acid). However, at 9.3% magnesium stearate coating the free magnesium stearate which remains may result in the reduction of filler dispersion in the matrix since excess magnesium stearate affects a decrease in viscosity of polymer.

Hutley and Darlington [70] have observed a correlation between the recrystallisation temperature (T_c) in calcium carbonate filled polypropylene and impact strength. In this thesis, the results go some way to confirming their results and show that high recrystallisation temperatures are observed for composites with an increased impact strength. It is possible that the nucleation of crystals occurs at higher crystallisation

temperatures, where crystal growth can proceed more rapidly, then smaller spherulites are formed leading to an increased crack propagation resistance. Surface modification of filler with magnesium stearate usually enhances impact strength and also increases the amount of crystallinity in the polymer.

4.4.4.2 Magnesium hydroxide modified with calcium stearate.

It appears again from Figure 4.28 that the addition of 40% w/w magnesium hydroxide reduces the impact strength. $\text{Mg}(\text{OH})_2$ filled composites containing calcium stearate coating agent give improvement in impact properties in comparison with the unmodified compound. In addition, the results illustrate that the compound containing $\text{Mg}(\text{OH})_2$ coated with a monolayer coverage of calcium stearate gives the highest falling weight impact resistance (and the lowest tensile and flexural modulus) compared with other filled composites. Although, comparing Figures 4.27 and 4.28, magnesium stearate coating gave higher impact properties than calcium stearate coating, however the results are not directly comparable. These results are affected by such things as variation of room temperature and the fact that the impact machine and injection moulder were upgraded between the two experiments. However, HDPE compounds containing $\text{Mg}(\text{OH})_2$ coated with one monolayer of magnesium and calcium stearate are directly compared in chapter 5.

From the microscopic view point, the competition between effects of an interfacial force between polymer and filler and lubricating effect of coating agent on mechanical properties of composites are not completely understood but some aspects have been explained based on the structure of compounds. For example, the addition of uncoated filler (rigid and brittle) at high % filler loading into polymer (soft and tough) increases tensile/flexural modulus of composites according to the rule of mixtures. The composites showed brittle fracture under tension with low elongation at yield. It may suggest that some degree of filler-matrix interaction is required to resist a tensile force. However, there are unlikely to be any chemical interactions at the

filler/polymer interface due to large differences in surface polarity. It appears that physical interaction occurs between the highly rough surfaces of filler particles and the polymer matrix as the mechanical keys. The results obtained from impact testing for the uncoated filled-composite also showed brittle failure under stress loading. This may imply that a filler/polymer interface is not strong to resist crack propagation and the compound may contain the agglomerated magnesium hydroxide leading to the fact that the crack will propagate between the agglomerated particles. If the interfacial force at the filler/polymer interface is extremely strong, like primary bonding, exceeding the strength of the matrix, the failure mechanism is restricted to the matrix and little or no discharged filler is observed on the fracture surface. Where the strength of the matrix is equivalent to that of the interface, a propagating crack will follow the filler-matrix boundary. With very low interfacial force, the filler and the matrix will separate completely and there may be a limitation to filler addition because of the overall impact properties of the composites.

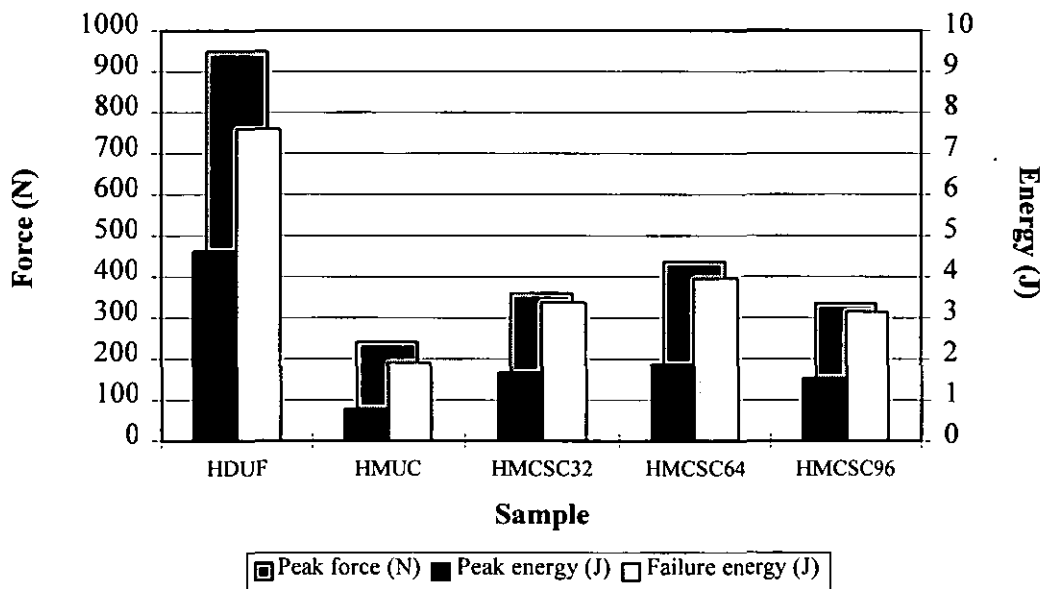


Figure 4.28: Falling Weight Impact properties of unfilled HDPE and compounds containing $Mg(OH)_2$ coated with different levels of calcium stearate (average of 10 tests).

Surface modification of magnesium hydroxide with 0.5, 1.0, and 1.5 monolayer of magnesium/calcium stearate reduced the tensile/flexural modulus and increased elongation at yield of all composites resulting in a tougher product compared to uncoated filled-composite. This may imply that magnesium stearate acts as a lubricating agent resulting in a slippage of polymer chains in the interphase. At low extension rate (5 mm/min) the molecular chains of polymer in the compound have time to align themselves under the influence of the applied stress. Thus the addition of coating agent means that the polymer chains are more able to move at the same rate as it is being strained. An increase in impact strength (more toughness) was also found in composites containing coated filler.

At one monolayer coverage of filler with magnesium/calcium stearate showed a minimum value of tensile/flexural modulus and a maximum value of elongation at yield, extension at maximum load, and impact properties. It is possible that one monolayer coverage of the filler with either coating agent gives the lowest interfacial force at filler/polymer interface as shown in Figure 4.29(b) resulting in a greater energy absorption with ductile fracture compared with the other filled composites and the interfacial force effect becomes dominant. Whereas at less than one monolayer coverage of filler the lubricating effect is less importance to the composite properties than the interfacial force effect, since the composites contain fillers coated imperfectly as shown in Figure 4.29(a).

In comparison with 1.0 monolayer coverage, tensile/flexural modulus of composite containing 1.5 monolayer increases while impact properties progressively decrease. It may indicate that the dispersion of filler decrease, because excess coating agents have remained in the system leading to a decrease in viscosity of polymer as shown in Figure 4.29(c-d). This excess coating agent leads to the reduction of interactions between polymer and coated filler. The proposed mechanisms of coating filler may be explained as below:

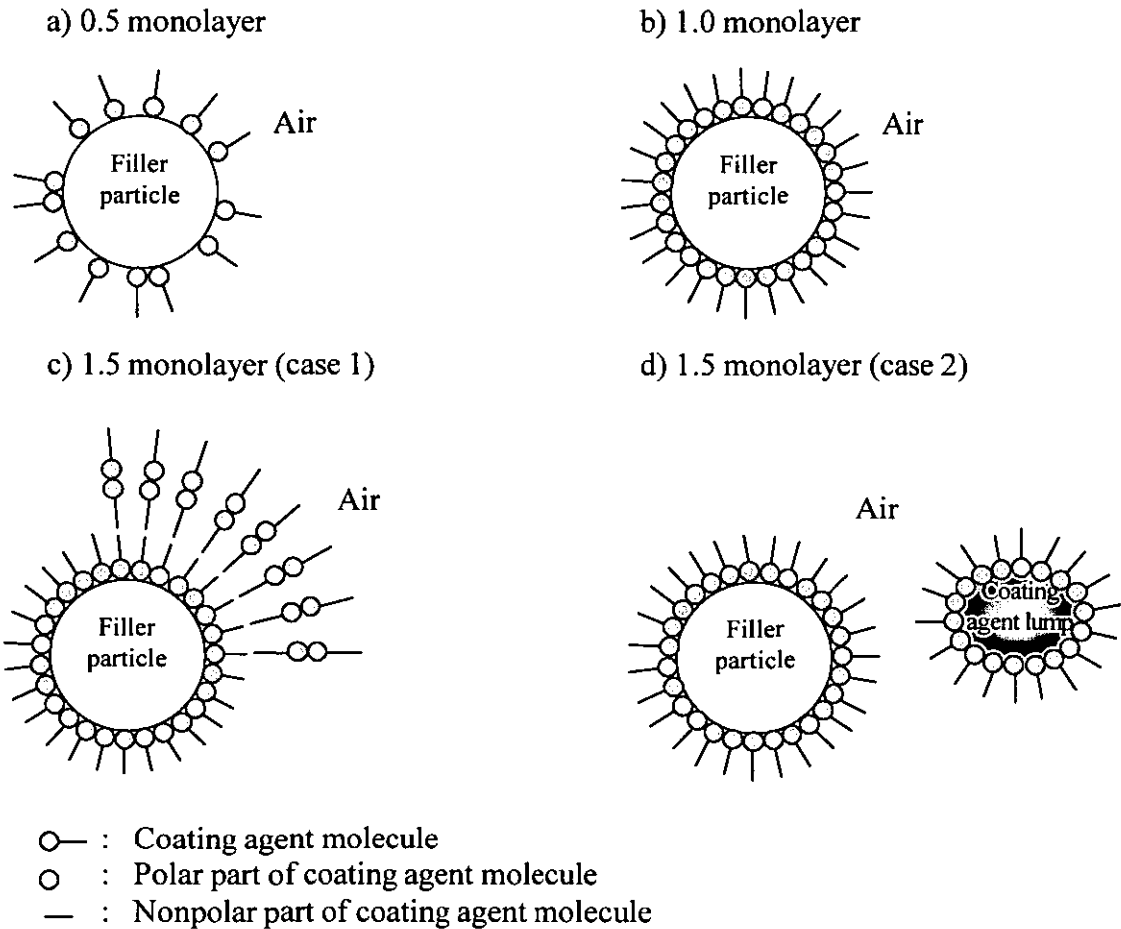


Figure 4.29: The proposed mechanisms of coating filler.

4.4.5 CRYSTALLISATION PROPERTES

Properties of polymer composites are significantly influenced by interfacial interaction. In the composites polymer adheres to the surface of the filler, and an interphase is formed the properties of which are different from those of the components. In semicrystalline polymers, however, other forms of interaction can also appear. Fillers can initiate crystallisation thus changing the morphology of the matrix. As an effect of nucleation the size of the crystallites decreases resulting in significant property changes in composites, such as an increase in toughness. To understand further the effect of coating concentration on mechanical properties of composites, DSC was used to investigate crystallisation properties of composites. Degree of crystallinity is determined by dividing heat of fusion of PE in compounds

by the heat of fusion of a 100% crystalline polyethylene (293 J/g) [139]. The DSC thermogram for the unfilled HDPE compound is shown in Figure 3.8. Crystallisation properties are summarised in Tables 4.5 and 4.6 for the coating with magnesium and calcium stearates, respectively.

By inspection of crystallisation properties, it is seen from Table 4.5 that the addition of magnesium hydroxide filler, both coated and uncoated, resulted in a significant decrease in melting temperature (T_m) and increases in recrystallisation temperature (T_c) and degree of crystallinity. This indicates the nucleation effect of magnesium hydroxide. Magnesium hydroxide particles evidently increase the number of heterogeneous crystallisation nuclei. The reductions of melting temperature and increase in recrystallisation temperature of filled composites implies the presence crystallites which are smaller in comparison with crystallites of unfilled HDPE. It suggests that because a filler acts as a nucleating agent to induce crystallisation in the matrix, the number of spherulites in a filled polymer is greater while the crystallite size is smaller than in an unfilled polymer. This result is in agreement with many other results [125, 129, 130]. However, filler coatings do not have significant effects on melting and recrystallisation temperatures.

Surface modification of magnesium hydroxide was applied using various magnesium stearate concentrations or stearic acid to increase the adhesive force at the filler/polymer interphase. The results show that surface modification of magnesium hydroxide makes it possible to change the filler to a nucleation active one producing a higher crystallinity compared to HDPE alone or HDPE with unmodified magnesium hydroxide. The sample containing a monolayer coverage of magnesium stearate shows a higher crystallinity than that with 0.5 and 1.5 monolayer coatings. However, at one monolayer coverage of filler with stearic acid shows a lower value than that with magnesium stearate, as the wetting and dispersion of filler particles in the sample coated with stearic acid is less than that coated with magnesium stearate (as above). However, the degree of crystallisation is not only a factor affecting the toughness of

modified filled-composites. Other important factors such as the interaction at the interface and lubrication effect of coating agents are also considered.

Table 4.5: Crystallisation properties for unfilled HDPE and compounds containing $Mg(OH)_2$ coated with various concentrations of magnesium stearate and stearic acid.

Code	Details	T_m (°C)	T_c (°C)	% Cryst
HDF	100% HDPE	136.9	113.4	56.5
HMUC	HDPE+40%uncoated $Mg(OH)_2$	133.7	114.9	64.8
HMMSC31	HDPE+40% $[Mg(OH)_2 + 3.1\%MS]$ (40 min)	133.2	115.5	69.1
HMMSC61	HDPE+40% $[Mg(OH)_2 + 6.2\%MS]$ (10 min)	133.6	114.4	69.6
HMMSC62	HDPE+40% $[Mg(OH)_2 + 6.2\%MS]$ (40 min)	133.9	114.6	75.2
HMMSC93	HDPE+40% $[Mg(OH)_2 + 9.3\%MS]$ (40 min)	132.8	115.2	56.8
HMSAC60	HDPE+40% $[Mg(OH)_2 + 6.0\%SA]$ (40 min)	131.7	114.7	58.4

Table 4.6: Crystallisation properties for unfilled HDPE and compounds containing $Mg(OH)_2$ coated with various calcium stearate concentrations.

Code	Details	T_m (°C)	T_c (°C)	% Cryst
HDF	100% HDPE	134.1	110.6	62.2
HMUC	HDPE+40%uncoated $Mg(OH)_2$	130.1	115.6	72.3
HMCSC32	HDPE+40% $[Mg(OH)_2 + 3.2\%CS]$ (40 min)	130.4	113.5	77.6
HMCSC64	HDPE+40% $[Mg(OH)_2 + 6.4\%CS]$ (40 min)	130.5	113.0	78.4
HMCSC96	HDPE+40% $[Mg(OH)_2 + 9.6\%CS]$ (40 min)	131.5	113.3	75.0

Table 4.6 shows again that particulate filled polymer gives a lower melting temperature, higher recrystallisation temperature and degree of crystallinity than unfilled polymer. Like magnesium stearate coating, calcium stearate coating has an insignificant effect on the melting and recrystallisation temperature of coated filled-compounds. The sample containing a monolayer coverage of calcium stearate also shows the highest crystallinity compared to 0.5 and 1.5 monolayer coating. All compounds in Tables 4.5 and 4.6 give difference in the crystallisation properties due to differences in the mould used (Figure 3.3) and injection conditions (see Appendices A.2 and A.3).

4.4.6 REVERSION MEASUREMENT

In order to estimate the molecular orientation in a moulding, the maximum reversion of the mouldings after a specified heat treatment was determined using a reversion test. The testing temperature used was 132 °C. The results are represented in Figures 4.30 and 4.31.

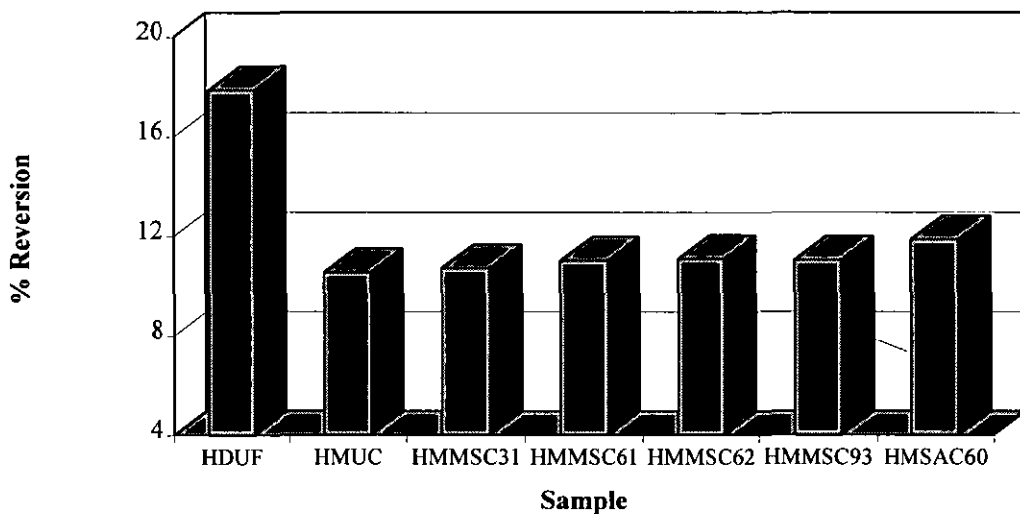


Figure 4.30: %Reversion test of unfilled HDPE and compounds containing $Mg(OH)_2$ coated with various magnesium stearate concentrations and stearic acid (average 4 of tests).

Figure 4.30 shows that the highest amount of reversion occurs with the unfilled polymer, and reversion decreases considerably with the addition of filler. The effect of coating is probably not significant. As all compounds are injection moulded, the chains of unfilled polymer are free to align in the flow direction but the chains of filled polymer are bound to the filler particle which acts as an anchorage, this may impede the polymer orientation. Moreover, with the filled polymer, the amount of polymer is diluted so the samples have less shrinkage.

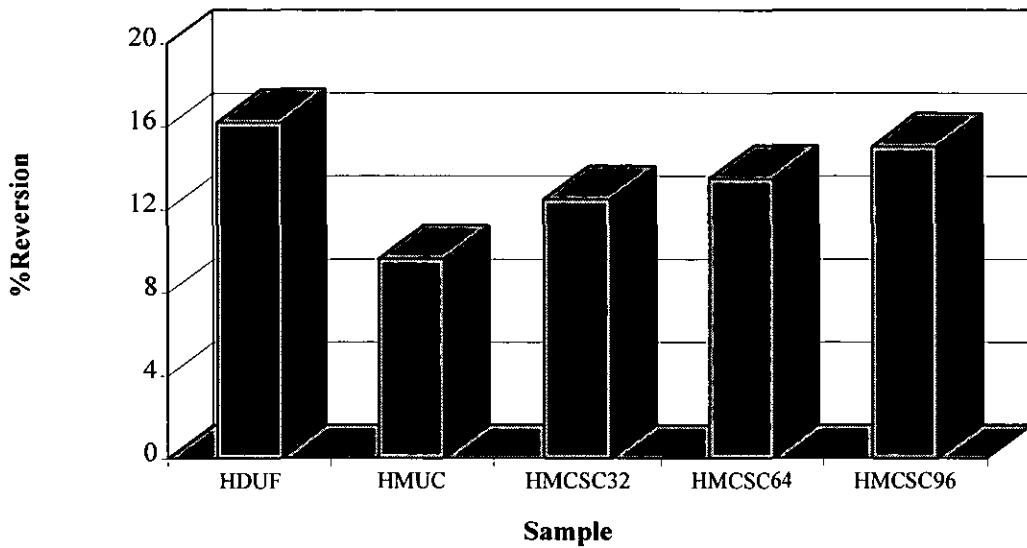


Figure 4.31: %Reversion test of unfilled HDPE and compounds containing $Mg(OH)_2$ coated with various calcium stearate concentrations (average of 4 tests).

It appears from Figure 4.31 that the addition of filler decreases the percentage of reversion as filler particles may disturb the polymer alignment in the composite. Surface modification of filler with calcium stearate shows that an increased reversion results from an increase in calcium stearate concentration. Calcium stearate acts as lubricant leading to the improvement of filler wettability, therefore, polymer alignment is easier in the injection direction compared with filled polymer containing uncoated filler. An unexpected result obtained from the HDPE compound containing magnesium hydroxide with 1.5 monolayer coverage calcium stearate shows a slightly higher %reversion compared to that with 1.0 monolayer coverage. This may be because the specimens lose their shape (thinner and wider) during heating.

4.4.7 FILLER/POLYMER ORIENTATION

Nearly all injection-moulded polymers are more or less oriented. The molecules tend to align themselves parallel to the flow direction during the viscous flow of the molten polymer. Hence the polymer orientation is no longer random, and part of this

orientation is retained in the moulded object as it cools [160]. In this case the polymer is spoken of as *preferentially oriented* or, more commonly, simply as *oriented* [162]. Preferential orientation of the polymer chains parallel in the injection direction can therefore result in optimal tensile and other mechanical properties.

Orientation can be predominantly either uniaxial or biaxial, but usually appears to be a combination of both [160]. Uniaxial orientation is easily accomplished by stretching a plastic bar or long strip in one direction at a temperature at which the polymer behaves as a rubber or very viscous liquid. The polymer chains or sections of the chains tend to line up parallel to the direction of stretching. Biaxial orientation results when a plastic sheet is stretched in two directions at right angles to each other so that the area of the sheet increases and its thickness decreases. The chain segments tend to line up parallel to the plane of the sheet but in a random direction in this plane [160].

For filled composites, the filler orientation in the matrix depends mostly on filler shape. In particular flake-like and needle shape filler particles tend to align themselves strongly parallel to the flow direction to reduce resistance between the filler particles and molten polymer. For this thesis, tensile specimens were produced by injection moulding. A mould was designed which consists of a gate at one end of each specimen, therefore, the flow direction is parallel to the longitudinal tensile specimen. The dimensions of the tensile specimen are shown in Figure 3.3. The use of coating agent moreover also affects the polymer and filler orientation leading to changes in mechanical properties as suggested by Nielsen, Bright and co-workers [154, 163]. Orientation can be measured by a number of methods. In crystalline polymers the orientation of the crystallites can be measured by X-ray diffraction. In this study, therefore X-ray diffraction was used to determine preferred orientation to relate its effect to mechanical properties. The polyethylene chain axes align in the *c* axis direction. This direction is parallel to the 200 planes and 110 planes [15-18]. Two biggest peaks of PE200 and PE110 can be ratioed to give an indication of two dimensional variation of polymer orientation (see Figure 4.32). The unit cell of

magnesium hydroxide is a hexagonal close packed structure and its basal plane lies in the 001 plane [30, 32] as illustrated in Figure 4.33. Filler orientation can, therefore, be determined from dividing the peak intensity of MH001 by MH101. By adjustment of processing conditions, non-direction flow (randomised) HDPE was produced to use as a base line for comparison. This is isotropic in plastic behaviour, either by achieving a completely random orientation of the crystals or by balancing two or more types of preferred orientation which are opposed in effect. X-ray diffraction patterns of HDPE show how preferred orientation arises when an isotropic (Appendix G.1(a)) and anisotropic samples (Appendix G.1(b)), produced using injection moulding, were compared. Figure 4.34 shows how polyethylene and magnesium hydroxide unit cells lie in the injection direction. The X-ray diffraction results of $\text{Mg}(\text{OH})_2$ filled HDPE containing magnesium and calcium stearate are shown as follows.

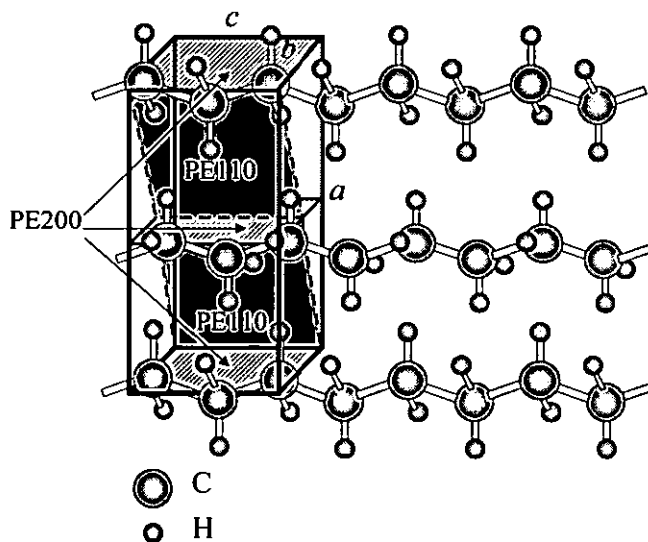


Figure 4.32: Base-centred orthorhombic structure [164] for polyethylene: $a = 7.40 \text{ \AA}$, $b = 4.93 \text{ \AA}$, $c = 2.53 \text{ \AA}$.

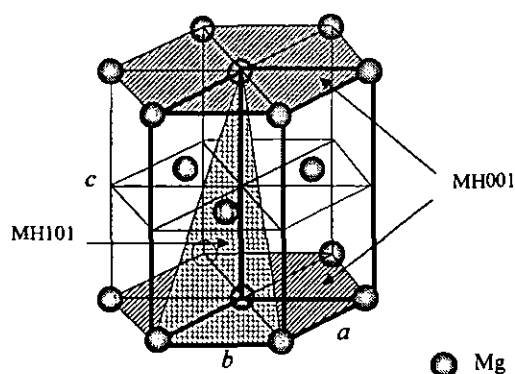


Figure 4.33: Hexagonal close-packed structure [164] for magnesium hydroxide:
 $a = b = 3.140 \text{ \AA}$, $c = 4.769 \text{ \AA}$.

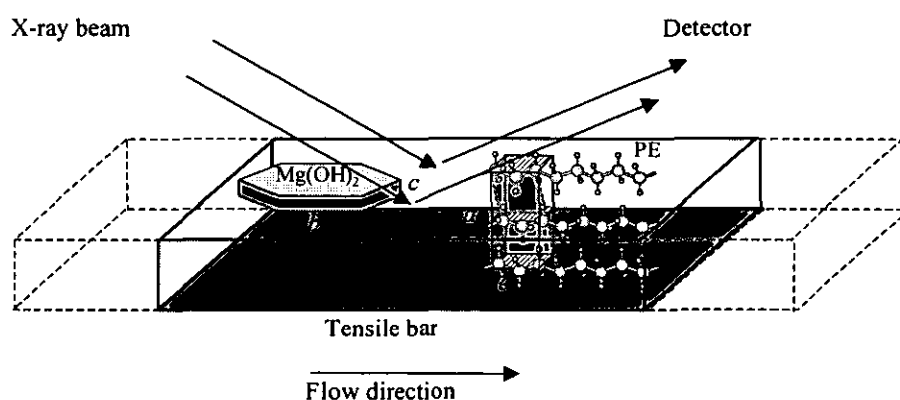


Figure 4.34: Scheme of test sample showing places and directions of the X-ray diffraction measurements and the orientation of the magnesium hydroxide and PE crystals.

4.4.7.1 Magnesium hydroxide modified with magnesium stearate.

Figure 4.35 shows that the injection moulding causes polymer deformation by reducing the intensity ratio of PE200/110 compared to isotropic HDPE. The PE200/110 intensity ratio increases with filler addition. It is clear that the degree of PE orientation in composites is considerably higher than PE alone. This result is in agreement with Rybnikar [165] who found that composites of polypropylene containing 5% talc show not only a preferred orientation of PP crystallites but also of talc. Compared with unmodified filled composite, the surface modification of filler give an increase in the intensity ratio PE200/110 with the maximum value observed at

one monolayer coverage. This ratio decreases with the presence of more than one monolayer of coating agent. This suggests a lower interfacial force at the interface and higher lubrication effect causing by excess coating agent in the system compared with one monolayer coating.

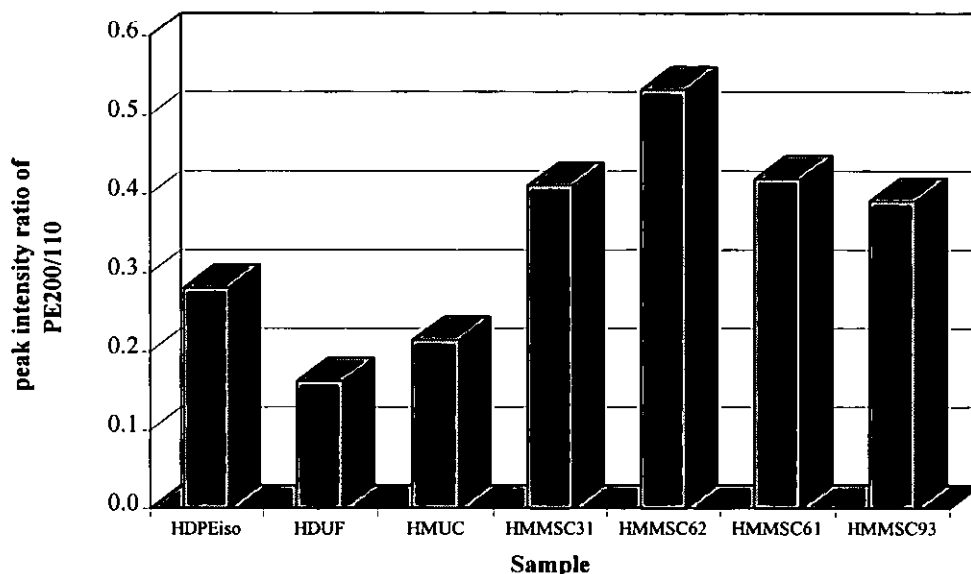


Figure 4.35: Plot of peak intensity ratio of PE200/110 for HDPE; isotropic, unfilled, and compounds containing $\text{Mg}(\text{OH})_2$ coated with various magnesium stearate concentrations.

The effect of HDPE orientation on machine performance was also studied by Guan and co-workers [92, 93]. They showed that the transmission pinhole pattern of samples without stress gave a number of sharp concentric rings indicating the crystallites are statistically random while that with stress showed an arclike shape. This effect arises from the orientation of the crystallites. The transmission pinhole pattern and X-ray diffraction pattern were also related. The sample showing an arclike pattern also showed increases in the intensity of PE 110, 200 and 020 peaks in the X-ray diffraction pattern. This implies that cylindrical distribution of the crystallographic planes (PE110, 200, 020) about the machine direction has increased. The increase in probability is most apparent for planes PE110 and PE200 relating to the probability that c axis orientation parallel to the machine direction has increased.

The enhanced alignment of 200 plane parallel to the surface can reasonably be expected to have some influence on the mechanical properties of the composites in the current work. For example, an increase in PE200/110 ratio for modified filled-composites relates to a decreased tensile/flexural modulus, and a increased elongation at yield/extension at maximum load compared to unmodified filled-compound. However, it is difficult to provide a simple explanation for this, since the PE200/110 intensity peak ratio correlates with polymer orientation in two dimensions only while the polymer structure is three dimensions which is much more complex.

Orientation has a significant effect on tensile strength and elongation at break [160]. Parallel to orientation the tensile strength is easily increased by at least 200 or even 500 percent. However, perpendicular to orientation the tensile strength may be only a half or a third of the tensile strength of an unoriented specimen. These effects are to be expected since parallel to the orientation, stresses are exerted largely on the primary bonds of the polymer chains, while in the direction perpendicular to the orientation, forces act to a large extent on the weak secondary bonds between polymer chains.

Filler orientation is determined from the peak intensity ratio of MH001/101. A greater value for this ratio indicates a higher number of filler particles with their basal planes [001] lying parallel to the specimen surface. The value of MH001/101 ratio taken from the magnesium hydroxide powder (randomised powder) is the value approximating to the value in the JCPDS X-ray powder diffraction file [140]. Therefore, this value is used as the basic line for comparison. Figure 4.36 shows that HDPE containing uncoated filler has a lower MH001/101 peak ratio than that containing coated filler. This implies that the magnesium hydroxide particles (plate-like structure) randomly align in the melted matrix when it is added to HDPE. The modification of filler surface with various magnesium stearate concentrations can improve the filler orientation, showing high values of MH001/101 ratio relating to increases in

elongation at yield and extension at load of their composites. 6.2% magnesium stearate coating is the optimum concentration giving the highest preferred orientation of filler. The mixing conditions also have an effect on the filler orientation as the surface of magnesium hydroxide may not be covered perfectly by magnesium stearate after a short period of coating (10 min), therefore the result shows a low value of MH001/101 in comparison with long period coating (40 min). However, it is also found that with the use of high coating levels (more than one monomolecular coverage) the filler particles and polymer molecules tend to lose orientation relating to the reduction of elongation at yield and extension at maximum load of filled composites. This implies that at a high concentration of magnesium stearate (9.3%), magnesium stearate molecules build up in a head to head configuration to form a molecular bilayer along filler surfaces (Figure 4.29(c)) or remained free (Figure 4.29(d)). Hence, coated magnesium hydroxide particles can easily slip in the polymer matrix during processing and lose their orientation. This result is in agreement with Coupland and co-workers [166].

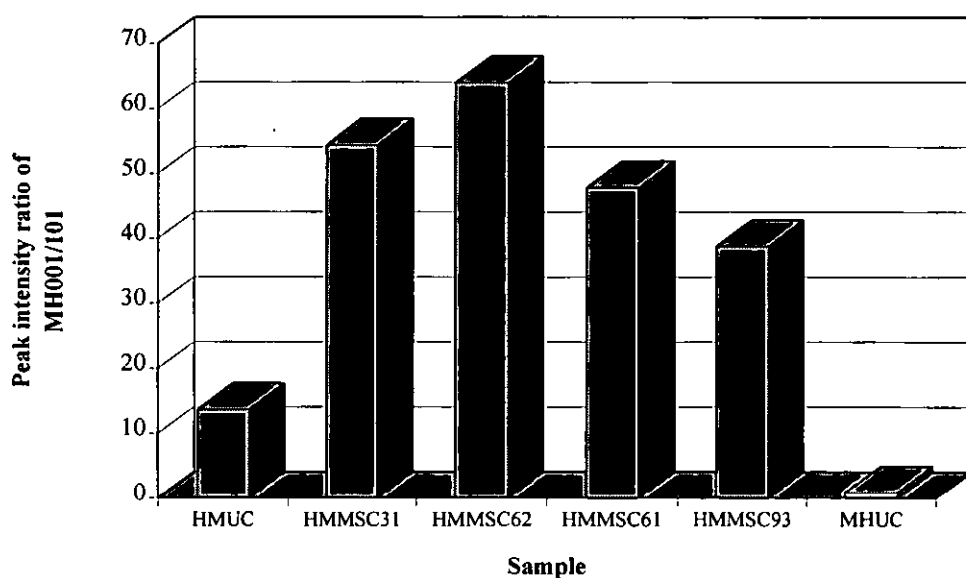


Figure 4.36: Plot of peak intensity ratio of MH001/101 for HDPE compounds containing $\text{Mg}(\text{OH})_2$ coated with various magnesium stearate concentrations and $\text{Mg}(\text{OH})_2$ powder.

4.4.7.2 Magnesium hydroxide modified with calcium stearate.

Figure 4.37 shows that again the peak intensity ratios of PE200/110 increase with addition of filler. Compared with unmodified filled-composite, the surface modification of filler with half monolayer coverage increases the intensity ratio of PE200/110 while this ratio seem to decrease with an increase in calcium stearate concentration. Unfilled HDPE gives the lowest ratio, filled polymer shows intermediate and modified filled-composites show the highest ratio. Again, the presence of a high concentration of coating agent (calcium stearate) leads to a reduction in polymer orientation.

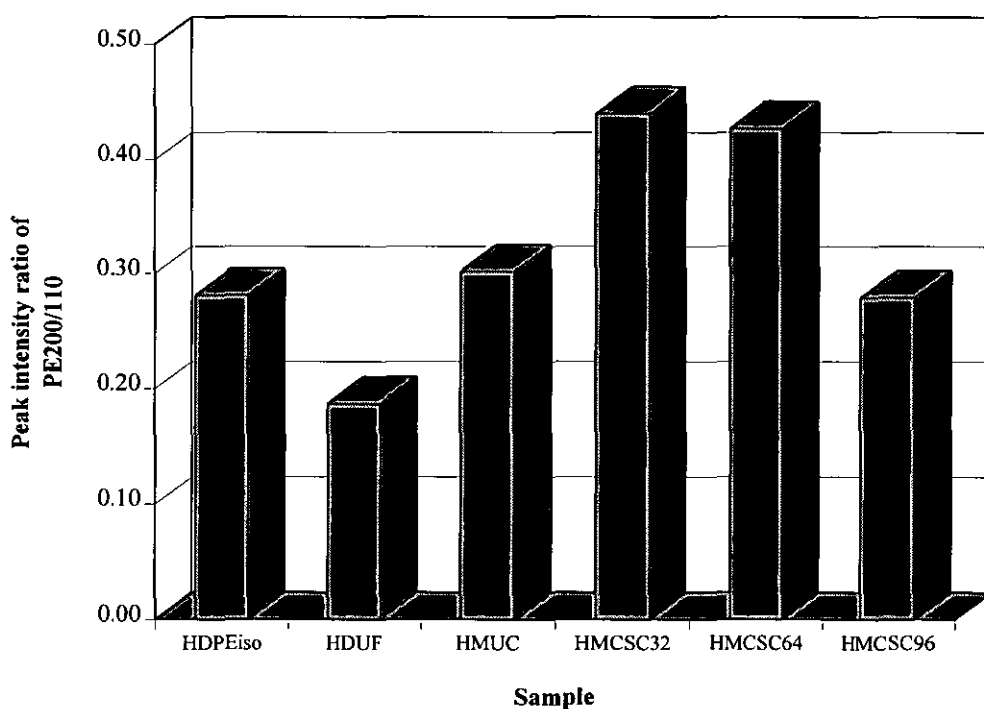


Figure 4.37: Plot of peak intensity ratio of PE200/110 for HDPE; isotropic, unfilled, and compounds containing $\text{Mg}(\text{OH})_2$ coated with various calcium stearate concentrations.

Comparing magnesium and calcium stearate coating, compounds containing $\text{Mg}(\text{OH})_2$ coated with magnesium stearate give slightly higher PE200/110 ratio of polymer orientation than those with calcium stearate. This may be caused by differences in the

mould characteristics/injection conditions, and also upgrading of injection machine. Samples containing magnesium stearate were prepared using a four part mould while samples containing calcium stearate were produced from a four piece tensile mould (characteristics of both moulds were shown in Figure 3.3), therefore the degree of polymer orientation could be different.

Again, Figure 4.38 shows that the lowest ratio of MH001/101 is obtained from the magnesium hydroxide powder (as above). HDPE containing uncoated filler has a lower MH001/101 peak ratio than that containing coated filler. The modification of filler surface with various calcium stearate concentrations can further improve the filler orientation reflecting an increase in elongation at yield and extension at maximum load. A 6.4% calcium stearate coating is the optimum concentration that gives the highest preferred orientation of filler.

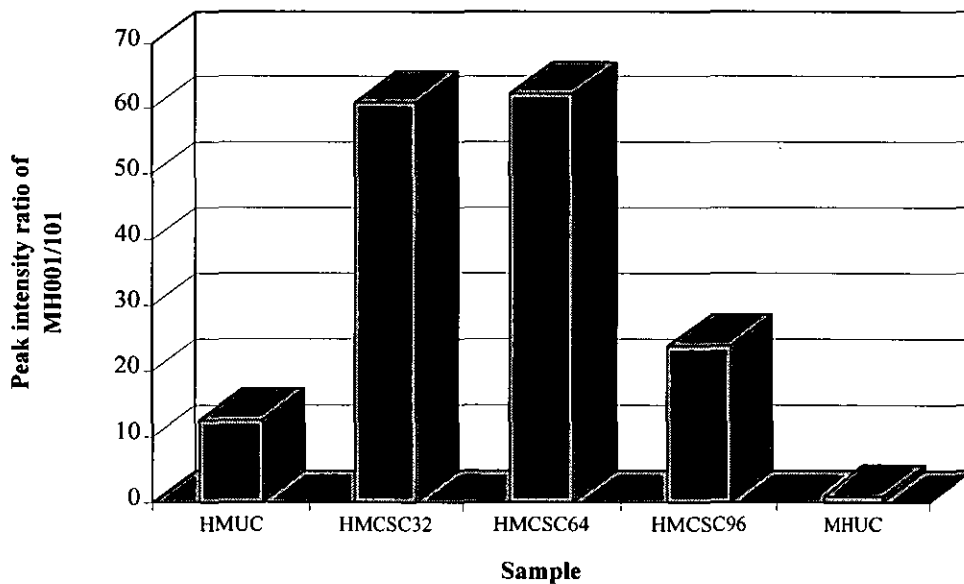


Figure 4.38: Plot of peak intensity ratio of MH001/101 for HDPE compounds containing $\text{Mg}(\text{OH})_2$ coated with various calcium stearate concentrations and $\text{Mg}(\text{OH})_2$ powder.

However, $\text{Mg}(\text{OH})_2$ filled compound with a 1.5 monolayer of calcium stearate coating shows a lower filler orientation than that of magnesium stearate coating. This is not

readily explained but it may be because calcium stearate is more able to lubricate than magnesium stearate, therefore, the surfaces of magnesium hydroxide coated with excess calcium stearate are more slippery than those coated with excess magnesium stearate resulting in less filler orientation for the sample containing excess calcium stearate coating.

4.4.8 SURFACE FREE ENERGY

Surface free energies of uncoated/coated fillers and coating agents have been discussed earlier (4.2.3). The contact angle on an exterior surface of the mould sample of all composites was measured with four different liquid types. The surface free energies calculated from the contact angles of composites are shown in Table 4.7.

Table 4.7: Contact angle measurement and surface free energies (average of 5 tests).

Code	Contact angle (degree)				Surface free energy (mJm ⁻²)
	Water	Glycerol	DIM	BNL	
HDUF	94.4	79.0	55.4	43.8	32.92
HMUC	89.2	72.6	53.6	31.0	36.82
HMCS32	92.0	74.8	55.0	34.0	35.51
HMCS64	93.6	75.6	57.6	39.4	33.80
HMCS96	93.8	76.8	58.8	38.0	33.52

Table 4.7 shows that the surface free energy of composites slightly increases with the filler addition, since magnesium hydroxide has higher surface free energy than HDPE. Compared with uncoated filled-composite, the surface free energy of coated filled-composites gradually decreases with increased amount of coating agent applied because of the fact that the coating agent has a lower surface free energy than magnesium hydroxide (see section 4.2.3). However, surface free energy of all composites are nearly equal (34 ± 2 mJ/m²). This implies that when a polymer melts and is injected into a mould cavity, the filler particles are totally covered by the matrix. In injection moulding polymer is melted, mixed with filler and become a

viscous fluid before it is injected into the mould cavity by applying large forces. The mould is filled with melt and solidification starts. An additional amount of melt must be packed into the mould to offset polymer shrinkage during solidification and to achieve an accurate reproduction of the mould. Therefore, the wall region of specimen usually contains only polyethylene resulting in the similar values for the surface free energy. This also may be due to contamination on specimen surfaces from spraying the mould with releasing agent.

4.5 SUMMARY

The effects of various magnesium and calcium stearate concentrations coated on magnesium hydroxide on mechanical properties of filled HDPE have been studied. The results of this study showed that :

- increased temperature of mixing is a significant factor affecting the coating performance while increased coating time after temperature reaches the melting point of coating agents is a minor factor;
- DRIFT is an useful technique which can be used to differentiate between melted and unmelted coating agents on magnesium hydroxide surfaces;
- thermal analysis showed a decreased amount of a polymorphic C-form with increased coating time. Other polymorphic structures (A- and B-form) were detectable during coating process for magnesium stearate coating while they were undetectable for calcium stearate coating;
- X-ray diffraction can be used to identify monolayers of coating agent on filler surfaces and also for investigating of polymer/filler orientation;
- surface free energy of magnesium hydroxide decreased when the filler was modified with calcium stearate which led to a better dispersion and wettability of coated filler in the molten HDPE;

- one monolayer is the optimum coverage to obtain the characteristics at the filler/polymer interface leading to the best mechanical properties of filled composites (i.e. greatest impact toughness);
- surface modification of magnesium hydroxide with one monolayer of coating agent improved mechanical properties of filled composites, such as increase in elongation at yield/ extension at load, and increase in peak force, and peak/failure energies for impact properties. Filled composites containing magnesium stearate coatings showed higher toughness than with stearic acid;
- coating agents act as nucleating and lubricating agents at the same time. Therefore, a modification of filler results in an increase in crystallinity, decrease in melting temperature of modified $\text{Mg}(\text{OH})_2$ composites and also improved filler/polymer orientation of composites.

CHAPTER 5

RESULTS AND DISCUSSION: SERIES II

THE EFFECTS OF VARIOUS COATING AGENT TYPES ON PROPERTIES OF $Mg(OH)_2$ AND $CaCO_3$ FILLED HDPE : SERIES II

From the previous chapter, one monolayer coverage of coating on magnesium hydroxide gave the best properties, while the optimum coating conditions in the Fielder mixer were 140°C for 40 minutes. In order to understand further the effects of various filler and coating agent types, magnesium hydroxide and calcium carbonate were used as fillers. They were coated with one monolayer of various coating agents i.e. magnesium stearate, calcium stearate, zinc stearate, and stearic acid using the Fielder mixer. The mixing conditions were also the same as Series I (140°C for 40 minutes). In practice one monolayer coverage of magnesium hydroxide corresponds to 6.0% w/w stearic acid which is equivalent to 6.2% w/w magnesium stearate, 6.4% w/w calcium stearate, and 6.7% w/w zinc stearate, respectively (the calculations are shown in Appendix D.2). Similarly one monolayer of calcium carbonate theoretically corresponds to 4.0% w/w stearic acid which is equivalent to 4.2% w/w magnesium stearate, 4.3% w/w calcium stearate, and 4.5% w/w zinc stearate. Effects of coating conditions on mechanical properties of compounds was also considered, therefore mixtures of 6.2% w/w magnesium stearate and magnesium hydroxide, and 4.3% w/w calcium stearate and calcium carbonate were prepared using the Fielder mixer at low mixing speed and room temperature.

The results and discussion are divided into three main sections. The first section is concerned with characterisation of the coated fillers. The second section is the effect of coating agents on filled compound properties. The final section discusses the effect of coating agents on polymer properties.

5.1. CHARACTERISATION OF COATED FILLERS

To understand the effect of coating fillers on the mechanical properties of resulting composites, a variety of fundamental techniques were used to characterise the fillers. This included Fourier transform infrared spectroscopy, thermal analysis, X-ray diffraction and X-ray photoelectron spectroscopy.

5.1.1 FOURIER TRANSFORM INFRARED SPECTROSCOPY (FTIR)

Two FTIR analysis techniques are used for different purposes. The DRIFT technique was used for characterising filler, both modified magnesium hydroxide and calcium carbonate, samples taken from the Fielder Mixer at 10 minute intervals, to examine coating efficiencies for the fillers modified with various coating agents. The transmission technique was used to examine the final products of coated fillers extracted by toluene to investigate the adsorption/deposition of each individual coating agent on filler surfaces.

5.1.1.1 DRIFT technique

The FTIR spectra of unmodified magnesium hydroxide and magnesium hydroxide modified with one monolayer of various stearate types using a coating time of 40 minutes are shown in Figure 5.1. For modified $\text{Mg}(\text{OH})_2$, integrated absorbances of the CH peak at $2767\text{-}3078\text{ cm}^{-1}$ and COO^- band at $1327\text{-}1648\text{ cm}^{-1}$ from metal stearates and stearic acid are ratioed to that of the OH peak at 3697 cm^{-1} from the magnesium hydroxide. Results for CH/OH, COO^-/OH ratios for modified $\text{Mg}(\text{OH})_2$ against coating time are shown in Figures 5.2 and 5.3, respectively.

From Figure 5.1, the FTIR spectrum for magnesium hydroxide with magnesium stearate added (the third spectrum from the bottom : MMSA62), which was prepared using a low mixing speed at room temperature shows that the RCOO^- band contains

several peaks having the middle peak at 1580 cm^{-1} . On the other hand the spectra of all coated fillers prepared using the Fielder mixer at high speed and temperature do not have this middle peak in the RCOO^- band. This implies melting or changing in crystalline structure of coating agents at high mixing speed and temperature. Under these conditions the coating agents are melted and coated on to the magnesium hydroxide surfaces. These results are consistent with those from Series I which showed that the middle peak in the RCOO^- band disappeared when the temperature rose to the melting point of the coating agents. Therefore, it reveals that the effectiveness of coating depends upon the coating agent properties and also the mixing conditions. The area under the CH band of samples coated with zinc stearate was found to be greater than other samples. It is possible that zinc stearate gives a more an effective coating than other stearates.

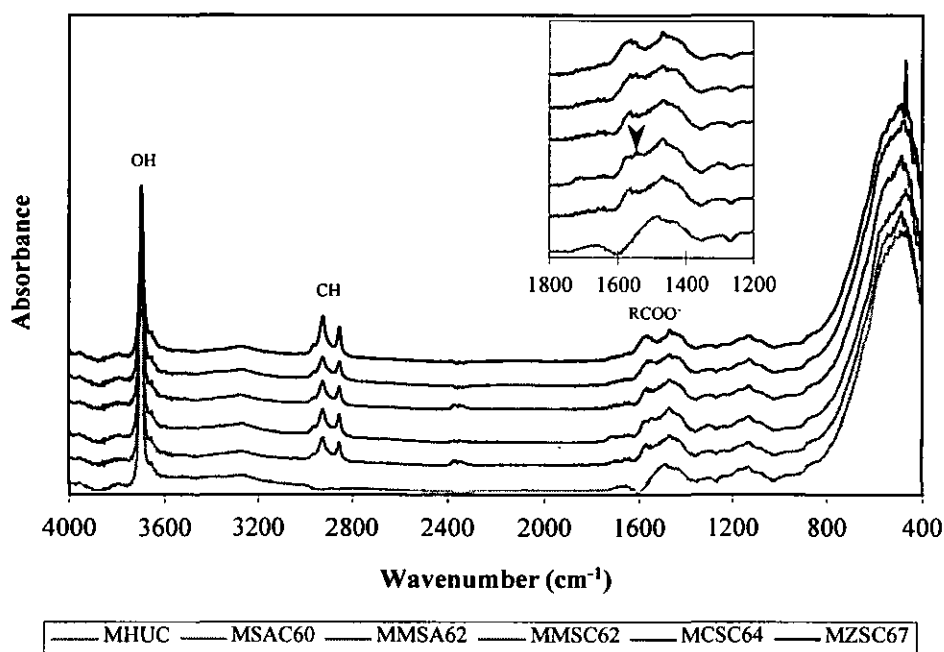


Figure 5.1: FTIR spectra of $\text{Mg}(\text{OH})_2$ uncoated and coated with 6.2% magnesium stearate, 6.4% calcium stearate, 6.7% zinc stearate, 6.0% stearic acid and $\text{Mg}(\text{OH})_2$ with 6.2% magnesium stearate added after 40 minutes coating in the Fielder mixer.

It is seen from Figure 5.2 that the CH/OH ratios for most coated magnesium hydroxides increase with increased coating time and reach a plateau region after about

20 minutes, except for the calcium stearate coated sample. This result implies that the coating agents are increasingly melted and mixed with magnesium hydroxide particles during the initial period. After 20 minutes of mixing coating agents are fully melted and coated on to $\text{Mg}(\text{OH})_2$. Zinc stearate gives the highest CH/OH ratio. This is not fully understood but it may be because of characteristics of zinc stearate such as its fluffy properties. Consistent with Series I, stearic acid produced smaller CH/OH ratios in comparison with metal stearates. Stearic acid and zinc stearate may also react with magnesium hydroxide producing magnesium stearate as shown in Equations 4.1 and 4.4. FTIR transmission spectra of both coated fillers are shown in Appendix F.2(c) and (d). Magnesium hydroxide with added magnesium stearate shows ratios that are fairly constant with increased coating time indicating no phase transformation when a low speed of mixing at room temperature is used. The RCOO⁻/OH ratios represented in Figure 5.3 are found mostly constant with an increase in coating time. It may be to difficult to detect small changes in carboxylate groups of coating agents coated on fillers during mixing.

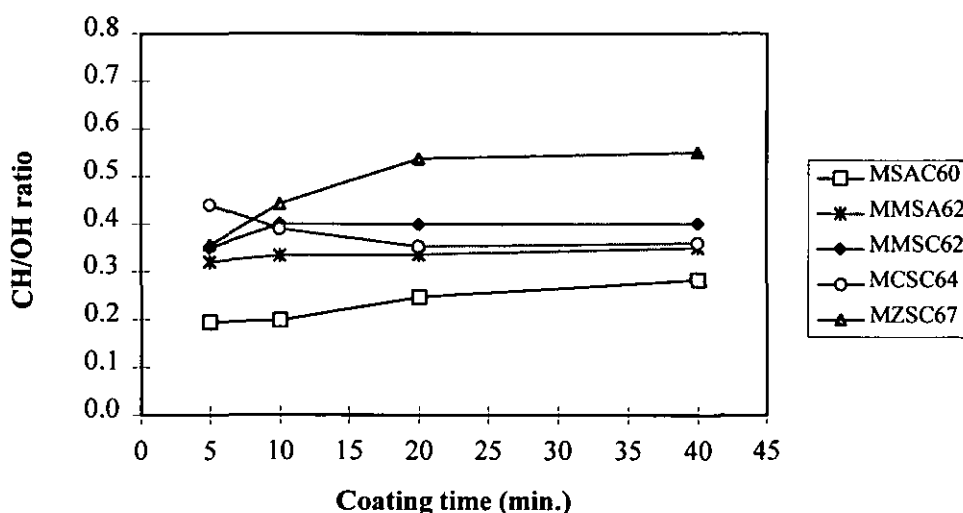


Figure 5.2: CH/OH ratio versus time for magnesium hydroxide coated with metal stearates and stearic acid in the Fielder high speed mixer.

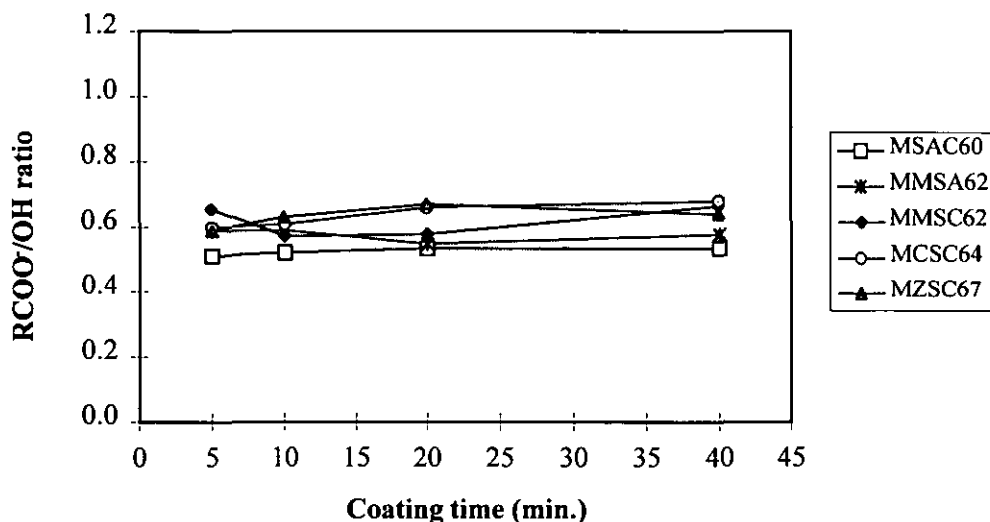


Figure 5.3: RCOO⁻/OH ratio versus time for magnesium hydroxide coated with metal stearates and stearic acid in the Fielder high speed mixer.

The FTIR spectra of unmodified calcium carbonate and calcium carbonate modified with one monolayer of various stearates after coating for 40 minutes are shown in Figure 5.4. In order to determine the efficiency of filler coating, the integrated absorbances of the CH peak corresponding to metal stearates and stearic acid are ratioed to the combination vibration of the CO peak at 2395-2700 cm⁻¹ due to CaCO₃. Since the COO⁻ band from metal stearates and stearic acid (1600-1800 cm⁻¹) is at the same position as the fundamental vibration of the CO peak from CaCO₃, the ratio of COO⁻/CO cannot be determined for the modified calcium carbonate. Results for CH/CO ratios from modified CaCO₃ against coating time are shown in Figure 5.5.

Figure 5.4 shows that the samples treated with metal stearates and stearic acid give an increase in absorbance intensities at 2800-3000 cm⁻¹, which may be assigned to C-H vibrations in the alkyl chain of the stearates. The samples coated with stearic acid and zinc stearate show greater integrated absorbance for the CH band than the samples with coated/added calcium stearate and magnesium stearate. These results can be observed from the CH/CO ratio in Figure 5.5.

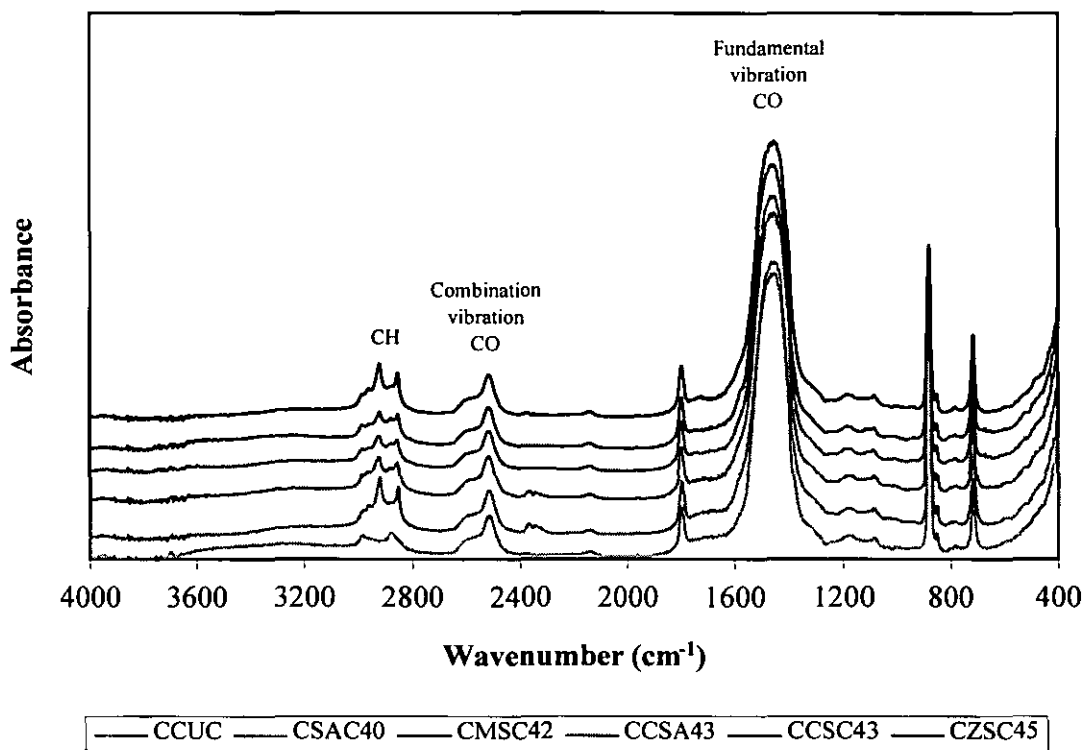


Figure 5.4: FTIR spectra of CaCO_3 uncoated and coated with 4.2% magnesium stearate, 4.3% calcium stearate, 4.5% zinc stearate, 4.0% stearic acid and CaCO_3 with 4.2% magnesium stearate added after 40 minutes coating in the Fielder mixer.

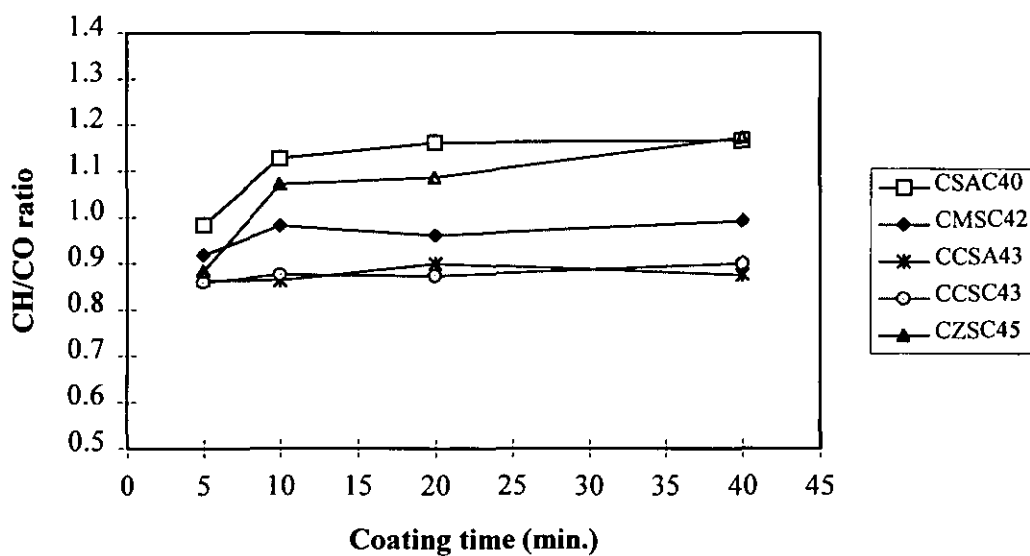


Figure 5.5: CH/CO ratio versus time for calcium carbonate coated with metal stearates and stearic acid in the Fielder high speed mixer.

Figure 5.5 reveals that the CH/CO ratios of most coating agents increase with increased time up to 20 minutes and then become constant. Calcium carbonate both coated with calcium stearate and with calcium stearate “added” give the lowest value of the CH/CO ratio. It is seen from DRIFT results in Figure 5.2 and 5.5 that stearic acid appears to be the best coating agent for calcium carbonate but it is the poorest coating for magnesium hydroxide. This result is not fully understood, but it may be due to free stearate (C-form) component produced during the coating of calcium carbonate with stearic acid, which is detected by DSC as shown in section 5.1.2.2 (Figure 5.7(d)). For both fillers coated with metal stearates, the amount of detected coating decreases as follows:

zinc stearate > magnesium stearate > calcium stearate

5.1.1.2 Transmission technique

Final products of coated fillers (at 40 minutes coating time) were extracted with toluene for 20 hours as described in chapter 3. Extracts were investigated using the FTIR transmission technique. The spectra of coating agents and extracted samples are shown in Appendices F.1-F.3.

It was found that FTIR spectra of samples extracted from $\text{Mg}(\text{OH})_2$ coated with stearic acid, magnesium or zinc stearate all showed similar characteristics to the spectrum obtained from magnesium stearate (see Appendix F.2). Initial tests had shown that stearic acid and all three metal stearates were soluble in toluene at high temperature, however it is possible that once the magnesium hydroxide is coated with zinc stearate a reaction may occur that might affect the solubility of the coating. Another possibility is that at the interfaces of both $\text{Mg}(\text{OH})_2$ /stearic acid and $\text{Mg}(\text{OH})_2$ /zinc stearate there may be a chemical reaction or an ion exchange between filler/coating producing magnesium stearate according to Equations 4.1 and 4.4. The presence of magnesium stearate and the absence of zinc stearate in the toluene extract is quite clear, however it is not possible to preclude the possibility that the reaction in

Equation 4.4 occurred during solvent extraction rather than at the mixing stage. In the case of $\text{Mg}(\text{OH})_2$ /magnesium stearate interface no ion exchange occurs as both substances contain Mg^{2+} ion. The extracted sample from calcium stearate coated- $\text{Mg}(\text{OH})_2$ illustrates the spectrum of a mixture containing calcium stearate and an unknown substance. It is difficult to identify the unknown substance but it is presumed to be ketone as reported by Reid [168] that ketone may be produced when the calcium salt loses carbon dioxide from its molecule.

Compared to magnesium hydroxide, calcium carbonate is more inert to chemical reaction. The FTIR spectra of samples extracted from coated CaCO_3 show that no chemical reaction between any of the metal stearates and CaCO_3 occur (see Appendix F.3(a)-(c)). The extracted sample of zinc stearate coated- CaCO_3 shows a combination spectrum which includes zinc stearate and an unknown substance. Stearic acid is the only coating agent which reacts with calcium carbonate to produce calcium stearate or a new substance (see the spectrum in Appendix F.3 (d)). These results are consistent with the DSC examination. However, it is not fully understood how stearic acid interacts with calcium carbonate during the coating process but stearic acid may react with calcium carbonate according to Equations 4.2 or 4.3.

5.1.2 THERMAL ANALYSIS

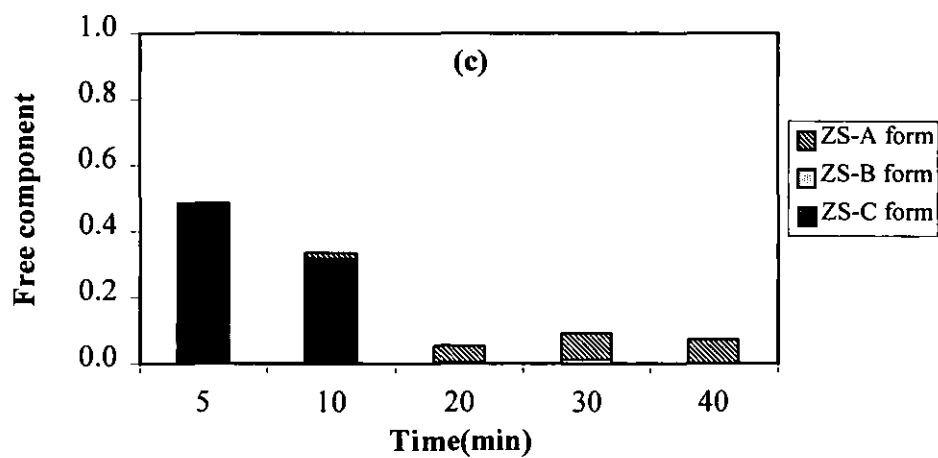
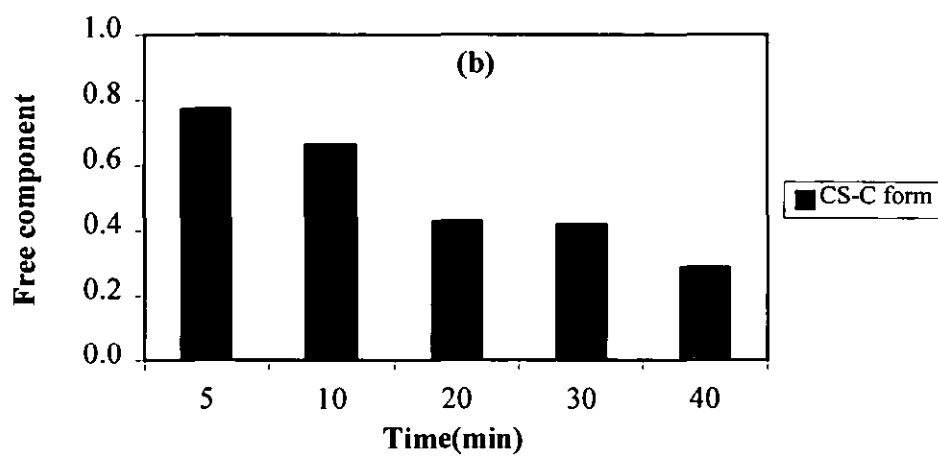
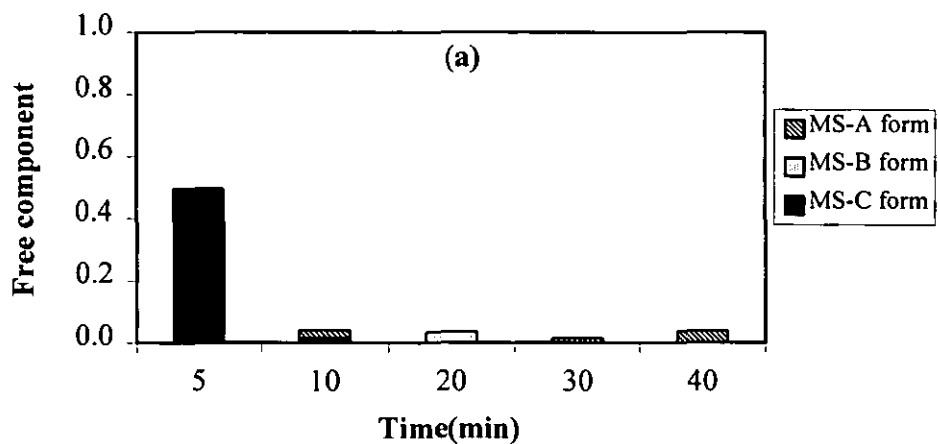
The melting temperature and heat of fusion of monolayer coated fillers was examined and analysed using a thermal analyser fitted with DSC cell. Metal stearates and stearic acid are polymorphic materials which show multiple transition stages when they are heated [64, 169, 170]. Each transition corresponds to a change of one crystal form to another form at a specific temperature. In this study, transitions have been detected at three temperature ranges for coated fillers as indicated in section 4.3.1. DSC traces of these coated fillers, magnesium hydroxide and calcium carbonate, are shown in Appendices E.2 and E.3. The thermal analysis data of free components were calculated from the heat of fusion divided by the heat of fusion of stearates/acid ratioed to stearate/acid concentration. An example of calculation was shown in

chapter 4 (section 4.3.1). A summary of the free components detected is shown in Figures 5.6 and 5.7 for coated magnesium hydroxide and calcium carbonate, respectively.

5.1.2.1 Magnesium hydroxide modified with various coating agent types.

Using data calculated from DSC traces for coated magnesium hydroxide samples, it is shown in Figure 5.6 that the amount of free mesomorphic C-form obviously decreases with increased coating time. It implies that free particles of coating agent are progressively deposited upon the magnesium hydroxide surfaces during the mixing process. Figure 5.6(a) for magnesium hydroxide coated with magnesium stearate shows that after 5 minutes of coating, some of magnesium stearate has been deposited on magnesium hydroxide and the other particles are free in the mixture. The amount of free magnesium stearate particles (C-form) rapidly decreases and a small amount of the A-forms of magnesium stearate are produced after 10 minutes. A change in form between A- and B-form is observed after 20 minutes of coating. A small amount of free particle (A-form) remains in the end product.

Magnesium hydroxide coated with calcium stearate shows a progressive decrease of free calcium stearate component with coating time as shown in Figure 5.6(b). Similar to the result from Series I, only C-form of polymorphic structure has been detected during the melting of calcium stearate. This result is in agreement with Rek [146] who reported that polymorphic forms become more stable with an increase in atomic weight of cation.



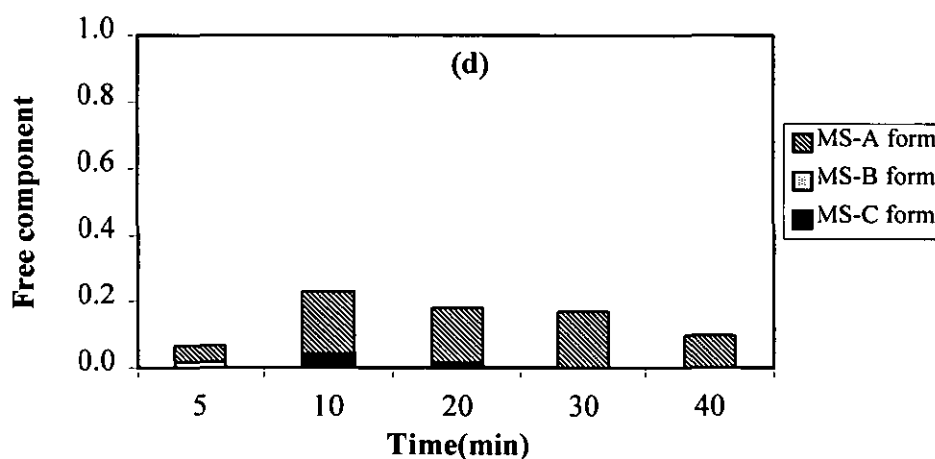


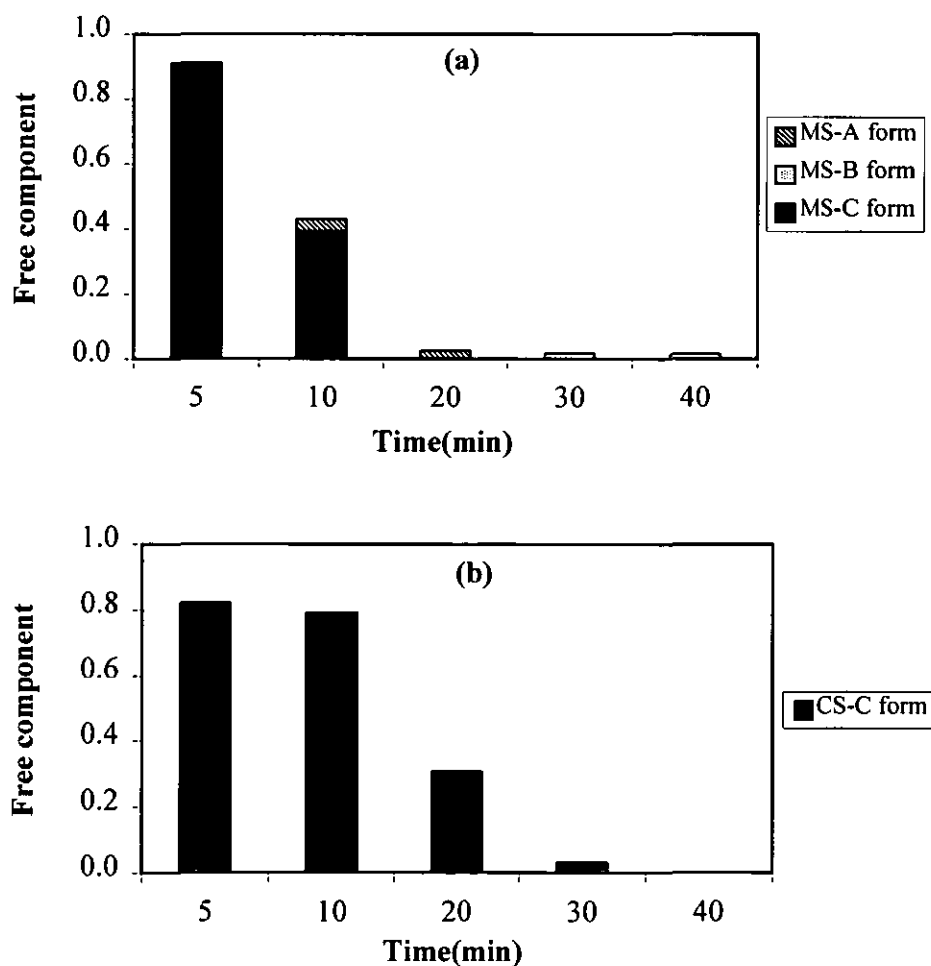
Figure 5.6: Free components versus coating time for magnesium hydroxide coated with one monolayer of different coating agent types: a) magnesium stearate, b) calcium stearate, c) zinc stearate and d) stearic acid.

Figure 5.6 (c) shows DSC results for magnesium hydroxide coated with zinc stearate. The amount of free zinc stearate particles (C-form) progressively decrease when the coating is carried out for longer periods. An A-mesomorphic structure is produced after 10 minutes and gradually increases over 30 minutes. After 30 minutes a small amount of B-form is detected. The final product shows a residue of free component of A-form only. Results for magnesium hydroxide coated with stearic acid magnesium stearate are shown in Figure 5.6(d). It is found that the A- and B-mesomorphic structure of magnesium stearate are produced during the initial period of coating. As expected C-form also is detected. The amount of A- and C-form decrease when the sample was left in the mixer for a longer period. However, A-form still remains in the end product. These results suggest that there are interactions/reactions between stearic acid and magnesium hydroxide producing magnesium stearate (C-form). This magnesium stearate may change to A- and B-form during heating. This result is consistent with FTIR results that show magnesium stearate in the spectrum after an extraction of stearic acid coated-Mg(OH)₂ with toluene. The spectra of extracted magnesium hydroxide samples are shown in Appendix F.2. Moreover, these results are consistent with those of Markley, Gardiner

et. al., and McBain and Lee [64, 169, 170] who report that the alkali metal salts of fatty acid produce several transitions when they are heated. This is because these compounds can exist in several polymorphic forms and may show one or more transitions of unstable forms during heating.

5.1.2.2 Calcium carbonate modified with various coating agent types.

Figure 5.7 shows the DSC results obtained from the coating of calcium carbonate with various types of coating agent. Figure 5.7(a) for calcium carbonate coated with magnesium stearate shows that the amount of free stearate (C-form) rapidly reduces with longer coating time. A little mesomorphic A-form is produced after 10 minutes. The decrease of A-form continues and disappears after 30 minutes, then B-form is detected. The final product contains a small amount of B-form.



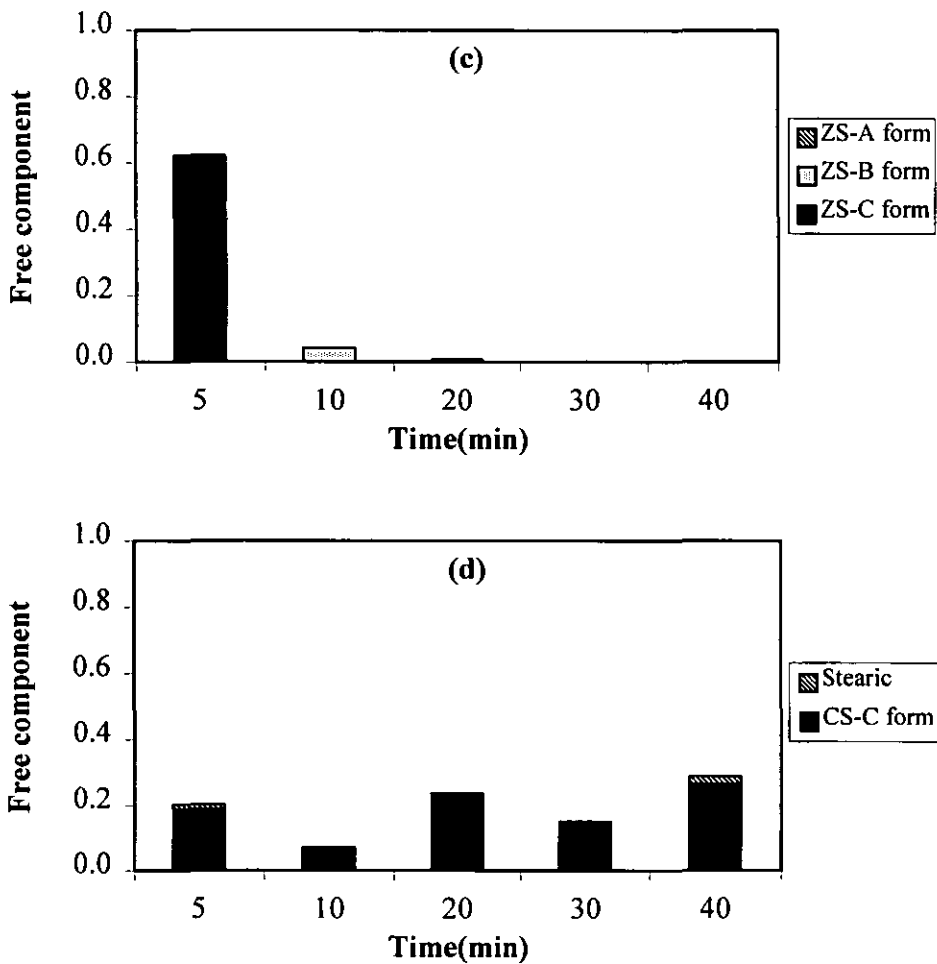


Figure 5.7: Free components versus coating time for calcium carbonate coated with one monolayer of different coating agent types: a) magnesium stearate, b) calcium stearate, c) zinc stearate and d) stearic acid.

Figure 5.7(b) illustrates the reduction of free stearate (C-form) during the calcium stearate coating of calcium carbonate. Like magnesium hydroxide coating (Figure 5.6(b)), calcium carbonate coated with calcium stearate shows only one mesomorphic structure. No free calcium stearate is detected at the end of coating. This suggests that all free calcium stearate adsorbs on calcium carbonate surfaces without changing form. Figure 5.7(c) for calcium carbonate coated with zinc stearate shows a disappearance of free stearate (C-form) particles, which indicates the deposition of coating agent on the filler surfaces. A free mesomorphic B-form component is found

after 10 minutes of coating. After 20 minutes B-form vanishes while a small amount of A-form is found. However, all components have disappeared after the final period of coating. Again, no reaction between zinc stearate and calcium carbonate is found. Figure 5.7(d) shows that when calcium carbonate is coated with stearic acid, substantial free stearate (C-form) is detected while a small amount of free stearic acid is also found. It suggests that stearic acid may react with calcium carbonate following Equation 4.2 or 4.3. This is supported by the FTIR result (as shown in Appendix F.3(d)).

As a result of high mixing speed and temperature, it is possible that all coating agents may coat on magnesium hydroxide/calcium carbonate surfaces as a very thin film, which cannot be detected using the DSC technique. This agrees with results obtained from X-ray diffraction as discussed in next section. Calcium stearate disappears more slowly than magnesium stearate and (in order) than zinc stearate with magnesium hydroxide, when the filler is calcium carbonate, the reverse is true.

5.1.3 X-RAY DIFFRACTION (XRD)

To study the surface coating of fillers, X-ray diffraction was used to determine the crystal structure of both free particles of coating agents and coating agents deposited on filler surfaces. Samples of uncoated and coated magnesium hydroxide extracted from the Fielder mixer at various coating times were scanned from 19 to 24 degree 2θ in which region magnesium hydroxide gives an X-ray pattern corresponding to a flat line (only background). The XRD patterns of magnesium hydroxide with 6.2% magnesium stearate added (low mixing speed and temperature), and magnesium hydroxide coated with 6.2% magnesium stearate, 6.4% calcium stearate, 6.7% zinc stearate, and 6.0% stearic acid (high mixing speed and temperature) are shown in Figures 5.8 to 5.12, respectively.

Figure 5.8 shows that after 5 minutes the mixing between magnesium hydroxide and magnesium stearate is not achieved and the magnesium hydroxide pattern is observed

at the beginning of mixing. After 10 minutes the magnesium stearate pattern appears and remains until the end of the coating process. After 20 minutes more mixing will have occurred and the coating is probably deposited on the filler surface. Little further change occurs as mixing time is increased to 40 minutes. This indicates neither melting of nor changing in crystalline structure of magnesium stearate because the added sample is prepared using low mixing speed and temperature. Hence, the coverage of the filler with the coating agent has not been completely melted.

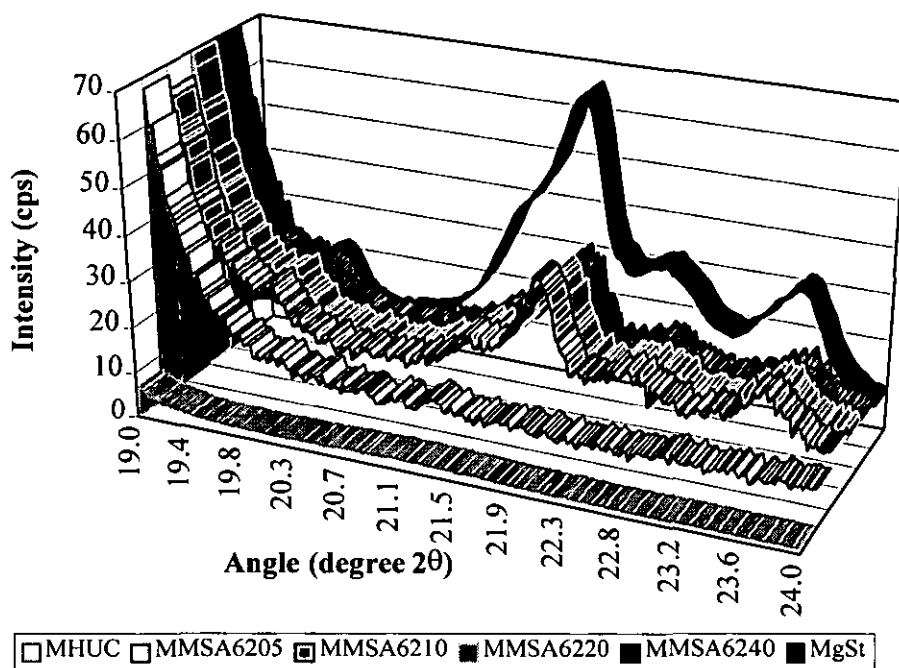


Figure 5.8: X-ray diffraction patterns of magnesium hydroxide with 6.2% w/w magnesium stearate added taken from the Fielder mixer after 5 min, 10 min, 20 min, 40 min, and magnesium stearate.

X-ray results of magnesium hydroxide coated with 6.2% w/w magnesium stearate as shown in Figure 5.9 reveal that after 5 minutes of mixing magnesium stearate has already melted and deposited on magnesium hydroxide surfaces due to the high mixing speed and temperature, showing one single broad peak patterns for all coating time. It suggests that there is complete coating and no chemical reaction between magnesium hydroxide and magnesium stearate. The X-ray diffraction technique can detect a change

in crystal structure of magnesium stearate from free particles to thin film layer coated on magnesium hydroxide. Since the X-ray patterns of coated samples at all coating times show a single broad peak rather than multiple peaks, a monolayer of magnesium stearate coated on magnesium hydroxide may have been produced and the thin layer of adsorbed magnesium stearate on magnesium hydroxide surfaces can not recrystallise to the former crystalline structure of free magnesium stearate particles. This result is consistent with that reported by Jefferson [171] who states that the crystal structure of stearic acid and metal stearates consist of bilayers of molecules (head to head or tail to tail) aligned perpendicular to the horizontal plane. Therefore, at one monolayer coverage of magnesium hydroxide the X-ray diffraction pattern shows one single broad peak representing the deposited coating agent.

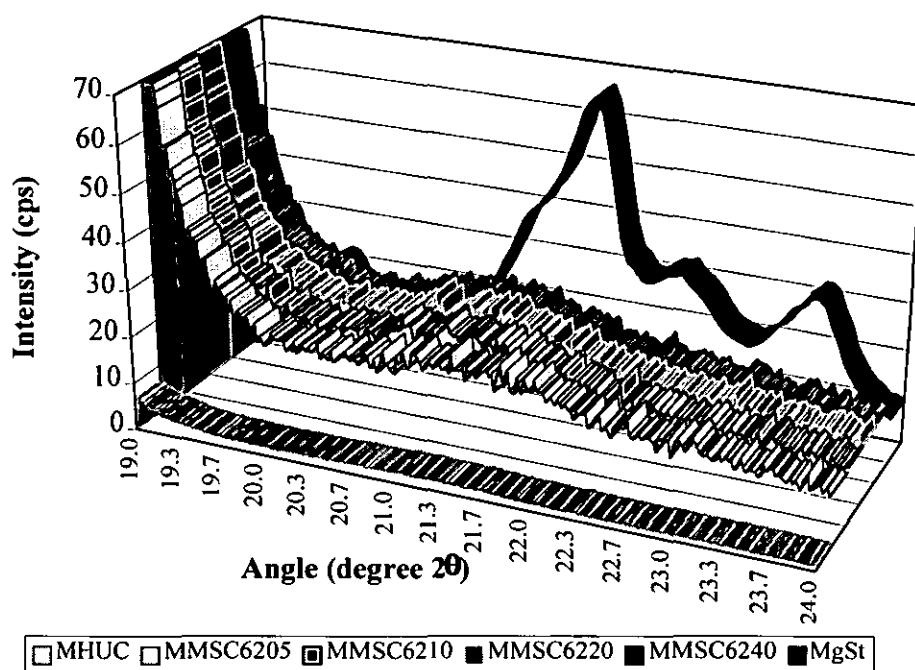


Figure 5.9: X-ray diffraction patterns of magnesium hydroxide coated with 6.2% w/w magnesium stearate taken from the Fielder mixer after 5 min, 10 min, 20 min, 40 min and magnesium stearate.

Figure 5.10 shows that at the beginning of mixing X-ray patterns of magnesium hydroxide coated with calcium stearate are characteristic of calcium stearate. It

indicates that there are some free calcium stearate particles in the mixture. Free calcium stearate particles gradually deposit upon the filler surfaces during progressive mixing. This is observed from the change of X-ray patterns from a set of several peaks to a single broad peak by the end of mixing. They may be explained by the fact that calcium stearate is more difficult than magnesium stearate to change from free particles to a thin film layer due to its higher melting point.

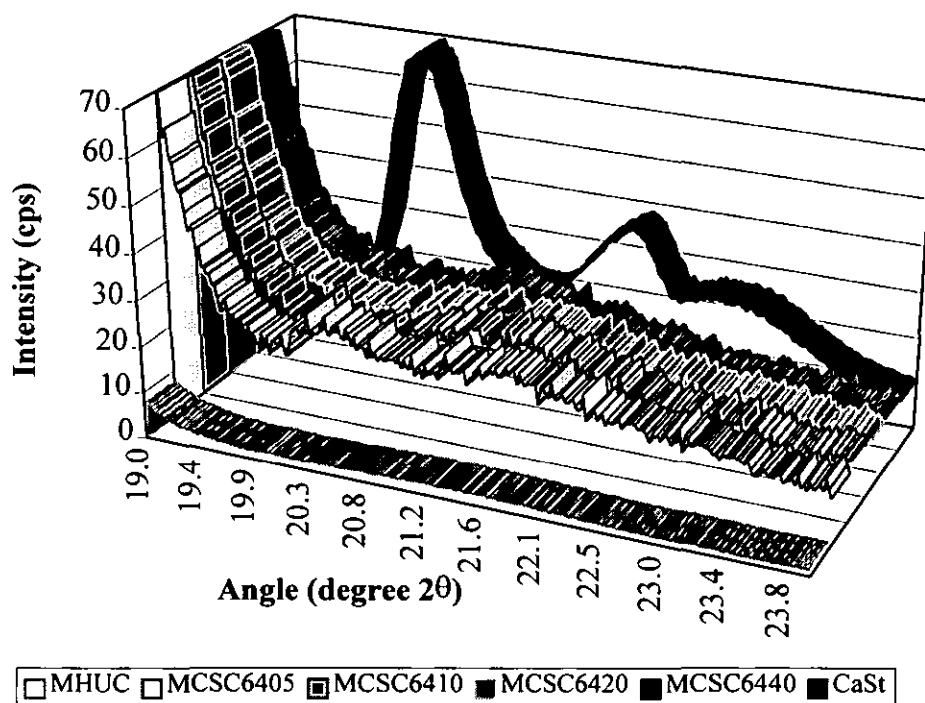


Figure 5.10: X-ray diffraction patterns of magnesium hydroxide coated with 6.4% w/w calcium stearate taken from the Fielder mixer after 5 min, 10 min, 20 min, 40 min and calcium stearate.

X-ray patterns of magnesium hydroxide coated with zinc stearate as shown in Figure 5.11 indicate that free particles of zinc stearate are detected from the beginning until 10 minutes of mixing and after that the particles melt and deposit upon the magnesium hydroxide surfaces. This results in the changing X-ray patterns from multiple peaks to one single broad peak. It implies that zinc stearate (free particles) melts and coats as a thin film on the filler surfaces. Therefore, crystalline structure has been detected. Again, since the zinc stearate coating is one monolayer coverage

the coating layer is not thick enough to reform the former crystalline structure, so only one broad peak is detected from X-ray diffraction.

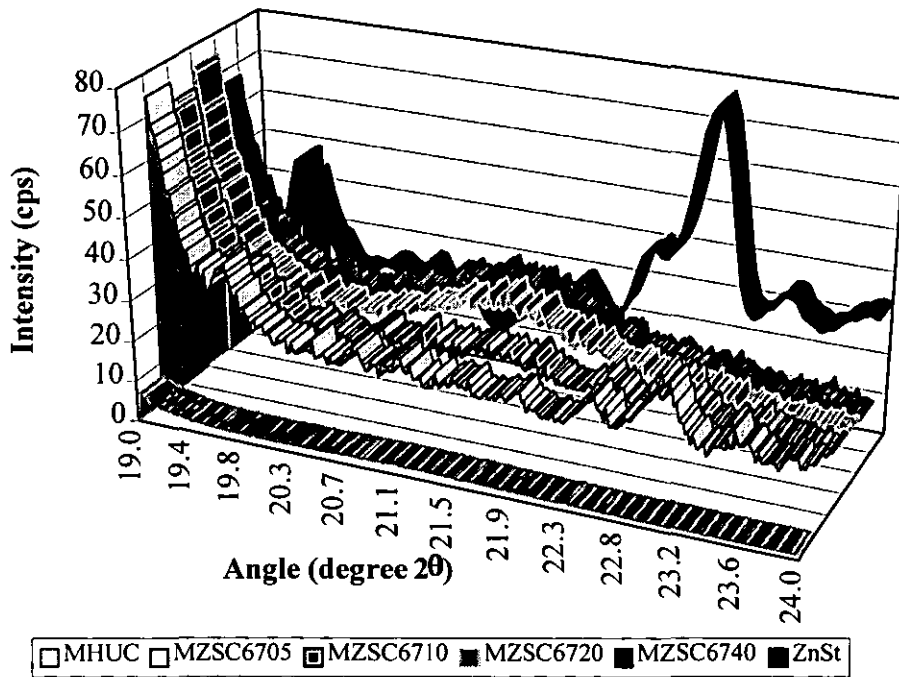


Figure 5.11: X-ray diffraction patterns of magnesium hydroxide coated with 6.7% w/w zinc stearate taken from the Fielder mixer after 5 min, 10 min, 20 min, 40 min and zinc stearate.

Figure 5.12 shows X-ray pattern of stearic acid powder contains two peaks as shown in Appendix G.3(d). One single broad peak is detected through out the coating process due to the lower melting point and easier coating with stearic acid in comparison with metal stearates. The disappearance of sharp peak for the samples coated with stearic acid may imply that free stearic acid particles, which have crystal structures consisting of bilayers of molecules (head to head) aligned perpendicular to the horizontal plane [171], have been melted and absorbed on magnesium hydroxide surfaces as a thin monolayer film.

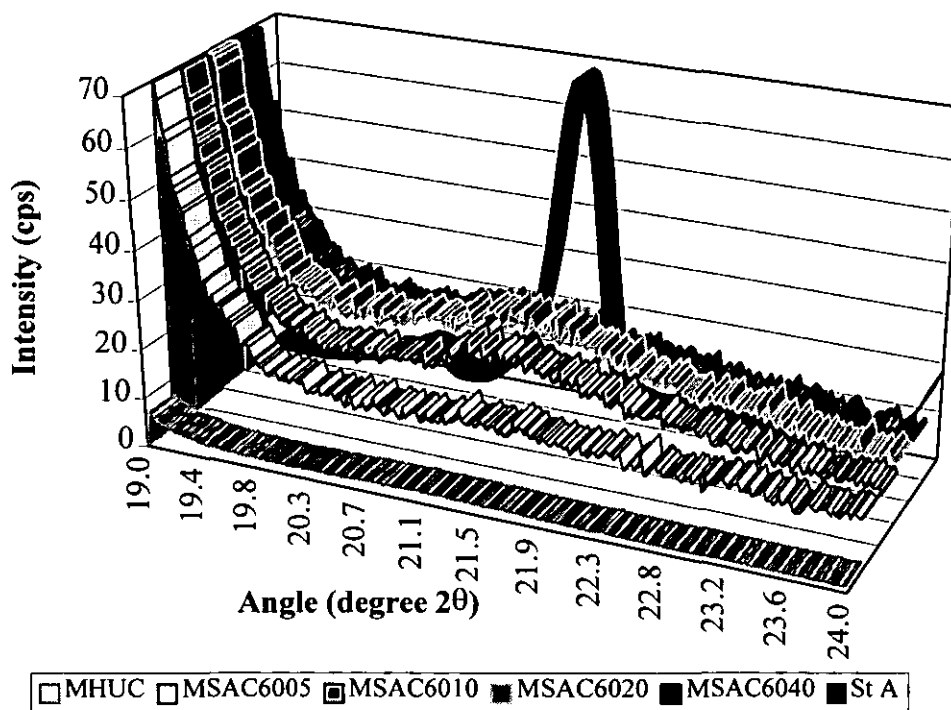


Figure 5.12: X-ray diffraction patterns of magnesium hydroxide coated with 6.0% w/w stearic acid taken from the Fielder mixer after 5 min, 10 min, 20 min, 40 min and stearic acid.

5.1.4 CONTACT ANGLE MEASUREMENT

Contact angles of samples measured with four different kinds of liquids are recorded. The calculations of surface free energy are shown in Appendix D.6. The contact angle and surface free energy results for magnesium hydroxide and calcium carbonate with the various types of coating agents coated/added are summarised in Table 5.1

The results show that uncoated fillers give higher surface free energy than modified fillers, indicating the high polarity (hydrophilic) of both magnesium hydroxide and calcium carbonate. Calcium carbonate shows the highest surface free energy. The surface modification of the filler seems to decrease polarity of the fillers. It suggests that the addition of coating agent helps to improve the filler surfaces to be hydrophobic resulting to better dispersion and distribution of filler in molten plastic during processing [7]. Metal stearate coatings give lower surface energies than stearic acid

coating. This is because stearic acid itself has a higher surface free energy than metal stearates. This may result in poorer dispersion of stearic acid coated filler in comparison with metal stearate coated ones during mixing in the Fielder mixer. For modified magnesium hydroxide, calcium stearate coating gives the lowest surface free energy indicating the best dispersion of the coated filler, and magnesium stearate coating gives a better result than zinc stearate coating. The magnesium hydroxide with 6.2% magnesium stearate “added” shows a higher value of surface free energy than coated sample. This may be due to incomplete coverage of magnesium hydroxide with magnesium stearate, consequently giving a high surface free energy closer to magnesium hydroxide.

Table 5.1: Contact angles and surface free energy of uncoated fillers, and coated/added fillers with various types of coating agents (average of 5 tests).

Code	Contact angle (degree)				Surface free energy (mJm ⁻²)
	Water	Glycerol	DIM	BNL	
MHUC	35.0	40.5	27.8	26.6	62.02
MMSA62	75.4	62.2	49.6	35.5	41.05
MMSC62	104.6	88.0	56.4	49.0	30.52
MCSC64	109.9	89.0	57.5	49.5	30.09
MZSC67	100.0	82.5	58.3	48.0	30.82
MSAC60	105.0	87.5	54.6	47.2	31.51
CCUC	32.6	28.6	29.6	28.8	64.77
CMSC42	105.9	88.7	56.5	49.6	30.38
CCSA43	62.0	86.5	41.4	35.0	48.54
CCSC43	104.2	86.0	57.0	49.4	30.46
CZSC45	105.9	88.5	55.5	47.1	31.25
CSAC40	105.1	87.5	54.1	45.6	32.01
MgSt	105.8	92.2	78.4	67.2	20.54
CaSt	106.5	92.4	76.0	66.0	21.29
ZnSt	108.2	93.5	75.0	67.0	21.19
StA	85.9	72.0	53.2	44.2	35.23

For modified calcium carbonate, magnesium and calcium stearate coatings give similar surface free energy values which are lower than the surface free energy with zinc stearate and stearic acid coating. A similar result to magnesium hydroxide with 6.2% magnesium stearate coated/added, calcium carbonate with 4.3% calcium stearate coated/added shows different values of surface free energy implying that the mixing conditions have an effect on the surface properties of filler. The “added” sample gives higher surface free energy than the coated one due to unsuccessful coverage of calcium stearate on the calcium carbonate surface. Surface free energies of coating agents demonstrate that stearic acid has the highest surface free energy in comparison with the stearate salts. Magnesium stearate has a surface free energy lower than calcium and zinc stearate. Therefore, it is concluded that the surface treatment of magnesium hydroxide and calcium carbonate can improve wetting and dispersion of the fillers in a polymer matrix thereby reducing and preventing agglomeration of the fillers, leading to tougher composites.

5.1.5 X-RAY PHOTOELECTRON SPECTROSCOPY (XPS)

XPS is a well established surface analysis technique providing quantitative elemental analysis (for all element excepts hydrogen) of the outer 2-5 nm of solid surfaces. In XPS the sample is irradiated with soft X-rays and the photoelectrons generated are collected and energy analysed to yield a spectrum. High energy resolution spectra can be used to study surface chemistry and identify functional groups present at the surface, in addition to providing elemental composition [85]. Since the technique provides quantitative data it is possible to relate the extent of coating to mechanical properties of the filled polymer, so coated fillers were also examined using XPS with VG ESCALAB Mk1 spectrometer. High energy resolution carbon 1s photoelectron peaks for uncoated/coated magnesium hydroxide with various concentrations of magnesium stearate coating, uncoated/coated magnesium hydroxide with various types of coating agents, and uncoated/coated calcium carbonate with various types of coating agents are shown in Figures 5.13-5.15, respectively. Broad scan XPS spectra

of filler samples are also shown in Appendix F.5. An example of the calculation of the percentage of atoms is shown in Appendix D.8. Surface composition results are shown in Tables 5.2 and 5.3.

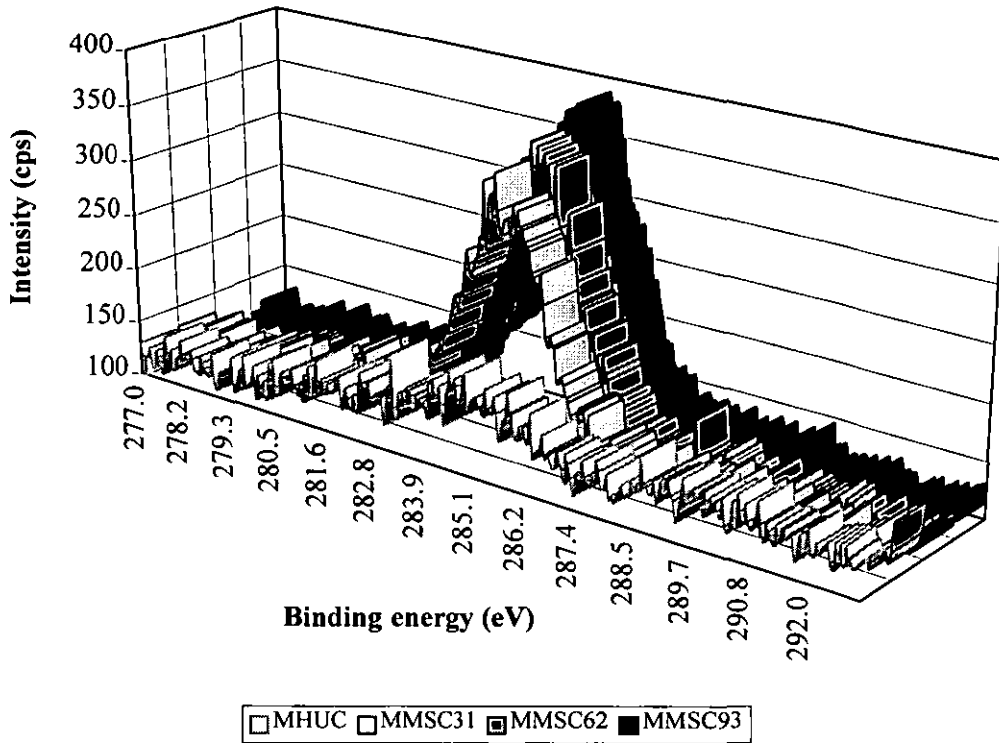


Figure 5.13: High energy resolution carbon 1s photoelectron peaks for uncoated/coated magnesium hydroxide with various magnesium stearate concentrations.

Figure 5.13 shows typical XPS spectra of the carbon 1s spectra for uncoated and coated magnesium hydroxide. One form of organic carbon is detected. The small amount of hydrocarbon present on the surface of the uncoated filler is due to atmospheric contamination and is found to some extent on all air exposed inorganic surfaces. This is often referred to as adventitious carbon. The carbon peak from the stearate anion is too weak to be clearly resolved, but would be expected at a slightly lower binding energy than that in the magnesium hydroxide. The amount of organic carbon increases significantly in the presence of coatings.

Figure 5.14 and Table 5.2 shows typical carbon 1s XPS spectra for uncoated magnesium hydroxide and magnesium hydroxide coated with different stearates. Coated magnesium hydroxide containing 6.7% zinc stearate gives the highest intensity, 6.0% stearic acid (with higher background intensity) shows the second highest intensity. 6.2% magnesium stearate coated magnesium hydroxide shows a slightly higher intensity than 6.4% calcium stearate coated one. Uncoated magnesium hydroxide gives the lowest intensity.

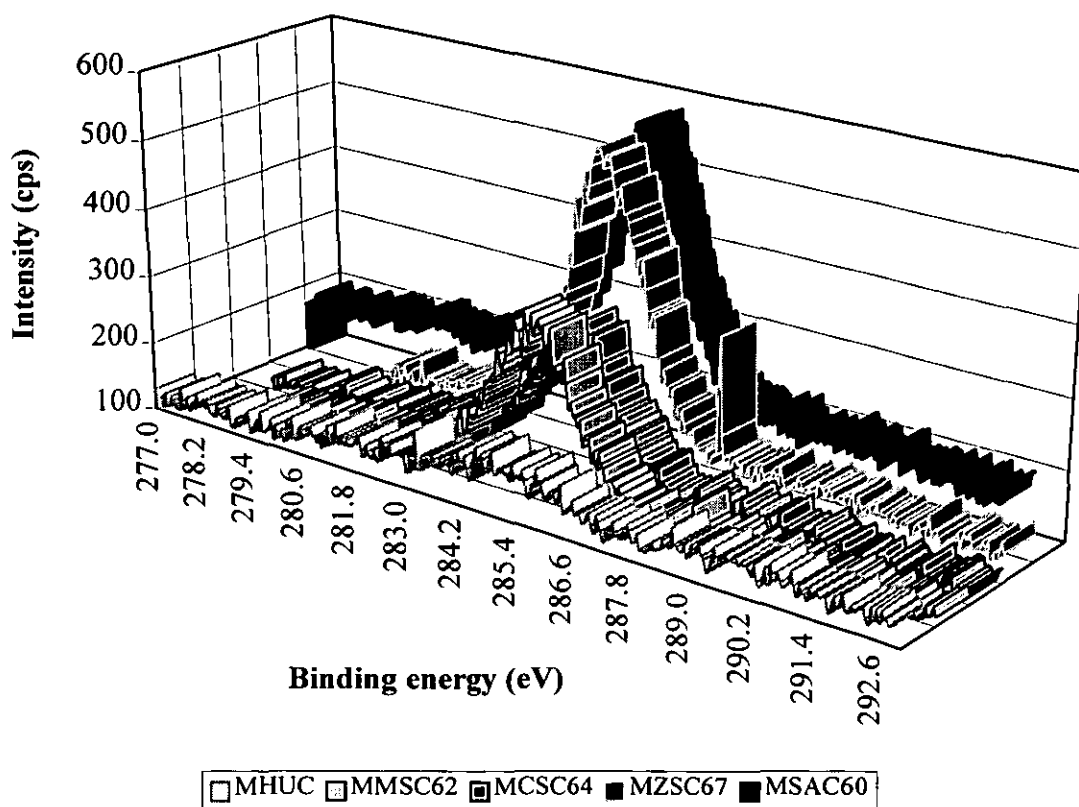


Figure 5.14: High energy resolution carbon 1s photoelectron peaks for uncoated/coated magnesium hydroxide with 6.2% magnesium stearate, 6.4% calcium stearate, 6.7% zinc stearate and 6.0% stearic acid.

Surface compositions of uncoated and coated magnesium hydroxide are shown in Table 5.2. The ratio C/Mg reflects the amount of organic substances on the surface of the magnesium hydroxide. The results shows that zinc stearate produces the highest

C/Mg ratios relative to other stearates. The ratios C/Mg increase with increased magnesium stearate concentrations. This suggests that the deposition of coating agent on magnesium hydroxide surface depends on the amount of coating agent.

Table 5.2: Surface compositions of uncoated and coated magnesium hydroxide.

Sample	Surface composition excluding H (atom%)				atomic ratio
	C	O	Mg	Zn	C/Mg
Uncoated Mg(OH) ₂	8.1	51.4	40.5	-	0.2
Mg(OH) ₂ +3.1% Mg stearate	32.1	33.8	34.1	-	0.9
Mg(OH) ₂ +6.2% Mg stearate	37.8	31.0	31.1	-	1.2
Mg(OH) ₂ +9.3% Mg stearate	40.7	28.8	30.5	-	1.3
Mg(OH) ₂ +6.4% Ca stearate	30.9	33.8	35.3	-	0.9
Mg(OH) ₂ +6.7% Zn stearate	49.1	25.5	25.3	0.2	1.9
Mg(OH) ₂ +6.0% stearic acid	36.1	32.0	31.9	-	1.1

Figure 5.15 shows typical the carbon 1s XPS spectra for uncoated calcium carbonate and calcium carbonate coated with different stearates. Two forms of carbon are detected. These can be attributed to the organic carbon and carbonate carbon. Carbonate carbon peaks decrease when organic carbon peaks increase. The amount of organic carbon detected gives very high intensity when 4.0% stearic acid was coated on calcium carbonate compared with other coating agents. For the metal stearates, the amount of organic carbon detected is lowest with calcium stearate, for both calcium carbonate and magnesium hydroxide. This may be because calcium stearate has the highest melting point, so is more difficult to melt and coat on filler surfaces than the others. A high level of organic carbon is observed on calcium carbonate when zinc stearate is used. Again, this result correlates with rapid disappearance of zinc stearate during coating (DSC results). It is also seen that zinc itself can be detected as zinc has a lower detection limit than calcium or magnesium by XPS.

Table 5.3 shows surface compositions of uncoated and coated calcium carbonate. The atomic ratios C/Ca and CH/CO₃ reflect the amount of organic material on the surface

of calcium carbonate. Results imply that zinc stearate gives the biggest C/Ca ratios relative to above. Stearic acid is also particularly good for calcium carbonate.

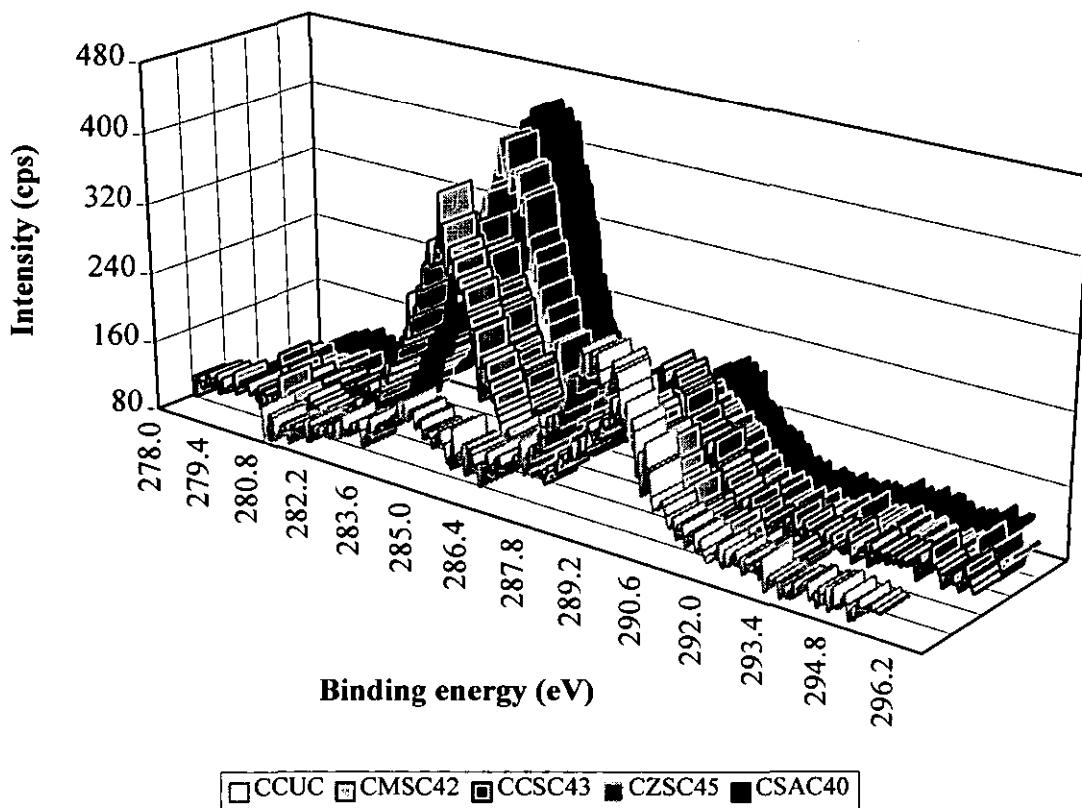


Figure 5.15: High energy resolution carbon 1s photoelectron peaks for uncoated and coated calcium carbonate with 4.2% magnesium stearate, 4.3% calcium stearate, 4.5% zinc stearate and 4.0% stearic acid.

Table 5.3: Surface compositions of uncoated and coated calcium carbonate.

Sample	Surface composition					Atomic ratio	
	C	O	Ca	Mg	Zn	C/Ca	CH/CO ₃
Uncoated CaCO ₃	26.9	51.3	21.7	-	-	1.2	0.3
CaCO ₃ +4.2% Mg stearate	49.3	35.3	15.4	-	-	3.2	2.4
CaCO ₃ +4.3% Ca stearate	43.3	40.3	16.4	-	-	2.6	1.7
CaCO ₃ +4.5% Zn stearate	58.8	29.0	11.5	-	0.7	5.1	4.4
CaCO ₃ +4.0% stearic acid	60.6	27.3	12.1	-	-	5.0	4.6

5.2. EFFECT OF COATING AGENTS ON FILLED COMPOUND PROPERTIES

The addition of filler in polymer and the surface treatment of fillers have effects on compound properties. From the discussion in the previous chapter, it has been shown that one monolayer coverage of filler affects mechanical properties of the composites by reducing hydrophilicity of filler, increasing dispersivity and wettability of filler, modifying the interfacial force at polymer/filler interphase, and increasing the slippage of polymer chains in the interphase causing by a lubricating effect. In order to understand further how one monolayer coverage of filler with various coating agent types affects compound properties, physical/mechanical properties of individual compounds were investigated. Filler content is determined to confirm the amount of the polymer, filler, and coating agent components. Tensile, flexural and impact properties have been determined. Crystallinity and reversion of compounds have also been investigated. Filler/polymer orientation were determined from X-ray diffraction. All results are discussed as follows:

5.2.1 FILLER CONTENTS

Polymer, filler and coating agent contents were determined using an ashing test, burning samples to produce ash. All samples such as unfilled and filled polymers; uncoated and coated fillers as well as coating agents were heated in a furnace for 3 hours at 850 °C. An example of filler content calculation is shown as Appendix D.7. The results are shown in Table 5.4.

It was known from Series I that some filler and coating agent particles leaked between the vessel and lid due to pressure developing inside the vessel during mixing, this problem was solved in Series II by reducing of the pressure inside the vessel during mixing more often. The ashing results show that in almost cases the coating contents are close to the planned values. However, the filler contents are difficult to control because filler and polymer feed rates depend on not only room temperature and

humidity but also depend on the characteristics of compounder, extrusion conditions, and also characteristics of fillers and coating agents. $\text{Mg}(\text{OH})_2$ filled-compounds containing 6.7% zinc stearate and 6.0% stearic acid give higher filler contents than those containing 6.2% magnesium stearate and 6.4% calcium stearate, respectively. These results may cause slightly poorer tensile/flexural modulus of magnesium hydroxide composites containing zinc stearate and stearic acid. For CaCO_3 filled-compounds, the results show that filled compounds containing uncoated CaCO_3 , CaCO_3 coated with 4.3% calcium stearate, and 4.5% zinc stearate give lower filler contents than other samples. This may again produce a lower tensile/flexural modulus for the compounds.

Table 5.4: Polymer, filler, and coating agent contents (average of 2 tests).

Code	Details	%Polymer Content	%Filler Content	%Coating* Content
HDUF	100% HDPE	100	0.00	(0.00)
HMUC	HDPE+40% $\text{Mg}(\text{OH})_2$ UNCOATED	59.22	40.78	(0.00)
HMMSA62	HDPE+40% $[\text{Mg}(\text{OH})_2+6.2\%\text{MS}]$ (ADDED)	61.50	38.50	(6.19)
HMMSC62	HDPE+40% $[\text{Mg}(\text{OH})_2+6.2\%\text{MS}]$ (COATED)	62.37	37.63	(6.14)
HMCSC64	HDPE+40% $[\text{Mg}(\text{OH})_2+6.4\%\text{CS}]$ (COATED)	62.35	37.65	(6.34)
HMZSC67	HDPE+40% $[\text{Mg}(\text{OH})_2+6.7\%\text{ZS}]$ (COATED)	59.88	40.12	(6.78)
HMSAC60	HDPE+40% $[\text{Mg}(\text{OH})_2+6.0\%\text{SA}]$ (COATED)	58.73	41.27	(6.06)
HCUC	HDPE+40% CaCO_3 UNCOATED	60.82	39.18	(0.00)
HCMSC42	HDPE+40% $[\text{CaCO}_3+4.2\%\text{MS}]$ (COATED)	59.18	40.82	(4.22)
HCCSA43	HDPE+40% $[\text{CaCO}_3+4.3\%\text{CS}]$ (ADDED)	59.16	40.84	(4.32)
HCCSC43	HDPE+40% $[\text{CaCO}_3+4.3\%\text{CS}]$ (COATED)	60.74	39.26	(4.34)
HCZSC45	HDPE+40% $[\text{CaCO}_3+4.5\%\text{ZS}]$ (COATED)	61.18	38.82	(4.58)
HCSAC40	HDPE+40% $[\text{CaCO}_3+4.0\%\text{SA}]$ (COATED)	59.54	40.46	(3.97)

*: %coating agent in the filler

5.2.2 TENSILE PROPERTIES

In order to study physical and mechanical properties, tensile bars were produced using a Negri Bossi NB55 injection moulder. Tensile properties of filled HDPE containing magnesium hydroxide and calcium carbonate surface treated with different types of

metal stearates and stearic acid were determined using a Lloyd tensile testing machine, type L200R. The results are summarised in two subsections.

5.2.2.1 Magnesium hydroxide modified with various coating agent types.

It is seen from Figure 5.16 that all $\text{Mg}(\text{OH})_2$ filled-composites give higher tensile modulus (380%) and lower elongation at yield (65%) than unfilled HDPE. The composite containing uncoated magnesium hydroxide gives the highest modulus and the lowest elongation at yield with brittle failure under tension. This is due to a higher interfacial force between polymer and filler (as explained in section 4.4.2.). Like Series I, the surface modification of the filler with one monolayer coverage effects a decrease in modulus and an increase in elongation at yield resulting from the reduction of interfacial force at the filler/polymer interphase and the lubricating effect of the coating agent. The filler coating decreases surface free energy (section 5.1.4) of magnesium hydroxide resulting in increased hydrophobicity of the filler. This leads to better dispersibility and wettability of filler in the melted matrix resulting in increased toughness of the modified filled-compounds afterward. The calcium stearate coating gives better tensile properties (lower modulus and higher elongation at yield) than stearic acid, magnesium stearate, and zinc stearate coatings, respectively. This indicates that the coating of magnesium hydroxide with calcium stearate is more effective than with stearic acid and other stearates. This may be because the coating of magnesium hydroxide with calcium stearate give the lowest value of surface free energy (see Table 5.4) leading to the highest flexibility of interaction at polymer/filler interphase, compared with other coated-magnesium hydroxides. The result also may relate to polymer content as the sample containing calcium stearate has a slightly higher polymer content than other samples. However, it is evident that the one monolayer coverage of filler can improve ductility of composites. The various types of coating agents have little effect on yield strength. Coating agents also act as lubricants causing a reduction of tensile modulus by the slippage of polymer chains as shown in section 5.3.2.

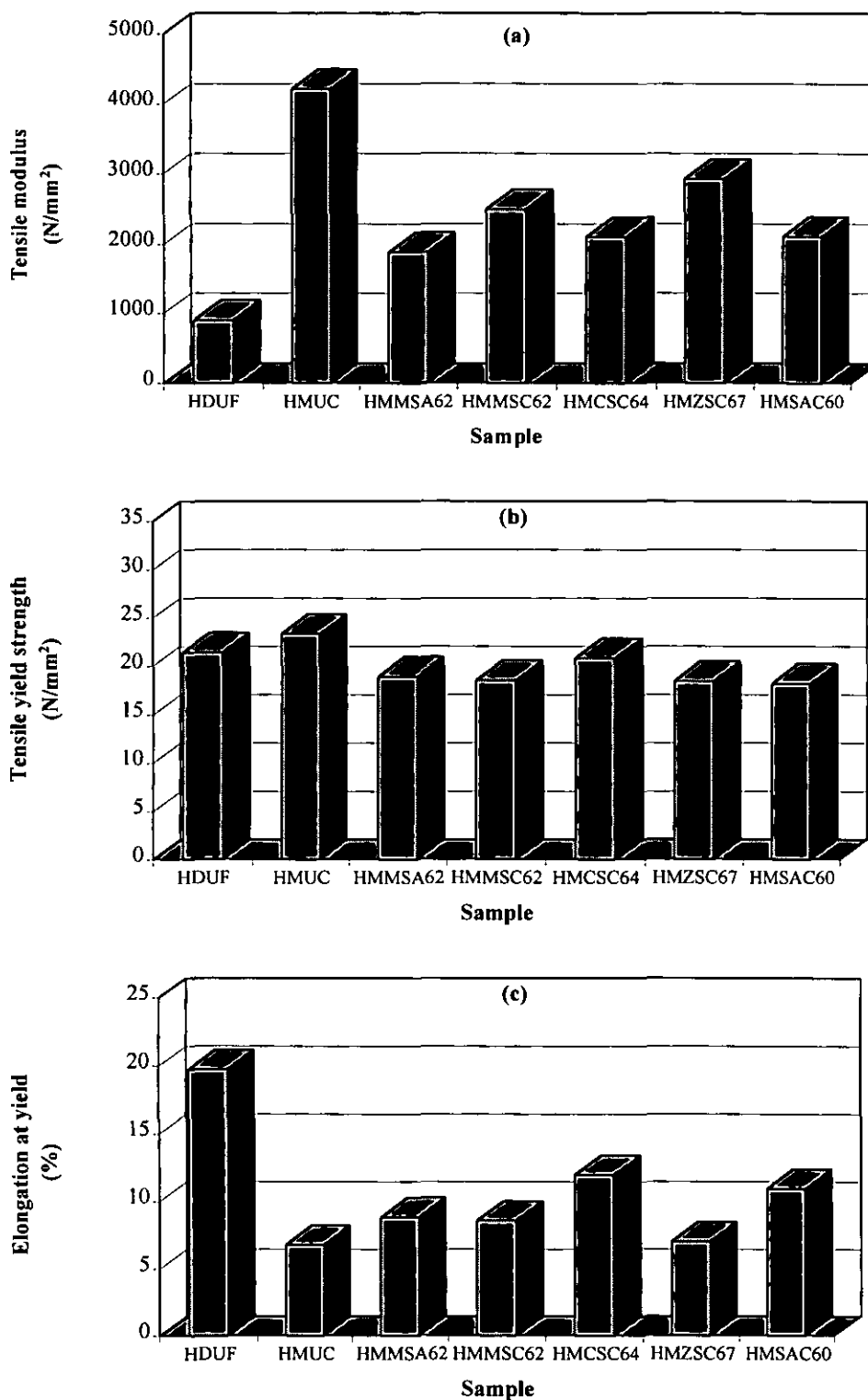
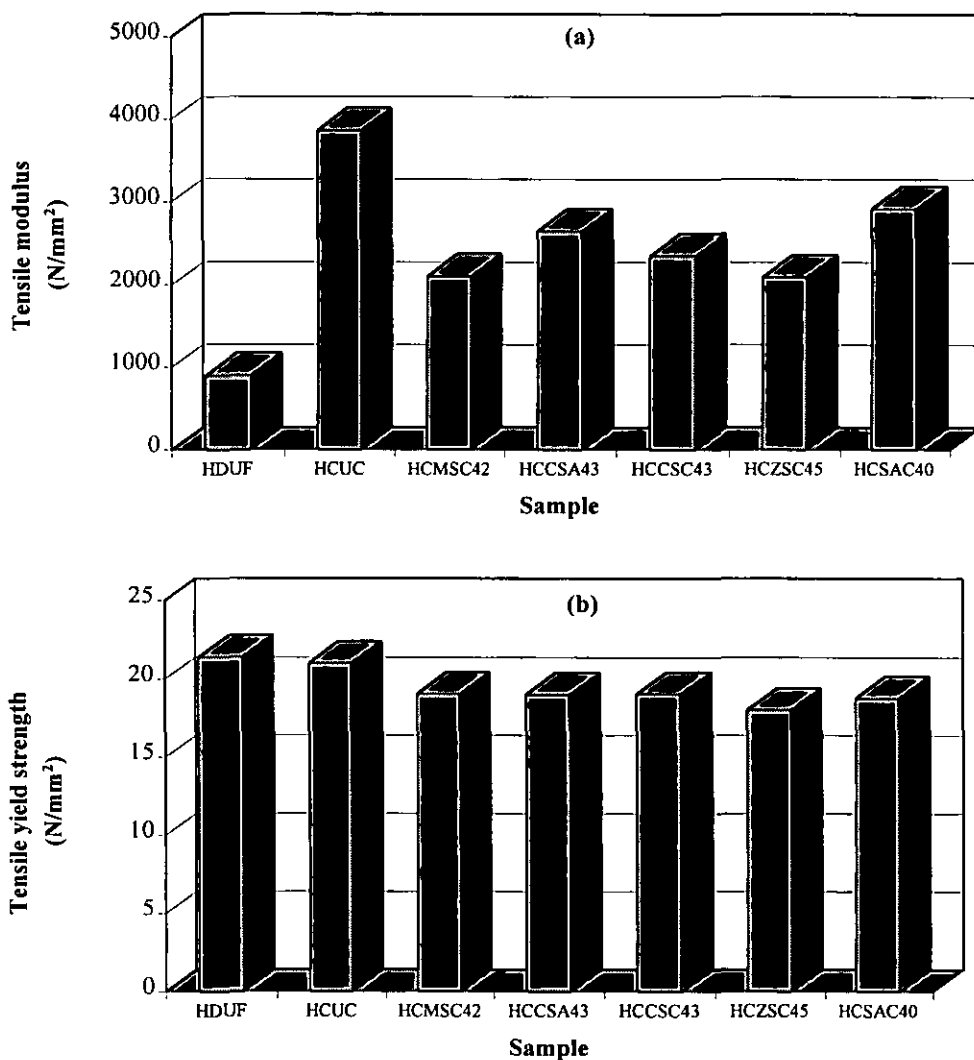


Figure 5.16: Tensile properties of unfilled HDPE and HDPE compounds containing $Mg(OH)_2$ coated with various coating agent types; (a) tensile modulus, (b) yield strength, (c) elongation at yield (average of 8 tests).

5.2.2.2 Calcium carbonate modified with various coating agent types.

Figure 5.17 shows that like $Mg(OH)_2$ filled-composites, $CaCO_3$ filled-composites give higher modulus and lower elongation at yield than unfilled polyethylene. Surface modification of the filler has a significant effect in reducing tensile modulus while a smaller effect in decreasing tensile yield strength and increasing in elongation at yield compared to uncoated filled-compound.



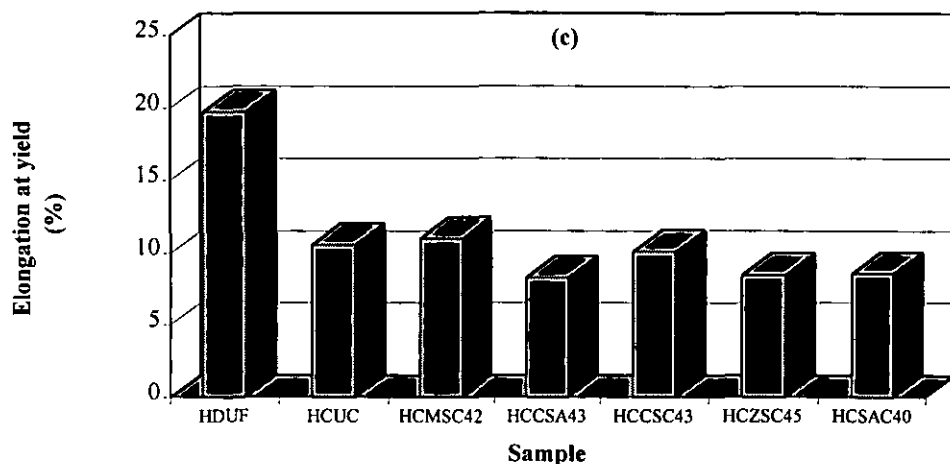


Figure 5.17: Tensile properties of unfilled HDPE and HDPE compounds containing CaCO_3 coated with various coating agent types; (a) tensile modulus, (b) yield strength, (c) elongation at yield (average of 8 tests).

Compared with stearic acid coated filled-compound, the coating of CaCO_3 with a monolayer coverage of metal stearates again resulted in much decreased tensile modulus, but not obviously enhanced strength and elongation at yield as reported by Hancock, Pukanszky and co-workers [71, 172]. A CaCO_3 filled-composite containing magnesium stearate give the best tensile properties as above.

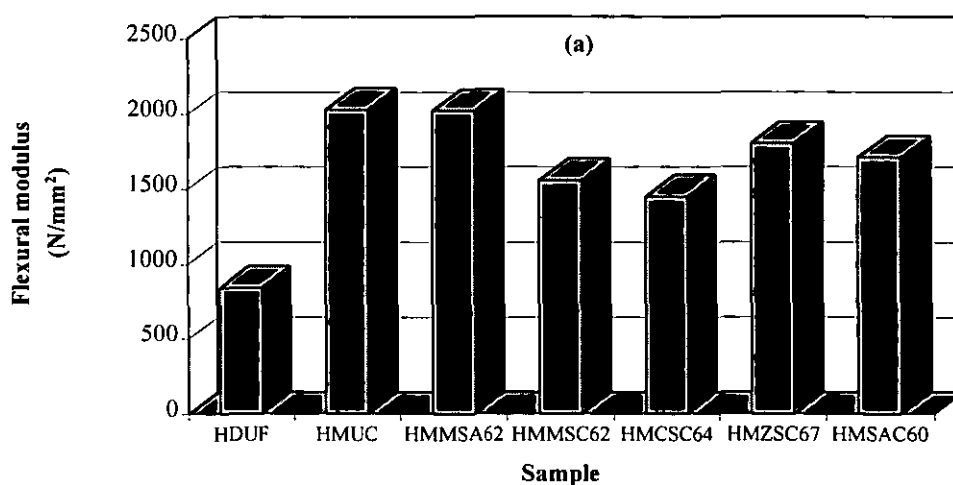
The various coating agent types (one monolayer) for calcium carbonate and magnesium hydroxide give different tensile properties, i.e. magnesium stearate is the best coating for calcium carbonate while calcium stearate is the best coating for magnesium hydroxide. This result suggests that changes in coating type cause less variation in tensile properties for calcium carbonate filled-compounds than for the magnesium hydroxide one. This may be because the amount of coating agent added into calcium carbonate in each sample is less than that added into magnesium hydroxide. However, the results give no general trend, possibly because the change in coating agent types gives the small effects observed.

5.2.3 FLEXURAL PROPERTIES

Flexural properties of filled HDPE containing magnesium hydroxide and calcium carbonate modified with one monolayer of various coating agent types were examined using the same tensile testing machine in three point flexural mode. The results are summarised in two subsections.

5.2.3.1 Magnesium hydroxide modified with various coating agent types.

Similar to the effect on tensile modulus, Figure 5.18 shows that the 40% uncoated filled-composite gives an increase in flexural modulus by 140% and yield strength by 47% but extension at maximum load is decreased by 20%, in comparison with unfilled composite.



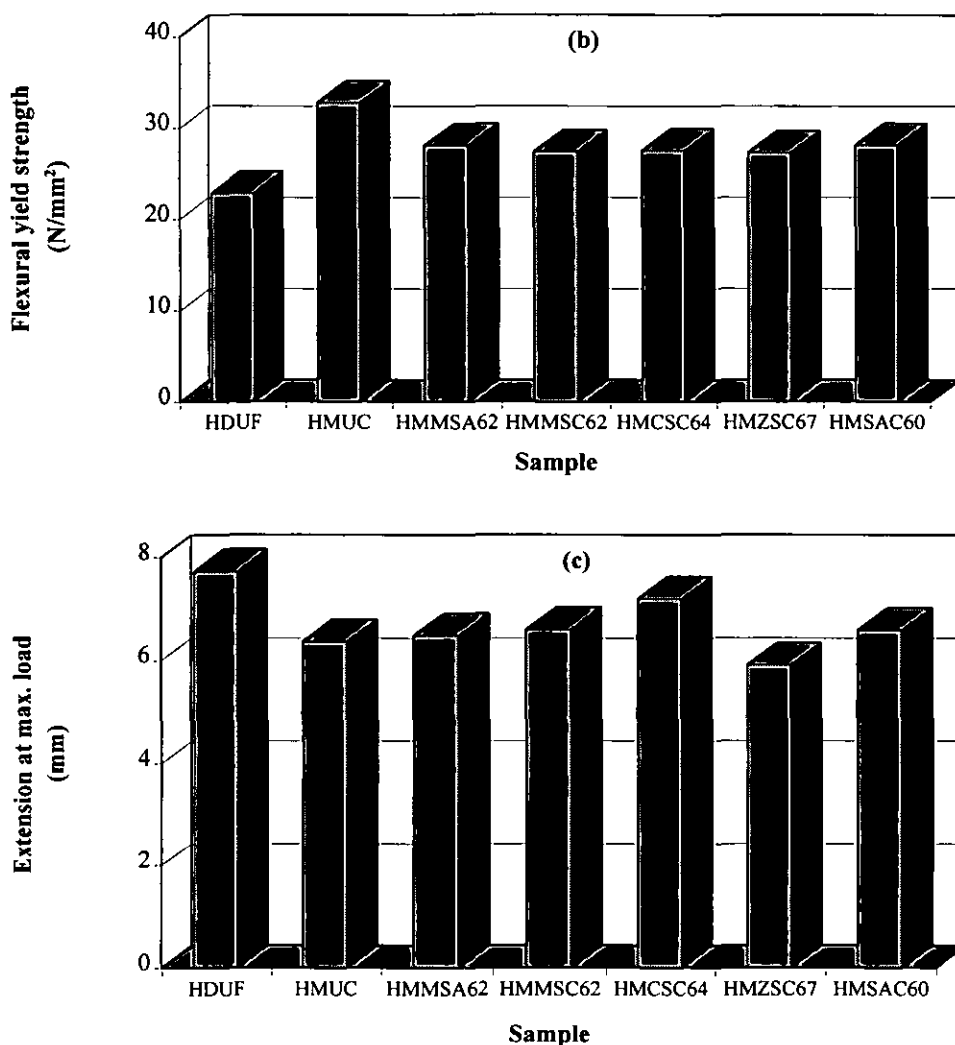


Figure 5.18: Flexural properties of unfilled HDPE and HDPE compounds containing $\text{Mg}(\text{OH})_2$ coated with various coating agent types; (a) flexural modulus, (b) flexural yield strength, (c) extension at maximum load (average of 8 tests).

As expected, the composite containing uncoated filler shows a higher flexural modulus than the modified-filled and unfilled HDPE. The presence of magnesium and calcium stearate treatments leads to an obvious decline in flexural modulus (20%) and flexural yield strength (16%) compared to uncoated filled composite.

In comparison with zinc stearate and stearic acid coatings, the magnesium and calcium stearate coatings give more evident reduction of the modulus and increase in

extension at maximum load, though the effects of coating types on yield strength are small. It appears that magnesium stearate and calcium stearate enhance wettability of the filler more than stearic acid and zinc stearate do, as they have lower surface free energy than stearic acid and zinc stearate. Particularly, magnesium hydroxide filled HDPE containing calcium stearate gives the best flexural properties (lowest flexural modulus and highest extension at maximum load). These results are consistent with tensile properties. Comparing filled composites containing “added” and coated magnesium stearate, the added filled-composite gives poorer flexural properties due to poorer wettability and dispersibility of filler particles (see explanation in section 4.4.3). However, the effects of different coating types on yield strength and extension at yield are not significant. This result is in agreement with many workers [71, 124].

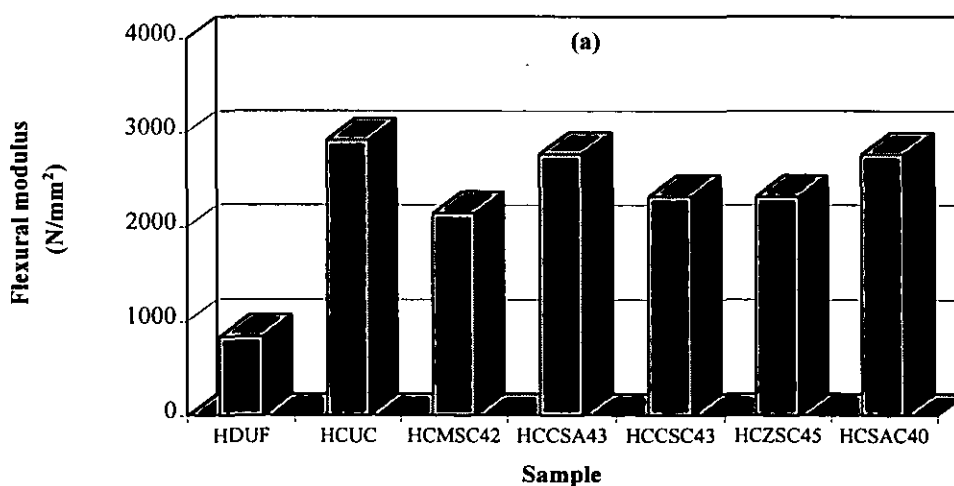
The addition of coating agents, equivalent to one monolayer coverage, to a polymer causes a decrease in flexural properties of composites (as shown in Figure 5.35) by reducing the flexural modulus and yield strength of compounds containing coating agent. This indicates no chemical bonding between polymer and coating. However, the difference in type of coating agent has little effect on the flexural property changes.

5.2.3.2 Calcium carbonate modified with various coating agent types.

The effect of surface modification of calcium carbonate with various stearate types on flexural properties of filled HDPE is shown in Figure 5.19. Like magnesium hydroxide, the addition of 40% calcium carbonate results in an increase of flexural modulus of uncoated filled-composites by 370% and yield strength by 50%, compared with unfilled HDPE. However, the filler addition results in a brittle compound, showing the lowest value of extension at maximum load. The addition of filler increased flexural yield strength while slightly decreasing tensile yield strength. This result is not clear but it may be due to a difference in mode of applied force. Compared with stearic acid coating, filled composites with metal stearate coatings

show considerable reduction of flexural modulus while a slight decline in flexural yield strength implying a lower interfacial force between the coated calcium carbonate and HDPE at the polymer/filler interface. Extensions at maximum load of the composites were found to decrease with the filler addition but the decrease was less when the filler was treated with metal stearates. The flexural modulus is also found to have the lowest value while the extension at maximum load shows the greatest value when calcium carbonate is coated with magnesium and calcium stearate. This is due to the fact that similar to the coatings on magnesium hydroxide described above, the magnesium and calcium stearate treatments provide some improvement in dispersing and lubricating the calcium carbonate particles in the polymer matrix influencing the increase of flexural properties of composites as reported by McKane and Grossman [159].

It is concluded that the presence of surface coatings (one monolayer) improves filler wettability and markedly enhances the flexibility of interaction between filler and polymer. Compared with calcium stearate coating, calcium carbonate with “added” calcium stearate gave higher flexural modulus indicating higher interfacial force.



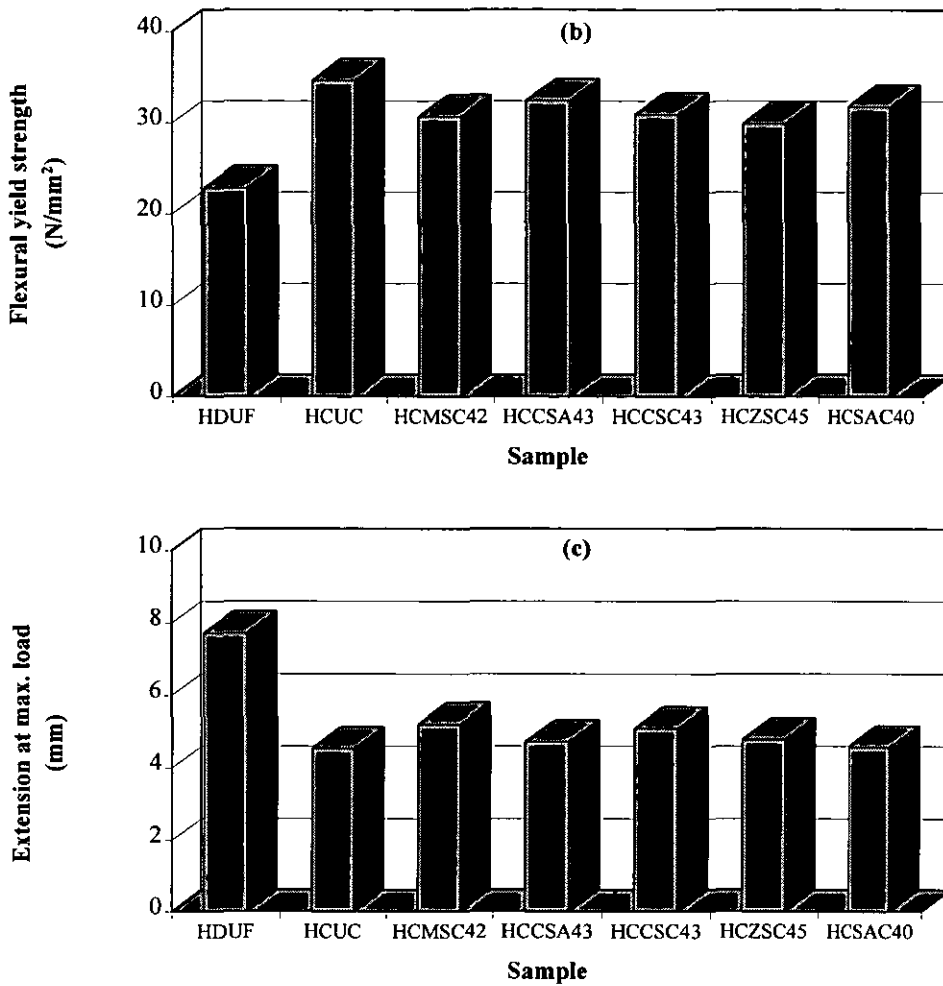


Figure 5.19: Flexural properties of unfilled HDPE and HDPE compounds containing CaCO_3 coated with various coating agent types; (a) flexural modulus, (b) flexural yield strength, (c) extension at maximum load (average of 8 tests).

5.2.4 IMPACT PROPERTIES

The circular disks produced by injection moulding were used for impact testing. Impact strength was measured using a Rosand Falling Weight Impact tester with a dropping height of 461 mm and impact velocity approximately of 3 m/s. Impact properties are summarised in two subsections.

5.2.4.1 Magnesium hydroxide modified with various coating agent types.

Figure 5.20 shows that the addition of magnesium hydroxide reduces the impact strength of polyethylene. This observation is consistent with results reported from many other polymer composites, where the presence of inorganic fillers (such as talc and mica) is detrimental to toughness properties [113].

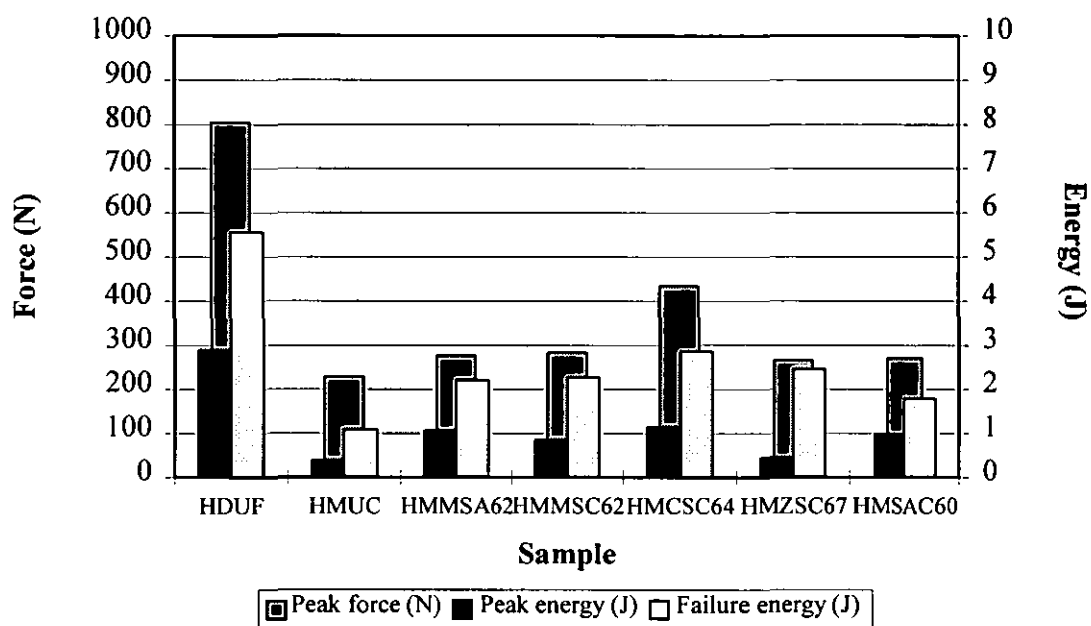


Figure 5.20: Impact properties of unfilled HDPE and HDPE compounds containing $Mg(OH)_2$ coated with different types of coating agents (average of 10 tests).

Modification of the filler surface gives better impact properties (higher peak force, peak energy, and failure energy) compared with uncoated filled-composite. Like in Series I, a monolayer coverage of metal stearates gave higher impact resistance in comparison with that of stearic acid. No evident difference in impact properties was observed when the magnesium stearate was either “coated” or “added”. The impact properties of the filled composite with calcium stearate were greater in value (lower tensile/flexural modulus) than other stearates. The poorer impact properties obtained from the equivalent zinc stearate and stearic acid coated compounds may relate to higher filler contents in their composites (as shown in Table 5.4) in comparison with

the other composites. Overall compounds containing coated magnesium hydroxide show ductile behaviour, except for the uncoated compound which showed brittle fracture. This may be because the presence of coating improves dispersion and wettability of filler in the polymer matrix and also increases the flexibility of interaction between polymer and filler leading to greater resistance to the propagation of cracks.

5.2.4.2 Calcium carbonate modified with various coating agent types.

It is apparent from Figure 5.21 that the addition of 40% w/w calcium carbonate reduces the impact strength of HDPE. Calcium carbonate filled composites containing magnesium stearate coating agent give the highest increased impact properties in comparison with other modified filled-compounds. Like magnesium hydroxide coating, the compounds containing calcium carbonate coated with a monolayer coverage of metal stearates give higher falling weight impact resistance (and lower tensile/flexural modulus) compared with stearic acid coated filled-composites. The increase in impact properties is because of the effective wetting and dispersibility of filler in the matrix, hence more energy is absorbed before fracture. This result is in agreement with Bajaa *et.al.* [57] and Riley and co-workers [113] who also suggested that good dispersion resulting from surface modification of filler enhanced the impact strength of the composites.

The mixing conditions have an effect on impact properties of calcium carbonate modified with calcium stearate. Calcium carbonate coated with calcium stearate shows better results than that "added" with calcium stearate. This is due to the fact that the mixing at high speed and temperature gives better coating performance than the mixing at low speed and temperature (see surface free energy of both samples in section 5.1.4).

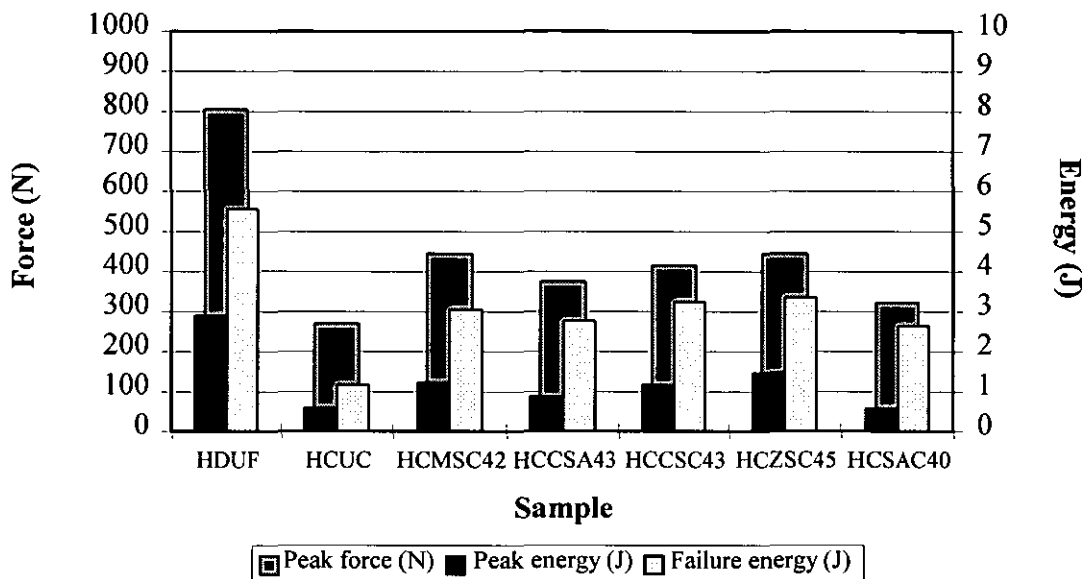


Figure 5.21: Impact properties of unfilled HDPE and HDPE compounds containing CaCO_3 coated with different types of coating agents (average of 10 tests).

It is concluded that the addition of 40% w/w of both magnesium hydroxide and calcium carbonate fillers to HDPE reduced its impact strength by about 70% and 50%, respectively, compared with unfilled HDPE. Compounds containing coating agents give higher impact properties in comparison with the composite containing uncoated filler. The results also show that filler coated with metal stearates results in greater impact properties than with stearic acid, and especially the filled compound containing calcium stearate show good impact properties in both $\text{Mg}(\text{OH})_2$ filled and CaCO_3 filled compounds. It is evident that the presence of surface-modified filler caused a substantial rise in impact strength. This effect corresponded to a change from brittle to ductile failure in the material, accompanied by the appearance of stress whitening at the failure position. The filler coating promotes the dispersion of filler particles thus it produces a larger number of available filler particles to retard crack propagation for the fracture of composites. Again, like tensile and flexural properties, the addition of various coating agents types (equivalent amount to one monolayer coverage) to polymer does not have a great effect on impact properties of composites as shown in section 5.3.4.

Although X-ray results showed that modified $\text{Mg}(\text{OH})_2$ filled-composites gives a better alignment resulting in a higher extension at maximum load compared with modified calcium carbonate one, the modified $\text{Mg}(\text{OH})_2$ filled-composites give lower impact properties than modified calcium carbonate filled-composites. This is because magnesium hydroxide particles exist as plate-like particles with a higher aspect ratio than calcium carbonate (sphere-like particles), therefore magnesium hydroxide particles act as stress-promoter reducing the necessary crack initiation energy in impact properties. This implies that the increase in the filler alignment does not have a significant effect on impact properties while it strongly affects tensile and flexural properties of composites. This is due to the fact that the increased filler alignment reinforces only the force resistance in the longitudinal direction, which is 90° to the direction of impact passed through the specimen, but it does not support the force resistance in the vertical direction of the composites. This result is in agreement with Riley and co-workers [113].

5.2.5 CRYSTALLISATION PROPERTIES

From DSC thermograms, melting temperature (T_m) and crystallisation temperature (T_c) were recorded to investigate crystallisation properties. Further information about the differences in the nucleating activity of unmodified and modified fillers ($\text{Mg}(\text{OH})_2$ and CaCO_3) can be obtained from analysis of DSC melting data. The heat of fusion attributed to melting of compounds was also determined and divided by heat of fusion of a 100% crystalline polyethylene (293 J/g) [139] to give the degree of crystallinity of samples. Crystallisation properties of $\text{Mg}(\text{OH})_2$ filled- and CaCO_3 filled-compounds are shown in Table 5.5.

Table 5.5 clearly shows that the addition of magnesium hydroxide and calcium carbonate, either uncoated or coated, results in a decrease in melting temperature, but an increase in recrystallisation temperature of $\text{Mg}(\text{OH})_2/\text{CaCO}_3$ filled-composites.

This implies that filler acts as nucleating agent leading to the presence of a greater number of crystallites, which are smaller and less perfect in comparison with unfilled-HDPE crystallites.

Table 5.5: Crystallisation properties for unfilled HDPE and $\text{Mg}(\text{OH})_2/\text{CaCO}_3$ filled HDPE containing various coating agents.

Code	Details	T_m (°C)	T_c (°C)	% Cryst
HDUF	100% HDPE	133.6	110.7	56.6
HMUC	HDPE+40%uncoated $\text{Mg}(\text{OH})_2$	131.3	114.7	58.5
HMMSA62	HDPE+40%[$\text{Mg}(\text{OH})_2$ +6.2%MS (added)]	132.3	112.3	65.0
HMMSC62	HDPE+40%[$\text{Mg}(\text{OH})_2$ +6.2%MS coated]	132.2	111.6	73.5
HMCSC64	HDPE+40%[$\text{Mg}(\text{OH})_2$ +6.4%CS (coated)]	132.6	111.1	78.5
HMZSC67	HDPE+40%[$\text{Mg}(\text{OH})_2$ +6.7%ZS (coated)]	132.8	111.0	77.0
HMSAC60	HDPE+40%[$\text{Mg}(\text{OH})_2$ +6.0%SA (coated)]	131.0	112.2	70.6
HCUC	HDPE+40%uncoated CaCO_3	131.8	113.0	68.6
HCMSC42	HDPE+40%[CaCO_3 +4.2%MS (coated)]	132.7	111.7	77.5
HCCSA43	HDPE+40%[CaCO_3 +4.3%CS (added)]	132.4	112.5	70.4
HCCSC43	HDPE+40%[CaCO_3 +4.3%CS (coated)]	132.4	111.3	72.6
HCZSC45	HDPE+40%[CaCO_3 +4.5%ZS (coated)]	132.7	111.6	75.0
HCSAC40	HDPE+40%[CaCO_3 +4.0%SA (coated)]	131.5	111.5	73.9

The results show that surface modification of magnesium hydroxide and calcium carbonate induces inert surfaces of fillers to be active surfaces (hydrophobic) which is compatible with polymer resulting in an increase in crystallinity compared with unfilled HDPE or HDPE with unmodified $\text{Mg}(\text{OH})_2/\text{CaCO}_3$. This result can be observed from adding the same amount of coating agent without filler to polymer which is shown in section 5.3.5. In all cases considered, unfilled-HDPE gives the lowest crystallinity, filled-HDPE compounds show intermediate, and HDPE filled with treated fillers produce the highest value. The highest crystallinity was found in compounds with a monolayer coverage of calcium stearate for magnesium hydroxide and magnesium stearate for calcium carbonate relating to the best in impact properties of their composites as above. This implies that calcium/magnesium stearate coating gives smaller and less perfect crystallites in comparison with other stearates and

stearic acid. These results are also consistent with the surface free energy of coated fillers and the result obtained from Series I.

5.2.6 REVERSION MEASUREMENT

In order to estimate the molecular orientation in composites produced from injection moulding, the maximum reversion was determined using the reversion test. The results are represented in Figures 5.22 and 5.23.

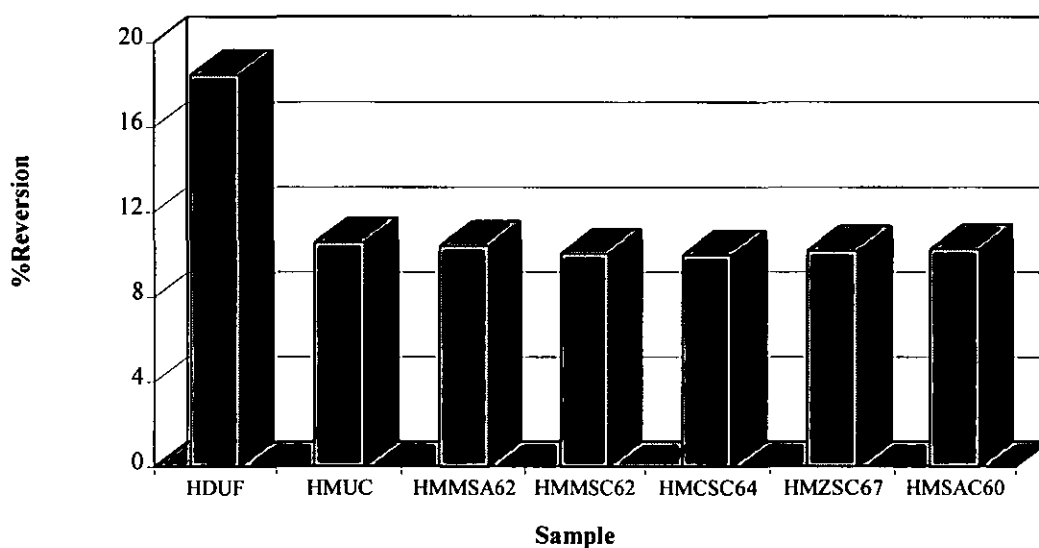


Figure 5.22: %Reversion test of unfilled HDPE and HDPE compounds containing $\text{Mg}(\text{OH})_2$ coated with various coating agent types (average of 4 tests).

Figures 5.22 and 5.23 show that unfilled polymer gives the highest percentages of reversion while the addition of either magnesium hydroxide or calcium carbonate to the polymer causes considerable decrease in these values. However, the effect of coating is probably not significant. As all compounds are produced from an injection moulder, the polymer chains of filled polymer are physically bound to the filler particles, which act as an anchorage. This may impede the polymer reorientation. Moreover, with the filled polymer, the amount of polymer is diluted so the compounds have less shrinkage than unfilled polymer. Another contribution is that

the specimens lose their former shape during melting, therefore, it is difficult accurately to remeasure the sample after the test.

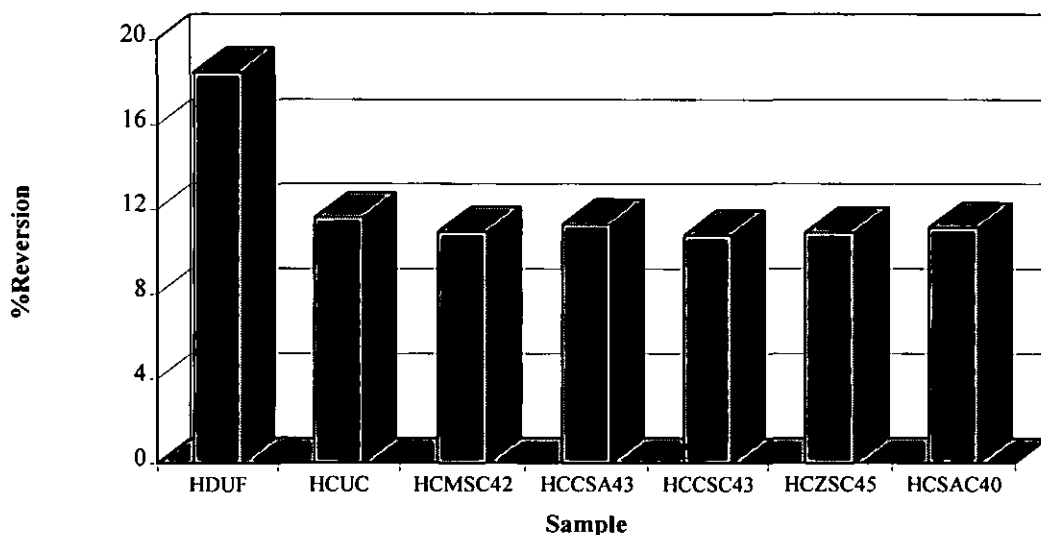


Figure 5.23: %Reversion test of unfilled HDPE and HDPE compounds containing CaCO_3 coated with various coating agent types (average of 4 tests).

5.2.7 FILLER/POLYMER ORIENTATION

One of the most important matters for injection moulders is orientation of the polymer as it enters the mould cavity and then freezes. In injection moulding the orientation pattern of products is described as follows. When the melt enters the mould there is little orientation as the material contacts the mould wall, leading to low orientation at sample skin. The bulk flow is laminar and highly orientated, hence inside the skin appears a highly orientated layer. The centre may be less orientated because it remains hot and it is insulated by the outer layers, so it has a long enough time to anneal [173]. Therefore, the orientations can cause variation in mechanical properties through a sample.

In order to determine filler/polymer orientation, tensile bars produced by injection moulding were scanned from 2-50 degree 2θ using X-ray diffraction. The X-ray patterns obtained for each scan are given in Appendices G.1 and G.2. The peak

intensity ratios of PE200/110 and MH001/101 for magnesium hydroxide filled compounds are shown in section 5.2.7.1 and the peak intensity ratios of PE200/110 and CC104/110 for calcium carbonate filled composites are shown in section 5.2.7.2.

5.2.7.1 Magnesium hydroxide modified with various coating agent types.

Figure 5.24 shows that the simple process of injection moulding causes a significant decrease in the PE200/110 ratio compared with isotropic HDPE. The addition of filler gives an increase in the peak intensity ratio of PE200/110 compared to unfilled HDPE sample. This result is consistent with the result reported by Raymond [134]. It is clear that the PE200/110 ratio indicating polymer orientation in filled composites is higher than in unfilled HDPE. It implies that the filler addition alters the way in which HDPE deforms during injection moulding. Surface modification of filler gives considerably further increase in the PE200/110 ratio of polymer orientation. An increase in the intensity of PE200, 110, and 020 implies an increase in amount of polymer chain axes (*c*-axes) parallel to the specimen surface and injection moulding flow [92, 93]. Again, various coating agent types do not have significant effects on the PE200/110 ratio. However, when pinhole photograph transmission was used to investigate more about the preferred polymer orientation for the injection moulded specimen of modified filled-compounds, the difference between the intensity of the rings at 90° to each other can be observed. It indicates an increase in the preferred polymer orientation of the specimen compared to unfilled HDPE and uncoated filled-compound, however it is difficult to quantify without using a photometer.

For the magnesium stearate modified filled-compound, the compound containing magnesium stearate “added” on magnesium hydroxide shows a lower value of PE200/110 ratio in comparison with the one containing magnesium stearate “coated”. It implies that the using of low mixing speed and temperature results in a lower PE200/110 ratio of polymer orientation in comparison with high mixing speed and temperature due to imperfect coverage of magnesium stearate on the filler surfaces.

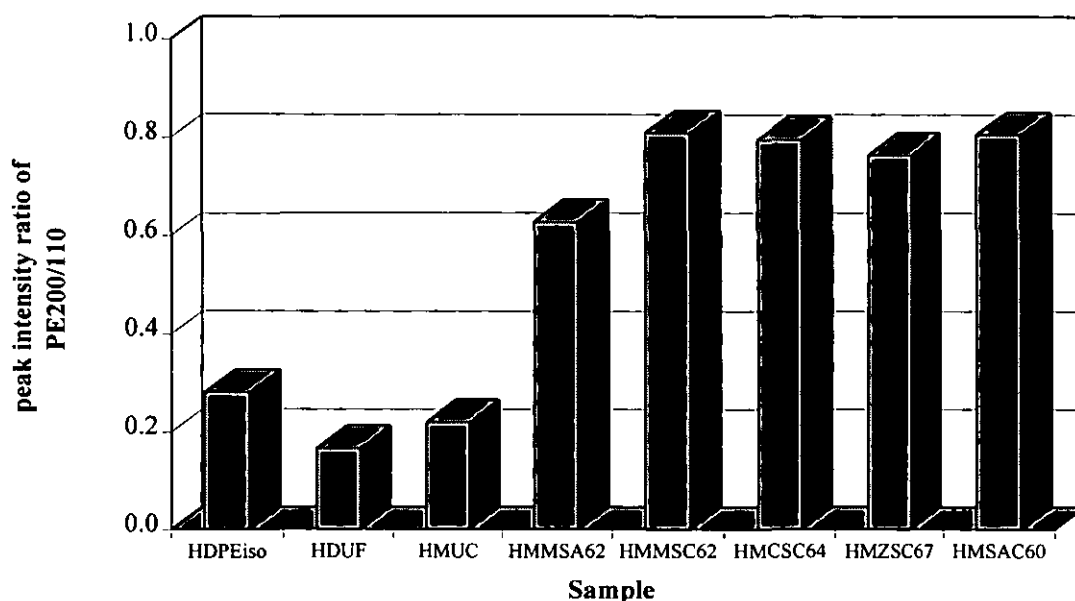


Figure 5.24: Peak intensity ratio of PE200/110 of isotropic HDPE, unfilled HDPE and $\text{Mg}(\text{OH})_2$ filled-compounds containing various coating agent types.

The effects of injection moulding on the alignment of $\text{Mg}(\text{OH})_2$ are shown in Figure 5.25. As for Series I, the value of MH001/101 ratio taken from the randomised magnesium hydroxide powder (plate-like particles) is used as the reference for the comparison of the filler alignment (as indicated in section 4.4.7.1). A greater number of magnesium hydroxide particles aligned parallel to the flow direction are detected in magnesium hydroxide filled-HDPE compound produced using injection moulding. Much greater orientation of the filler particles is achieved when the filler was coated with various coating agents because of shearing action during liquid flow plates end up parallel to the sample surface (see Figure 4.34). It suggests that the increase in the filler orientation may increase reinforcement of the composite to resist to longitudinal force applied. The compounds with metal stearate coatings give higher MH001/101 ratio than stearic acid coating. Magnesium stearate coating shows the highest result for filler orientation followed by calcium stearate, zinc stearate and stearic acid coating. The results show a slightly lower value of MH001/101 ratio for the “added” sample. This indicates that the mixing with less severe conditions gives lower filler

orientation of compound than with high speed and temperature but still higher than calcium/zinc stearate coating.

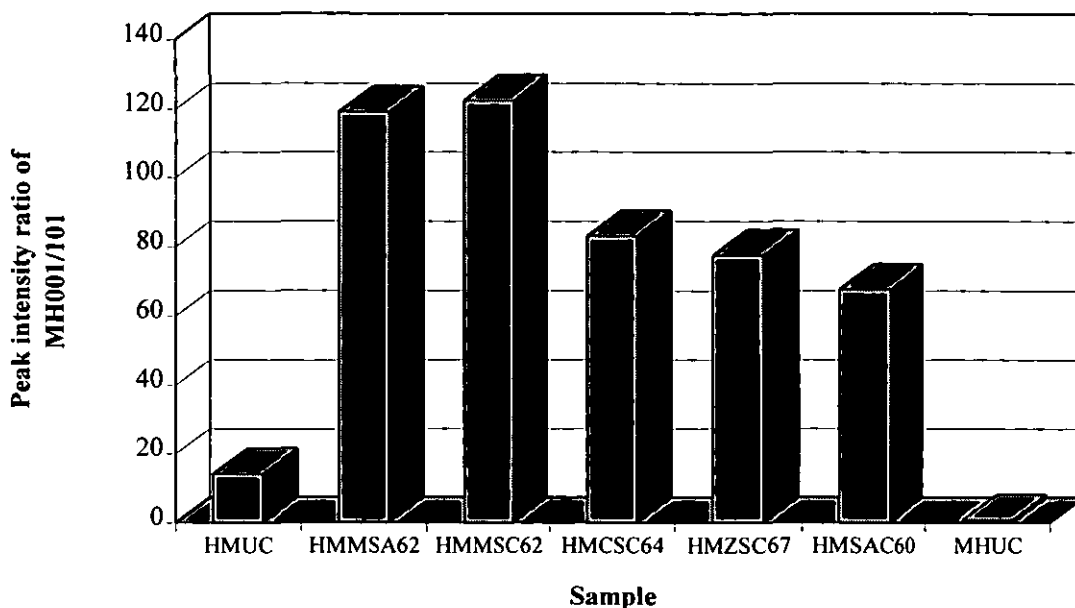


Figure 5.25: Peak intensity ratio of MH001/101 for magnesium hydroxide and $\text{Mg}(\text{OH})_2$ filled compounds containing various coating agents types.

5.2.7.2 Calcium carbonate modified with various coating agent types.

Figure 5.26 shows that again the peak intensity ratio of PE200/110 increases with the filler addition. In comparison with the uncoated CaCO_3 filled-composite, the surface modification of calcium carbonate with a monolayer coverage of different coating agent types obviously increases the intensity PE200/110 ratio of coated CaCO_3 filled-composites. The PE200/110 ratio for uncoated CaCO_3 filled-compound is considerably higher than that for the uncoated $\text{Mg}(\text{OH})_2$ filled-compound. It is not clear about the phenomenon of polymer flow with filler during injection moulding but it may be because the asymmetric shape of magnesium hydroxide particles promote more turbulent flow of the molten polymer compared with symmetric calcium carbonate particles. Like magnesium hydroxide, the surface modification of calcium carbonate give a higher PE200/110 ratio of polymer orientation than isotropic and

unfilled HDPE. This indicates that the surface modification of filler increases alignment of polymer chains (*c* axis) to be parallel to the specimen surface as reported by Guan and co-workers [92, 93].

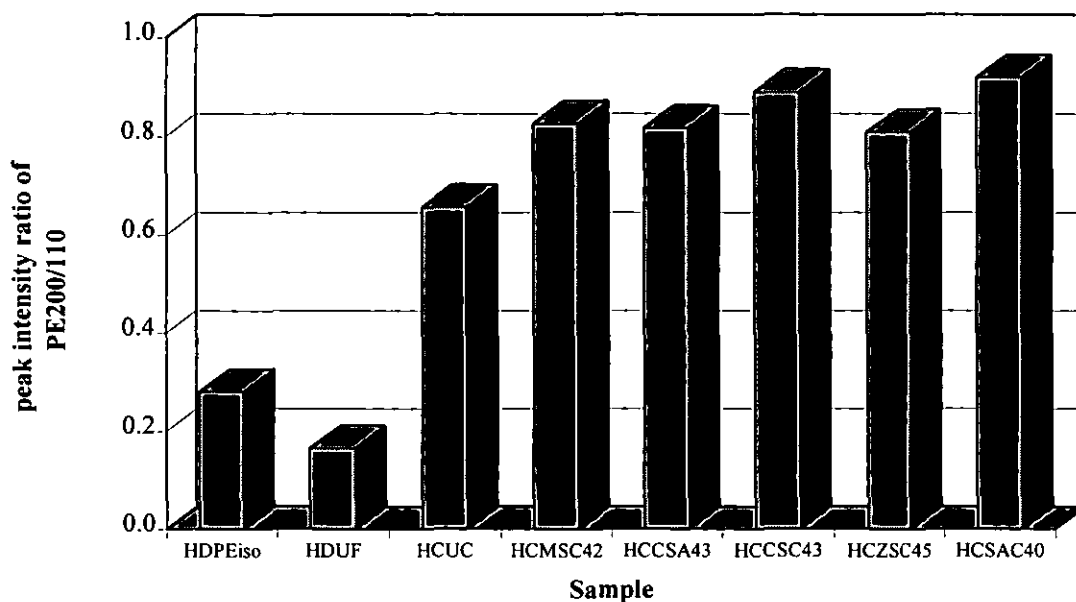


Figure 5.26: Peak intensity ratio of PE200/110 for isotropic HDPE, unfilled HDPE and CaCO_3 filled compounds containing various coating agent types.

From Figure 5.27, the peak intensity ratio of CC104/110 for calcium carbonate powder is approximately the same as that ratio taken from X-ray diffraction powder index file [140], hence this value was used as the reference to compare the calcium carbonate orientation in the injection moulding. Like magnesium hydroxide, the orientation of calcium carbonate increases when it was added to the polymer matrix. The CC104/110 ratio increases further when calcium carbonate is coated with coating agents but this effect is much less than the MH001/101 in magnesium hydroxide filled compounds. This is because crystals of CaCO_3 cleave fairly readily. The angle between the cleavage face is 78° and 102° [174]. Hence CaCO_3 particles are only slightly non-equiaxed compared to $\text{Mg}(\text{OH})_2$ and consequently the degree of alignment in injection moulded samples would not be expected to be great. This is seen in

Figure 5.27 where the maximum of CC104/110 ratio is only about double that of the powder sample. The equivalent figure for $\text{Mg}(\text{OH})_2$ is about 16 times.

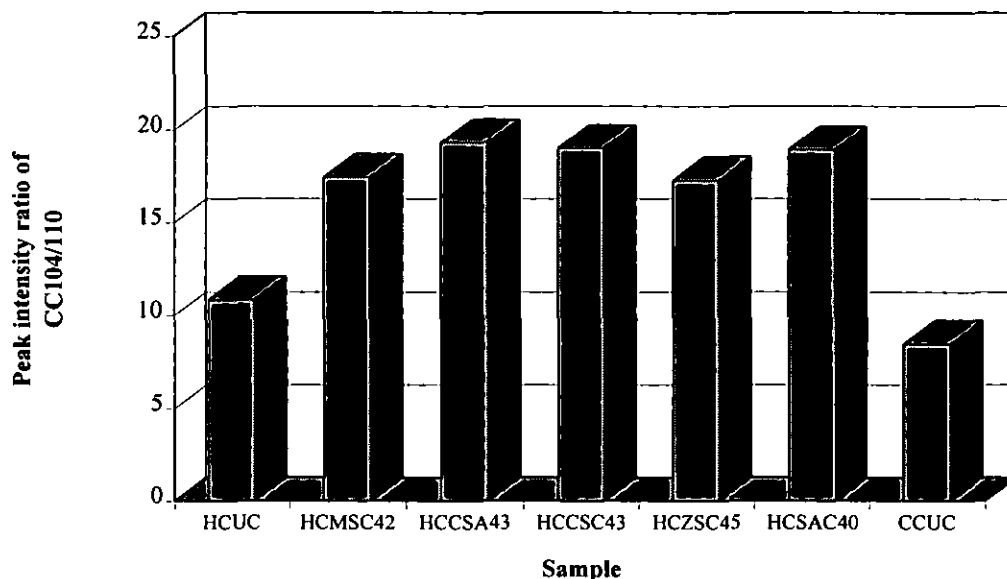


Figure 5.27: Peak intensity ratio of CC104/110 for calcium carbonate and CaCO_3 filled compounds containing various coating agent types.

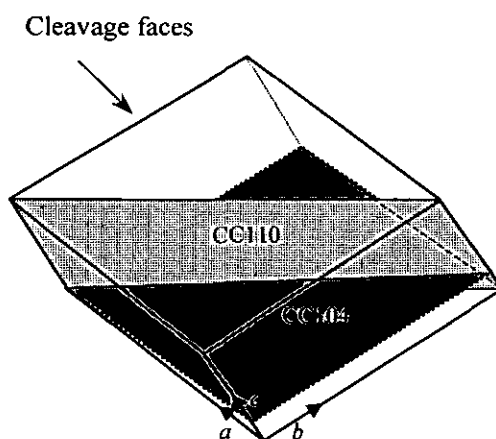


Figure 5.28: Rhombohedral structure and plane axes of calcium carbonate.

The modification of filler surfaces with various coating agent types gives further increase in CC104/110 ratio due to filler orientation compared with the unmodified filled-composite. It is considered that calcium carbonate particles align their long diagonal plane (CC110) to be perpendicular to the specimen surfaces and parallel to the injection flow direction (see Figures 5.28 and 5.29) to reduce the resistance for the

melted polymer flow as much as possible. It is revealed that the filler treatment results in the lubrication of filler, the improvement of filler wettability in matrix, and aids the alignment of filler particles in the injection direction. These results may correlate with an improvement of toughness, increased elongation at yield/extension at maximum load for coated filled-composites, in comparison with uncoated filled-composites.

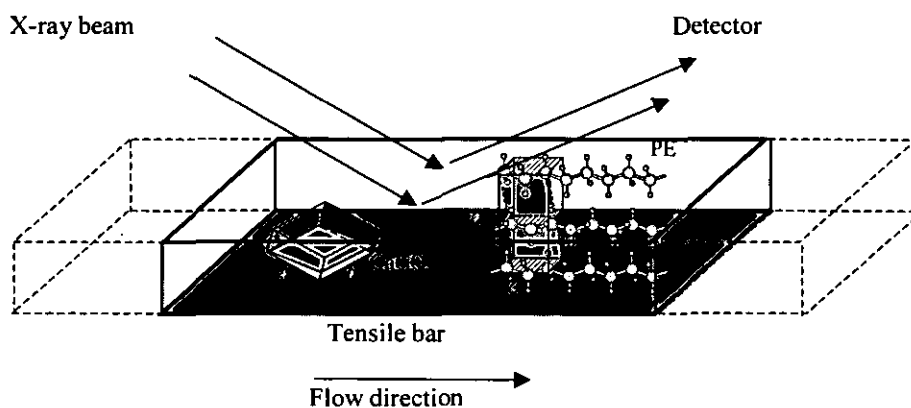


Figure 5.29: Scheme of a test sample showing places and directions of the X-ray diffraction measurements and the orientation of calcium carbonate and polyethylene crystals.

5.2.8 SURFACE FREE ENERGY

Surface free energies of uncoated/coated fillers and coating agents have been discussed in section (5.1.4). An example calculation of surface free energy is shown in Appendix D.6. The surface free energies of composites are shown in Table 5.6.

Table 5.6 shows that unfilled HDPE has the lowest surface free energy. The filler additions (either magnesium hydroxide or calcium carbonate) cause an increase in surface free energy of compounds due to high surface energy of the fillers (see Table 5.1). Surface modification of filler shows a decrease in surface free energy of compounds. This is due to the lower polarity of coating agents compared with the fillers. However, surface free energies of all composites are close to each other. It is considered that the specimen skin may contain only polyethylene. This may also be

due to contamination of mould release agent on specimen surfaces which is sprayed on mould surface before injection moulding is operated. However, filled HDPE composites containing uncoated magnesium hydroxide and calcium carbonate give slightly higher surface energy than unfilled HDPE and HDPE containing coated filler. This is due to the high polarity of magnesium hydroxide and calcium carbonate (see Table 5.1).

Table 5.6: Contact angles and surface free energy of compounds (average of 5 tests).

Code	Contact angle (degree)				Surface free energy (mJm^{-2})
	Water	Glycerol	DIM	BNL	
HDFU	96.0	80.0	51.6	46.2	33.16
HMUC	82.2	73.0	50.8	33.8	37.04
HMSA62	90.0	76.0	48.5	38.8	36.08
HMSC62	94.2	79.0	51.4	48.2	34.14
HMCSC64	95.0	78.5	53.0	42.8	33.76
HMZSC67	93.5	78.0	51.0	42.0	34.48
HMSAC60	92.2	76.5	54.3	38.0	34.72
HCUC	89.8	73.5	50.2	28.4	37.78
HCMSC42	93.0	75.8	52.2	42.0	34.61
HCCSA43	92.4	77.4	51.8	38.6	35.03
HCCSC43	93.6	76.6	53.6	43.8	33.79
HCZSC45	92.8	76.4	51.6	41.6	34.73
HCSAC40	91.6	76.0	64.8	42.4	31.62

5.2.9 SPECIFIC ENERGY

Specific energy is defined as energy consumption in the compounding machine per unit mass of polymer during compounding. An example of calculation of specific energy is shown in Appendix D.9. Values of specific energy are summarised in Table 5.7.

The specific energies of unfilled HDPE and HDPE filled with magnesium hydroxide and calcium carbonate represented in Table 5.7 show that the addition of each filler results to an increase in the specific energy of compounding machine to produce filled

compounds compared with unfilled HDPE. The surface modification of filler promotes a decrease in specific energies of compounding machine. As coating agents are coated on the fillers, they act as lubricating agents which can change the rheological properties by reducing the melt viscosity of the polymer [44] and may also modify considerably temperature stability characteristics of composites. Metal stearates produce a more effective coating than stearic acid for magnesium hydroxide. Calcium stearate coating is the best coating agent for both magnesium hydroxide and calcium carbonate. Stearic acid is also particularly good for calcium carbonate. These results are consistent with surface free energy of uncoated fillers, coated fillers, and coating agents (see Table 5.1).

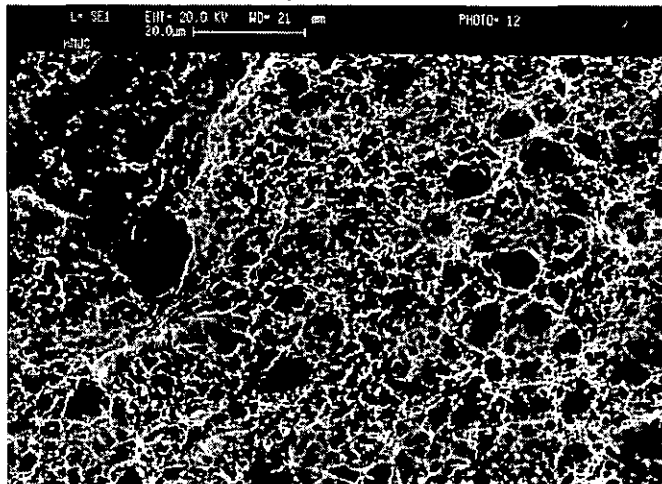
Table 5.7: Specific energy of compounding machine to produce each HDPE compound.

Code	Screw speed (rpm)	Torque (%)	Specific energy (kWhr/kg)
HDPE	350	70.0	0.245
HMUC	353	65.0	0.287
HMMSA62	350	60.0	0.211
HMMSC62	352	55.0	0.194
HMCSC64	351	60.0	0.193
HMZSC67	351	57.5	0.202
HMSAC60	351	60.0	0.211
HCUC	352	60.0	0.264
HCMSC42	352	60.0	0.211
HCCSA43	352	60.0	0.211
HCCSC43	351	55.0	0.193
HCZSC45	350	60.0	0.210
HCSAC40	351	55.0	0.193

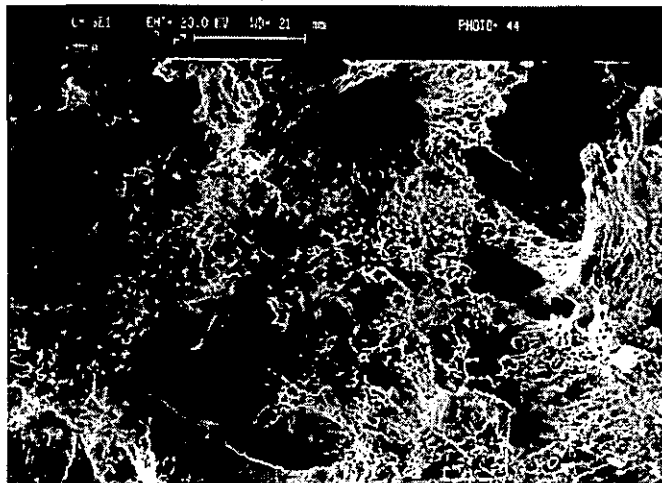
5.2.10 MICROSTRUCTURE AND MORPHOLOGY

Microstructure of fractured samples was studied using scanning electron microscopy (SEM) to investigate morphology of composites. All samples were cut from a fractured part which had been tested using falling weight impact as described in section 3.5.5. The SEM micrographs are shown in the Figures 5.30 and 5.31.

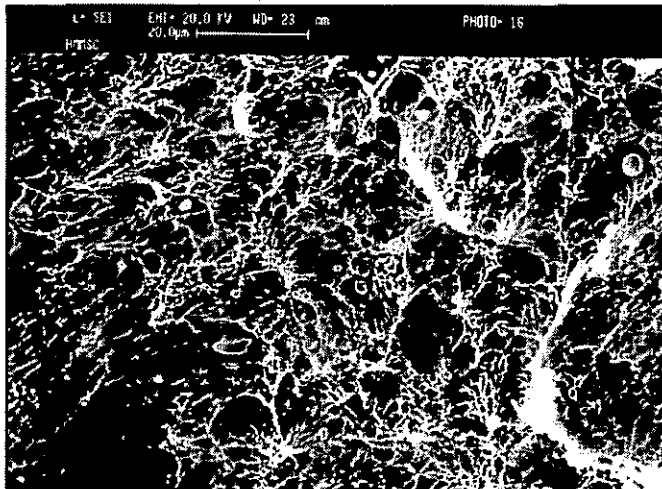
a) HMUC



b) HMMSA62



c) HMMSC62



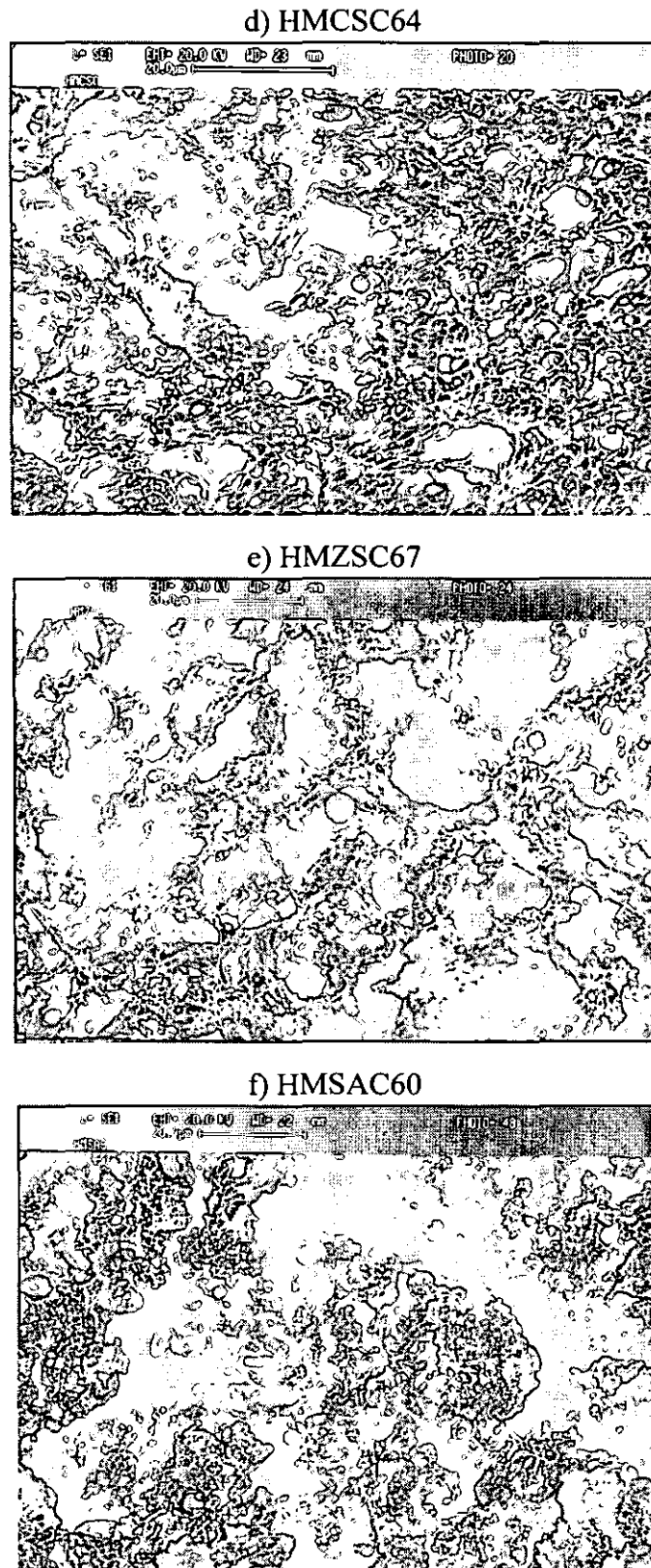
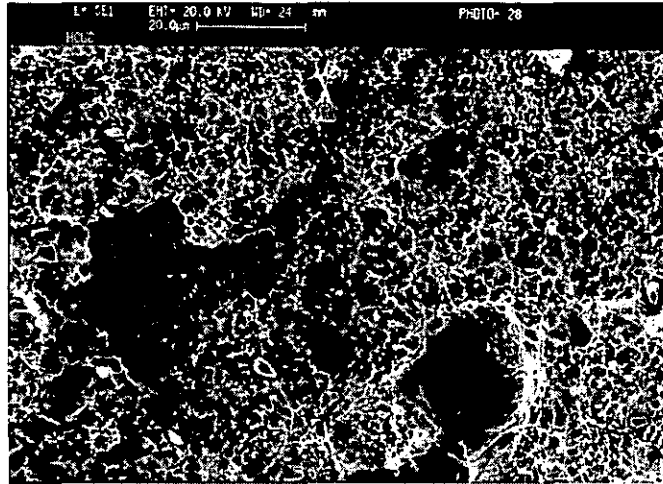
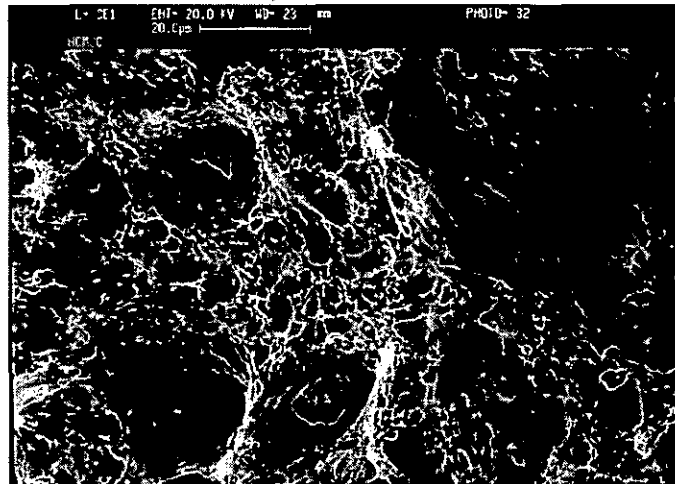


Figure 5.30: Microstructure of filled high density polyethylene containing Mg(OH)₂: a) uncoated, b) added with Mg stearate, c) coated with Mg stearate, d) coated with Ca stearate, e) coated with Zn stearate, and f) coated with stearic acid.

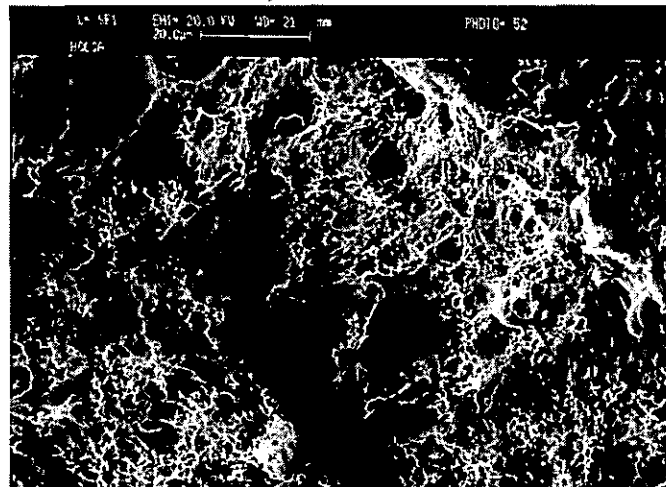
a) HCUC



b) HCMSC42



c) HCCSA43



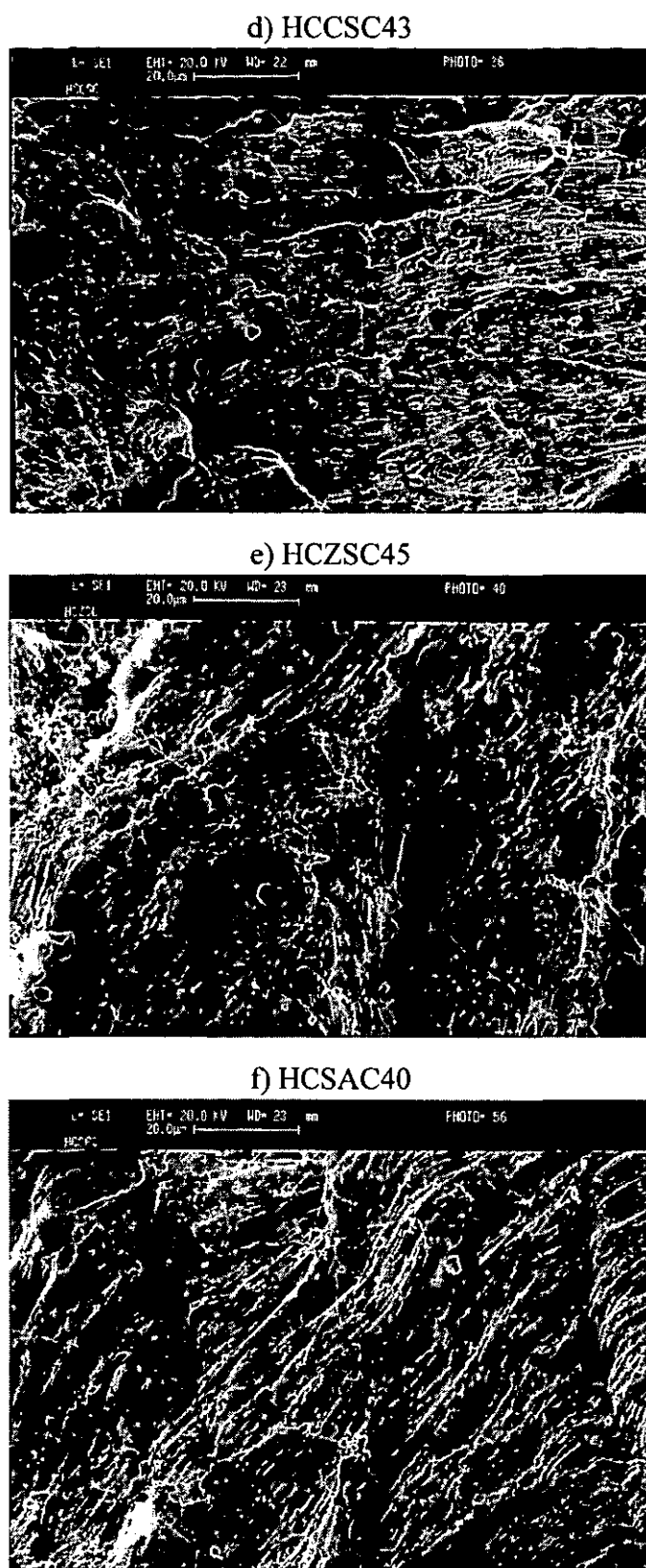


Figure 5.31: Microstructure of filled high density polyethylene containing CaCO_3 : a) uncoated, b) coated with Mg stearate, c) added with Ca stearate, d) coated with Ca stearate, e) coated with Zn stearate, and f) coated with stearic acid.

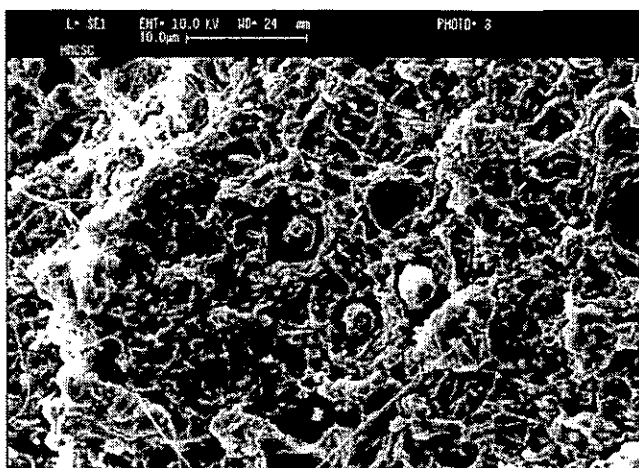
Examination of fracture surfaces obtained from impact test specimens reveals extensive cracking and lack of bonding at the filler/matrix interface for HDPE filled with untreated magnesium hydroxide (Figure 5.30 (a)). The results obtained from mechanical properties indicate that the surface coating of $\text{Mg}(\text{OH})_2$ gives an increase in matrix yielding relating to the fibre-like structures created from applied stress as shown in Figure 5.30 (b) to (d). These results are supported by increasing impact properties with ductile failure of filled compounds containing metal stearates. As a result of the reduced value of surface free energy for coated filler compared with the uncoated one, it suggests that filler particles are generally well dispersed in the polymer matrix. However, compounds containing one monolayer coverage of $\text{Mg}(\text{OH})_2$ with stearic acid (Figure 5.30 (f)) shows a slightly smoother surface reflecting low impact properties of the composite compared with metal stearates. This may be because stearic acid has a higher surface free energy than metal stearates leading to poorer filler dispersion.

For CaCO_3 filled-composites, the morphology of the compound containing uncoated CaCO_3 shows slightly smooth surfaces with brittle failure under impact force (Figure 5.31 (a)). Again, compounds containing treated CaCO_3 show ductile failure as shown in Figure 5.31 (c-f) implying an increase in dispersibility and wettability of filler. This result leads to an increase in matrix yielding and impact properties of modified CaCO_3 filled-compounds.

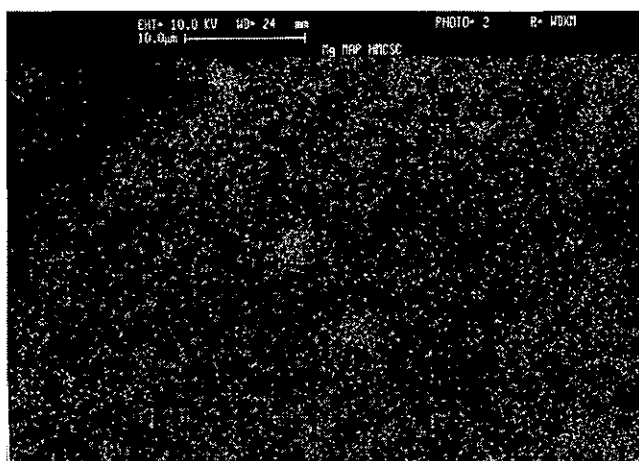
5.2.11 WAVELENGTH DISPERSIVE X-RAY MAPPING (WDXM)

To understand the surface treatment of fillers, wavelength dispersive X-ray mapping was used for scanning filled compounds containing the different elements in fillers and coating agents for example a compound containing CaCO_3 coated with magnesium stearate. The white dots on micrographs correspond to the position where the element is being investigated. The results of mapping for two compounds, which are high density polyethylene containing $\text{Mg}(\text{OH})_2$ coated with calcium stearate (HMCSC64) and that containing CaCO_3 coated with magnesium stearate (HCMSC42), are shown in Figures 5.32 and 5.33.

a) HMCSC



b) HMCSC (Mg mapping)



c) HMCSC (Ca mapping)

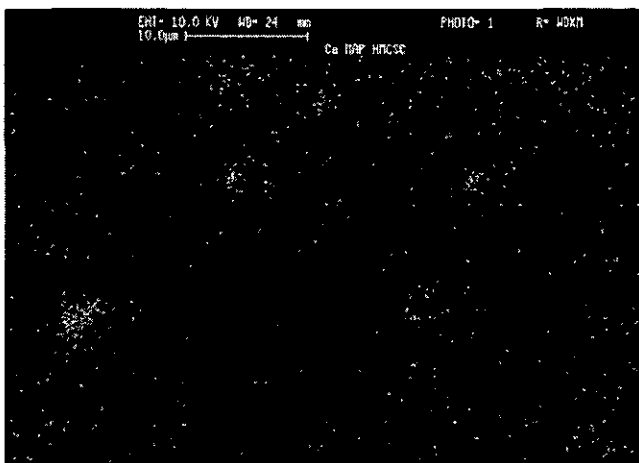
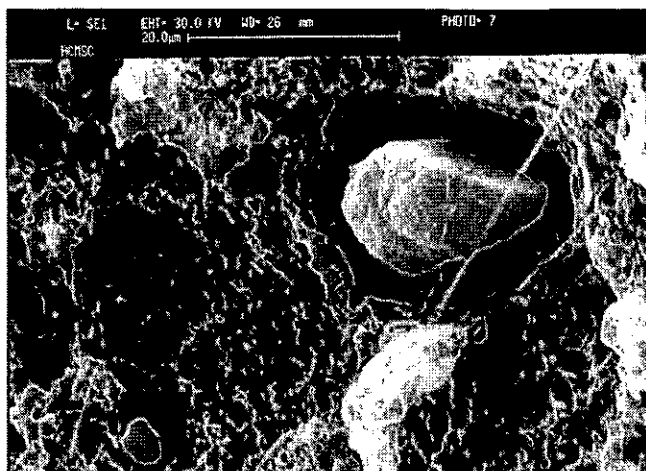
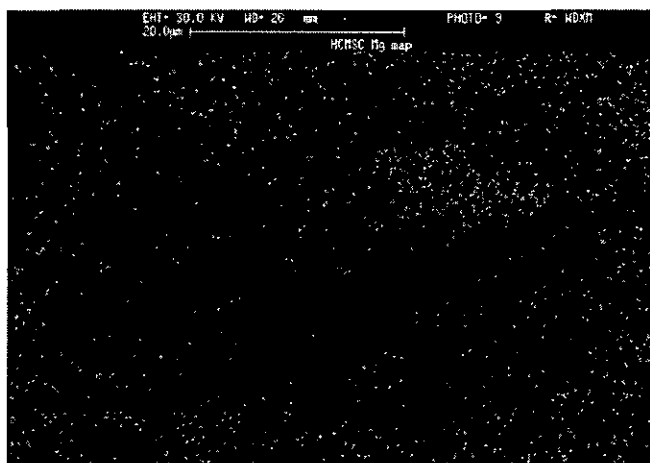


Figure 5.32: Micrographs of HDPE compounds containing Mg(OH)₂ coated with calcium stearate a) image, b)Mg mapping, c) Ca mapping.

a) HCMSC



b) HCMSC (Mg mapping)



c) HCMSC (Ca mapping)

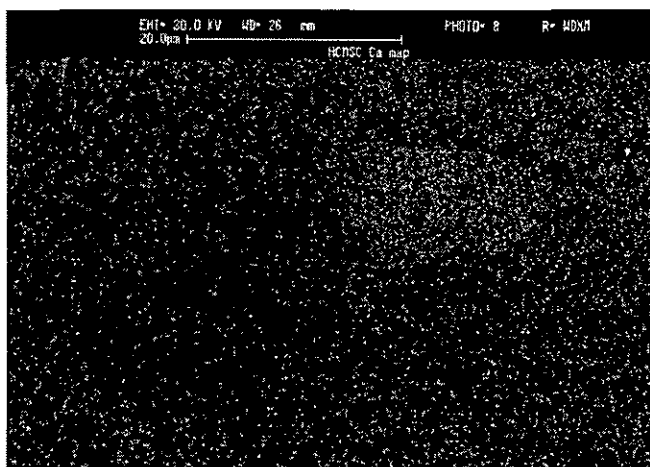


Figure 5.33: Micrographs of HDPE compounds containing CaCO_3 coated with magnesium stearate a) image, b) Mg mapping, c) Ca mapping.

The filled HDPE compound containing $\text{Mg}(\text{OH})_2$ coated with Ca stearate showed X-ray signals of both Ca and Mg elements when it was mapped. Mg mapping shows randomly dispersed white dots and several groups of dense regions of white dots are found in the position of magnesium hydroxide particles. Ca mapping shows less intensity of dispersed white dots compared with Mg mapping. On the surface of $\text{Mg}(\text{OH})_2$ particles, the signal from Mg has a higher intensity than that of Ca due to more opportunities of finding Mg on the $\text{Mg}(\text{OH})_2$ surface. Some strong Ca signals are found on the other areas of magnesium hydroxide particles, due to the roughness of the sample surface. X-ray signals cannot penetrate deeply into areas under the surface.

A CaCO_3 filled compound containing Mg stearate as shown in Figure 5.33 shows strong signals of Ca on the surface of calcium carbonate and also on the matrix during Ca mapping. Mg element is also found on the calcium carbonate particles and randomly distributed in the matrix. Impact fracture samples cut from HDPE compounds containing $\text{Mg}(\text{OH})_2$ and CaCO_3 coated with zinc stearate are shown in Appendix H (Figures H.1 and H.2). Mg and Ca mapping give distinct signals (a high concentration of white dots) in the position of magnesium hydroxide and calcium carbonate particles, Figures H.1(b) and H.2(b), respectively. Zinc mapping shows a random distribution of white dots and does not show groups of white dots on either filler coated with zinc stearate (Figures H.1(c) and H.2(c)). It implies less adsorption of zinc stearate on the surface of both fillers. Although XPS and FTIR results shows the highest coating thickness for zinc coated $\text{Mg}(\text{OH})_2$ and CaCO_3 , desorption of zinc stearate from the filler surface may occur when the compounds are ruptured. However, the mapping technique has limitations and is better used for smooth surfaces but this technique still gives some useful information for further understanding the filler coating.

5.3 EFFECT OF COATING AGENTS ON POLYMER PROPERTIES

To see whether coating agents alone affect polymer properties, the equivalent amount of each coating agent which had been used for one monolayer coated $\text{Mg}(\text{OH})_2$ was incorporated into HDPE to produce specimens using injection moulding. The amount of the polymer and coating agent components are confirmed from polymer/coating agent contents. Tensile, flexural, impact, and crystallisation properties are determined. Reversion, polymer orientation, surface free energy, specific energy and melt flow index are also investigated. These results are discussed below.

5.3.1 POLYMER/COATING AGENT CONTENTS

The polymer/coating agent contents were determined using an ashing test and the results of measurements are given in Table 5.8. Each sample of unfilled HDPE, coating-agent filled HDPE, and coating agent was burned in a furnace for 3 hours at 850 °C to produce ash. The polymer/coating agent contents from Table 5.8 illustrate that in all cases the coating contents are slightly lower than the intended values.

Table 5.8: Polymer/coating agent contents.

Code	DETAILS	%Polymer Content	%Filler Content	%Coating Content
HDPE	100% HDPE	99.95	0.00	0.00
HDMS	HDPE+4.0%Mg STEARATE	96.16	0.00	3.84
HDCS	HDPE+4.1%Ca STEARATE	95.97	0.00	4.03
HDZS	HDPE+4.3%Zn STEARATE	95.76	0.00	4.24
HDSA	HDPE+3.9%STEARIC ACID	96.22	0.00	3.78

5.3.2 TENSILE PROPERTIES

In order to study effects of coating agents alone on mechanical properties of polymer, tensile bar specimens were produced using a Negri Bossi NB55 injection moulder. The tensile properties were determined using a Lloyd tensile testing machine, type L200R. Tensile properties are summarised as shown in Figure 5.34.

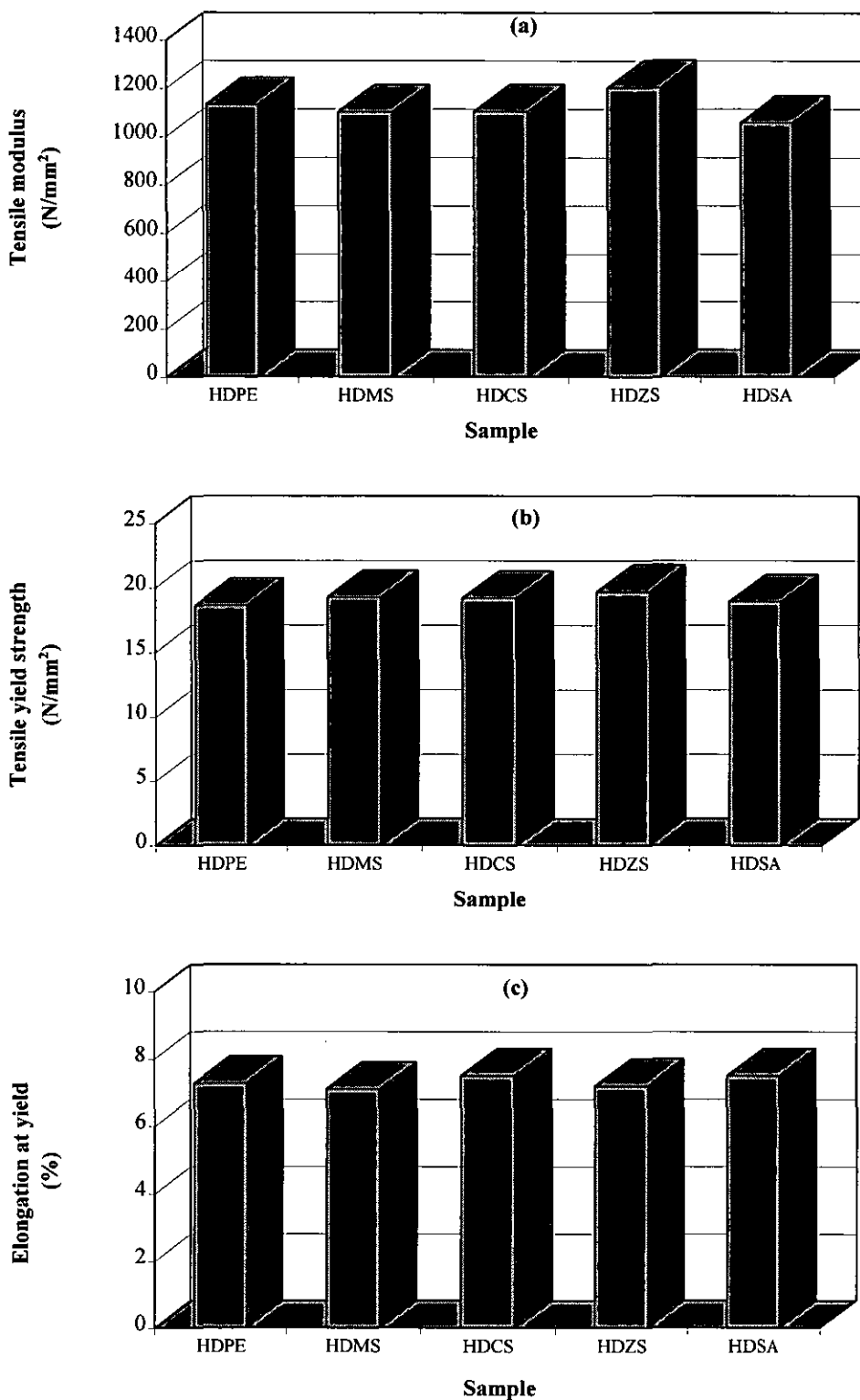
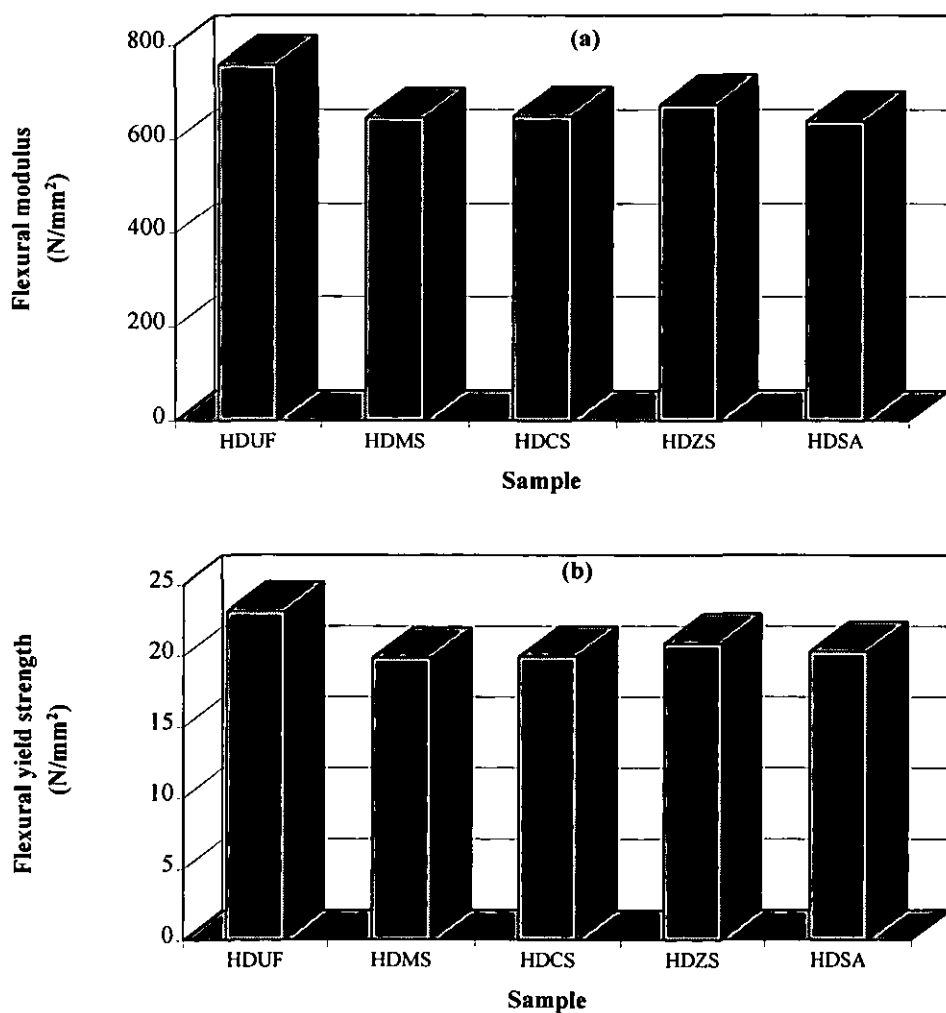


Figure 5.34: Tensile properties of unfilled HDPE and HDPE compounds containing various coating agent types; (a) tensile modulus, (b) yield strength, (c) elongation at yield.

It is seen from Figure 5.34 that all compounds containing various coating agent types give similar modulus, yield strength and elongation at yield, compared with unfilled HDPE. It indicates that the addition of coating agent has minimal effect on tensile properties.

5.3.3 FLEXURAL PROPERTIES

Flexural properties of HDPE filled with various coating agents were determined using the same tensile testing machine in three point flexural mode. The results are summarised in Figure 5.35.



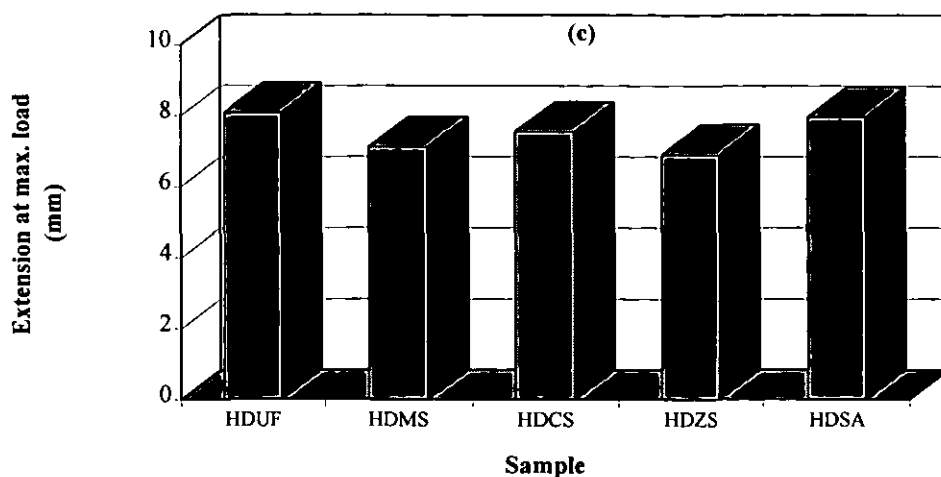


Figure 5.35: Flexural properties of unfilled HDPE and HDPE compounds containing various coating agent types; (a) tensile modulus, (b) yield strength, (c) extension at maximum load.

Figure 5.35 reveals that the addition of coating agent gives a slight reduction of flexural modulus, yield strength and extension at maximum load. The results show no specific effects of coating agent type on flexural properties. It is possible that the coating agents may act as plasticisers which promote mobility of polymer chains and reduce the operating temperature for polymer processing, thereby increasing the tendency for adding higher amount of filler and improving processing characteristics.

5.3.4 IMPACT PROPERTIES

Figure 5.36 shows that an addition of coating agent slightly decreases the peak force, peak energy and failure energy. It is due to the fact that the coating agents act as lubricant resulting in reduction of polymer orientation and impact properties.

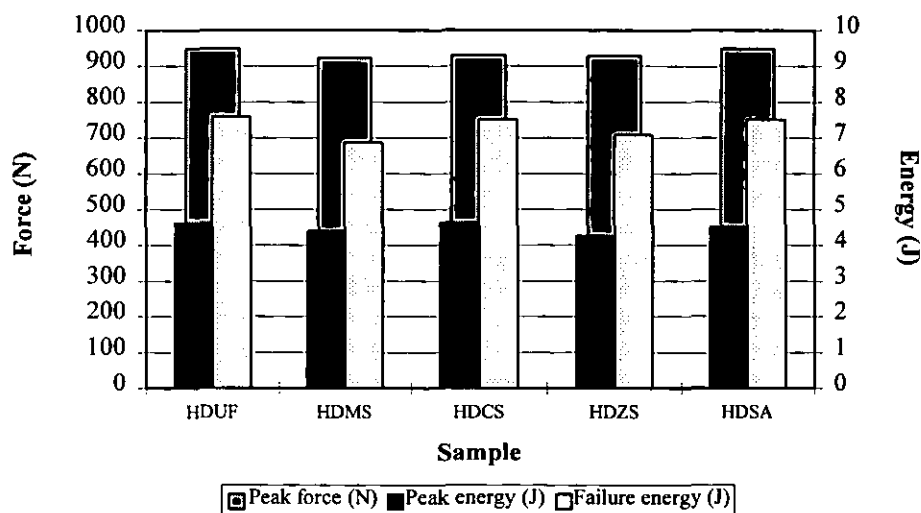


Figure 5.36: Impact properties of unfilled HDPE and HDPE compounds containing various coating agents.

5.3.5 CRYSTALLISATION PROPERTIES

To understand further the effect of coating agents on mechanical properties of polyethylene, crystallisation properties of compounds obtained from DSC results are determined and summarised in Table 5.9.

Table 5.9: Crystallisation properties for HDPE unfilled and filled with various coating agents.

Code	Details	T_m ($^{\circ}\text{C}$)	T_c ($^{\circ}\text{C}$)	% Cryst
HDUF	100% HDPE	134.1	110.6	62.18
HDMS	HDPE+4.0%Mg STEARATE	132.2	112.1	73.11
HDCS	HDPE+4.1%Ca STEARATE	133.0	111.9	72.76
HDZS	HDPE+4.3%Zn STEARATE	132.0	112.7	70.89
HDSA	HDPE+3.9%STEARIC ACID	131.7	112.2	71.37

By inspection of crystallisation properties, it is seen that the addition of coating agent results in a slight decrease in melting temperature but increase in recrystallisation temperature due to the nucleation effect of metal stearates and stearic acid. These samples have higher overall crystallinity compared with the unfilled one. The compound containing magnesium stearate gives the highest degree of crystallinity, calcium stearate compound gives the second, stearic acid compound gives the third and zinc stearate compound give the lowest value.

5.3.6 REVERSION MEASUREMENT

In order to estimate the molecular orientation in moulded specimens, the maximum reversion of the moulded specimens after a specified heat treatment was determined using a reversion test. The testing temperature used was 132 °C. The results are represented in Figure 5.37.

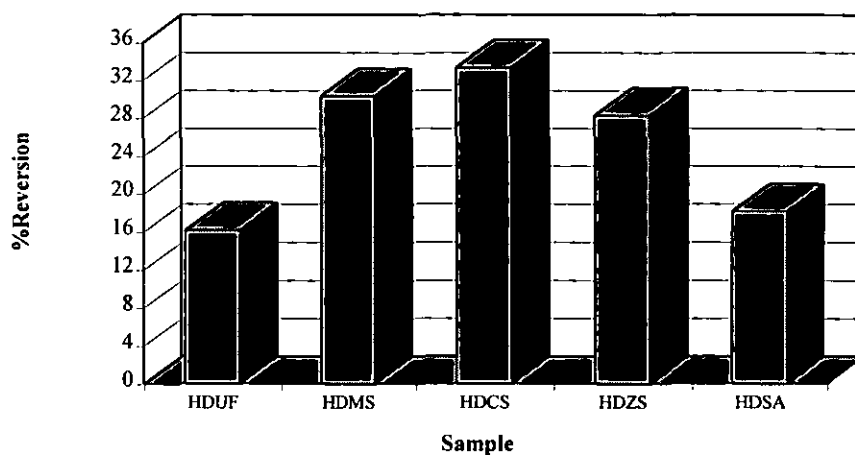


Figure 5.37: %Reversion of unfilled HDPE and HDPE compounds containing various coating agents.

It is apparent that the addition of coating agent gives an increase in percentages of reversion compared with unfilled HDPE. The addition of metal stearates results in a higher percentage of reversion than that of stearic acid. Calcium stearate filled HDPE shows highest percentage of reversion, magnesium stearate filled HDPE is second, and zinc stearate filled HDPE is third. This implies that the addition of coating agents gives more polymer alignment in compounds. However, stearic acid provides less opportunity for chain mobility than the other coating agents which may stimulate recoiling and twisting of the polymer chains as lubricating effect.

5.3.7 POLYMER ORIENTATION

In order to understand further about effect of coating agents on mechanical properties, X-ray diffraction is used to examine the orientation of the polymer. The peak intensity ratio of PE200/110 is plotted for the different samples as shown in Figure 5.38.

Figure 5.38 shows that the peak intensity ratios of PE200/110 for filled HDPE are lower than unfilled HDPE which is a lot different to what happens when the coating agents are on the filler particles. It implies that the presence of the coating agents cause the reduction of polymer alignment. These coating agents act as lubricant hence the polymer molecules may move freely during processing and relax back to random coiled configurations relating to slightly reduced elongation at yield and extension at maximum load in the flexural test.

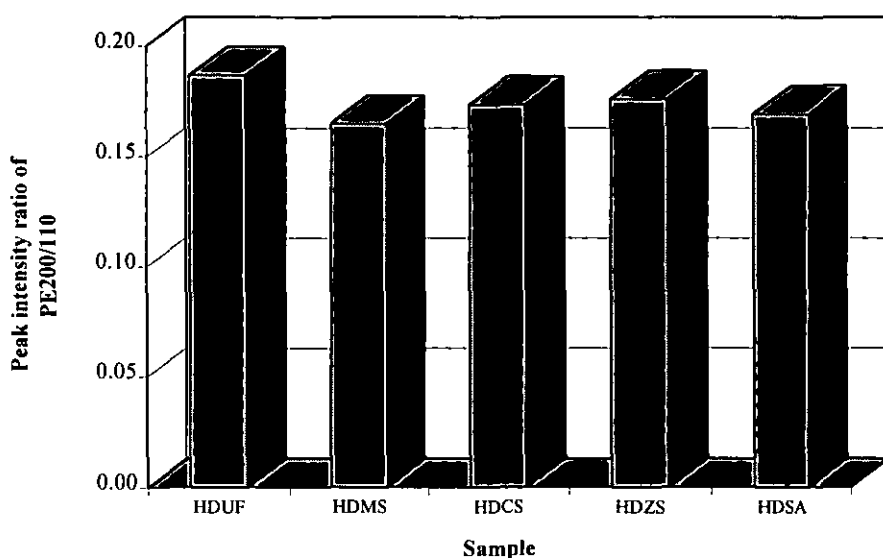


Figure 5.38: Plot of the peak intensity ratio of PE200/110 for unfilled HDPE and HDPE compounds containing various coating agents.

5.3.8 SURFACE FREE ENERGY

Surface free energies of magnesium hydroxide and calcium carbonate filled HDPE containing different coating types have been discussed in an earlier section (5.2.8). The surface free energies of HDPE containing various coating agent types are shown in Table 5.10.

Table 5.10 shows that surface free energies of all filled compounds are fairly constant and close to each other, but are less than unfilled HDPE. This is because the surface free energies of the coating agents are slightly lower than HDPE.

Table 5.10: Contact angles and surface free energy of HDPE containing various coating agents (average of 5 tests).

Code	Contact angle (degree)				Surface free energy (mJm ⁻²)
	Water	Glycerol	DIM	BNL	
HDUF	94.4	79.0	55.4	43.8	32.92
HDMS	93.8	77.8	64.2	41.2	31.49
HDCS	93.4	76.4	65.8	40.0	31.57
HDZS	94.2	78.0	64.4	40.2	31.55
HDSA	91.6	76.0	64.8	42.4	31.64

5.3.9 SPECIFIC ENERGY

Specific energies obtained during compounding for HDPE alone and HDPE containing various coating agents are investigated and the results are shown in Table 5.11.

Table 5.11: Specific energies obtained during compounding for HDPE alone and HDPE containing various of coating agents.

Code	Screw Speed (rpm)	Torque (%)	Specific energy (kWhr/kg)
HDUF	351	70.0	0.245
HDMS	351	35.0	0.123
HDCS	350	35.0	0.122
HDZS	350	37.5	0.131
HDSA	351	37.5	0.132

Table 5.11 shows that HDPE with various coating agents gave lower specific energies than HDPE. It indicates that these coating agents act as lubricant, thus compounding and injection moulding can be carried out using lower torque and temperature than usual conditions.

5.3.10 MELT FLOW INDEX (MFI)

The Melt Flow Index test is a method used to characterise the flow of polymer melts. The apparatus consists of a single point ram extruder and test conditions are followed using standard testing (BS 2782) method. The polymer sample is heated in the barrel to a temperature of 190°C and then extruded through a standard die (diameter of

internal bore 0.2096 mm, die length 8.0 mm) using a standard weight (2.16 kg) on the piston, and the weight (in gms) of polymer extruded in 10 minutes is quoted as the melt flow index (MFI) of the polymer. Melt flow indices of HDPE containing various coating agents were determined and the results are shown in Table 5.12.

Table 5.12: Melt flow indices of HDPE containing various coating agents.

Code	Composition	MFI (g/10 min)
HDPE	HDPE virgin	20.20
HDUF	HDPE unfilled	20.86
HDMS	HDPE+Mg STEARATE	23.46
HDCS	HDPE+Ca STEARATE	23.66
HDZS	HDPE+Zn STEARATE	24.76
HDSA	HDPE+STEARIC ACID	23.20

Table 5.12 shows that unfilled HDPE gives a slightly higher MFI than virgin HDPE, indicating chain scission of the polymer molecules at high temperature, pressure, and shear during compounding. The chain scission causes a decrease in average molecular weight of polymer resulting in the reduction of viscosity. Filled HDPE compounds containing various coating agent types show higher melt flow indices than unfilled HDPE. The presence of coating agents shows an improvement of flow properties of compounds. These coating agents help to lubricate polymer chains, reduce viscosity of the molten polymer and also reduce the friction force between polymer and mechanical equipment.

5.4 SUMMARY

The aim of this series was to study the effects of various coating agent types on mechanical properties of magnesium hydroxide and calcium carbonate filled HDPE compounds.

5.4.1 CHARACTERISATION AND MECHANICAL PROPERTIES

From characterisation of coated filler surfaces, it was found that:

- The coverage of fillers with individual coating agents using a mixer operated at high speed and temperature gave better results for surface coating than one operating at low speed and room temperature.
- The DSC technique can be used to detect phase transformations in coating agents.
- DSC also indicates that metal stearates have polymorphic structures showing several transitions up to the melting point.
- X-ray diffraction results showed differences of patterns between initial and final period of coating indicating the progress to monolayer coverage of coating agent on the filler. X-ray diffraction can also be used for investigating of polymer/filler orientation.
- Information obtained from XPS is in agreement with FTIR results, zinc stearate coating gave the highest thickness, followed by stearic acid coating. However, their composites showed less toughness than composites containing magnesium/calcium stearate coating. As zinc stearate and stearic acid have higher surface energies than magnesium and calcium stearates causing poorer dispersion and distribution of fillers, the interfacial force between HDPE and filler coated with stearic acid and zinc stearate are higher than that with other stearates.
- Detailed characterisation of coated fillers, and the coating process can be carried out by the combined use of thermal analysis, DRIFT and XPS; these three techniques serve to produce complementary information.

From mechanical property testing, the results can be concluded as follow:

- The addition of filler to polymer results in the deterioration of mechanical properties.
- The surface modification of filler with one monolayer of coating can improve toughness of composites.
- As a result of low polarity of coating agents, filler coating can help to improve the wettability and dispersibility of filler and to promote filler/polymer orientation.
- Further increase in crystallisation is caused from the nucleating effect of coating agents.

5.4.2 STRUCTURE/PROPERTIES/INTERACTIONS

Metal stearates coated on both magnesium hydroxide and calcium carbonate in filled HDPE-composites were effective for improving impact properties, decreasing

tensile/flexural modulus, and increasing elongation at yield while the effects on tensile and flexural strength were insignificant. The level of surface treatment applied to magnesium hydroxide has a significant effect on the composite properties. The optimum impact properties were achieved using experimental monolayer coverage of the fillers. Coating of metal stearates produced tougher, but less stiff compounds than when stearic acid was used, even when the concentration of coating was equivalent. Calcium stearate gave the toughest filled-compound containing magnesium hydroxide while both calcium and magnesium stearate produced the optimum impact properties for calcium carbonate filled-compounds. Calcium stearate was also found to be more stable than the other coating agents. From DSC results calcium stearate gave one transition (C-form) and did not change polymorphic forms while both magnesium and zinc stearates gave three polymorphic forms (A-, B-, and C-form) during coating at high temperature. Calcium stearate remained free at the end of coating process resulting in the reduction of tensile/flexural modulus causing by lubricating effect. In order to understand the observed changes in mechanical properties of the composites, the following possible causes, i.e. changing in surface free energy, crystallinity, polymer/filler orientation, specific energy, and MFI were investigated. The surface modification of filler gave a decrease in the surface free energy of the filler resulting in a modified interfacial force between polymer and filler. However, the decrease in surface free energy of coated fillers was similar for all the coating agent types used. An increased flexibility of interaction between the polymer and filler at the interface in the presence of coating agents could account for the increase in elongation at yield of composites. This interaction may also cause an increase in both polymer and filler orientation in a similar way. The different types of coating agent affected the orientation of composites similarly. However, the increased filler orientation seemed to have little effect on impact properties. Compounds containing coating agents (both with and without filler) showed lower specific energies and higher MFI than unfilled composite. This suggests that the lubricating effect was a controlling parameter for increasing toughness of coated filled-compounds. Crystallinity increased with filler coating but did not appear to have a major effect on tensile, flexural, and impact properties.

CHAPTER 6

CONCLUSIONS AND SUGGESTIONS FOR FURTHER WORK

6.1 CONCLUSIONS

Magnesium hydroxide and calcium carbonate were used as fillers for studying the effect of stearic acid/stearate coating on filled HDPE properties. Filler surfaces were modified using four types of coating agents, i.e. stearic acid, magnesium stearate, zinc stearate, and calcium stearate. Coating was carried out using a Fielder mixer and compounds were prepared using a twin screw compounder with a filler loading of 40%w/w. FTIR, DSC, XRD, XPS and contact angle measurements were used to characterise fillers. The effect of various coating agent concentrations and types on mechanical properties of compounds were investigated using a variety of methods including tensile, flexural and impact measurements.

Coating results showed that mixing temperature influences the coating performance. The higher the operating temperature the faster and more effective the coating. FTIR results using a DRIFT technique showed increases in integrated CH absorbances with increased coating concentration. Zinc stearate and stearic acid coating gave higher integrated CH absorbances than magnesium and calcium stearate coatings. Information obtained from XPS was in agreement with the FTIR results, zinc stearate coating gave the highest thickness followed by stearic acid, magnesium stearate, and calcium stearate coatings.

Interactions/reactions between fillers and coating agents have been observed. FTIR transmission results showed that stearic acid reacted with magnesium hydroxide and produced magnesium stearate but did not react simply with calcium carbonate to produce calcium stearate. The reactivity of coating agents to the fillers can be listed as below:

stearic acid > zinc stearate > magnesium stearate > calcium stearate

DSC traces showed that magnesium stearate and zinc stearate have several transitions up to their melting points. Three kinds of mesomorphic forms were detected at various temperatures. Thermal analysis was also used to examine the disappearance of free components in the mixture relating to the adsorption of coating agent onto the filler surfaces, for samples taken at various coating times from the Fielder mixer. It appeared that the adsorption of coating agent on the fillers increased with increased coating time. The higher the melting temperature of the coating agent the slower coverage of the filler. 40 minutes and 140°C were the optimum conditions for the coating of filler with one monolayer of coating agent in this study.

From contact angle measurements, fillers gave a much higher surface free energy than polymer. The surface free energies of fillers decreased progressively with the addition of coating agents. Metal stearates gave lower surface free energies than stearic acid. Calcium stearate showed the lowest surface free energy, magnesium and zinc stearate gave moderate values.

The addition of filler to polymer increased the specific energy required to mechanically process the filled composites. This specific energy reduced when the filler was coated. MFI results also showed that the addition of coating agents reduced viscosity of the melted polymer. The filler addition gave an increase in crystallinity (from 57% to 64%) and crystallisation temperature (from 111 to 114°C) while the melting temperature of composite decreased (from 134 to 131°C). Coating filler gave a further increase in crystallinity.

Mechanical properties of magnesium hydroxide and calcium carbonate filled compounds have been determined. The addition of filler increased tensile/flexural modulus, but decreased elongation at yield, extension at maximum load, and peak/energy force for impact properties with brittle fracture. Surface modification of filler increased toughness of filled composites. Filled composites containing metal

stearates were tougher than those containing stearic acid. Magnesium hydroxide filled-composites containing calcium stearate gave the highest toughness compared to those containing magnesium stearate, followed by these coating zinc stearate and stearic acid. The calcium carbonate filled-composite containing magnesium stearate was tougher than those with calcium stearate, zinc stearate and stearic acid, respectively.

Surface modification of filler gave a higher polymer orientation for filled composites compared to unfilled HDPE. A higher filler orientation was also obtained when filler was coated. Better filler orientation relates to an increase in tensile/flexural elongation compared with uncoated filled-composites. A single monolayer coating gave the highest polymer and filler orientation compared with the other coating concentrations. X-ray diffraction results also showed that a monolayer coverage of coating agent markedly increased the alignment of filler in the matrix for magnesium hydroxide filled composites while slightly enhanced filler orientation was found for calcium carbonate filled composites. This leads to HDPE compounds containing coated magnesium hydroxide having lower impact properties than compounds with coated calcium carbonate. A decrease in surface free energy of filler due to coating gives increased filler dispersion and wettability of filler leading to a higher toughness when fillers are coated. Fillers coated with calcium and magnesium stearate gave lower surface free energies than with zinc stearate and stearic acid resulting in tougher composites containing calcium/magnesium stearate in comparison with composites containing zinc stearate and stearic acid.

6.2 SUGGESTIONS FOR FURTHER WORK

To understand more about interaction between filler/coating agent/polymer at the interfaces, a polar polymer such as ethylene vinyl acetate (EVA) can be used for studies instead of a non polar polymer like HDPE.

The DSC technique gave considerable information about the adsorption of coating agent on filler surfaces at various coating times. To obtain more details of polymorphic forms, the examination should be done with very low heating rate. However, it also needs a high sensitivity apparatus to gain more information about coating agent properties to understand the mechanism of coverage of coating agent on filler surfaces.

Although contact angle measurements give excellent results about surface forces, direct force measurements such as an atomic force microscope (AFM) are an alternative method. For composite specimens it would be useful to measure contact angle under the skin surfaces of finished product to obtain real effect of the uncoated/coated filler contained in the polymer.

To understand further about polymorphism of metal stearates and stearic acid, the most common modifications are α , β' , and β which, in that order, display an increasing thermodynamic stability, heat of phase transformation, heat of fusion. The change in polymorphic forms of coating agents can be characterised by X-ray diffraction method with heating and cooling of sample units to examine each mesomorphic structure during heating.

Pole figures could be used to examine the compounds to understand more about the effect of injection moulding on polymer/filler alignment and the interaction between polymer, and coating agents.

REFERENCES

1. Katz S (1984) *Classic Plastics*, Thames and Hudson, London.
2. Touval I (1992) in *Kirk-Othmer Encyclopedia of chemical Technology*, Vol 10, 4th ed., John Wiley & Sons, New York.
3. Hornsby P R and Watson C L (1990) "A study of the mechanism of flame retardance and smoke suppression in polymers filled with magnesium hydroxide." *Polymer Degradation and Stability*, Vol. 30, p. 73-87.
4. Hornsby P R and Watson C L (1986) "Magnesium hydroxide-a combined flame retardant and smoke suppressant filler for thermoplastics." *Plastics and Rubber Processing and Applications*, Vol. 6, No. 2, p. 169-175.
5. Hornsby P R (1994) "The application of magnesium hydroxide as a fire retardant and smoke suppressing additive for polymers." *Fire and Materials*, Vol. 18, p. 269-276.
6. Sobolev I and Woycheshin E A (1987) "Alumina Trihydrate" in *Handbook of Fillers for Plastics*, edited by Katz H S and Milewski J V, Van Nostrand Reinhold Company, New York.
7. Rothon R (1995) *Particulate-filled polymer composites*, Longman Scientific & Technical, Essex.
8. Doak K W (1986) *Encyclopedia of Polymer Science and Engineering*, Vol.6, John Wiley & Sons Inc., New York.
9. Paiin G R (1967) *Plastics for Engineers an Introductory Course*, Pergamon Press, London.
10. Raff R A W and Doak K W, eds. (1965) "Crystalline Olefin Polymers", Pt.I, No. 20, in *High Polymer Series*, Wiley-Interscience, New York.
11. Boor J, Jr. (1979) *Ziegler-Natta Catalysts and Polymerizations*, Academic Press, Inc., New York.
12. Mandelkern L, *Crystallization of Polymers*, Maidenhead: McGraw-Hill, New York.
13. Boening H V (1966) *Polyolefins: Structure and Properties*, Elsevier Publishing Co., Ammsterdam.
14. Gordon M (1963) *High polymers: Structure and Physical Properties*, 2nd ed., Iliffe Books Ltd., London.
15. Geil P H (1963) *Polymer Single Crystals*, Interscience Publishers, New York.

16. Rybnikar F (1991) "Interactions in the system isotactic polypropylene-calcite." *Journal of Polymer Science*, Vol. 42, p. 2727-2737.
17. Murray G T (1993) *Introduction to Engineering Materials*, Marcel Dekker, Inc., New York.
18. Tobolsky A V (1960) *Properties and Structure of Polymers*, John Wiley & Sons, Inc., New York.
19. Hornsby P R and Mthupha A (1994) "Rheological characterisation of polypropylene composites filled with magnesium hydroxide." *Journal of Materials Science*, Vol. 30, p. 5293-5301.
20. Hornsby P R and Watson C L (1989) "Mechanism of smoke suppression and fire retardancy in polymer containing magnesium hydroxide filler." *Plastics and Rubber Processing and Applications*, Vol. 11, No. 1, p. 45-51.
21. Wyckoff R W G (1964) *Crystal structures*, 2nd ed., Interscience Publishers, New York.
22. Megaw H D (1973) *Crystal Structures*, W.B. Saunders Company, Philadelphia.
23. Goodenough R D and Stenger V A (1973) *Comprehensive Inorganic Chemistry*, Vol. 1, Pergamon Press, Oxford.
24. Whisson R R (1971) "Mineral powders.", in *Fillers for Plastics*, edited by Wake W C, Iliffe Books, London.
25. Baker R A, Koller L L, and Kummer P E (1987) "Calcium carbonate." in *Handbook of Fillers for Plastics*, edited by Katz H S and Milewski J V, Van Nostrand Reinhold Company, New York.
26. Wypych G (1993) *Fillers*, Chem Tec Publishing, Ontario.
27. Briggs C and Rutherford A. (1990) "A unique flame retardant filler for polyethylene and other cable compounds", *Antec '90*, p.1216-1220.
28. Oleesky S S and Morh J G (1964) *Handbook of Reinforce Plastics*, Reinhold Publishing corporation, New York.
29. Wan Hanafi W Z A W and Hornsby P R (1993) "Smoke suppression and fire retardancy in unsaturated polyesters containing hydrated fillers." *Plastic, Rubber and Composites Processing and Application*, Vol. 19, p. 175-184.
30. Mellor J W (1923) *A Comprehensive Treatise on Inorganic and Theoretical Chemistry*, Vol 4, Longmans, Green and Co., London.
31. Lewis R J (1993) *Hawley's Condensed Chemical Dictionary*, 12th ed., Van Nostrand Reinhold Company, New York.

32. Mason B and Berry L G (1959) *Elements of Mineralogy*, W. H. Freeman and Company, London.
33. Benzing E P (1967) "Fillers for Thermosetting plastics." in *The Encyclopedia of Basic Materials for Plastics*, edited by Simonds H R and Church J M, Reinhold Publishing Corporation, New York.
34. Jenkner H (1985) "Flame Retardants for Thermoplastics.", in *Plastics Additives Handbook*, edited by Gachter R and Muller H, Hanser Publishers, Munich.
35. Pasternak M, Zinn B T, and Browner R F (1982) "Studied of the chemical mechanism of smoke particulates formation during the combustion of chlorinated polymers." *Combustion Science and Technology*, Vol. 28, p. 263-270.
36. Lyons J W (1970) *The Chemistry and Uses of Fire Retardants*, Wiley-Interscience, New York.
37. Kuryla W C and Papa A J (1975) *Flame Retardancy of Polymeric Materials*, Vol. 3, Marcel Dekker, Inc., New York.
38. Hornsby P R and Watson C L (1987) "Development of halogen-free flame retardant and smoke suppressing thermoplastics compositions." *Antec '87*, p. 1301-1304.
39. Stinson J M and Horn W E (1994) "Flame retardant performance of a modified aluminum trihydroxide with increased thermal stability.", *Antec '94*, p. 2829-2833.
40. Kirschbaum G (1989) "Halogen free flame retardant with metal oxides." *Kunststoffe German plastics*, Vol. 79, No. 11, p.1205-1208.
41. Aseeva R M and Zaikov G E (1986) *Combustion of Polymer Materials*, Carl Hanser Verlag, Munich.
42. Beekman G F, Petrie S and Keating L (1986) "Magnesium hydroxide as a flame and smoke suppressant for polypropylene." *Antec '86*, p. 1167-1171.
43. Hornsby P R, Wang J, Cosstick K, Rotheron R, Jackson G, and Wilkinson G (1994) "Mechanism of fire retardancy of polyamides filled with magnesium hydroxide." *Antec '94*, p. 2834-2839.
44. Miyata S, Imahashi T, and Anabuki H (1980) "Fire-retarding polypropylene with magnesium hydroxide." *Journal of Applied Polymer Science*, Vol. 25, p.415-425.
45. Holloway L R (1987) "Application of magnesium hydroxide as a flame retardant and smoke suppressant in elastomers." *Rubber Chemistry and Technology*, Vol. 61, No. 2, p. 186-193.

46. Ferrigno T H (1987) "Principles of filler selection and use." in *Handbook of Fillers for Plastics*, edited by Katz H S and Milewski J V, Van Nostrand Reinhold Company, New York.
47. Van Oss C L (1993) "Acid-base effects at polymer interfaces." in *Polymer Surfaces and Interface II*, edited by Feast, W J, Munro, H S, and Richards, R W, John Wiley & Sons Ltd., London.
48. Adamson A W (1976) *Physical Chemistry of Surfaces*, 3rd ed., Wiley, New York.
49. Hiller L A Jr and Herber R H (1960) *Principles of Chemistry*, McGraw-Hill Book Company, Inc., New York.
50. Wu S (1982) *Polymer Interface and Adhesion*, Marcel Dekker, New York.
51. Miller J D, Hoh K and Ishida H (1984) "Studies of the simulation of silane coupling agent structures on particulate fillers; The pH effect." *Polymer Composite*, Vol. 5, No. 1, p. 18-28.
52. Favis B D, Blanchard, L P, Leonard, J and Prud'Homme R E (1989) "The formation of coupling agent monolayer on the surface of mica." *Polymer Composites*, January, Vol.5, No. 1, p.11-17.
53. Johnson R E and Ford D I (1994) "Stability and reactivity of dimethyl-ethoxysilane.", in *Chemically modified Surface.*, edited by Pesek J J and Leigh I E, Royal Society of Chemistry, Cambridge.
54. Monte S J and Sugerman G (1978) "Theory and application of organo-titanium coupling agents in filled polymers." *Plastics and Rubber; Materials and Applications*, August, p. 117-121.
55. Morrell S H (1981) "A review of the effects of surface treatments on polymer-filler interactions." *Plastics and Rubber Processing and Applications*, Vol. 1, p. 179-186.
56. Ramos M A, Berna M S and Matheu J P V (1991) "Effect of talc surface treatment on the mechanical properties of composites based on PP/LDPE blend matrices." *Polymer Engineering and Science*, Vol. 31, No. 4, February, p. 245-252.
57. Bajaa P, Jha N K and Jha R. K (1989) "Effect of titanate coupling agents on mechanical properties of mica-filled polypropylene." *Polymer Engineering and Science*, April, Vol. 29, No. 8, p. 557-563.
58. Evans M B, Rothon R N and Ryan T A (1988) "Carboxylated polybutadienes as coupling agents for mineral filled elastomers." *Plastics and Rubber Processing and Applications*, Vol. 9, No. 4, p. 215-220.

59. Liauw C M, Lees G C, Hurst J S, Rotheron R N and Dobson D C (1995) "The effect of filler surface modification on the mechanical properties of aluminium hydroxide filled polypropylene." *Plastics, Rubber and Composites Processing and Applications*, Vol.24, No.5, p. 249-260.
60. Fu Q and Wang G (1992) "Polyethylene toughened by rigid inorganic particles." *Polymer Engineering and Science*, January, Vol. 32, No. 2, p. 94-97.
61. Liu Z and Gilbert M (1996) "Structure and properties of talc-filled polypropylene: Effect of phosphate coating." *Journal of Applied Polymer Science*, Vol.59, p. 1087-1098.
62. Mitsuishi K, Ueno S, Kodama S and Kawasaki H (1991) "Crystallization behavior of polypropylene filled with surface-modified calcium carbonate." *Journal of Applied Polymer Science*, Vol. 43, p. 2043-2049.
63. Gunston F D (1996) *Fatty Acid and Lipid Chemistry*, Blackie Academic & Professional, London.
64. Markley K S (1960) *Fatty Acids*, Part 1, 2nd ed., Interscience Publishers, New York.
65. Pett M C (1987) "Molecular Engineering using the Langmuir-Blodgett technique.", *Polymer Surfaces and Interfaces*, Edited by W J Feast and H S Munro, John Wiley & Sons Ltd., London.
66. Nogami Y, Hamanaka H, and Ishiguro T (1991) "Anomalous X-ray diffraction line shift in heterogeneous Langmuir-Blodgett multilayer films." *Journal of The Physical Society of Japan*, Vol. 60, No. 6, p. 1860-1863.
67. Papirer E, Schultz J, and Turchi C (1984) "Surface properties of calcium carbonate filler treated with stearic acid." *Euro. Polym. J.*, Vol. 20, No. 12, p. 1155-1158.
68. Jefferson M E (1951) "Fatty Acids (Survey)-Crystal Properties", *Encyclopedia of Chemical Technology* (Kirk and Othmer, eds.) Vol. 6, Interscience, New York.
69. Cook M and Harper J F (1996) "Influence of magnesium hydroxide morphology and surface coating on physical and mechanical properties of heterophasic polypropylene." *Plastics, Rubber and Composites Processing and Applications*, Vol. 25. No. 2, p. 99-105.
70. Hutley T J and Darlington M W (1984) "Impact strength-d.s.c. correlation in mineral-filled polypropylene." *Polymer Communications*, Vol. 25, August, p.226-228.
71. Hancock M, Tremayne P, and Rosevear J (1980) "Filler in polypropylene II" *Journal of Polymer Science, Polymer Chemistry Edition*, Vol. 18, p. 3211-3217.

72. Ishida H and Koenig J L (1978) "Fourier transform infrared spectroscopic study of the silane coupling agent/porous silica interface." *Journal of Colloid and Interface Science*, Vol. 64, No. 3, p. 555-564.
73. Ishida H and Koenig J L (1978) "Fourier transform infrared spectroscopic study of the silane coupling agent on E-glass." *Journal of Colloid and Interface Science*, Vol. 64, No. 3, p. 565-576.
74. Ishida H and Koenig J (1979) "Molecular organization of the coupling agent interphase of fibre-glass reinforced plastics." *Journal of Polymer Science: Polymer Physics Edition*, Vol. 17, p. 1807-1813.
75. Chiang C H, Ishida H and Koenig J L (1980) "The structure of γ -aminopropyltriethoxysilane on glass surfaces." *Journal of Colloid and Interface Science*, Vol. 74, No. 2, p. 396-404.
76. Chiang C H and Koenig J L (1981) "Fourier transform infrared spectroscopic study of the adsorption of multiple amino silane coupling agents on glass surfaces." *Journal of Colloid and Interface Science*, Vol. 83, No. 2, p. 361-370.
77. Ishida H (1987) "Quantitative surface FT-IR spectroscopic analysis of polymers." *Rubber Chemistry and Technology*, Vol. 60, No. 6, p. 497-554.
78. Miller J D and Ishida H (1984) "Quantitative monomolecular coverage of inorganic particulates by methacryl-functional silanes." *Surface Science*, Vol. 148, p. 601-622.
79. Ishida H and Miller J D (1984) "Substrate effects on the chemisorbed and physisorbed layers of methacryl silane modified particulate minerals." *Macromolecules*, Vol. 17, p.1659-1666.
80. Ishida H and Miller J D (1985) "Cyclization of methacrylate-functional silane on particulate clay." *Journal of Polymer Science*, Vol. 23, p.2227-2242.
81. Miller J D and Ishida H (1985) "Quantitative intermolecular reaction of hydrolyzed trialkoxysilanes at submonolayer, monolayer, and multilayer surface coverages." *Langmuir*, Vol. 2, p. 127-131.
82. McKenzie M T, Culler S R, and Koenig J L (1984) "Applications of diffuse reflectance FT-IR to the characterization of an E-glass fiber/ γ -APS coupling agent system." *Applied Spectroscopy*, Vol. 38, No. 6, p.786-790.
83. Culler S R, Ishida H and Koenig J L (1985) "Structure of silane coupling agents adsorbed on silicon powder." *Journal of Colloid and Interface Science*, Vol. 106, No. 2, August, p.334-346.

-
84. Gilbert M, Sutherland I, and Guest A (1992) "Filler/coating interaction in thermoplastics." Conf. Proc. Fillers'92, Manchester, British Plastics Federation, May 19-20.
 85. Sutherland I, Maton D and Harrison D L (1996) "Characterisation of coated fillers by FTIR and XPS." *Loughborough Fillers Symposium II*, 17th-18th September.
 86. Klug H P and Alexander L E (1974) *X-ray Diffraction Procedures*, 2nd ed., John Wiley & Sons, Inc., New York.
 87. Hatada M and Nishi M (1977) "Polymerization induced by electron-beam irradiation of octadecyl methacrylate in the form of a multilayer or monolayer." *Journal of Polymer Science: Polymer Chemistry Edition*, Vol. 15, p. 927-935.
 88. Naegele D, Yoon D Y, and Broadhurst M G (1978) "Formation of a new crystal form (α_p) of poly(vinylidene fluoride) under electric field." *Macromolecules*, Vol. 11, No. 6, p.1297-1298.
 89. Dismore P F and Statton W O (1964) "Chain folding oriented 66-nylon fibres." *Journal of Polymer Science: Part B-2, Polymer Letter*, Vol. 2, p.1113-1116.
 90. Beresford D R and Bevan H (1963) "The effect of tension and annealing on the x-ray diffraction pattern of drawn 6.6 nylon." *Polymer*, Vol. 5, No. 5, p. 247-256.
 91. Sakaoku K, Morosoff N, and Peterlin A (1973) "Drawing of nylon 6 fibers (Bristles)." *Journal of Polymer Science: Polymer Physics Edition*, Vol. 11, p. 31-42.
 92. Guan Q, Shen K, and Zhu J (1995) "Structure and properties of self-reinforced polyethylene prepared by oscillating packing injection moulding under low pressure." *Journal of Applied Polymer Science*, Vol. 55, p. 1797-1804.
 93. Guan Q, Lai F S, McCarthy S P, Chiu D, Zhu X, and Shen K (1997) "Morphology and properties of self-reinforced high density polyethylene in oscillating stress field." *Polymer*, Vol. 38, No. 20, p. 5251-5253.
 94. Seto T, Hara T, and Tanaka K (1968) "Phase Transformation and deformation processes in oriented polyethylene." *Japanese Journal of Applied Physics*, Vol. 7, No. 1, p. 31-42.
 95. Kiho H, Peterlin A, and Geil P H (1964) "Polymer deformation. VI. Twinning and phase transformation of polyethylene single crystals as a function of stretching direction." *Journal of Applied Physics*, Vol.35, No. 5, p. 1599-1605.

-
96. Tanaka K, Seto T, and Hara T (1962) "Crystal structure of a new form of high-density polyethylene, produced by press." *Journal of the Physical Society of Japan*, Vol. 17, p. 873-874.
 97. Bevis M and Crellin E B (1971) "The geometry of twinning and phase transformations in crystalline polyethylene." *Polymer*, Vol. 12, p.666-684.
 98. Kiho H, Peterlin A, and Geil P H (1965) "Polymer deformation. VIII. Stability of the monoclinic phase of polyethylene." *Journal of Polymer Science: Part B-3*, p. 157.
 99. Kroschwitz J I (1990) *Polymers: Polymer characterization and analysis*, John Wiley & Sons, New York.
 100. Garbassi F, Occhiello E, Bastioli C, Romano G, and Brown A (1986) "XPS and SSIMS (FABMS) studies on silane treated filler surfaces." in *Composite Interface*, edited by Ishida H and Koenig J L, Elsevier Science Publishing Co., Inc., p.241-250.
 101. Pantano C G and Wittberg (1990) "XPS analysis of silane coupling agents and silane-treated E-glass fibers." *Surface and Interface Analysis*, Vol. 15, p. 498-501.
 102. Sheng E, Sutherland I, Brewis D M, Heath R J and Bradley R H (1994) "Surface studies of polyethylene modified by flame treatment." *Journal of Materials and Chemistry*, Vol.4, No. 3, p.487-490.
 103. Occhiello E, Morra M, Morini G, Garbassi F and Johnson D (1991) "On oxygen plasma-treated polypropylene interfaces with air, water, and epoxy resins. II. Epoxy resins." *Journal of Applied Polymer Science*, Vol. 42, p. 2045-2052.
 104. Zhong X, Yu L, Sun J and Zhang Y (1993) "XPS studies on radiation-induced structural changes in the copolymer of tetrafluoroethylene and ethylene." *Journal of Applied Polymer Science*, Vol. 47, p. 21-24.
 105. Jaycock M J and Parfitt G D (1981) *Chemistry of interfaces*, Ellis Horwood Limited, London.
 106. Dann J R (1970) "Forces involved in the adhesive process I. Critical surface tensions of polymeric solids as determined with polar liquids." *Journal of Colloid and Interface Science*, Vol. 32, No. 2, p. 302-320.
 107. Dann J R (1970) "Forces involved in the adhesive process II. Nondispersion forces of solid-liquid interface." *Journal of Colloid and Interface Science*, Vol. 32, No. 2, p. 321-331.
 108. Fowkes, F M (1964) "Attractive forces at interfaces." *Industrial and Engineering Chemistry*, Vol. 56, No. 12, p. 40-52.

-
109. Van Oss (1994) *Interfacial Forces in Aqueous Media*, Marcel Dekker, Inc., New York.
 110. Fowkes F.M (1968) *Chemistry and Physics Interfaces*, American Chemical Society, Washington D.C.
 111. Schultz J, Tsutsump K and Donnet J B (1977) "Surface properties of high-energy solids II. Determination of the nondispersive component of the surface free energy of mica and its energy of adhesion to polar liquids." *Journal of Colloid and Interface Science*, Vol. 59, No. 2, p.277-282.
 112. Kessaissia Z, Papirer E, and Donnet J B (1981) "The surface energy of silicas, grafted with alkyl chains of increasing lengths, as measured by contact angle techniques." *Journal of Colloid and Interface Science*, Vol. 82, No. 2, p.526-533.
 113. Riley A M, Paynter C D, Mc Genity P M, and Adams,J M (1990) " Factors affecting the impact properties of mineral filled polypropylene." *Plastics and Rubber Processing and Applications*, Vol. 14, No.2, p. 85-93.
 114. Busugin C, Martinez G M, Woodhams R T and Lahtinen R (1983) "Factors affecting the mechanical properties of mica-filled polypropylenes." *Polymer Engineering and Science*, Mid-October, Vol. 23, No. 14, p. 766-770.
 115. Jancar J (1989) "Influence of filler particle shape on elastic moduli of PP/Mg(OH)₂ composites." *Journal of Materials Science*, Vol. 24, p. 3947-3955.
 116. Fernando P L (1988) "Fracture toughness of filled polypropylene copolymer systems." *Polymer Engineering and Science*, June, Vol. 28, No. 12, p. 806-814.
 117. Chow T S (1980) "Review the effect of particle shape on the mechanical properties of filled polymers." *Journal of Material Science*, Vol. 15, p. 1873-1888.
 118. Turcsanyi B, Pukanszky B and Tudos F (1988) "Composition dependence of tensile yield stress in filled polymers." *Journal of Material Science Letter*, Vol. 7, p. 160-162.
 119. Tanaka H and White J L (1980) "Experimental investigations of shear and elongational flow properties of polystyrene melts reinforced with calcium carbonate, titanium dioxide, and carbon black." *Polymer Engineering and Science*, Vol. 20, p. 949-956.
 120. Kosinski L E, Caruthers J M (1986) "The effect of particle concentration on the rheology of polydimethylsiloxane filled with fumed silica." *Journal of Applied Polymer Science*, Vol. 32, p. 3393-3406.

121. Li L and Masuda T (1990) "Effect of dispersion of particles on viscoelasticity of CaCO₃-filled polypropylene melts." *Polymer Engineering and Science*, July, Vol. 30, No. 14, p. 841-847.
122. Fekete E, Pukanszky B, Toth, A and Bertoti I (1990) "Surface modification and characterization of particulate mineral fillers." *Journal of Colloid and Interface Science*, Vol. 135, No. 1, March 1, p. 200-208.
123. Schreiber H P, Viau J M, Fetoul A and Deng Z (1990) "Some properties of polyethylene compounds with surface-modified fillers." *Polymer Engineering and Science*, Mid-March, Vol. 30, No. 15, p. 263-269.
124. Hornsby P R and Watson C L (1995) "Interfacial modification of polypropylene composites filled with magnesium hydroxide." *Journal of Materials Science*, Vol. 30, p. 5347-5355.
125. Hutley T J and Darlington M W (1985) "Further observations on impact strength-d.s.c. correlation in mineral-filled polypropylene." *Polymer Communications*, Vol. 26, September, p. 264-267.
126. Abram J, Bowman J, Behiri J C, and Bonfield W (1984) "The influence of compounding route on the mechanical properties of highly loaded particulate filled polyethylene composites." *Plastics and Rubber Processing and Applications*, Vol. 4, p. 261-269.
127. Jancar J, Dibenedetto A T and Dianselmo A (1993) "Effect of adhesion on the fracture toughness of calcium carbonate-filled polypropylene." *Polymer Engineering and Science*, Vol. 33, No. 9, p. 559-563.
128. Pukanszky B, Belina K and Volk J (1991) "Effect of nucleation, filler anisotropy and orientation on the properties of PP composites." in *Interfacial Phenomena in Composite Materials'91*, edited by Verpoest I and Jones F, Butterworth, Heinemann.
129. Chen L S, Mai Y W and Cotterell B (1989) "Impact fracture energy of mineral-filled-polypropylene." *Polymer Engineering and Science*, April, Vol. 29, No. 8, p. 505-512.
130. Kowalewski T and Galeski A (1986) "Influence of chalk and its surface treatment on crystallisation of filled polypropylene." *Journal of Applied Science*, Vol. 32, p. 2919-2934.
131. Rybnikar F (1981) "Interactions in the system polyethylene-solid filler." *Journal of Macromolecule, Science-Physics.*, Part B, Vol. 19, No. 1, p. 1-11.

-
132. Wellinghoff S, Rybniker F, and Baer E (1974) "Epitaxial crystallization of polyethylene." *Journal of Macromolecule, Science-Physics Part, Part B*, Vol. 10, No. 1, p. 1-39.
 133. Mercier J P (1990) "Nucleation in polymer crystallization: A physical or a chemical mechanism." *Polymer Engineering and Science*, Mid-March, Vol. 30, No. 5, p. 270-278.
 134. Raymond C L (1997) "*Coating for magnesium hydroxide fillers in polyethylene compounds*" PhD Thesis, Loughborough University, Loughborough Leics, LE11 3TU.
 135. Markley K S (1961) *Fatty Acids*, Part 2, 2nd ed., Interscience Publishers, New York.
 136. Kroschwite J I (1990) *Polymers: Polymer Characterization and Analysis*, John Wiley & Sons, New York.
 137. Campbell D and White J R (1989) *Polymer Characterization*, Chapman and Hall, New York.
 138. Mathot V B V (1994) *Calorimetry and Thermal Analysis of Polymers*, Hanser Publishers, Munich.
 139. Runt J P (1986) *Encyclopedia of Polymer Science and Engineering*, Vol.4, John Wiley & Sons Inc., New York.
 140. Joint Committee on Chemical Analysis by Powder Diffraction Methods, *X-ray Powder Data File*, American Society for Testing Materials, Philadelphia, 1987.
 141. British Standard BS 2782 (1978): Part 4, Method 454A "Determination of ash".
 142. British Standard BS 2782 (1989): Part 9, Method 941 "Determination of maximum reversion of amorphous thermoplastics moulding materials".
 143. British Standard BS 2782 (1979): Method 720A "Determination of melt flow rate of thermoplastics".
 144. British Standard BS 2782 (1976): Part 3, Method 320A "Tensile strength, elongation and elastic".
 145. British Standard BS 2782 (1993): Part 3, Method 335A "Determination of flexural properties".
 146. Rek J H M (1972) "Oil, Fat, Soaps and Waxes." in *Differential Thermal Analysis*, edited by Mackenzie R C, Vol.2, Academic Press Inc., London.
 147. Umemura J, Takeda S, Hasegawa T, Kamata T and Takenaka T (1994) "Effect of thickness and monolayer location on thermostability of metal stearate LB films studied by FT-IR reflection-absorption spectroscopy." *Spectrochimica Acta*, Vol. 50A, No. 8/9, p. 1563-1571.

148. Barrall E M, II and Johnson J F (1970) "Differential scanning calorimetry." in *Thermal Characterization Techniques*, edited by Slade P E, Jr., and Jenkins L T, Marcel Dekker, Inc., New York.
149. Hattiangdi G S, Vold M J, and Vold R D (1949) "Differential thermal analysis of metal soaps." *Industrial and Engineering Chemistry*, Vol. 41, No. 10, p.2320-2324.
150. Wada Y and Matsubara T (1994) "Pseudo-polymorphism and lubricating properties of magnesium stearate." *Powder Technology*, Vol. 78, p. 109-114.
151. Peiser H S , Rooksby H P and Wilson A J C (1960) *X-ray diffraction by polycrystalline materials*, Reinhold Publishing Corporation, New York.
152. Baker T W (1974) "*X-ray diffraction*" in *Modern Physical Techniques in Materials Technology*, Edited by Mulvey T and Webster R K, Oxford University Press, Oxford.
153. Baxter D V, Cayton R H, Chisholm M H, Huffman, Putilina E F, Tagg S L, Wesemann J L, Zwanziger J W and Darrington F D (1994) "Multiple bonds between metal atoms in ordered assemblies. 2. Quadruple bonds in the mesomorphic state." *Journal of American Chemistry Society*, Vol. 116, p. 4551-4566.
154. Nielsen L E (1967) "Mechanical properties of particulate-filled systems." *Journal of Composite Materials*, Vol. 1, p. 100-119.
155. Shenoy A V (1999) *Rheology of filled polymer systems*, Kluwer Academic Publishers, London.
156. Maiti S N and Mahapatro (1991) "Mechanical properties of i-PP/CaCO₃ composites." *Journal of Applied Polymer Science*, Vol. 42, p. 3101-3110.
157. Manson J A and Sperling L H (1976) *Polymer Blends and Composites*, Plenum, New York.
158. Dieckmann D (1992) "Fatty acids and their derivatives." in *Plastics Additives and Modifiers Handbook*, edited by Edenbaum J, Van Nostrand Reinhold, New York.
159. McKane Jr. F W and Grossman F (1988) "Stearate choice depends on compound ingredients." in *RPN Technical Notebook*, edited by School R.
160. Nielsen L E (1967) *Mechanical properties of polymer*, Reinhold Publishing Corporation, New York.
161. Galeski A (1990) "Toughening of crystallisation polyolefins containing particulate fillers by interface modification." in *Controlled Interphases in*

- Composite Materials*. edited by Ishida H, Proceedings of Third International Conference on Composite Interfaces (ICCI-III), Elsevier Science Publishing Company, New York.
162. Alexander L E (1969) *X-ray diffraction methods in polymer science*, Wiley - Interscience, John Wiley & Sons, Inc., New York.
 163. Bright P F and Darlington M W (1981) "Factor influencing fibre orientation and mechanical properties in fibre reinforced thermoplastics injection mould." *Plastics and Rubber Processing and Applications*, Vol. 1, No. 2, p.139-147.
 164. Cullity B D (1978) *Elements of X-ray diffraction*, 2nd edition, Addison-Wesley Publishing Company, Inc., Massachusetts.
 165. Rybnikar F (1989) "Orientation in composite of polypropylene and talc." *Journal of Polymer Science*, Oct 20, Vol.38, No.8, p.1479-1490.
 166. Coupland K, Maltby A J and Parker D A (1997) "Why fatty amides are the preferred slip agents for polyolefin films." *Addcon Asia '97*, Paper 15.
 167. Osipow L I (1962) *Surface Chemistry*, Reinhold Publishing Corporation, New York.
 168. Reid K F (1968) *Properties and reactions of bonds in organic molecules*, Longmans, UK.
 169. Gardiner, K W, Buerger, M J, and Smith, L B (1945) *Journal of Physical Chemistry*, Vol. 49, p. 417-428.
 170. McBain J W and Lee, W W (1943) *Oil & Soap*, Vol. 20, p. 1943.
 171. Jefferson, M.E. (1951) "Fatty Acids (Survey)-Crystal Properties", *Encyclopedia of Chemical Technology* (Kirk and Othemer, eds.), Vol. 6, Interscience, New York.
 172. Pukanszky B, Fekete E, Tudos F (1989) *Makromolekul Chemistry Macromol Symp*, Vol. 28, p. 165.
 173. Morton-Jones D H (1989) *Polymer Processing*, Chapman and Hall, London.
 174. Jenkins F A and White H E (1957) *Fundamentals of Optics*, 3rd edition, McGraw-Hill, New York.
 175. Jumba S (1998) "Elongational rheometry and processing of filled polyethylene melts" PhD Thesis, Loughborough University, Loughborough Leics, LE11 3TU.

APPENDIX A: THE MACHINE PARAMETERS

Appendix A.1: The conditions of compounding.

SERIES I-a: Unfilled HDPE and HDPE compounds containing Mg(OH)₂ coated with various levels of Mg stearate and stearic acid							
CONDITION	HDUF	HMUC	HMMSC31	HMMSC61	HMMSC62	HMMSC93	HMSAC60
Screw speed (rpm)	350	350	352	352	351	350	351
Torque (%)	70	70	60	55	55	55	55
Die pressure (psi)	345	350	290	290	330	290	290
Polymer feed rate (kg/hr)	15	7.2	9	9	9	9	9
Filler feed rate (kg/hr)	0	4.8	6	6	6	6	6
Actual temp1 (°C) at die	163	175	166	167	165	166	166
Actual temp2 (°C)	175	172	178	161	168	168	165
Actual temp3 (°C)	170	172	167	170	177	177	171
Actual temp4 (°C)	163	170	160	166	167	167	166
Actual temp5 (°C)	158	162	159	158	158	158	158
Actual temp6 (°C) at feeder	141	137	137	135	138	135	139
SERIES I-b: Unfilled HDPE and HDPE compounds containing Mg(OH)₂ coated with various levels of calcium stearate							
CONDITION	HDUF	HMUC	HMCSC32	HMCSC64	HMCSC96		
Screw speed (rpm)	351	351	350	350	350		
Torque (%)	70	65	60	50	40		
Die pressure (psi)	345-350	330	250	280	290		
Polymer feed	15	7.2	9	9	9		
Filler feed	0	4.8	6	6	6		
Actual temp1 (°C) at die	183	166	165	165	163		
Actual temp2 (°C)	183	172	179	177	172		
Actual temp3 (°C)	176	177	178	169	168		
Actual temp4 (°C)	169	163	168	160	158		
Actual temp5 (°C)	158	166	161	162	161		
Actual temp6 (°C) at feeder	141	145	144	145	144		
SERIES II-a: Unfilled HDPE and HDPE compounds containing Mg(OH)₂ treated with various types of metal stearates and stearic acid							
CONDITION	HDUF	HMUC	HMMSA62	HMMSC62	HMCSC64	HMZSC67	HMSAC60
Screw speed (rpm)	350	353	350	352	351	351	351
Torque (%)	70	65	60	55	60	57.5	60
Die pressure (psi)	345-350	340	240	270	270	240	260
Polymer feed rate (kg/hr)	15	7.2	9	9	9	9	9
Filler feed rate (kg/hr)	0	4.8	6	6	6	6	6
Actual temp1 (°C) at die	183	160	183	165	166	165	162
Actual temp2 (°C)	183	159	183	161	168	179	171
Actual temp3 (°C)	176	167	176	160	177	168	177
Actual temp4 (°C)	169	155	169	160	167	162	159
Actual temp5 (°C)	158	155	155	159	158	158	159
Actual temp6 (°C) at feeder	141	133	125	129	135	143	139

SERIES II-b: Unfilled HDPE and HDPE compounds containing CaCO₃ treated with various types of metal stearates and stearic acid							
CONDITION	HDUF	HCUC	HCMSC42	HCCSA43	HCCSC43	HCZSC45	HCSAC40
Screw speed (rpm)	350	352	352	352	351	350	351
Torque (%)	70	60	60	60	55	60	55
Die pressure (psi)	345-350	330	250	280	290	270	260
Polymer feed	15	7.2	9	9	9	9	9
Filler feed	0	4.8	6	6	6	6	6
Actual temp1 (°C) at die	183	166	165	165	163	165	164
Actual temp2 (°C)	183	172	179	177	172	179	171
Actual temp3 (°C)	176	177	178	169	168	174	177
Actual temp4 (°C)	169	163	168	160	158	166	161
Actual temp5 (°C)	158	166	161	162	161	160	156
Actual temp6 (°C) at feeder	141	145	144	145	144	143	138
SERIES II-c: HDPE containing metal stearates and stearic acid							
CONDITION	HDUF	HDMS	HDCS	HDZS	HDSA		
Screw speed (rpm)	351	351	350	350	351		
Torque (%)	70	35	35	37.5	37.5		
Die pressure (psi)	345-350	330	250	280	290		
Polymer feed	15	15	15	15	15		
Filler feed	0	0	0	0	0		
Actual temp1 (°C) at die	183	166	165	165	163		
Actual temp2 (°C)	183	172	179	177	172		
Actual temp3 (°C)	176	177	178	169	168		
Actual temp4 (°C)	169	163	168	160	158		
Actual temp5 (°C)	158	166	161	162	161		
Actual temp6 (°C) at feeder	141	145	144	145	144		

Appendix A.2: The conditions of injection moulding for four part mould.

SERIES I-a: Unfilled HDPE and HDPE compounds containing Mg(OH)₂ coated with various levels of Mg stearate and stearic acid							
CONDITION	HDUF	HMUC	HMMSC31	HMMSC61	HMMSC64	HMMSC93	HMSAC64
1. Nozzel Temperature (°C)	190	220	220	220	220	220	220
2. Barrel Temperature (°C)	180	210	210	210	210	210	210
3. Barrel Temperature (°C)	170	200	200	200	200	200	200
4. Barrel Temperature (°C)	160	190	190	190	190	190	190
5. Actual Screw Position (mm.)	50.6	52.6	50.6	52.6	52.6	50.7	52.6
6. 1st injection speed, Position (mm.)	40	30	30	30	20	30	30
7. 2nd injection speed, Position (mm.)	40, 20	40, 40	40, 40	40, 40	40, 40	40, 40	40, 40
8. 3rd injection speed, Position (mm.)	40, 13	40, 30	40, 30	40, 30	40, 30	40, 30	40, 30
9. 4th injection speed, Position (mm.)	40, 12	40, 20	40, 20	40, 20	40, 20	40, 20	40, 20
10. 5th injection speed, Position (mm.)	20, 10	10, 10	10, 10	10, 10	10, 10	10, 10	10, 10
11. Max. injection Pressure (bar)	140	140	140	140	140	140	140
12. 1st hold pressure (bar), time (sec.)	40, 10	50, 5	40, 10	35, 10	40, 10	40, 10	35, 10
13. 2nd hold pressure (bar), time (sec.)	20, 10	20, 5	20, 10	20, 10	20, 10	20, 10	20, 10
14. 3rd hold pressure (bar), time (sec.)	0, 0	0, 0	0, 0	0, 0	0, 0	0, 0	0, 0
15. 4th hold pressure (bar), time (sec.)	0, 0	0, 0	0, 0	0, 0	0, 0	0, 0	0, 0
16. 5th hold pressure (bar), time (sec.)	0, 0	0, 0	0, 0	0, 0	0, 0	0, 0	0, 0
17. Shot size (Max. 125.0) (mm.)	53	52	50	50	52	50	50
18. 1st screw speed (%)	60	50	50	50	50	50	50
19. 2nd screw speed (%), position	30, 45	20, 45	20, 45	20, 45	20, 45	20, 45	20, 45
20. 1st back pressure (bar)	10	10	10	10	10	10	10
21. 2nd back pressure (bar)	2, 45	2, 45	2, 45	2, 45	2, 45	2, 45	2, 45
22. Cooling (sec.)	40	40	40	40	40	40	40
23. Recycle (sec.)	0.2	0.2	0.2	0.2	0.2	0.2	0.2

SERIES I-b: Unfilled HDPE and HDPE compounds containing Mg(OH)₂ coated with various levels of calcium stearate					
CONDITION	HDUF	HMUC	HMCSC32	HMCSC64	HMCSC96
1. Nozzel Temperature (°C)	190	220	220	220	220
2. Barrel Temperature (°C)	180	210	210	210	210
3. Barrel Temperature (°C)	170	200	200	200	200
4. Barrel Temperature (°C)	160	190	190	190	190
5. Actual Screw Position (mm.)	50.6	52.6	50.6	52.6	52.6
6. 1st injection speed, Position (mm.)	40	30	30	30	20
7. 2nd injection speed, Position (mm.)	40, 20	40, 40	40, 40	40, 40	40, 40
8. 3rd injection speed, Position (mm.)	40, 13	40, 30	40, 30	40, 30	40, 30
9. 4th injection speed, Position (mm.)	40, 12	40, 20	40, 20	40, 20	40, 20
10. 5th injection speed, Position (mm.)	20, 10	10, 10	10, 10	10, 10	10, 10
11. Max. injection Pressure (bar)	140	140	140	140	140
12. 1st hold pressure (bar), time (sec.)	40, 10	50, 5	40, 10	35, 10	40, 10
13. 2nd hold pressure (bar), time (sec.)	20, 5	20, 5	20, 5	20, 5	20, 5
14. 3rd hold pressure (bar), time (sec.)	0, 0	0, 0	0, 0	0, 0	0, 0
15. 4th hold pressure (bar), time (sec.)	0, 0	0, 0	0, 0	0, 0	0, 0
16. 5th hold pressure (bar), time (sec.)	0, 0	0, 0	0, 0	0, 0	0, 0
17. Shot size (Max. 125.0) (mm.)	47.2	47.2	47.2	47.2	47.2
18. 1st screw speed (%)	60	60	60	60	60
19. 2nd screw speed (%), position	30, 35	30, 35	30, 35	30, 35	30, 35
20. 1st back pressure (bar)	10	10	10	10	10
21. 2nd back pressure (bar), position	2, 10	2, 10	2, 10	2, 10	2, 10
22. Cooling (sec.)	50	50	50	50	50
23. Recycle (sec.)	0.2	0.2	0.2	0.2	0.2

SERIES II-a: Unfilled HDPE and HDPE compounds containing Mg(OH)₂ treated with various types of metal stearates and stearic acid							
CONDITION	HDUF	HMUC	HMMSA62	HMMSC62	HMCSC64	HMZSC67	HMSAC60
1. Nozzel Temperature (°C)	190	220	220	220	220	220	220
2. Barrel Temperature (°C)	180	210	210	210	210	210	210
3. Barrel Temperature (°C)	170	200	200	200	200	200	200
4. Barrel Temperature (°C)	160	190	190	190	190	190	190
5. Actual Screw Position (mm.)	50.6	52.6	50.6	52.6	52.6	50.7	52.6
6. 1st injection speed, Position (mm.)	40	30	30	30	20	30	30
7. 2nd injection speed, Position (mm.)	40, 20	40, 40	40, 40	40, 40	40, 40	40, 40	40, 40
8. 3rd injection speed, Position (mm.)	40, 13	40, 30	40, 30	40, 30	40, 30	40, 30	40, 30
9. 4th injection speed, Position (mm.)	40, 12	40, 20	40, 20	40, 20	40, 20	40, 20	40, 20
10. 5th injection speed, Position (mm.)	20, 10	10, 10	10, 10	10, 10	10, 10	10, 10	10, 10
11. Max. injection Pressure (bar)	140	140	140	140	140	140	140
12. 1st hold pressure (bar), time (sec.)	40, 10	50, 5	40, 10	35, 10	40, 10	40, 10	35, 10
13. 2nd hold pressure (bar), time (sec.)	20, 10	20, 5	20, 10	20, 10	20, 10	20, 10	20, 10
14. 3rd hold pressure (bar), time (sec.)	0, 0	0, 0	0, 0	0, 0	0, 0	0, 0	0, 0
15. 4th hold pressure (bar), time (sec.)	0, 0	0, 0	0, 0	0, 0	0, 0	0, 0	0, 0
16. 5th hold pressure (bar), time (sec.)	0, 0	0, 0	0, 0	0, 0	0, 0	0, 0	0, 0
17. Shot size (Max. 125.0) (mm.)	53	52	50	50	52	50	50
18. 1st screw speed (%)	60	50	50	50	50	50	50
19. 2nd screw speed (%), position (mm.)	30, 45	20, 45	20, 45	20, 45	20, 45	20, 45	20, 45
20. 1st back pressure (bar)	10	10	10	10	10	10	10
21. 2nd back pressure (bar), position (mm)	2, 45	2, 45	2, 45	2, 45	2, 45	2, 45	2, 45
22. Cooling (sec.)	40	40	40	40	40	40	40
23. Recycle (sec.)	0.2	0.2	0.2	0.2	0.2	0.2	0.2

SERIES II-b: Unfilled HDPE and HDPE compounds containing CaCO₃ treated with various types of metal stearates and stearic acid							
CONDITION	HDUF	HCUC	HCMSC42	HCCSA43	HCCSC43	HCZSC45	HCSAC40
1. Nozzel Temperature (°C)	190	220	220	220	220	220	220
2. Barrel Temperature (°C)	180	210	210	210	210	210	210
3. Barrel Temperature (°C)	170	200	200	200	200	200	200
4. Barrel Temperature (°C)	160	190	190	190	190	190	190
5. Actual Screw Position (mm.)	50.6	52.6	50.6	52.6	52.6	50.7	52.6
6. 1st injection speed, Position (mm.)	40	30	30	30	20	30	30
7. 2nd injection speed, Position (mm.)	40, 20	40, 40	40, 40	40, 40	40, 40	40, 40	40, 40
8. 3rd injection speed, Position (mm.)	40, 13	40, 30	40, 30	40, 30	40, 30	40, 30	40, 30
9. 4th injection speed, Position (mm.)	40, 12	40, 20	40, 20	40, 20	40, 20	40, 20	40, 20
10. 5th injection speed, Position (mm.)	20, 10	10, 10	10, 10	10, 10	10, 10	10, 10	10, 10
11. Max. injection Pressure (bar)	140	140	140	140	140	140	140
12. 1st hold pressure (bar), time (sec.)	40, 10	50, 5	40, 10	35, 10	40, 10	40, 10	35, 10
13. 2nd hold pressure (bar), time (sec.)	20, 10	20, 5	20, 10	20, 10	20, 10	20, 10	20, 10
14. 3rd hold pressure (bar), time (sec.)	0, 0	0, 0	0, 0	0, 0	0, 0	0, 0	0, 0
15. 4th hold pressure (bar), time (sec.)	0, 0	0, 0	0, 0	0, 0	0, 0	0, 0	0, 0
16. 5th hold pressure (bar), time (sec.)	0, 0	0, 0	0, 0	0, 0	0, 0	0, 0	0, 0
17. Shot size (Max. 125.0) (mm.)	53	52	50	50	52	50	50
18. 1st screw speed (%)	60	50	50	50	50	50	50
19. 2nd screw speed (%), position (mm.)	30, 45	20, 45	20, 45	20, 45	20, 45	20, 45	20, 45
20. 1st back pressure (bar)	10	10	10	10	10	10	10
21. 2nd back pressure (bar), position (mm)	2, 45	2, 45	2, 45	2, 45	2, 45	2, 45	2, 45
22. Cooling (sec.)	40	40	40	40	40	40	40
23. Recycle (sec.)	0.2	0.2	0.2	0.2	0.2	0.2	0.2
SERIES II-c: HDPE containing metal stearates and stearic acid							
CONDITION	HDUF	HDMS	HDCS	HDZS	HDSA		
1. Nozzel Temperature (°C)	190	180	180	180	180		
2. Barrel Temperature (°C)	180	170	170	170	170		
3. Barrel Temperature (°C)	170	160	160	160	160		
4. Barrel Temperature (°C)	160	150	150	150	150		
5. Actual Screw Position (mm.)	48.2	48.2	48.2	48.2	48.2		
6. 1st injection speed, Position (mm.)	40	40	40	40	40		
7. 2nd injection speed, Position (mm.)	40, 40	40, 40	40, 40	40, 40	40, 40		
8. 3rd injection speed, Position (mm.)	40, 30	40, 30	40, 30	40, 30	40, 30		
9. 4th injection speed, Position (mm.)	40, 20	40, 20	40, 20	40, 20	40, 20		
10. 5th injection speed, Position (mm.)	20, 10	20, 10	20, 10	20, 10	20, 10		
11. Max. injection Pressure (bar)	72	72	72	72	72		
12. 1st hold pressure (bar), time (sec.)	50, 5	50, 5	50, 5	50, 5	50, 5		
13. 2nd hold pressure (bar), time (sec.)	20, 5	20, 5	20, 5	20, 5	20, 5		
14. 3rd hold pressure (bar), time (sec.)	0, 0	0, 0	0, 0	0, 0	0, 0		
15. 4th hold pressure (bar), time (sec.)	0, 0	0, 0	0, 0	0, 0	0, 0		
16. 5th hold pressure (bar), time (sec.)	0, 0	0, 0	0, 0	0, 0	0, 0		
17. Shot size (Max. 125.0) (mm.)	47.2	47.2	47.2	47.2	47.2		
18. 1st screw speed (%)	60	60	60	60	60		
19. 2nd screw speed (%), position (mm.)	30, 35	30, 35	30, 35	30, 35	30, 35		
20. 1st back pressure (bar)	10	10	10	10	10		
21. 2nd back pressure (bar), position (mm)	2, 10	2, 10	2, 10	2, 10	2, 10		
22. Cooling (sec.)	50	50	50	50	50		
23. Recycle (sec.)	0.2	0.2	0.2	0.2	0.2		

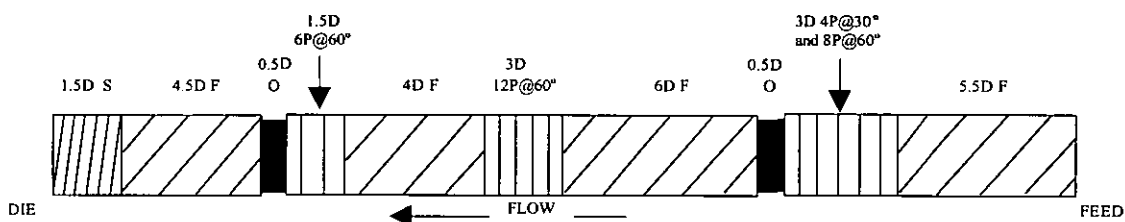
Appendix A.3: The conditions of injection moulding for a four piece tensile mould.

SERIES I-a: Unfilled HDPE and HDPE compounds containing Mg(OH)₂ coated with various levels of Mg stearate and stearic acid							
CONDITION	HDF	HMUC	HMMSC31	HMMSC61	HMMSC62	HMMSC93	HMSAC60
1. Nozzel Temperature (°C)	190	220	220	220	220	220	220
2. Barrel Temperature (°C)	180	210	210	210	210	210	210
3. Barrel Temperature (°C)	170	200	200	200	200	200	200
4. Barrel Temperature (°C)	160	190	190	190	190	190	190
5. Actual Screw Position (mm.)	48.2	48.2	48.2	48.2	48.2	48.2	48.2
6. 1st injection speed, Position (mm.)	40	40	40	40	40	40	40
7. 2nd injection speed, Position (mm.)	40, 40	40, 40	40, 40	40, 40	40, 40	40, 40	40, 40
8. 3rd injection speed, Position (mm.)	40, 30	40, 30	40, 30	40, 30	40, 30	40, 30	40, 30
9. 4th injection speed, Position (mm.)	40, 20	40, 20	40, 20	40, 20	40, 20	40, 20	40, 20
10. 5th injection speed, Position (mm.)	20, 10	20, 10	20, 10	20, 10	20, 10	20, 10	20, 10
11. Max. injection Pressure (bar)	140	140	140	140	140	140	140
12. 1st hold pressure (bar), time (sec.)	50, 5	50, 5	50, 5	50, 5	50, 5	50, 5	50, 5
13. 2nd hold pressure (bar), time (sec.)	20, 5	20, 5	20, 5	20, 5	20, 5	20, 5	20, 5
14. 3rd hold pressure (bar), time (sec.)	0, 0	0, 0	0, 0	0, 0	0, 0	0, 0	0, 0
15. 4th hold pressure (bar), time (sec.)	0, 0	0, 0	0, 0	0, 0	0, 0	0, 0	0, 0
16. 5th hold pressure (bar), time (sec.)	0, 0	0, 0	0, 0	0, 0	0, 0	0, 0	0, 0
17. Shot size (Max. 125.0) (mm.)	47.2	47.2	47.2	47.2	47.2	47.2	47.2
18. 1st screw speed (%)	60	60	60	60	60	60	60
19. 2nd screw speed (%), position (mm.)	30, 35	30, 35	30, 35	30, 35	30, 35	30, 35	30, 35
20. 1st back pressure (bar)	10	10	10	10	10	10	10
21. 2nd back pressure (bar), position (mm)	2, 10	2, 10	2, 10	2, 10	2, 10	2, 10	2, 10
22. Cooling (sec.)	40	40	40	40	40	40	40
23. Recycle (sec.)	0.2	0.2	0.2	0.2	0.2	0.2	0.2
SERIES I-b: Unfilled HDPE and HDPE compounds containing Mg(OH)₂ coated with various levels of calcium stearate							
CONDITION	HDF	HMUC	HMCS34	HMCS64	HMCS94		
1. Nozzel Temperature (°C)	190	220	220	220	220		
2. Barrel Temperature (°C)	180	210	210	210	210		
3. Barrel Temperature (°C)	170	200	200	200	200		
4. Barrel Temperature (°C)	160	190	190	190	190		
5. Actual Screw Position (mm.)	48.2	48.2	48.2	48.2	48.2		
6. 1st injection speed, Position (mm.)	40	40	40	40	40		
7. 2nd injection speed, Position (mm.)	40, 40	40, 40	40, 40	40, 40	40, 40		
8. 3rd injection speed, Position (mm.)	40, 30	40, 30	40, 30	40, 30	40, 30		
9. 4th injection speed, Position (mm.)	40, 20	40, 20	40, 20	40, 20	40, 20		
10. 5th injection speed, Position (mm.)	20, 10	20, 10	20, 10	20, 10	20, 10		
11. Max. injection Pressure (bar)	140	140	140	140	140		
12. 1st hold pressure (bar), time (sec.)	50, 5	50, 5	50, 5	50, 5	50, 5		
13. 2nd hold pressure (bar), time (sec.)	20, 5	20, 5	20, 5	20, 5	20, 5		
14. 3rd hold pressure (bar), time (sec.)	0, 0	0, 0	0, 0	0, 0	0, 0		
15. 4th hold pressure (bar), time (sec.)	0, 0	0, 0	0, 0	0, 0	0, 0		
16. 5th hold pressure (bar), time (sec.)	0, 0	0, 0	0, 0	0, 0	0, 0		
17. Shot size (Max. 125.0) (mm.)	47.2	47.2	47.2	47.2	47.2		
18. 1st screw speed (%)	60	60	60	60	60		
19. 2nd screw speed (%), position (mm.)	30, 35	30, 35	30, 35	30, 35	30, 35		
20. 1st back pressure (bar)	10	10	10	10	10		
21. 2nd back pressure (bar), position (mm)	2, 10	2, 10	2, 10	2, 10	2, 10		
22. Cooling (sec.)	40	40	40	40	40		
23. Recycle (sec.)	0.2	0.2	0.2	0.2	0.2		

SERIES II-a: Unfilled HDPE and HDPE compounds containing Mg(OH)₂ treated with various types of metal stearates and stearic acid							
CONDITION	HDF	HMUC	HMMSA62	HMMSC62	HMCS64	HMZSC67	HMSAC60
1. Nozzel Temperature (°C)	190	220	220	220	220	220	220
2. Barrel Temperature (°C)	180	210	210	210	210	210	210
3. Barrel Temperature (°C)	170	200	200	200	200	200	200
4. Barrel Temperature (°C)	160	190	190	190	190	190	190
5. Actual Screw Position (mm.)	48.2	48.2	48.2	48.2	48.2	48.2	48.2
6. 1st injection speed, Position (mm.)	40	40	40	40	40	40	40
7. 2nd injection speed, Position (mm.)	40, 40	40, 40	40, 40	40, 40	40, 40	40, 40	40, 40
8. 3rd injection speed, Position (mm.)	40, 30	40, 30	40, 30	40, 30	40, 30	40, 30	40, 30
9. 4th injection speed, Position (mm.)	40, 20	40, 20	40, 20	40, 20	40, 20	40, 20	40, 20
10. 5th injection speed, Position (mm.)	20, 10	20, 10	20, 10	20, 10	20, 10	20, 10	20, 10
11. Max. injection Pressure (bar)	140	140	140	140	140	140	140
12. 1st hold pressure (bar), time (sec.)	50, 5	50, 5	50, 5	50, 5	50, 5	50, 5	50, 5
13. 2nd hold pressure (bar), time (sec.)	20, 5	20, 5	20, 5	20, 5	20, 5	20, 5	20, 5
14. 3rd hold pressure (bar), time (sec.)	0, 0	0, 0	0, 0	0, 0	0, 0	0, 0	0, 0
15. 4th hold pressure (bar), time (sec.)	0, 0	0, 0	0, 0	0, 0	0, 0	0, 0	0, 0
16. 5th hold pressure (bar), time (sec.)	0, 0	0, 0	0, 0	0, 0	0, 0	0, 0	0, 0
17. Shot size (Max. 125.0) (mm.)	47.2	47.2	47.2	47.2	47.2	47.2	47.2
18. 1st screw speed (%)	60	60	60	60	60	60	60
19. 2nd screw speed (%), position (mm.)	30, 35	30, 35	30, 35	30, 35	30, 35	30, 35	30, 35
20. 1st back pressure (bar)	10	10	10	10	10	10	10
21. 2nd back pressure (bar), position (mm)	2, 10	2, 10	2, 10	2, 10	2, 10	2, 10	2, 10
22. Cooling (sec.)	40	40	40	40	40	40	40
23. Recycle (sec.)	0.2	0.2	0.2	0.2	0.2	0.2	0.2
SERIES II-b: Unfilled HDPE and HDPE compounds containing CaCO₃ treated with various types of metal stearates and stearic acid							
CONDITION	HDF	HCUC	HCMSC42	HCCSA43	HCCSC43	HCZSC45	HCSAC40
1. Nozzel Temperature (°C)	190	220	220	220	220	220	220
2. Barrel Temperature (°C)	180	210	210	210	210	210	210
3. Barrel Temperature (°C)	170	200	200	200	200	200	200
4. Barrel Temperature (°C)	160	190	190	190	190	190	190
5. Actual Screw Position (mm.)	48.2	48.2	48.2	48.2	48.2	48.2	48.2
6. 1st injection speed, Position (mm.)	40	40	40	40	40	40	40
7. 2nd injection speed, Position (mm.)	40, 40	40, 40	40, 40	40, 40	40, 40	40, 40	40, 40
8. 3rd injection speed, Position (mm.)	40, 30	40, 30	40, 30	40, 30	40, 30	40, 30	40, 30
9. 4th injection speed, Position (mm.)	40, 20	40, 20	40, 20	40, 20	40, 20	40, 20	40, 20
10. 5th injection speed, Position (mm.)	20, 10	20, 10	20, 10	20, 10	20, 10	20, 10	20, 10
11. Max. injection Pressure (bar)	140	140	140	140	140	140	140
12. 1st hold pressure (bar), time (sec.)	50, 5	50, 5	50, 5	50, 5	50, 5	50, 5	50, 5
13. 2nd hold pressure (bar), time (sec.)	20, 5	20, 5	20, 5	20, 5	20, 5	20, 5	20, 5
14. 3rd hold pressure (bar), time (sec.)	0, 0	0, 0	0, 0	0, 0	0, 0	0, 0	0, 0
15. 4th hold pressure (bar), time (sec.)	0, 0	0, 0	0, 0	0, 0	0, 0	0, 0	0, 0
16. 5th hold pressure (bar), time (sec.)	0, 0	0, 0	0, 0	0, 0	0, 0	0, 0	0, 0
17. Shot size (Max. 125.0) (mm.)	47.2	47.2	47.2	47.2	47.2	47.2	47.2
18. 1st screw speed (%)	60	60	60	60	60	60	60
19. 2nd screw speed (%), position (mm.)	30, 35	30, 35	30, 35	30, 35	30, 35	30, 35	30, 35
20. 1st back pressure (bar)	10	10	10	10	10	10	10
21. 2nd back pressure (bar), position (mm)	2, 10	2, 10	2, 10	2, 10	2, 10	2, 10	2, 10
22. Cooling (sec.)	40	40	40	40	40	40	40
23. Recycle (sec.)	0.2	0.2	0.2	0.2	0.2	0.2	0.2

SERIES II-c: HDPE containing metal stearates and stearic acid					
CONDITION	HDUF	HDMS	HDCS	HDZS	HDSA
1. Nozzel Temperature (°C)	190	180	180	180	180
2. Barrel Temperature (°C)	180	170	170	170	170
3. Barrel Temperature (°C)	170	160	160	160	160
4. Barrel Temperature (°C)	160	150	150	150	150
5. Actual Screw Position (mm.)	48.2	48.2	48.2	48.2	48.2
6. 1st injection speed, Position (mm.)	40	40	40	40	40
7. 2nd injection speed, Position (mm.)	40, 40	40, 40	40, 40	40, 40	40, 40
8. 3rd injection speed, Position (mm.)	40, 30	40, 30	40, 30	40, 30	40, 30
9. 4th injection speed, Position (mm.)	40, 20	40, 20	40, 20	40, 20	40, 20
10. 5th injection speed, Position (mm.)	20, 10	20, 10	20, 10	20, 10	20, 10
11. Max. injection Pressure (bar)	72	72	72	72	72
12. 1st hold pressure (bar), time (sec.)	50, 5	50, 5	50, 5	50, 5	50, 5
13. 2nd hold pressure (bar), time (sec.)	20, 5	20, 5	20, 5	20, 5	20, 5
14. 3rd hold pressure (bar), time (sec.)	0, 0	0, 0	0, 0	0, 0	0, 0
15. 4th hold pressure (bar), time (sec.)	0, 0	0, 0	0, 0	0, 0	0, 0
16. 5th hold pressure (bar), time (sec.)	0, 0	0, 0	0, 0	0, 0	0, 0
17. Shot size (Max. 125.0) (mm.)	47.2	47.2	47.2	47.2	47.2
18. 1st screw speed (%)	60	60	60	60	60
19. 2nd screw speed (%), position (mm.)	30, 35	30, 35	30, 35	30, 35	30, 35
20. 1st back pressure (bar)	10	10	10	10	10
21. 2nd back pressure (bar), position (mm)	2, 10	2, 10	2, 10	2, 10	2, 10
22. Cooling (sec.)	50	50	50	50	50
23. Recycle (sec.)	0.2	0.2	0.2	0.2	0.2

Appendix A.4: Screw configuration of APV type MP30TC twin-screw extruder.



S: Single lead discharge screw; F: Feed screw; P: Paddles; O: Full bore orifice plug with diameter of 28.1 mm; and D: screw diameter (30 mm).

APPENDIX B: SUMMARISED RESULTS (Series I)

Appendix B.1: Effect of temperature on coating time of magnesium hydroxide coated with 6.2% magnesium stearate from the Waring blender.

Time (min)	Temperature (°C)				
	0 volts	20 volts	40 volts	60 volts	80 volts
0	22	21	20	21	21
2	24	25	28	38	48
4	25	27	33	59	72
5	28	31	35	64	85
6	31	34	39	74	93
8	34	37	46	76	106
10	36	39	67	87	113
12	37	46	71	96	119
14	40	55	75	104	121
15	41	62	78	107	128
16	42	65	79	111	132
18	44	68	84	114	139
20	46	71	91	119	143
22	47	74	92	122	144
24	48	77	98	126	144
25	48	76	99	129	144
26	49	75	100	126	145
28	54	78	104	128	142
30	56	80	109	130	142
32	56	82	108	135	143
34	56	85	111	137	143
35	55	87	113	137	143
36	54	88	114	137	142
38	55	87	115	137	142
40	55	88	115	139	144
42	55	89	113	138	145
44	54	89	115	138	144
45	54	89	117	138	144
46	55	88	117	137	144
48	55	87	117	137	144
50	55	88	117	138	144
52	54	89	116	138	144
54	54	89	116	138	143
55	55	89	116	138	143
56	54	89	116	137	143
58	54	88	115	137	143
60	53	88	114	136	142

Appendix B.2: Effect of temperature on coating time of magnesium hydroxide coated with calcium stearate from the Waring blender.

Time (min)	Temperature (°C)				
	0 volts	20 volts	40 volts	60 volts	80 volts
0	19	20	20	22	19
2	20	21	25	32	36
4	24	28	32	45	50
6	27	34	40	55	65
8	28	35	45	60	72
10	28	40	48	64	85
12	29	40	53	70	96
14	30	42	54	72	110
16	32	42	58	74	115
18	33	43	59	79	123
20	34	45	63	85	127
22	35	43	60	90	127
24	36	46	64	91	130
26	36	48	62	91	132
28	39	49	63	92	133
30	39	49	63	96	133
32	39	50	62	96	134
34	38	52	62	97	134
36	38	54	63	97	134
38	37	56	63	97	135
40	37	56	63	99	135
42	39	55	64	99	135
44	38	56	64	100	135
46	38	55	64	100	135
48	39	55	64	101	138
50	40	55	64	102	135
52	40	56	64	102	135
54	40	55	64	103	135
56	40	55	64	104	135
58	40	55	64	103	135
60	40	55	64	103	135

Appendix B.3: Effect of various voltages on 6.2 % magnesium stearate coating on magnesium hydroxide from the Waring blender using DRIFT technique.

TIME (min.)	CH/OH				
	0 volts	20 volts	40 volts	60 volts	80 volts
5	0.3598	0.3449	0.3463	0.3070	0.3170
10	0.3542	0.3675	0.3351	0.3687	0.3633
15	0.3474	0.3589	0.3688	0.3841	0.3997
20	0.3746	0.3555	0.3613	0.3938	0.4293
25	0.3740	0.3585	0.3619	0.3980	0.3705
30	0.3646	0.3731	0.3785	0.3980	0.3926
35	0.3477	0.3832	0.3914	0.3980	0.3873
40	0.3731	0.3701	0.3719	0.4060	0.3768

TIME (min.)	COO/OH				
	0 volts	20 volts	40 volts	60 volts	80 volts
5	0.7744	0.7438	0.7724	0.6675	0.7938
10	0.7659	0.7468	0.6912	0.7273	0.7499
15	0.7650	0.7402	0.7054	0.6908	0.7091
20	0.7553	0.7368	0.6875	0.7077	0.7100
25	0.7642	0.7116	0.6712	0.6371	0.7465
30	0.7227	0.6882	0.6759	0.6468	0.7293
35	0.6559	0.7105	0.6636	0.6473	0.7190
40	0.7058	0.7009	0.6199	0.6624	0.7146

Appendix B.4: Temperature at various coating time in the Fielder mixer for Mg(OH)₂ coated with various coating agent concentrations using DRIFT technique.

TIME (min.)	Temperature (°C)				
	MMSC31	MMSC61	MMSC62	MMSC93	MSAC60
0	60	60	60	60	60
5	119	118	120	118	116
10	137	138	137	138	136
15	138	-	139	139	138
20	139	-	138	138	138
25	139	-	139	139	139
30	140	-	139	139	140
35	139	-	140	140	139
40	140	-	140	140	140

Appendix B.5: Effect of various levels of coating agents on Mg(OH)₂ from a Fielder blender using DRIFT technique.

a) magnesium stearate and stearic acid

TIME (min.)	CH/OH				
	MMSC31	MMSC61	MMSC62	MMSC93	MSAC60
5	0.1756	0.4015	0.3554	0.3502	0.2141
10	0.1786	0.4049	0.3639	0.4488	0.2379
15	0.2012	-	0.3710	0.5240	0.2162
20	0.1983	-	0.3652	0.5303	0.2249
25	0.2051	-	0.3763	0.5142	0.2605
30	0.2047	-	0.3776	0.5057	0.2617
35	0.2023	-	0.3913	0.5122	0.2563
40	0.2076	-	0.3729	0.5134	0.2819

TIME (min.)	COO/OH				
	MMSC31	MMSC61	MMSC62	MMSC93	MSAC60
5	0.5881	0.6298	0.6635	0.6782	0.5579
10	0.5146	0.6472	0.6133	0.6849	0.5363
15	0.5231	-	0.6447	0.6716	0.5269
20	0.5065	-	0.6324	0.6902	0.5037
25	0.5151	-	0.6202	0.6996	0.5456
30	0.5060	-	0.5865	0.6547	0.5355
35	0.4961	-	0.6004	0.6770	0.5492
40	0.5090	-	0.6277	0.6965	0.5648

b) calcium stearate

TIME (min.)	CH/OH			COO/OH		
	MCSC32	MCSC64	MCSC96	MCSC32	MCSC64	MCSC96
5	0.2128	0.4310	0.5607	0.4050	0.6316	0.7289
10	0.2197	0.4228	0.5812	0.3751	0.6369	0.7208
20	0.2170	0.4522	0.5806	0.3650	0.6154	0.7236
30	0.2270	0.4445	0.5794	0.4186	0.6258	0.7258
40	0.2302	0.4504	0.5862	0.3950	0.6109	0.6995

Appendix B.6: Free component at various coating times, sample taken from DSC.

a) heat of fusion (J/g) of magnesium hydroxide coated with 3.1%, 6.2% and 9.3% magnesium stearate at different coating time in the Fielder mixer.

Time	MMSC31			MMSC62			MMSC93		
	C-form	B-form	A-form	C-form	B-form	A-form	C-form	B-form	A-form
5	1.799	-	-	4.310	-	-	7.740	0.160	-
10	0.057	-	0.106	0.129	-	0.227	6.185	-	0.359
20	-	0.103	-	-	0.304	-	1.971	0.427	-
30	-	-	0.022	-	-	0.116	0.787	-	0.950
40	-	-	0.087	-	-	0.333	0.492	-	0.289

b) heat of fusion (J/g) of 6.4% calcium stearate coating on magnesium hydroxide at various voltages and coating times in the Waring blender.

Time	0V		20V		40V		60V		80V	
	temp	heat of fusion								
0	25	1.397	30	1.281	35	1.313	50	1.292	60	1.198
20	34	1.351	45	1.298	63	1.498	86	1.570	127	2.184
60	41	1.586	55	1.535	64	1.435	103	1.808	135	4.275

c) heat of fusion (J/g) of magnesium hydroxide coated with 3.2%, 6.4%, and 9.6% calcium stearate at different coating time in the Fielder mixer.

Time	MCSC32 (C-form)	MCSC64 (C-form)	MCSC96 (C-form)
5	2.084	5.036	11.501
10	0.470	1.123	2.047
20	0.360	0.805	1.771
30	0.000	0.393	1.467
40	0.000	0.000	1.237

Appendix B.7: Ashing results.

a) HDPE compounds containing uncoated magnesium hydroxide and magnesium hydroxide coated with various magnesium stearate concentration and stearic acid.

No.	Code	Details	%ASH ₁	%ASH ₂	%ASH _{average}
1	HDUF	100% HDPE unfilled	0.058	0.048	0.053
2	HMUC	HDPE+40%Mg(OH) ₂ UNCOATED	30.034	30.532	30.283
3	HMMSC31	HDPE+40%[Mg(OH) ₂ +3.1%MgSTEARATE] 40min.	29.899	29.252	29.576
4	HMMSC61	HDPE+40%[Mg(OH) ₂ +6.2%MgSTEARATE] 10min.	28.601	28.632	28.616
5	HMMSC62	HDPE+40%[Mg(OH) ₂ +6.2%MgSTEARATE] 40min.	27.895	27.791	27.843
6	HMMSC93	HDPE+40%[Mg(OH) ₂ +9.3%MgSTEARATE] 40min.	24.176	24.160	24.168
7	HMSAC60	HDPE+40%[Mg(OH) ₂ +6.0%STEARIC ACID] 40min.	25.513	24.231	24.872
8	MHUC	Uncoated Mg(OH) ₂	70.003	70.157	70.080
9	MMSC31	Mg(OH) ₂ +3.1%MgSTEARATE 40 min.	67.603	68.147	67.875
10	MMSC61	Mg(OH) ₂ +6.2%MgSTEARATE 10min.	65.903	65.799	65.851
11	MMSC62	Mg(OH) ₂ +6.2%MgSTEARATE 40min.	65.897	65.836	65.866
12	MMSC93	Mg(OH) ₂ +9.3%MgSTEARATE 40min.	64.080	63.958	64.019
13	MSAC60	Mg(OH) ₂ +6.0%STEARIC ACID 40min.	65.871	65.808	65.840
14	MgSt	MgSTEARATE	6.920	7.148	7.034
15	StA	STEARIC ACID	0.000	0.000	0.000

b) HDPE compounds containing uncoated magnesium hydroxide and magnesium hydroxide coated with various calcium stearate concentrations.

No.	Code	Details	%ASH ₁	%ASH ₂	%ASH _{average}
1	HDUF	100% HDPE unfilled	0.053	0.053	0.053
2	HMUC	HDPE+40%Mg(OH) ₂ UNCOATED	27.042	26.893	26.967
3	HMCSC32	HDPE+40%[Mg(OH) ₂ +3.2%CaSTEARATE]	26.265	26.266	26.265
4	HMCSC64	HDPE+40%[Mg(OH) ₂ +6.4%CaSTEARATE]	25.706	25.686	25.696
5	HMCSC96	HDPE+40%[Mg(OH) ₂ +9.6%CaSTEARATE]	24.716	24.761	24.738
6	MHUC	Uncoated Mg(OH) ₂	68.658	68.663	68.661
7	MCSC32	Mg(OH) ₂ +3.2%CaSTEARATE	66.726	66.478	66.602
8	MCSC64	Mg(OH) ₂ +6.4%CaSTEARATE	64.291	64.310	64.301
9	MCSC96	Mg(OH) ₂ +9.6%CaSTEARATE	62.175	62.146	62.160
10	CaSt	CaSTEARATE	6.950	6.952	6.951

Appendix B.8: Tensile properties.

LOAD AXIS:	1000	N.
EXTENSION AXIS:	5	mm.
LOAD CELL:	10	kN.
GAUGE RANGE:	50	mm.
EXTENSOMETER:	EXTERNAL CLIP ON	
Range:	25	mm.
Temp.:	RT	°C
TEST SPEED:	5	mm/min.
SLOPE:		
Slope low:	100	N.
Slope high:	250	N.
JOG SPEED:	50	mm/min.
SAMPLE TYPE:	RECTANGULAR	

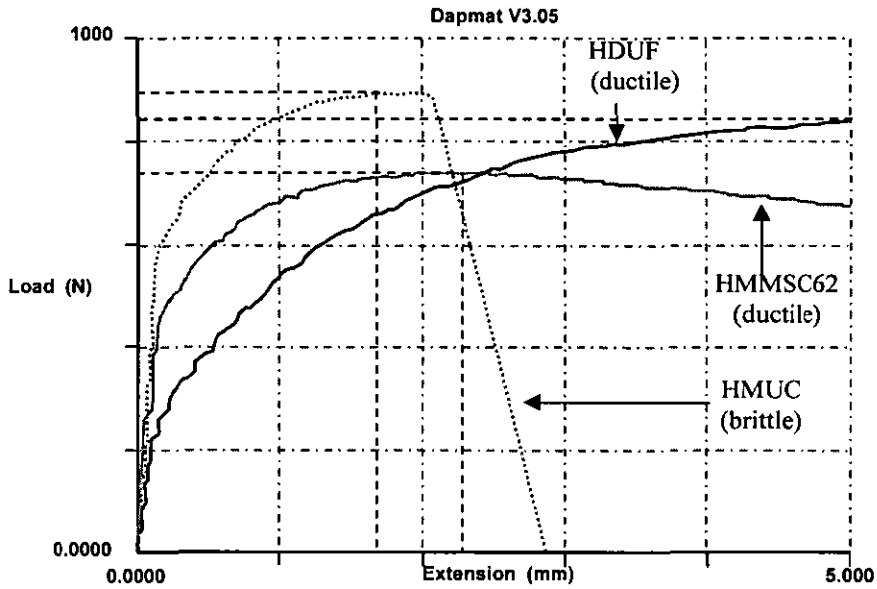


Figure B.1: Typical tensile trace of compounds.

a) HDPE unfilled/filled with magnesium hydroxide uncoated and coated with 3.1%, 6.2%, 9.3% magnesium stearate, and 6.0% stearic acid.

CODE	DETAILS	WIDTH (mm.)	THICK (mm)	MODULUS (N/mm ²)	YIELD STRENGTH (N/mm ²)	ELONGATION AT	
						yield (%)	break (%)
HDUF S/D	unfilled HDPE	12.616	3.133	836.7	20.277	12.71	-
		0.087	0.057	128.872	0.128	1.174	-
HMUC S/D	HDPE +40%Uncoated Mg(OH) ₂	12.584	3.10	3483.50	21.242	3.94	5.20
		0.226	0.049	1187.950	1.474	0.320	0.874
HMMS31 S/D	HDPE+40%[Mg(OH) 3.1%MS] (40 min)	12.681	3.098	1487.4	18.530	4.67	-
		0.026	0.027	702.734	0.389	1.134	-
HMMS61 S/D	HDPE+40%[Mg(OH) 6.2%MS] (10 min)	12.666	3.075	1105.4	18.472	6.01	-
		0.026	0.005	169.934	0.366	0.71	-
HMMS62 S/D	HDPE+40%[Mg(OH) 6.2%MS] (40 min)	12.683	3.075	1322.8	18.413	6.17	-
		0.013	0.011	324.787	0.379	0.804	-
HMMS93 S/D	HDPE+40%[Mg(OH) 9.3%MS] (40 min)	12.661	3.074	1501.0	18.629	5.94	-
		0.041	0.013	695.636	0.230	1.086	-
HMSAC60 S/D	HDPE+40%[Mg(OH) 6.0%SA] (40 min)	12.655	3.114	2079.1	17.953	4.36	-
		0.173	0.033	412.456	0.719	0.418	-

b) HDPE unfilled/filled with magnesium hydroxide uncoated and coated with 3.2%, 6.4% and 9.6% calcium stearate.

CODE	DETAILS	WIDTH (mm.)	THICK (mm)	MODULUS (N/mm ²)	YIELD STRENGTH (N/mm ²)	ELONGATION AT	
						yield (%)	break (%)
HDUF S.D	unfilled HDPE	12.376	3.146	1131.613	18.638	7.275	-
		0.072	0.031	172.522	0.102	0.604	-
HMUC S.D	HDPE +40%Uncoated Mg(OH) ₂	12.448	3.188	6452.875	20.265	2.306	2.695
		0.050	0.024	216.191	0.480	0.347	0.569
HMCSC32 S.D	HDPE+40%[Mg(OH) 3.2%CS] (40 min)	12.605	3.206	3336.250	17.855	2.897	-
		0.295	0.040	813.283	0.182	0.540	-
HMCSC64 S.D	HDPE+40%[Mg(OH) 6.4%CS] (40 min)	12.496	3.169	2237.500	17.790	2.920	-
		0.062	0.033	223.127	0.230	0.128	-
HMCSC96 S.D	HDPE+40%[Mg(OH) 6.6%CS] (40 min)	12.508	3.181	3438.125	16.865	2.638	-
		0.057	0.022	953.067	0.462	0.256	-

Appendix B.9: Flexural properties.

LOAD AXIS:	100	N.
EXTENSION AXIS:	10	mm.
LOAD CELL:	2.5	kN.
EXTENSOMETER:	INTERNAL	
Range:	25	mm.
Temp.:	RT	°C
TEST SPEED:	5	mm/min.

SLOPE:

Slope low: 5 N.

Slope high: 15 N.

JOG SPEED: 50 mm/min.

SAMPLE TYPE: RECTANGULAR

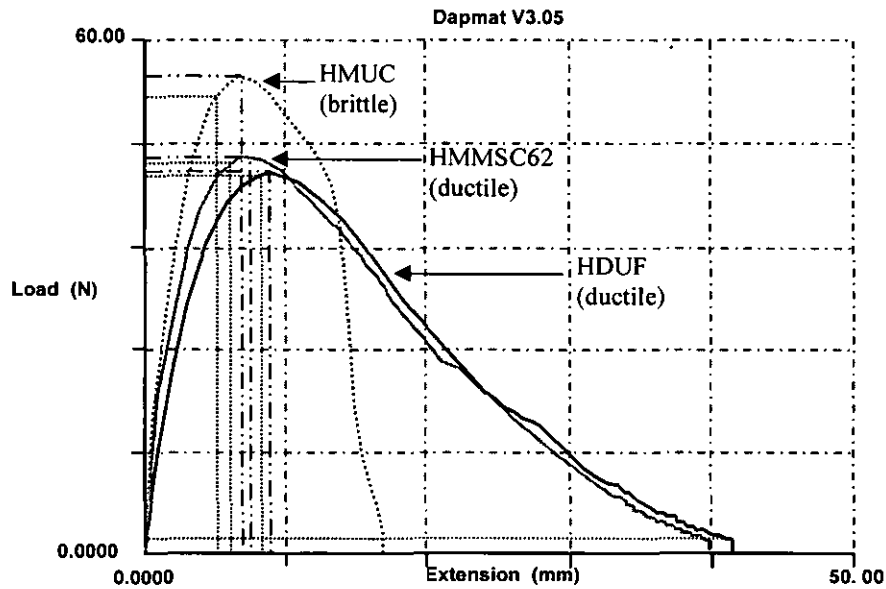


Figure B.2: Typical flexural trace of compounds.

a) HDPE unfilled and filled with magnesium hydroxide uncoated and coated with various levels of magnesium stearate.

Code	Max. Load (N)	Ext. @ Max Load (mm)	Strain @ Max Load (%)	Stress @ High Yield (N/mm ²)	Work Done (N-mm)	Flexural Modulus (N/mm ²)	Flexural Yield Strength (N/mm ²)	Sample Width (mm)	Sample Thick (mm)
HDUF	39.48	8.504	33.96	1.006	1002.3	862.7	24.38	12.69	3.09
S.D	1.63	0.759	12.17	0.041	61.9	88.5	1.02	0.01	0.01
HMUC	44.68	6.431	27.65	1.1320	1014.7	1649.4	27.43	12.70	3.10
S.D	0.69	1.291	3.17	0.0164	34.6	57.3	0.42	0.01	0.01
HMMSC32	37.34	6.558	26.23	0.9532	873.6	1215.9	23.18	12.70	3.08
S.D	1.28	0.681	2.72	0.0337	70.0	93.3	0.86	0.01	0.01
HMMSC61	38.43	6.804	27.22	0.9786	948.0	1058.2	23.86	12.70	3.08
S.D	1.80	0.392	1.57	0.0458	53.90	95.5	1.09	0.01	0.01
HMMSC62	39.29	7.067	28.27	1.0003	1017.4	1081.2	24.32	12.71	3.09
S.D	1.86	0.734	2.94	0.0453	53.8	108.8	1.02	0.02	0.02
HMMSC93	38.19	7.078	28.31	0.9755	895.6	1229.9	23.75	12.71	3.08
S.D	1.33	0.256	1.02	0.0332	46.7	80.7	0.79	0.01	0.01
HMSAC60	40.01	6.765	27.06	1.0180	942.1	1353.4	24.70	12.71	3.09
S.D	2.63	0.416	1.67	0.0672	131.4	79.7	1.65	0.02	0.01

b) HDPE unfilled and filled with magnesium hydroxide uncoated and coated with various levels of calcium stearate.

Code	Max. Load (N)	Max. Stress (N/mm ²)	Ext. @ Max Load (mm)	Strain @ Max Load (%)	Work Done (N-mm)	Flexural Modulus (N/mm ²)	Flexural Yield Strength (N/mm ²)	Sample Width (mm)	Sample Thick (mm)
HDUF	37.76	0.970	8.086	16.170	768.20	758.1	23.13	12.37	3.15
S.D	0.866	0.023	0.344	0.690	32.785	48.907	0.569	0.025	0.009
HMUC	51.98	1.294	6.309	12.498	281.59	1783.75	30.28	12.54	3.20
S.D	2.830	0.067	0.601	1.254	22.541	197.016	1.536	0.016	0.015
HMCSC32	40.63	1.019	7.156	14.311	744.10	1021.75	24.10	12.57	3.17
S.D	0.841	0.024	0.457	0.913	33.923	82.941	0.793	0.067	0.043
HMCSC64	38.34	0.959	7.141	14.283	663.14	978.38	22.55	12.54	3.19
S.D	1.454	0.039	0.766	1.533	40.044	91.420	1.005	0.020	0.033
HMCSC96	40.68	1.019	6.484	12.968	770.85	1128.38	24.00	12.53	3.19
S.D	0.643	0.014	0.462	0.925	84.349	61.951	0.401	0.032	0.030

Appendix B.10: Impact properties

Mass: 25 kg.
 Temperature: RT °C
 Sweep time: 4.92 ms.
 Impact velocity: 3.0 m/s.
 Filter frequency: 2.5 kHz.
 Thickness: 1.32 mm.

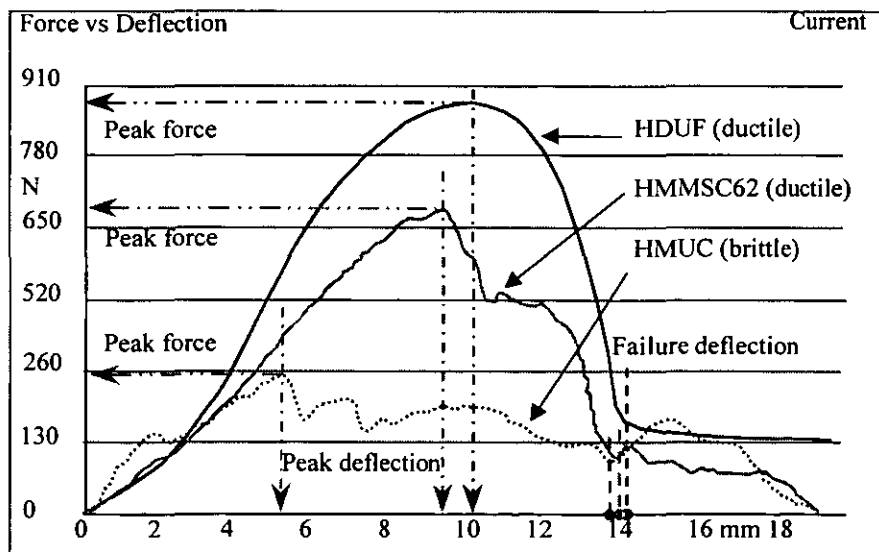


Figure B.3: Typical impact trace of compounds.

a) HDPE unfilled and filled with magnesium hydroxide uncoated and coated with various levels of magnesium stearate.

CODE	PEAK FORCE (N)	PEAK DEFL (mm)	PEAK ENERGY (J)	FAILURE DEFL (mm)	FAILURE ENERGY (J)
HDUF	904.762	9.893	4.492	13.146	6.662
S.D	13.862	0.438	0.299	0.579	0.436
HMUC	263.150	5.945	0.887	17.779	2.362
S.D	7.309	0.330	0.085	2.403	0.608
HMMSC31	399.463	5.421	1.112	18.327	3.737
S.D	54.901	0.717	0.334	0.389	0.242
HMMSC61	540.488	7.458	1.980	18.508	4.499
S.D	51.738	0.759	0.391	0.312	0.491
HMMSC62	580.415	7.489	2.171	18.324	4.986
S.D	52.994	1.012	0.464	0.353	0.558
HMMSC93	400.781	5.797	1.089	18.480	3.599
S.D	40.900	0.405	0.156	0.177	0.126
HMSAC60	451.990	6.080	1.287	18.267	3.729
S.D	63.516	0.788	0.344	0.571	0.333

b) HDPE unfilled and filled with magnesium hydroxide uncoated and coated with various levels of calcium stearate.

CODE	PEAK FORCE (N)	PEAK DEFL (mm)	PEAK ENERGY (J)	FAILURE DEFL (mm)	FAILURE ENERGY (J)
HDUF	949.10	9.540	4.618	15.329	7.592
S.D	9.74	0.155	0.084	0.036	0.120
HMUC	239.80	5.567	0.780	14.395	1.889
S.D	17.44	0.774	0.161	0.726	0.169
HMCSC32	358.60	7.822	1.652	15.949	3.363
S.D	9.34	0.281	0.081	0.345	0.075
HMCSC64	436.40	8.334	1.846	15.894	3.938
S.D	7.07	0.283	0.162	0.422	0.119
HMCSC96	334.60	7.069	1.514	15.919	3.130
S.D	16.30	1.668	0.463	0.565	0.097

Appendix B.12: Effect of types and levels of coating agent on crystallisation properties

a) HDPE unfilled and filled with magnesium hydroxide uncoated and coated with various levels of magnesium stearate and stearic acid.

Code	H_m (J/g)	H_c (J/g)	T_m (°C)	T_c (°C)	% Cryst
HDUF	165.4	204.3	136.9	113.4	56.45
HMUC	108.0	133.6	133.7	114.9	64.76
HMMSC31	114.3	150.3	133.2	115.5	69.09
HMMSC61	115.4	142.4	133.6	114.4	69.60
HMMSC62	127.3	156.4	133.9	114.6	75.20
HMMSC93	103.6	132.8	132.8	115.2	56.75
HMSAC60	106.6	137.5	131.7	114.7	58.42

b) HDPE unfilled and filled with magnesium hydroxide uncoated and coated with various levels of calcium stearate.

Code	H _m (J/g)	H _c (J/g)	T _m (°C)	T _c (°C)	% Cryst
HDUF	182.1	200.0	134.1	110.6	62.18
HMUC	128.8	139.3	130.1	115.6	72.34
HMCSC32	137.8	146.0	130.4	113.5	77.59
HMCSC64	138.0	159.9	130.5	113.0	78.38
HMCSC96	132.4	147.0	131.5	113.3	75.00

Appendix B.12: Reversion test

a) HDPE unfilled and filled with magnesium hydroxide uncoated and coated with various levels of magnesium stearate and stearic acid.

Code	R (%)	S.D
HDUF	17.86	0.53
HMUC	10.53	1.00
HMMSC31	10.70	0.78
HMMSC61	11.02	0.66
HMMSC62	11.07	0.64
HMMSC93	11.04	0.89
HMSAC60	11.86	0.99

b) HDPE unfilled and filled with magnesium hydroxide uncoated and coated with various levels of calcium stearate.

Code	%R	S.D
HDUF	16.18	1.361
HMUC	9.63	1.772
HMCSC32	12.48	2.497
HMCSC64	13.48	2.460
HMCSC96	15.02	1.991

Appendix B.13: X-ray diffraction.

a) HDPE unfilled and filled with magnesium hydroxide uncoated and coated with various levels of magnesium stearate and stearic acid.

CODE	Intensity (cps)					
	PE110	PE200	MH001	MH101	PE200/110	MH001/101
HDPEiso	4289	1205	-	-	0.28	-
HDUF	8562	1387	-	-	0.16	-
HMUC	1156	248	3013	221	0.21	13.63
HMMSC31	1849	759	11033	203	0.41	54.35
HMMSC62	1084	576	26809	419	0.53	63.98
HMMSC61	1401	587	18926	396	0.42	47.79
HMMSC93	1614	631	17820	460	0.39	38.74
HMSAC60	1342	679	19364	326	0.51	59.40
MHUC	-	-	1595	1835	-	0.87

b) HDPE unfilled and filled with magnesium hydroxide uncoated and coated with various levels of calcium stearate.

CODE	Intensity (cps)					
	PE110	PE200	MH001	MH101	PE200/110	MH001/101
HDPEiso	4289	1205	-	-	0.28	-
HDUF	4373	816	-	-	0.19	-
HMUC	1254	378	4786	384	0.30	12.46
HMCSC32	853	375	12284	202	0.44	60.81
HMCSC64	860	367	11935	192	0.43	62.16
HMCSC96	1112	310	7999	337	0.28	23.74
MHUC	-	-	1595	1835	-	0.87

APPENDIX C: SUMMARISED RESULTS (Series II)

Appendix C.1: Effect of various types of coating agents on filler in the Fielder blender from DRIFT analysis.

a) Magnesium Hydroxide

Time(min.)	CH/OH				
	MMSA62	MMSC62	MCSC64	MZSC67	MSAC60
5	0.3202	0.3499	0.4402	0.3559	0.1942
10	0.3342	0.4001	0.3897	0.4424	0.1985
20	0.3349	0.3986	0.3521	0.5367	0.2462
40	0.3507	0.4008	0.3601	0.5504	0.2828
Time(min.)	COO/OH				
	MMSA62	MMSC62	MCSC64	MZSC67	MSAC60
5	0.5869	0.6536	0.5972	0.5880	0.5111
10	0.5892	0.5719	0.6081	0.6301	0.5213
20	0.5475	0.5774	0.6591	0.6696	0.5335
40	0.5763	0.6637	0.6785	0.6389	0.5342

b) Calcium carbonate

Time(min.)	CH/CO				
	CMSC42	CCSA43	CCSC43	CZSC45	CSAC40
5	0.9178	0.8640	0.8593	0.8836	0.9836
10	0.9815	0.8628	0.8758	1.0720	1.1275
20	0.9612	0.8996	0.8734	1.0867	1.1619
40	0.9931	0.8757	0.9009	1.1735	1.1671

Appendix C.2 : Heat of fusion (J/g).

a) coated magnesium hydroxide.

Time	MMSC62			MCSC64	MZSC67			MSAC60		
	C-form	B-form	A-form	C-form	C-form	B-form	A-form	C-form	B-form	A-form
5	4.310	-	-	7.149	5.927	-	-	-	0.146	0.415
10	0.129	-	0.227	6.134	3.867	-	0.218	0.347	-	1.571
20	-	0.304	-	3.976	0.048	-	0.608	0.125	-	1.380
30	-	-	0.116	3.886	-	0.128	0.981	-	-	1.415
40	-	-	0.333	2.657	-	-	0.860	-	-	0.812

b) coated calcium carbonate.

Time	CMSC42			CCSC43	CZSC45			CSAC40		
	C-form	B-form	A-form	C-form	C-form	B-form	A-form	C-form	B-form	A-form
5	5.362	-	-	5.098	5.111	-	-	1.089	-	0.113
10	2.307	-	0.218	4.914	-	0.343	-	0.405	-	-
20	-	-	0.138	1.902	-	-	0.060	1.349	-	0.027
30	-	0.093	-	0.194	-	-	-	0.875	-	-
40	-	0.082	-	-	-	-	-	1.525	-	0.189

Appendix C.3 : Ashing test.

No.	Code	Details	%ASH ₁	%ASH ₂	%ASH _{average}
1	HDUF	100% HDPE unfilled	0.00	0.00	0.00
2	HMUC	HDPE+40%Mg(OH) ₂ UNCOATED	27.17	28.89	28.03
3	HMMS62	HDPE+40%[Mg(OH) ₂ +6.2%MS](COATED)	24.34	24.63	24.48
4	HMMSA62	HDPE+40%[Mg(OH) ₂ +6.2%MS](ADDED)	24.97	25.16	25.07
5	HMCSC64	HDPE+40%[Mg(OH) ₂ +6.4%CS](COATED)	24.45	24.65	24.59
6	HMZSC67	HDPE+40%[Mg(OH) ₂ +6.7%ZS](COATED)	25.76	25.65	25.70
7	HMSAC60	HDPE+40%[Mg(OH) ₂ +6.0%SA](COATED)	26.65	26.64	26.64
8	HCUC	HDPE+40%Ca(CO) ₃ UNCOATED	21.91	21.84	21.87
9	HCMSC42	HDPE+40%[Ca(CO) ₃ +4.2%MS](COATED)	22.07	21.91	21.99
10	HCCSC43	HDPE+40%[Ca(CO) ₃ +4.3%CS](COATED)	21.17	21.09	21.13
11	HCCSA43	HDPE+40%[Ca(CO) ₃ +4.3%CS](ADDED)	22.09	21.89	21.99
12	HCZSC45	HDPE+40%[Ca(CO) ₃ +4.5%ZS](COATED)	21.16	20.64	20.90
13	HCSAC40	HDPE+40%[Ca(CO) ₃ +4.0%SA](COATED)	21.67	21.72	21.69
14	MHUC	Mg(OH) ₂	68.77	68.70	68.73
15	MMS62	Mg(OH) ₂ +6.2%MS(COATED)	65.08	65.06	65.07
16	MMSA62	Mg(OH) ₂ +6.2%MS(ADDED)	65.04	65.07	65.06
17	MCSC64	Mg(OH) ₂ +6.4%CS(COATED)	65.22	65.20	65.21
18	MZSC67	Mg(OH) ₂ +6.7%ZS(COATED)	64.09	64.06	64.09
19	MSAC60	Mg(OH) ₂ +6.0%SA(COATED)	64.58	64.56	64.57
20	CCUC	Ca(CO) ₃ UNCOATED	55.84	55.84	55.84
21	CMSC42	Ca(CO) ₃ +4.2%MS(COATED)	53.86	53.88	53.87
22	CCSC43	Ca(CO) ₃ +4.3%CS(COATED)	53.84	53.82	53.83
23	CCSA43	Ca(CO) ₃ +4.3%CS(ADDED)	53.83	53.84	53.83
24	CZSC45	Ca(CO) ₃ +4.5%ZS(COATED)	53.89	53.90	53.89
25	CSAC40	Ca(CO) ₃ +4.0%SA(COATED)	53.62	53.63	53.62
26	MgSt	Mg STEARATE	9.06	9.14	9.10
27	CaSt	Ca STEARATE	9.41	9.46	9.43
28	ZnSt	Zn STEARATE	13.27	13.25	13.26
29	StA	STEARIC ACID	0.00	0.00	0.00

Appendix C.4 : Tensile Properties.

a) HDPE unfilled and filled with magnesium hydroxide and calcium carbonate.

SAMPLE CODE	DETAILS	WIDTH (mm.)	THICK (mm)	MODULUS (N/mm ²)	YIELD STRENGTH (N/mm ²)	ELONGATION At	
						yield (%)	break(%)
HDUF S.D	HDPE unfilled	12.708	3.096	896.463	21.409	19.739	-
		0.004	0.005	169.798	1.296	0.469	-
HMUC S.D	HDPE+40%Mg(OH) ₂	12.711	3.104	4208.625	23.341	6.763	5.198
		0.008	0.010	1646.874	0.733	1.445	0.818
HMMSA62 S.D	HDPE+40%[Mg(OH) ₂ +6.2%MS] (added)	12.706	3.101	1881.000	18.938	8.805	-
		0.005	0.003	292.394	0.635	0.975	-
HMMSA62 S.D	HDPE+40%[Mg(OH) ₂ +6.2%MS] (coated)	12.703	3.103	2488.625	18.529	8.568	-
		0.004	0.004	545.968	0.601	1.133	-
HMCSC64 S.D	HDPE+40%[Mg(OH) ₂ +6.4%CS] (coated)	12.706	3.096	2097.125	20.803	11.941	-
		0.005	0.005	34.156	0.238	1.630	-
HMZSC67 S.D	HDPE+40%[Mg(OH) ₂ +6.7%ZS] (coated)	12.709	3.098	2918.500	18.453	7.012	-
		0.003	0.007	173.357	0.735	0.826	-
HMSAC60 S.D	HDPE+40%[Mg(OH) ₂ +6.0%SA] (coated)	12.706	3.104	2104.625	18.186	10.924	-
		0.005	0.005	594.692	0.757	1.281	-
HCUC S.D	HDPE+40%CaCO ₃	12.710	3.099	3857.750	21.011	10.520	5.198
		0.000	0.003	208.255	0.754	0.648	0.818
HCMSC42 S.D	HDPE+40%[CaCO ₃ +4.2%MS] (coated)	12.709	3.103	2100.500	19.056	10.973	-
		0.006	0.008	39.784	0.427	0.614	-
HCCSA43 S.D	HDPE+40%[CaCO ₃ +4.3%CS] (added)	12.710	3.098	2641.000	19.013	8.270	-
		0.000	0.004	263.272	0.318	0.506	-
HCCSC43 S.D	HDPE+40%[CaCO ₃ +4.3%CS] (coated)	12.708	3.095	2346.750	19.053	10.086	-
		0.004	0.005	30.061	0.590	1.981	-
HCZSC45 S.D	HDPE+40%[CaCO ₃ +4.5%ZS] (coated)	12.706	3.099	2089.500	18.008	8.469	-
		0.005	0.006	27.600	0.215	0.475	-
HCSAC40 S.D	HDPE+40%[CaCO ₃ +4.0%SA] (coated)	12.708	3.099	2916.750	18.776	8.560	-
		0.004	0.008	63.035	0.338	1.059	-

b) HDPE unfilled and filled with coating agents.

SAMPLE CODE	DETAILS	WIDTH (mm.)	THICK (mm)	MODULUS (N/mm ²)	YIELD STRENGTH (N/mm ²)	ELONGATION At	
						yield (%)	break(%)
HDPE S.D	Unfilled HDPE	12.376	3.146	1131.613	18.638	7.275	-
		0.072	0.031	172.522	0.102	0.604	-
HDMS H.D	HDPE+Mg Stearate	12.388	3.140	1100.500	19.268	7.095	-
		0.045	0.018	76.364	0.294	0.558	-
HDCS S.D	HDPE+Ca Stearate	12.381	3.141	1103.013	19.190	7.505	-
		0.028	0.018	65.967	0.447	0.628	-
HDZS S.D	HDPE+Zn Stearate	12.346	3.134	1203.000	19.679	7.193	-
		0.037	0.033	70.431	0.149	0.751	-
HDSA S.D	HDPE+Stearic acid	12.340	3.151	1056.875	18.921	7.504	-
		0.031	0.013	23.735	0.151	0.360	-

Appendix C.5: Flexural properties.**a) HDPE unfilled and filled with magnesium hydroxide and calcium carbonate.**

Sample Code	Max. Load (N)	Stress @ High Yield (N/mm ²)	Ext. @ Max Load (mm)	Strain @ Max Load (%)	Work Done (N-mm)	Flexural Modulus (N/mm ²)	Flexural Yield Strength (N/mm ²)	Sample Width (mm)	Sample Thick (mm)
HDUF	36.86	0.850	7.722	15.45	677.11	841.5	22.85	12.39	3.13
S.D.	2.642	0.130	0.722	1.445	99.876	64.977	1.525	0.060	0.014
HMUC	55.27	1.320	6.365	12.730	739.04	2025.88	32.79	12.45	3.19
S.D.	2.075	0.079	0.390	0.779	211.003	135.989	1.375	0.073	0.030
HMMSA62	44.63	1.069	6.477	12.955	856.66	2021.25	28.09	12.53	3.08
S.D.	0.642	0.094	0.299	0.599	28.869	90.925	0.667	0.046	0.023
HMMSC62	44.82	1.059	6.597	13.194	892.55	1555.88	27.40	12.48	3.14
S.D.	0.977	0.173	0.425	0.850	33.074	68.135	0.738	0.084	0.029
HMCSC64	44.87	1.104	7.192	14.384	915.74	1446.88	27.53	12.47	3.13
S.D.	0.454	0.059	0.463	0.924	18.953	130.713	0.419	0.069	0.021
HMZSC67	43.41	1.105	5.903	11.806	841.38	1800.38	27.29	12.51	3.10
S.D.	0.757	0.032	0.404	0.806	31.473	67.528	0.722	0.062	0.015
HMSAC60	45.25	1.123	6.582	13.165	896.80	1707.13	28.11	12.50	3.11
S.D.	1.537	0.037	0.302	0.605	48.931	121.934	0.952	0.087	0.012
HCUC	56.17	1.428	4.528	18.111	856.08	2917.25	34.59	12.71	3.10
S.D.	1.713	0.046	0.180	0.717	26.844	294.777	1.158	0.005	0.009
HCMSC42	49.83	1.266	5.199	20.795	843.11	2142.75	30.63	12.71	3.10
S.D.	1.018	0.026	0.428	1.714	19.443	138.605	0.657	0.005	0.006
HCCSA43	52.79	1.341	4.719	18.875	894.86	2770.50	32.41	12.71	3.10
S.D.	2.342	0.057	0.185	0.740	58.051	190.081	1.337	0.005	0.010
HCCSC43	50.02	1.274	5.083	20.331	814.13	2318.25	30.88	12.70	3.09
S.D.	1.598	0.040	0.334	1.334	32.632	186.209	0.933	0.004	0.009
HCZSC45	48.50	1.234	4.778	19.290	794.91	2314.63	29.92	12.70	3.09
S.D.	1.008	0.026	0.296	1.570	22.360	59.462	0.632	0.007	0.011
HCSAC40	51.50	1.308	4.562	18.250	873.26	2765.25	31.73	12.71	3.10
S.D.	1.153	0.032	0.243	0.971	27.144	137.483	0.775	0.005	0.011

b) HDPE unfilled and filled with coating agents.

Sample Code	Max. Load (N)	Stress @ High Yield (N/mm ²)	Ext. @ Max Load (mm)	Strain @ Max Load (%)	Work Done (N-mm)	Flexural Modulus (N/mm ²)	Flexural Yield Strength (N/mm ²)	Sample Width (mm)	Sample Thick (mm)
HDUF	37.76	0.970	8.086	16.17	768.20	758.1	23.13	12.37	3.15
S.D.	0.866	0.023	0.344	0.690	32.785	48.907	0.569	0.025	0.009
HDMS	32.76	0.837	7.112	14.224	569.18	646.01	19.86	12.37	3.16
S.D.	1.505	0.042	0.549	1.098	37.664	63.959	1.189	0.076	0.040
HDCS	32.52	0.839	7.552	15.103	567.95	649.53	19.97	12.29	3.15
S.D.	0.994	0.032	0.698	1.395	31.136	55.348	0.985	0.057	0.050
HDZS	33.52	0.868	6.899	15.680	609.38	674.05	20.88	12.38	3.12
S.D.	1.434	0.035	2.584	1.693	40.504	55.386	0.810	0.031	0.016
HDSA	32.80	0.850	7.961	15.921	598.78	638.80	20.32	12.29	3.14
S.D.	1.706	0.051	0.580	1.160	38.397	65.634	1.334	0.064	0.021

Appendix C.6: Impact properties.

Mass:	26.2	kg.
Temperature:	RT	°C
Impact velocity:	2.95	m/s.
Filter frequency:	200	kHz.
Thickness:	1.32	mm.

a) HDPE unfilled and filled with magnesium hydroxide and calcium carbonate.

CODE	PEAK FORCE (N)	PEAK DEFL (mm)	PEAK ENERGY (J)	FAILURE DEFL (mm)	FAILURE ENERGY (J)
HDUF	804.50	5.421	2.893	14.514	5.560
S.D	21.58	0.792	0.488	2.783	0.577
HMUC	228.50	2.615	0.386	7.630	1.089
S.D	46.89	1.489	0.303	2.417	0.438
HMMSA62	275.60	6.923	1.056	12.183	2.202
S.D	20.23	2.039	0.439	2.481	0.343
HMMSC62	282.90	4.590	0.849	12.732	2.267
S.D	35.38	2.133	0.502	1.707	0.643
HMCSC64	433.50	4.768	1.144	13.135	2.865
S.D	58.24	0.727	0.306	1.095	0.246
HMZSC67	265.70	2.904	0.444	13.041	2.455
S.D	23.93	0.801	0.184	1.043	0.383
HMSAC60	269.80	5.428	0.980	10.221	1.785
S.D	18.14	1.402	0.238	1.553	0.295
HCUC	268.90	3.455	0.581	7.298	1.160
S.D	18.950	1.172	0.215	1.909	0.296
HCMSC42	444.00	4.731	1.220	13.118	3.050
S.D	41.08	0.675	0.263	0.596	0.243
HCCSA43	374.00	3.755	0.867	11.027	2.759
S.D	46.57	1.045	0.359	0.683	0.292
HCCSC43	415.40	4.446	1.150	13.800	3.239
S.D	48.68	0.705	0.305	2.533	0.547
HCZSC45	442.80	5.222	1.457	12.760	3.349
S.D	67.28	1.153	0.545	0.855	0.628
HCSAC40	366.80	3.117	0.645	12.762	2.773
S.D	46.07	0.785	0.297	0.579	0.192

b) HDPE unfilled and filled with coating agents.

CODE	PEAK FORCE (N)	PEAK DEFL (mm)	PEAK ENERGY (J)	FAILURE DEFL (mm)	FAILURE ENERGY (J)
HDUF	949.100	9.540	4.618	15.329	7.592
S.D	9.741	0.155	0.084	0.036	0.120
HDMS	922.80	9.348	4.391	15.157	6.875
S.D	10.19	0.206	0.161	0.746	0.423
HDCS	930.20	9.475	4.627	15.542	7.513
S.D	7.61	0.388	0.205	0.438	0.320
HDZS	928.20	9.187	4.264	15.571	7.091
S.D	11.48	0.249	0.250	0.896	0.573
HDSA	947.70	9.519	4.515	15.967	7.513
S.D	7.93	0.207	0.161	0.417	0.157

Appendix C.7: Crystallisation properties.

a) HDPE unfilled and filled with magnesium hydroxide and calcium carbonate.

CODE	H m (J/g)	H c (J/g)	T _m (°C)	T _c (°C)	% Cryst
HDUF	165.8	191.2	133.6	110.7	56.6
HMUC	101.5	117.9	131.3	114.7	58.5
HMMSA62	117.0	130.0	132.3	112.3	65.0
HMMSC62	134.3	148.0	132.2	111.6	73.5
HMCSC64	143.4	165.5	132.6	111.1	78.5
HMZSC67	135.2	151.1	132.8	111.0	77.0
HMSAC60	121.5	135.6	131.0	112.2	70.6
HCUC	122.2	138.6	131.8	113.0	68.6
HCMSC42	134.3	147.3	132.7	111.7	77.5
HCCSA43	122.0	154.1	132.4	112.5	70.4
HCCSC43	129.2	141.0	132.4	111.3	72.6
HCZSC45	134.5	147.9	132.7	111.6	75.0
HCSAC40	129.0	144.9	131.5	111.5	73.9

b) HDPE unfilled and filled with coating agents.

CODE	H m (J/g)	H c (J/g)	T _m (°C)	T _c (°C)	% Cryst
HDUF	182.1	200.0	134.1	110.6	62.18
HDMS	206.0	242.2	132.2	112.1	73.11
HDCS	204.6	234.5	133.0	111.9	72.76
HDZS	198.9	209.2	132.0	112.7	70.89
HDSA	201.2	224.2	131.7	112.2	71.37

Appendix C.8: Reversion test.

CODE	%R	S.D	CODE	%R	S.D	CODE	%R	S.D
HDUF	18.46	3.17	HDUF	18.46	3.17	HDUF	16.18	1.36
HMUC	10.56	0.41	HCUC	11.60	0.22	HDMS	30.37	2.00
HMMSA62	10.39	0.56	HCMSC42	10.92	0.71	HDCS	33.36	0.73
HMMSC62	10.03	0.46	HCCSA43	11.27	0.21	HDZS	28.30	1.15
HMCSC64	9.97	0.61	HCCSC43	10.76	0.49	HDSA	18.153	2.51
HMZSC67	10.16	0.32	HCZSC45	10.90	0.47			
HMSAC60	10.25	0.59	HCSAC40	11.12	0.31			

Appendix C.9: X-ray diffraction.

a) Magnesium hydroxide filled HDPE.

CODE	Intensity (cps)					
	PE110	PE200	MH001	MH101	PE200/110	MH001/101
HDUF	8734	1446	-	-	0.17	-
HMUC	1037	227	3112	219	0.22	14.21
HMMSC62	1084	876	26809	219	0.81	122.42
HMMSA62	1243	779	29655	249	0.63	119.10
HMCSC64	1337	1063	21519	259	0.80	83.08
HMZSC67	1092	833	22867	295	0.76	77.52
HMSAC60	1332	1072	21364	316	0.80	67.61
MHUC	-	-	1595	1835	-	0.87

b) Calcium carbonate filled HDPE.

CODE	Intensity (cps)					
	PE110	PE200	CC104	CC110	PE200/110	CC104/110
HDUF	8734	1446	-	-	0.17	-
HCUC	576	378	985	91	0.66	10.82
HCMSC42	442	365	1166	67	0.83	17.40
HCCSC43	398	354	1215	64	0.89	18.98
HCCSA43	409	334	1292	67	0.82	19.28
HCZSC45	528	427	1207	70	0.81	17.24
HCSAC40	346	318	1285	68	0.92	18.90
CCUC	-	-	1008	119	-	8.47

c) Coating agent filled HDPE.

CODE	Intensity (cps)		
	PE110	PE200	PE200/110
HDUF	4373	816	0.19
HDMS	6047	995	0.16
HDCS	5329	923	0.17
HDZS	5781	1016	0.18
HDSA	6514	1102	0.17

APPENDIX D: CALCULATIONS

Appendix D.1: The calculation of monolayer coverage of stearic acid.

Stearic acid molecule has a cross section area of 0.21 nm^2 . A monolayer is given by:

$$L_1 = \frac{S_f \times MW_a}{A_a \times N_A}$$

when S_f is specific area of filler, MW_a is molecular mass of the acid, A_a is cross section area of acid and N_A is Avogadro's number.

	$Mg(OH)_2$	$CaCO_3$	unit
Specific surface area	13.00×10^{18}	17.332×10^{18}	nm^2/g
Cross section area of stearic acid	0.21	0.21	$\text{nm}^2/\text{molecule}$
Avogadro's number	6.023×10^{23}	6.023×10^{23}	molecule/mole
MW of stearic acid	284	284	g/mole
\therefore monolayer coverage	$\frac{13 \times 10^{18} \times 284}{0.21 \times 6.023 \times 10^{23}}$ = 0.0292	$\frac{17.332 \times 10^{18} \times 284}{0.21 \times 6.023 \times 10^{23}}$ = 0.0389	$\text{g}_{\text{acid}}/\text{g}_{\text{filler}}$
That is	$\approx 3.0\%$ by weight	$\approx 4.0\%$ by weight	$\text{g}_{\text{acid}}/\text{g}_{\text{filler}}$

Appendix D.2: The calculation of acid-group equivalency between metal stearates and stearic acid.

According to the previous study, found that the amount of 6.0% stearic acid is practically performed monolayer coverage on magnesium hydroxide [134] whereas 4.0% stearic acid is completely coated on calcium carbonate [85].

	Stearic acid	Mg stearate	Ca stearate	Zn stearate
Formulation	$\text{CH}_3(\text{CH}_2)_{16}\text{COOH}$	$(\text{C}_{17}\text{H}_{35}\text{COO})_2\text{Mg}$	$(\text{C}_{17}\text{H}_{35}\text{COO})_2\text{Ca}$	$(\text{C}_{17}\text{H}_{35}\text{COO})_2\text{Zn}$
MW. (g/mol)	284	590.3	606.1	631.4
Atomic weight of (g/mole)	H: 1	Mg: 24	Ca: 40.1	Zn: 65.4
MW of stearate group (g/mol)	283	566	566	566

	Stearic acid (g)	Stearate group (g)
MW. of	284 contains	283
Weight of	6 contains	$\frac{283 \times 6}{284} = 5.98$

	Stearate group (g)	Mg stearate (g)	Ca stearate (g)	Zn stearate (g)
MW of	566	590.3	606.1	631.4
Weight of	5.98	$\frac{590.3 \times 5.98}{566} = 6.23$	$\frac{606.1 \times 5.98}{566} = 6.40$	$\frac{631.4 \times 5.98}{566} = 6.67$
\therefore $Mg(OH)_2$ coated with	6.0% stearic acid	= 6.2% Mg St	= 6.4% Ca St	= 6.7% Zn St

Appendix D.3: The calibration of polymer and filler feeders.

The calibration of polymer and filler feeders for HDPE+40% Mg(OH)₂ coated with 6.2% magnesium stearate is obtained from:

HDPE

Feed No.	Weight (g)	Feed rate (g/min)	Feed rate (kg/hr)
1	204.34	68.11	4.087
2	523.05	174.35	10.461
3	861.28	287.09	17.226

Mg(OH)₂+6.2% magnesium stearate

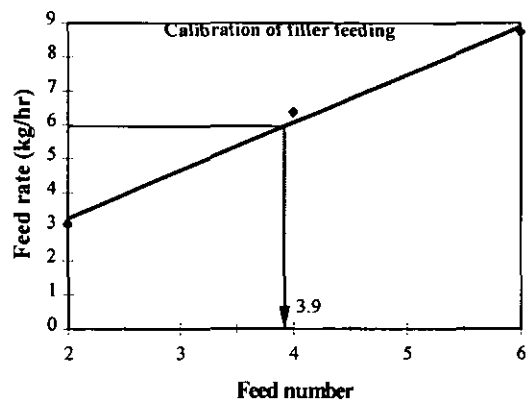
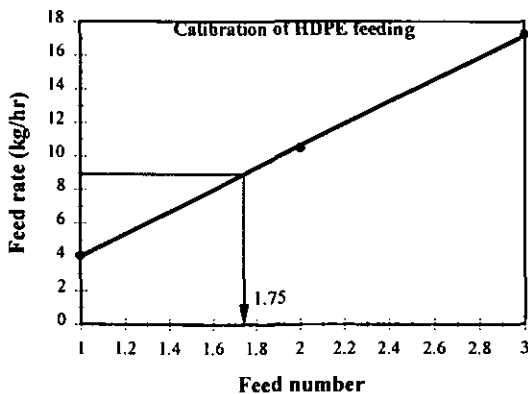
Feed No.	Weight (g)	Feed rate (g/min)	Feed rate (kg/hr)
2	153.76	51.25	3.075
4	318.07	106.02	6.361
6	436.73	145.58	8.735
2	156.84	52.28	3.137

Required production rate at 15 kg/hr,

Feeding of 60%HDPE = $15 \times 0.6 = 9$ kg/hr,

Feeding of 40%Mg(OH)₂ coated with 6.2% magnesium stearate = $15 \times 0.4 = 6$ kg/hr.

From the calibration of polymer and filler feedings, the polymer and filler feeders were set at 1.75 and 3.9, respectively.



Appendix D.4: %Crystallinity of compounds.

$$\% \text{ crystallinity of compound} = f_c = \frac{\Delta H_m}{\Delta H_{mc}} \times \frac{1}{\text{Polymer fraction}} \times 100 \quad (3.1)$$

Heat of fusion for HMMSC62 compound (ΔH_m) is 127.3 (J/g).

Heat of fusion of completely crystalline polyethylene (ΔH_{mc}) is 293.0 J/g [139].

%polymer content for HDPE compound containing $\text{Mg}(\text{OH})_2$ coated with 6.2% magnesium stearate (HMMSC62) obtained from ashing test is 57.77% .

$$\therefore \% \text{ crystallinity of HMMSC62} = f_c = \frac{127.3}{293.0} \times \frac{1}{0.5777} \times 100 = 75.21\%$$

Appendix D.5: The calculation of free components from DSC traces.

After 5 minutes of coating magnesium hydroxide with 6.2% (w/w) magnesium stearate in the Fielder mixer at temperature of $118 \pm 2^\circ\text{C}$, the coated filler sample was analysed using thermal analysis with DSC cell. The result showed that one transition were found at temperature 120.9°C (C-form) with heat of fusion 4.31 J/g and heat of fusion of magnesium stearate is 140.1 J/g. Therefore, free component for C form can be calculated as the following:

$$\text{Free component of C-form} = \frac{4.31 \times 100}{140.1 \times 6.2} = 0.496$$

After 10 minutes of coating, the DSC result showed that two transitions were found at temperature 65.6°C (A-form) and 120.05°C (C-form) with heat of fusion of 0.227 and 0.129 J/g, respectively Therefore, free component for A and B forms can be calculated as the following:

$$\text{Free component of A-form} = \frac{0.227 \times 100}{140.1 \times 6.2} = 0.026$$

$$\text{Free component of C-form} = \frac{0.129 \times 100}{140.1 \times 6.2} = 0.015$$

Appendix D.6: The calculation of surface free energy for HDPE.

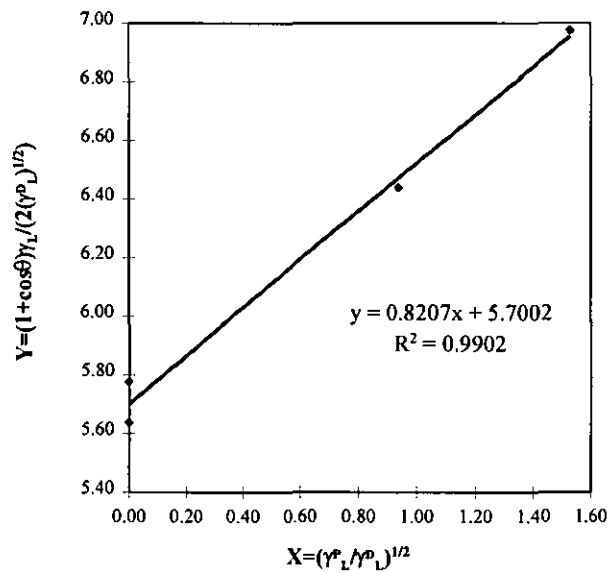
Surface free energy was determined using Equation (2.31).

$$\frac{(1 + \cos\theta_1)\gamma_L}{2\sqrt{\gamma_L^D}} = \sqrt{\gamma_S^D} + \sqrt{\gamma_S^P} \left(\sqrt{\frac{\gamma_L^P}{\gamma_L^D}} \right) \quad (2.31)$$

A straight line was plotted between variables $X = \sqrt{\frac{\gamma_L^P}{\gamma_L^D}}$ versus $Y = \frac{(1 + \cos\theta_1)\gamma_L}{2\sqrt{\gamma_L^D}}$.

$\sqrt{\gamma_S^P}$ and $\sqrt{\gamma_S^D}$ can be obtained from a slope and an intercept of the linear line including with R^2 which is a regression parameter. For HDPE the surface energy parameters and contact angle are given in Table below:

Liquids	γ_L (mJ/m ²)	γ_L^D (mJ/m ²)	γ_L^P (mJ/m ²)	X= (γ_L^P/γ_L^D) ^{1/2}	Contact angle (θ_1)	Y= (1+cos θ_1) $\gamma_L/2(\gamma_L^D)^{1/2}$
Water	72.8	21.8	51.0	1.529	96.0	6.976
Glycerol	64.0	34.0	30.0	0.939	80.0	6.438
DIM	50.8	50.8	0.0	0.000	51.6	5.776
BNL	44.4	44.4	0.0	0.000	46.2	5.637



The slope and intercept can be read from graph as 0.8207 and 5.7002, respectively and the values of γ_S^P and γ_S^D are calculated given as 0.6739 and 32.4911. Inserted both values into Equation (2.32).

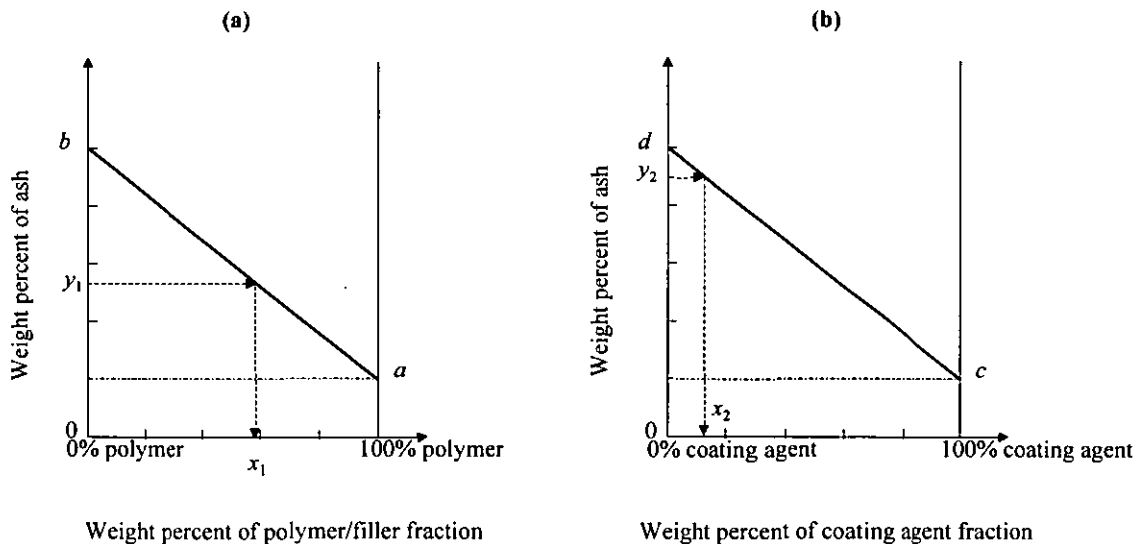
$$\gamma_S = \gamma_S^D + \gamma_S^P \quad (2.32)$$

Therefore, the surface energy of HDPE is 33.165 mJ/m².

Appendix D.7: The calculation of %polymer content, filler content, and %coating content for HDPE compound containing 40% (w/w) magnesium hydroxide coated with 6.2% (w/w) magnesium stearate.

Samples of high density polyethylene compounded (HDUF), HDPE compound containing magnesium hydroxide coated with 6.2% magnesium stearate (HMMSC62), magnesium hydroxide (Mg(OH)₂), magnesium hydroxide coated with 6.2% magnesium stearate (MMSC62), and magnesium stearate (MgSt) were burned in the furnace at temperature of 850 °C for 3 hours. The percentage of ash in each sample were recorded as shown in Table below.

Code	Details	% Ash
HDUF	HDPE unfilled	0.00
HMMSC62	HDPE+40%[Mg(OH) ₂ +6.2% Mg Stearate]	24.49
MHUC	Uncoated magnesium hydroxide	68.73
MMSC62	[Mg(OH) ₂ +6.2% Mg Stearate] (coated)	65.07
MgSt	Magnesium stearate	9.10



$$\text{Percent ash content of the compound } (y_1) = m_1 x_1 + b \tag{3.4}$$

$$y_1 = 24.485 = \left(\frac{65.088 - 0.000}{0 - 100} \right) (x_1) + 65.088$$

$$x_1 = \frac{(-40.603)(-100)}{65.088} = 62.38$$

∴ %Polymer content = 62.38%

$$\begin{aligned} \text{Final filler content} &= 100 - \text{weight percent of the polymer in that compound } (x_1) \quad (3.5) \\ &= 100 - 62.38 = 37.62 \end{aligned}$$

$$\therefore \% \text{Filler content} = 37.62$$

$$\text{Percent ash content of the coated filler } (y_2) = m_2 x_2 + d \quad (3.6)$$

$$y_2 = 65.069 = \left(\frac{68.733 - 9.099}{0 - 100} \right) (x_2) + 68.733$$

$$x_2 = \frac{(-3.664)(-100)}{59.634} = 6.14$$

$$\therefore \% \text{Coating content (in the filler)} = 6.14\% \frac{W_{\text{coating}}}{W_{\text{filler}}}$$

Appendix D.8: The calculation of %atom of XPS.

XPS information of calcium carbonate coated with 4.2% magnesium stearate

Sample: $\text{CaCO}_3 + 4.2\% \text{MgSt}$

Comments 100 eV 20 mS

Conditions B1 Al 10kV 20mA

element	peak	B.E	area	rsf*	At. Wt.	area/rsf	%Atom
C	REF.	285					0
C	1s	285	2713	0.23	12.01	11795.6	$\frac{11795.6 \times 100}{27233.9} = 43.3$
Ca	2p	347.3	5667	1.27	40.08	4462.2	$\frac{4462.2 \times 100}{27233.9} = 16.4$
O	1s	531.5	7354	0.67	16.0	10976.1	$\frac{10976.1 \times 100}{27233.9} = 40.3$

$\Sigma = 27233.9$

* rsf = relative sensitivity factor

Appendix D.9: The calculation of specific energies of compounding machine to produce HDPE composites.

Specific energy = {Drive power x (Screw speed/Max. screw speed) x Max. torque}/output rate

Drive power APV = 7.5 kW

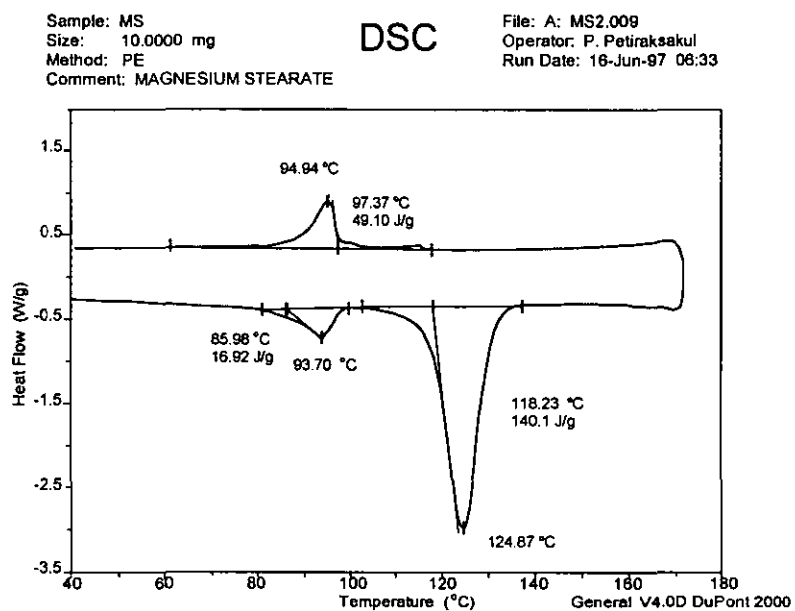
Max. screw speed = 500 rpm

Code	Screw speed (rpm)	Torque (%)	Out put rate (kg/hr)	Specific energy (kWhr/kg)
HDPE	350	70	15	$\frac{7.5 \times (350/500) \times (70/100)}{15} = 0.245$
HMUC	353	65	12	$\frac{7.5 \times (353/500) \times (65/100)}{12} = 0.282$
HMMSA62	350	60	15	$\frac{7.5 \times (350/500) \times (60/100)}{15} = 0.210$
HMMSC62	352	55	15	$\frac{7.5 \times (352/500) \times (55/100)}{15} = 0.194$
HMCSC64	351	55	15	$\frac{7.5 \times (351/500) \times (55/100)}{15} = 0.193$
HMZSC67	351	55	15	$\frac{7.5 \times (351/500) \times (55/100)}{15} = 0.193$
HMSAC60	351	60	15	$\frac{7.5 \times (351/500) \times (60/100)}{15} = 0.211$

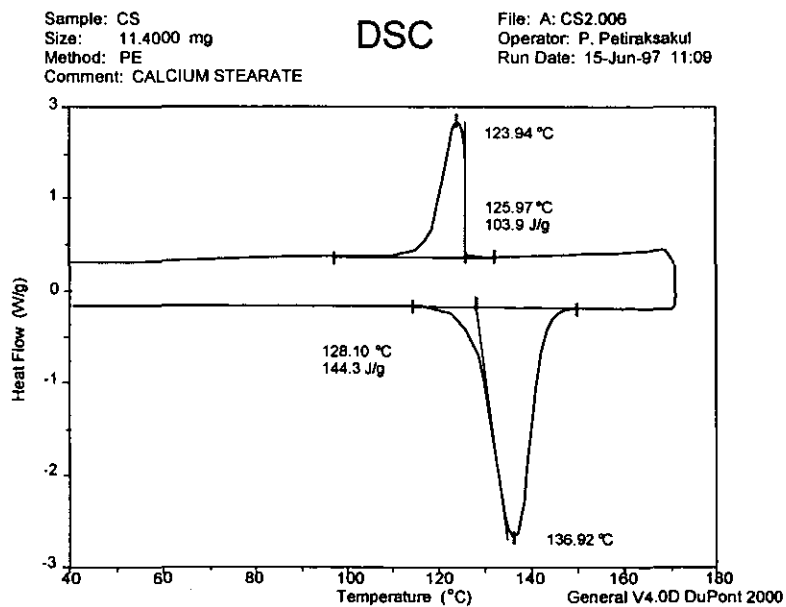
APPENDIX E: DSC TRACES

Appendix E.1: DSC traces of pure coating agents.

a: magnesium stearate



b: calcium stearate

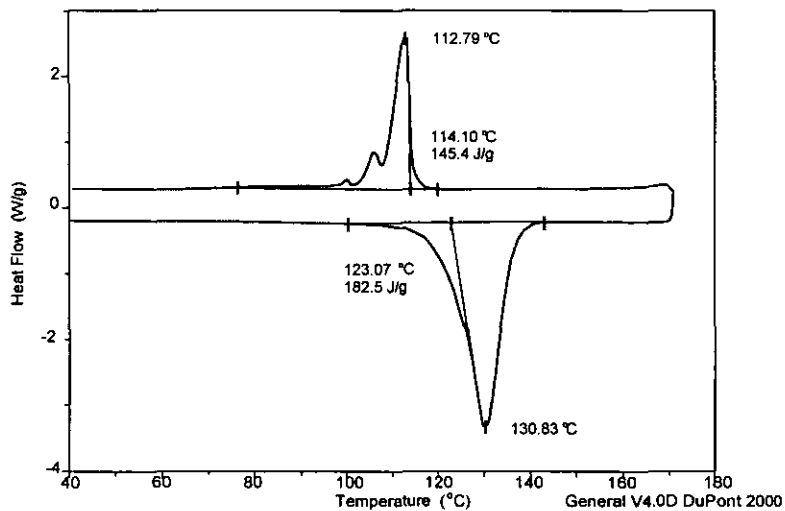


c: zinc stearate

Sample: ZS
Size: 13.6000 mg
Method: PE
Comment: ZINC STEARATE

DSC

File: A: ZS2.006
Operator: P. Petiraksakul
Run Date: 18-Jun-97 04:07

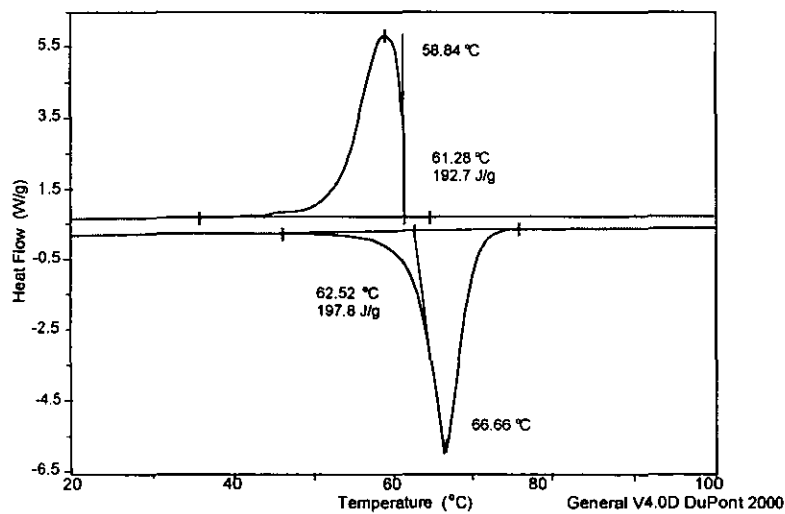


d: stearic acid

Sample: SA
Size: 4.5000 mg
Method: PE
Comment: STEARIC ACID

DSC

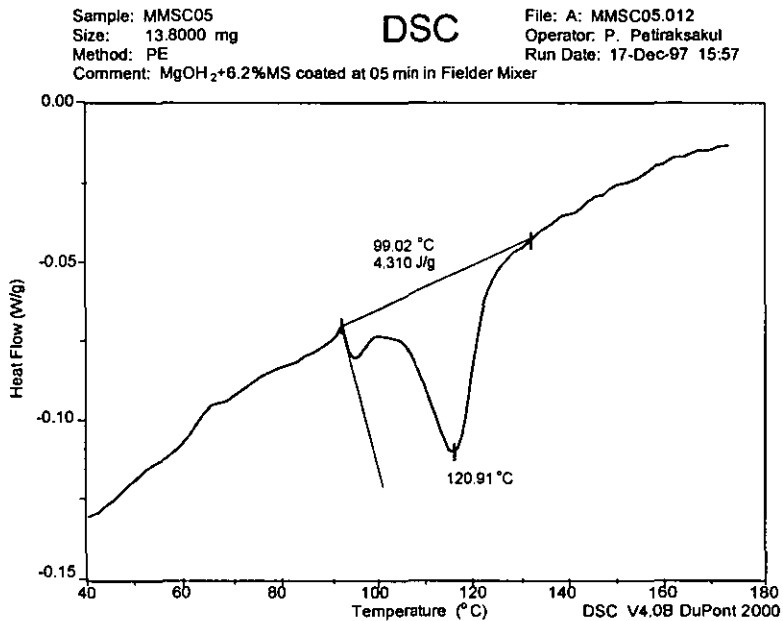
File: A: SA2.002
Operator: P. Petiraksakul
Run Date: 13-Jun-97 17:44



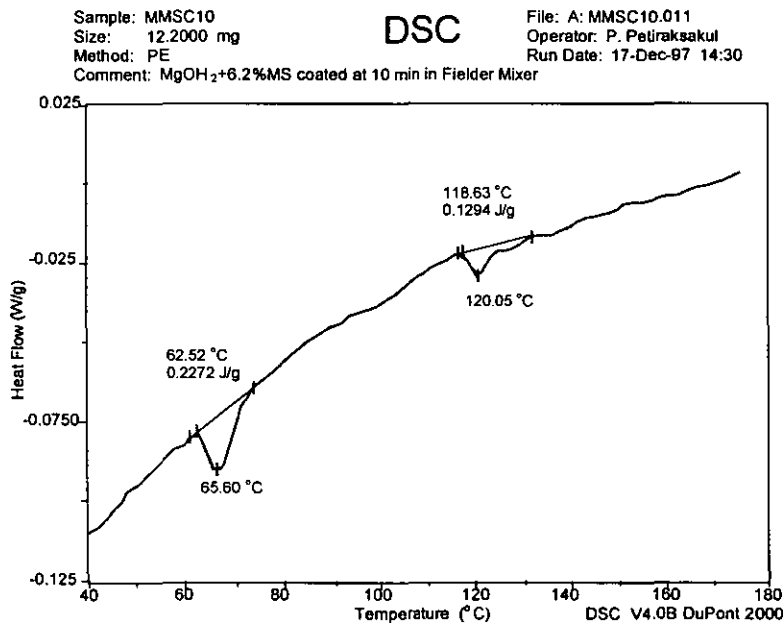
Appendix E.2: DSC traces of coated magnesium hydroxide.

a.: magnesium hydroxide coated with 6.2% magnesium stearate

- at 5 min of coating.



- at 10 min of coating.

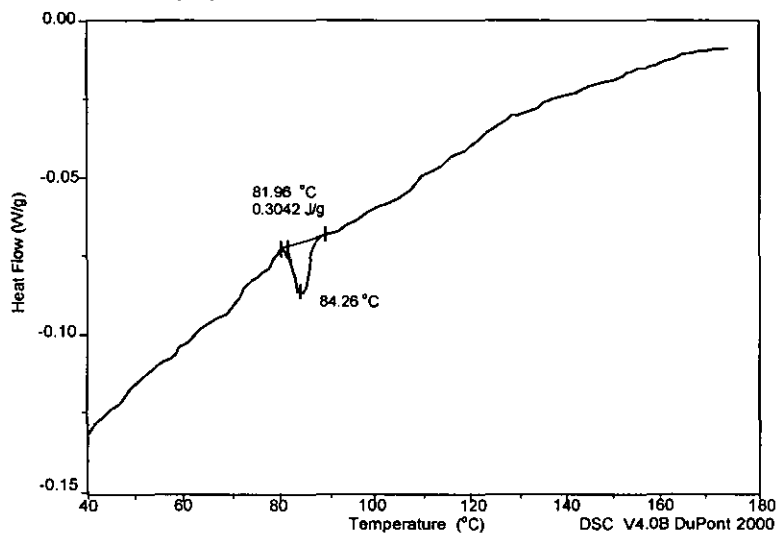


- at 20 min of coating.

Sample: MMSC20
Size: 13.4000 mg
Method: PE
Comment: MgOH₂+6.2%MS coated at 20 min in Fielder Mixer

DSC

File: A: MMSC20.011
Operator: P. Petiraksakul
Run Date: 17-Dec-97 14:53

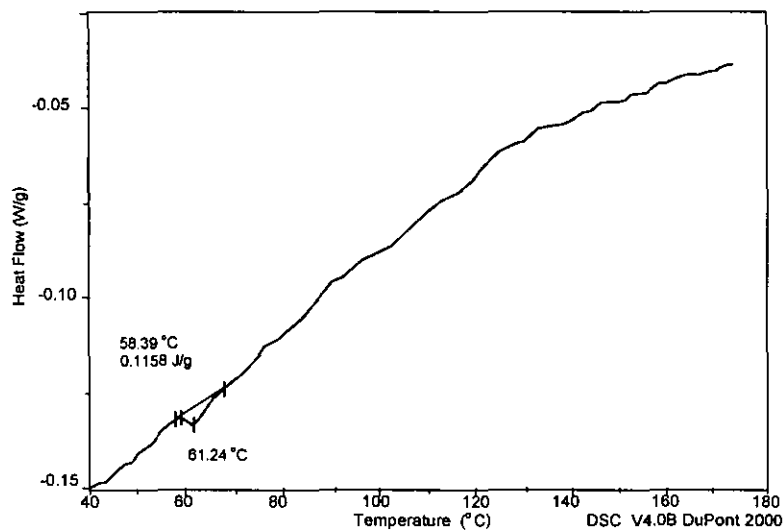


- at 30 min of coating.

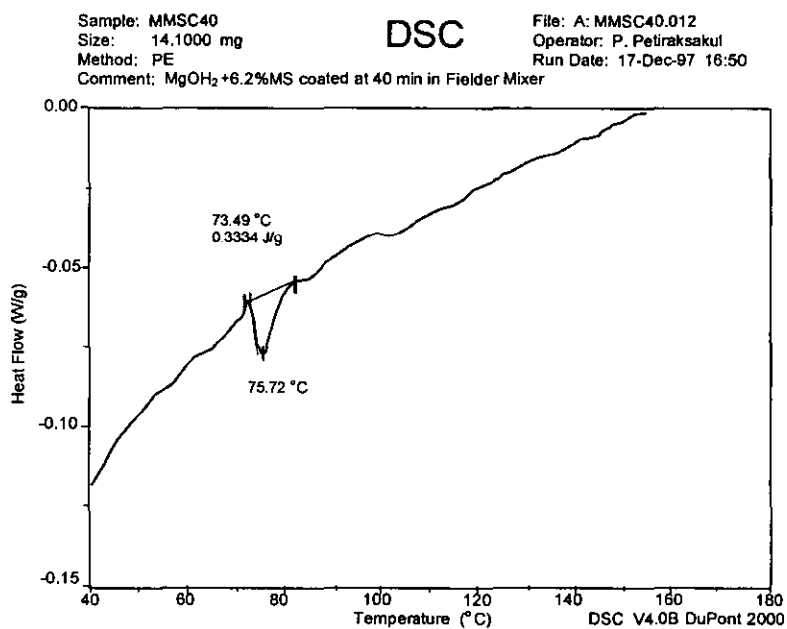
Sample: MMSC30
Size: 15.5000 mg
Method: PE
Comment: MgOH₂+6.2%MS coated at 30 min in Fielder Mixer

DSC

File: A: MMSC30.011
Operator: P. Petiraksakul
Run Date: 17-Dec-97 15:15

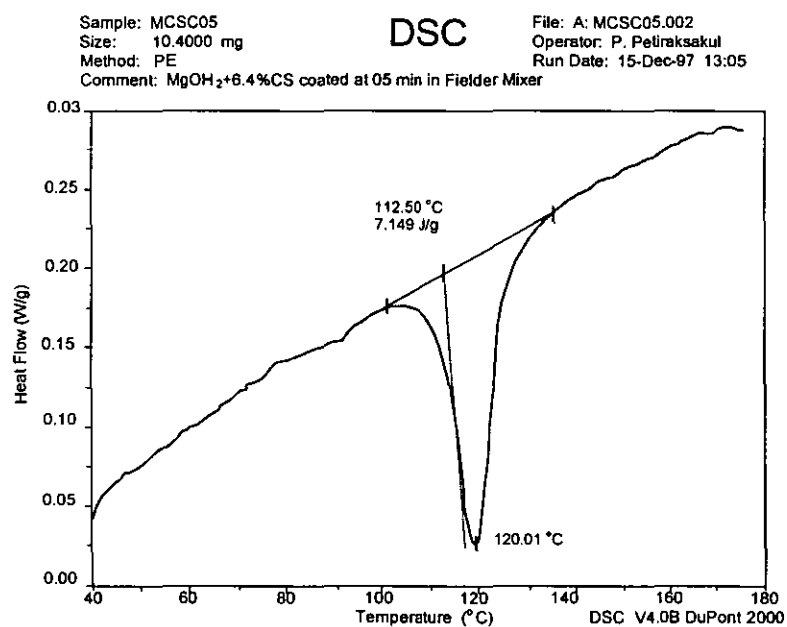


- at 40 min of coating.



b.: magnesium hydroxide coated with 6.4%calcium stearate

- at 5 min of coating.

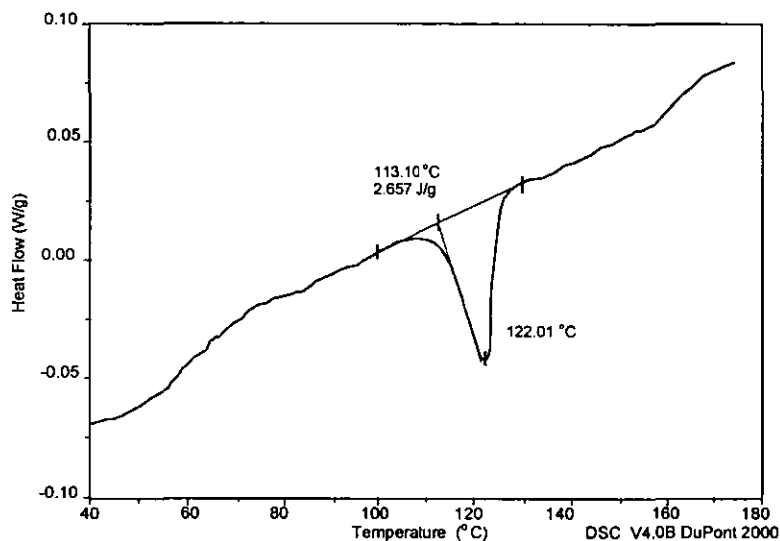


- at 40 min of coating

Sample: MCSC40
Size: 10.2000 mg
Method: PE
Comment: MgOH₂+6.4%CS coated at 40 min in Fielder Mixer

DSC

File: A: MCSC40.002
Operator: P. Petiraksakul
Run Date: 17-Dec-97 17:25



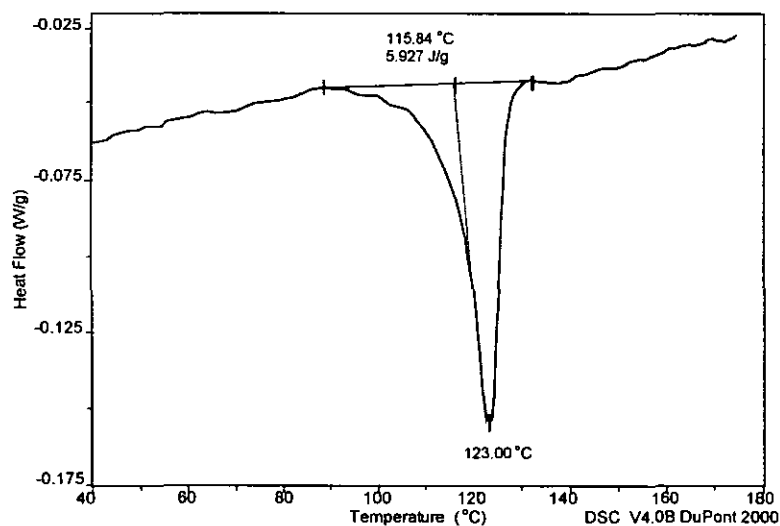
c.: magnesium hydroxide coated with 6.7% zinc stearate

- at 5 min of coating.

Sample: MZSC05
Size: 14.5000 mg
Method: PE
Comment: MgOH₂+6.7%ZS coated at 05 min in Fielder Mixer

DSC

File: A: MZSC05.011
Operator: P. Petiraksakul
Run Date: 17-Dec-97 13:27

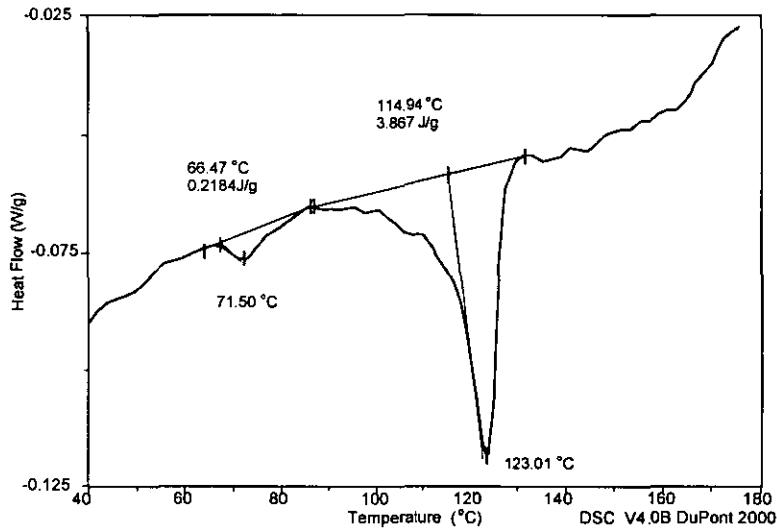


-at 10 min of coating.

Sample: MZSC10
 Size: 15.1000 mg
 Method: PE
 Comment: MgOH₂+6.7%ZS coated at 10 min in Fielder Mixer

DSC

File: A: MZSC10.011
 Operator: P. Petiraksakul
 Run Date: 17-Dec-97 12.55

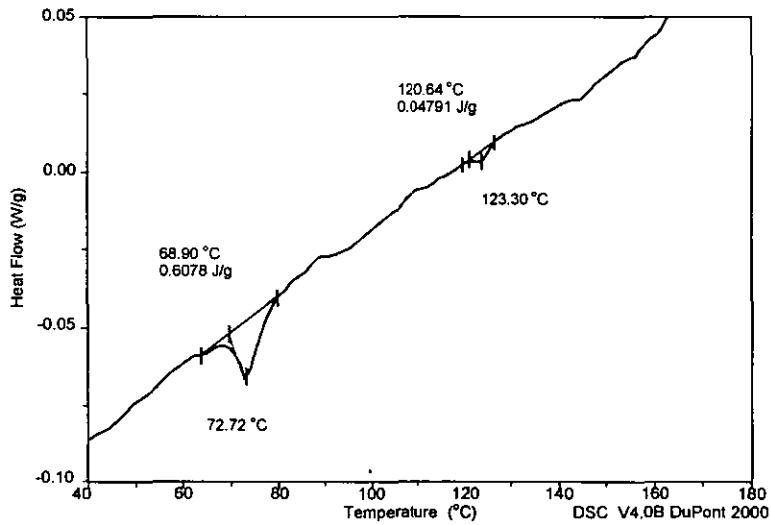


- at 20 min of coating.

Sample: MZSC20
 Size: 12.4000 mg
 Method: PE
 Comment: MgOH₂+6.7%ZS coated at 20 min in Fielder Mixer

DSC

File: A: MZSC20.012
 Operator: P. Petiraksakul
 Run Date: 17-Dec-97 12.29

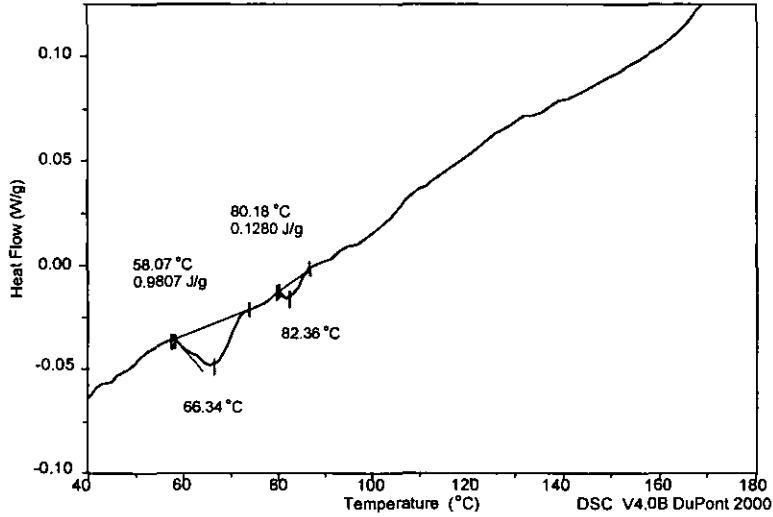


- at 30 min of coating.

Sample: MZSC30
 Size: 11.1000 mg
 Method: PE
 Comment: MgOH₂+6.7%ZS coated at 30 min in Fielder Mixer

DSC

File: A: MZSC30.011
 Operator: P. Petiraksakul
 Run Date: 15-Dec-97 12:43

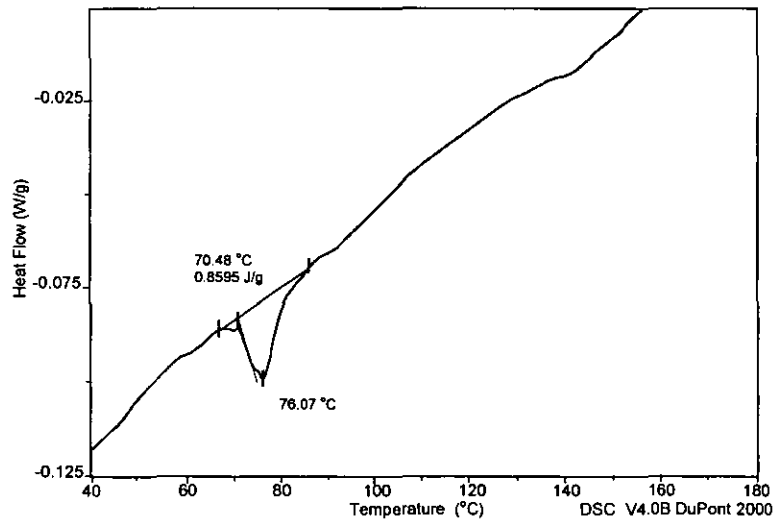


- at 40 min of coating.

Sample: MZSC40
 Size: 13.5000 mg
 Method: PE
 Comment: MgOH₂+6.7%ZS coated at 40 min in Fielder Mixer

DSC

File: A: MZSC40.011
 Operator: P. Petiraksakul
 Run Date: 17-Dec-97 12:03



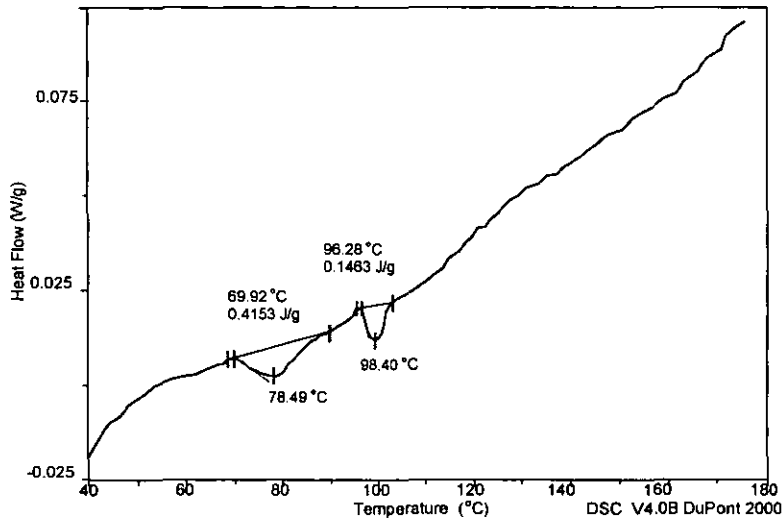
d.: magnesium hydroxide coated with 6.0% stearic acid

- at 5 min of coating.

Sample: MSAC05
Size: 8.4000 mg
Method: PE
Comment: MgOH₂+6.0%SA coated at 05 min in Fielder Mixer

DSC

File: A: MSAC05.002
Operator: P. Petiraksakul
Run Date: 15-Dec-97 10:45

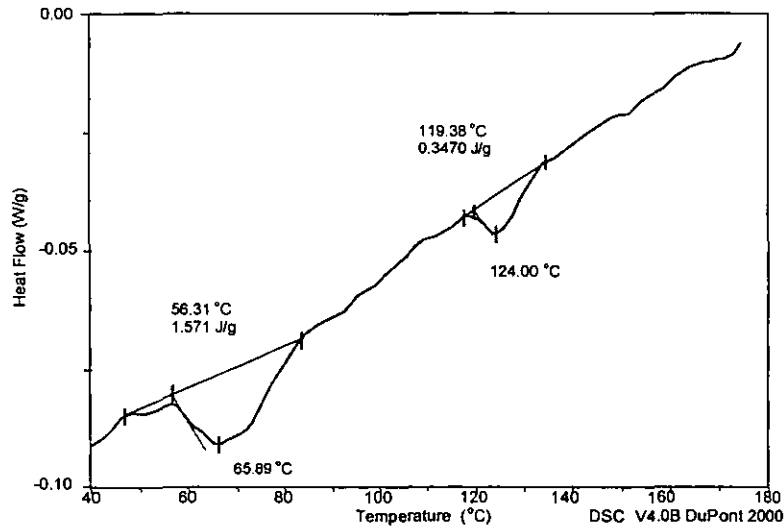


- at 10 min of coating.

Sample: MSAC10
Size: 10.6000 mg
Method: PE
Comment: MgOH₂+6.0%SA coated at 10 min in Fielder Mixer

DSC

File: A: MSAC10.001
Operator: P. Petiraksakul
Run Date: 15-Dec-97 09:20

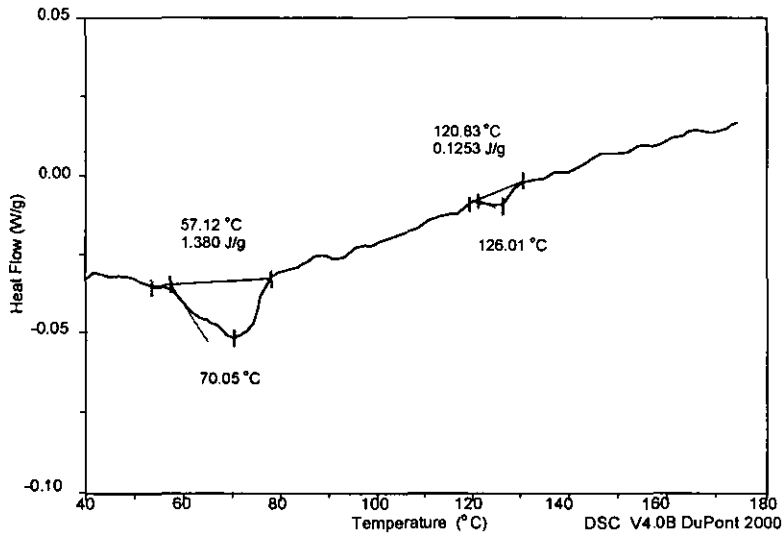


- at 20 min of coating.

Sample: MSAC20
Size: 10.0000 mg
Method: PE
Comment: MgOH₂+6.0%SA coated at 20 min in Fielder Mixer

DSC

File: A: MSAC20.001
Operator: P. Petiraksakul
Run Date: 15-Dec-97 08:54

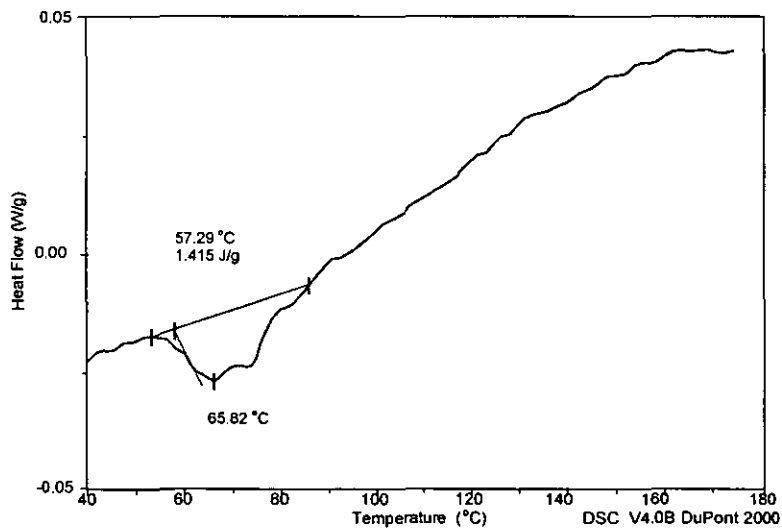


- at 30 min of coating.

Sample: MSAC30
Size: 10.5000 mg
Method: PE
Comment: MgOH₂+6.0%SA coated at 30 min in Fielder Mixer

DSC

File: A: MSAC30.001
Operator: P. Petiraksakul
Run Date: 15-Dec-97 08:23

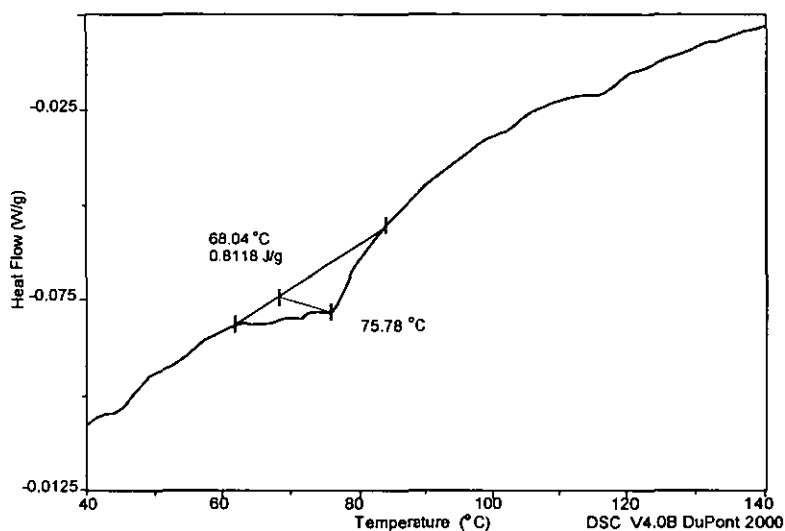


- at 40 min of coating.

Sample: MSAC40
Size: 12.0000 mg
Method: PE
Comment: MgOH₂+6.0%SA coated at 40 min in Fielder Mixer

DSC

File: A: MSAC40.011
Operator: P. Petiraksakul
Run Date: 17-Dec-97 11:18



Appendix E.3: DSC traces of coated calcium carbonate.

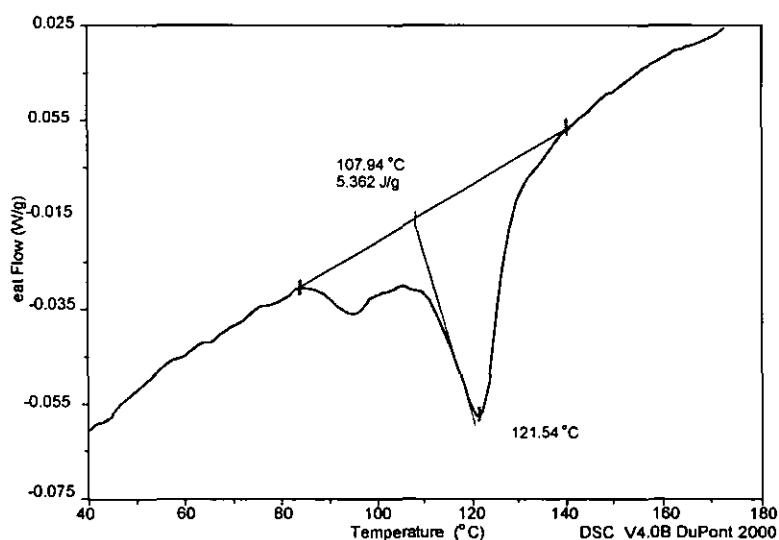
a.: calcium carbonate coated with 4.2% magnesium stearate

- at 5 min of coating.

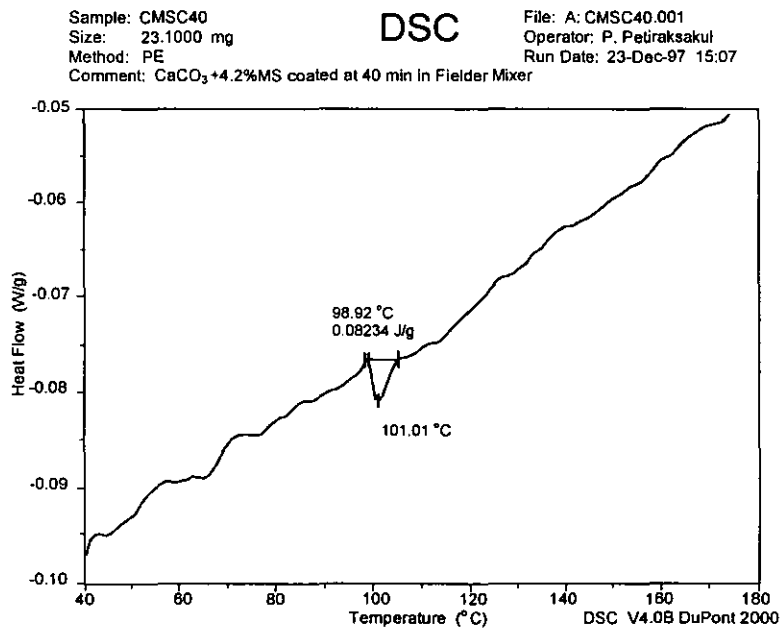
Sample: CMSC05
Size: 15.8000 mg
Method: PE
Comment: CaCO₃+4.2%MS coated at 05 min in Fielder Mixer

DSC

File: A: CMSC05.001
Operator: P. Petiraksakul
Run Date: 23-Dec-97 13:40

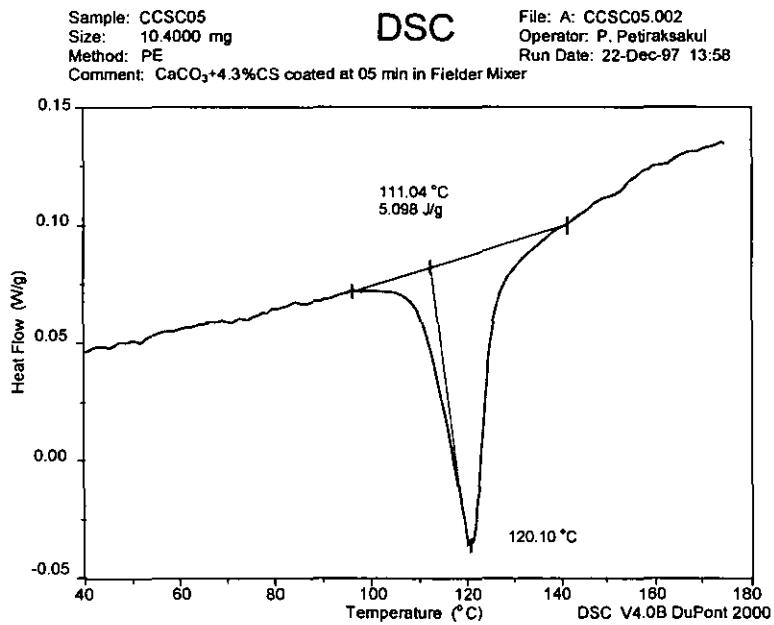


- at 40 min of coating.



b.: calcium carbonate coated with 4.3%calcium stearate

- at 5 min of coating.

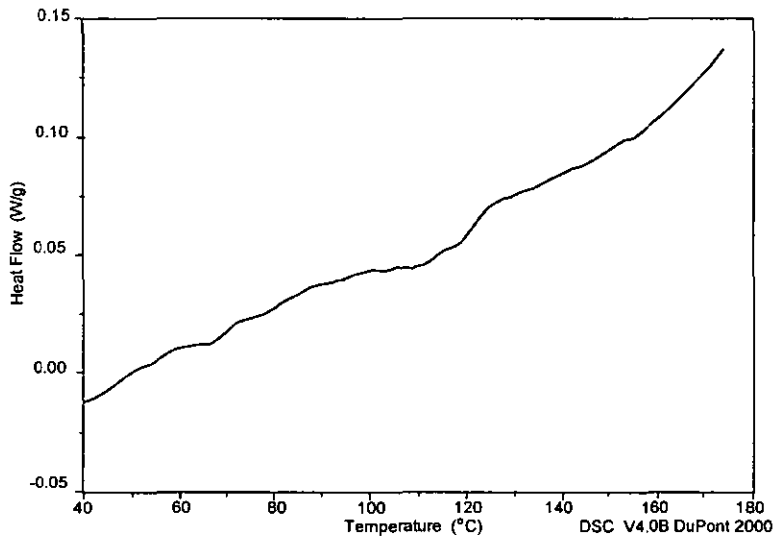


- at 40 min of coating

Sample: CCSC40
Size: 16.2000 mg
Method: PE
Comment: CaCO₃+4.3%CS coated at 40 min in Fielder Mixer

DSC

File: A: CCSC40.002
Operator: P. Petiraksakul
Run Date: 22-Dec-97 12:54



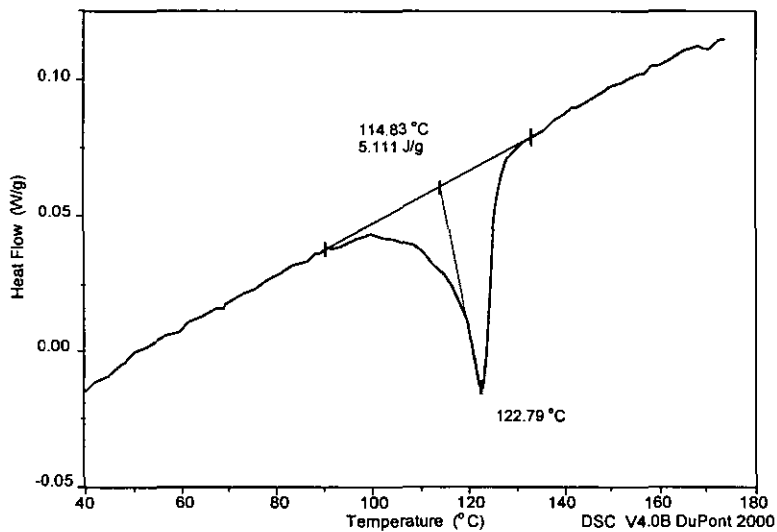
c.: calcium carbonate coated with 4.5% zinc stearate

- at 5 min of coating.

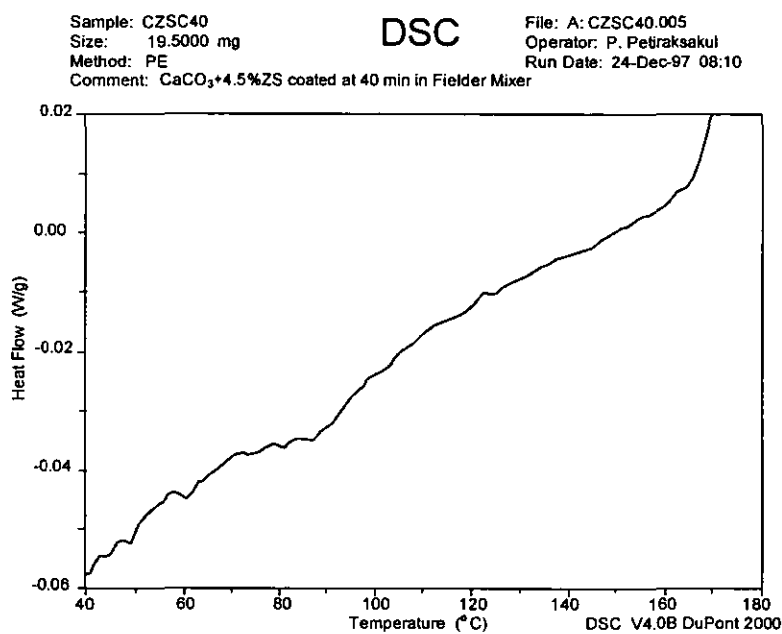
Sample: CZSC05
Size: 15.1000 mg
Method: PE
Comment: CaCO₃+4.5%ZS coated at 05 min in Fielder Mixer

DSC

File: A: CZSC05.001
Operator: P. Petiraksakul
Run Date: 22-Dec-97 14:20

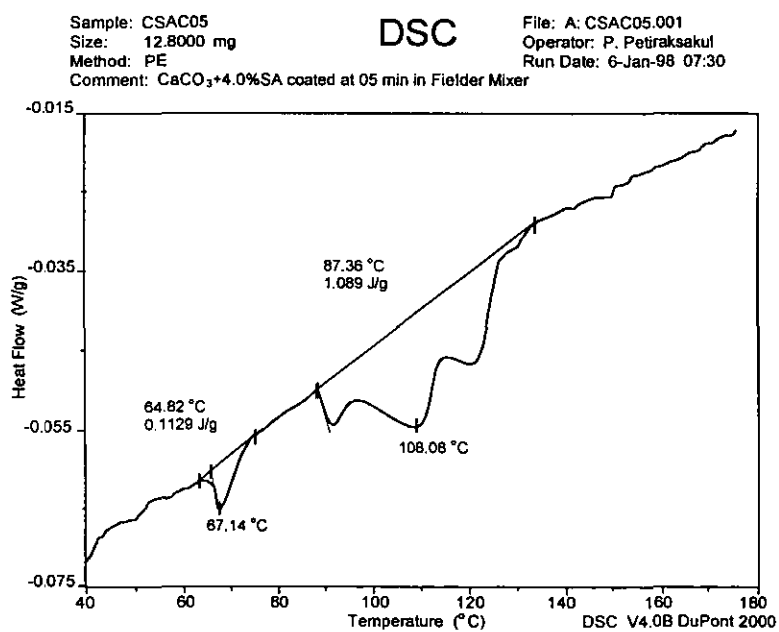


- at 40 min of coating.



d.: calcium carbonate coated with 4.0% stearic acid

- at 5 min of coating.

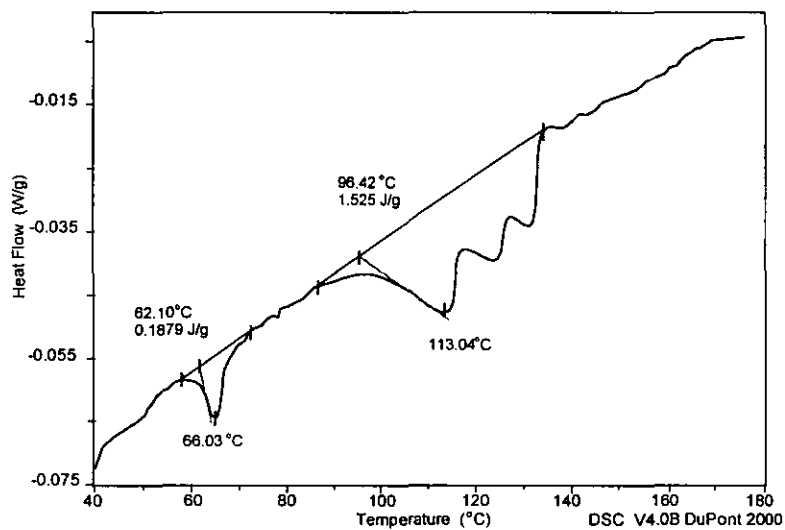


- at 40 min of coating.

Sample: CSAC40
Size: 13.6000 mg
Method: PE
Comment: CaCO₃+4.0%SA coated at 40 min in Fielder Mixer

DSC

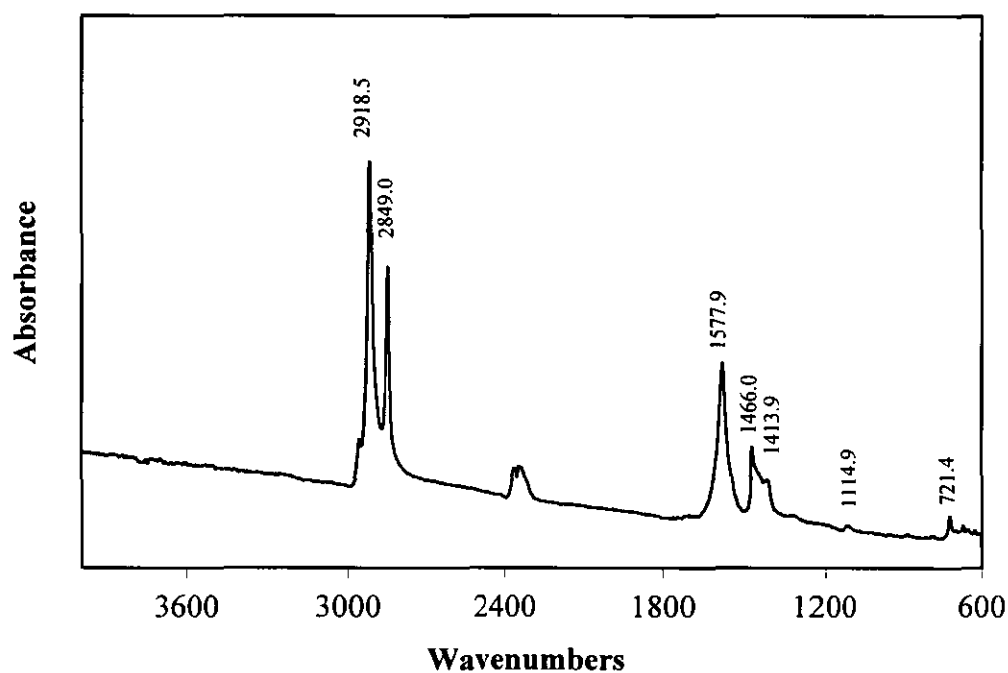
File: A: CSAC40.002
Operator: P. Petiraksakul
Run Date: 23-Dec-97 13:52



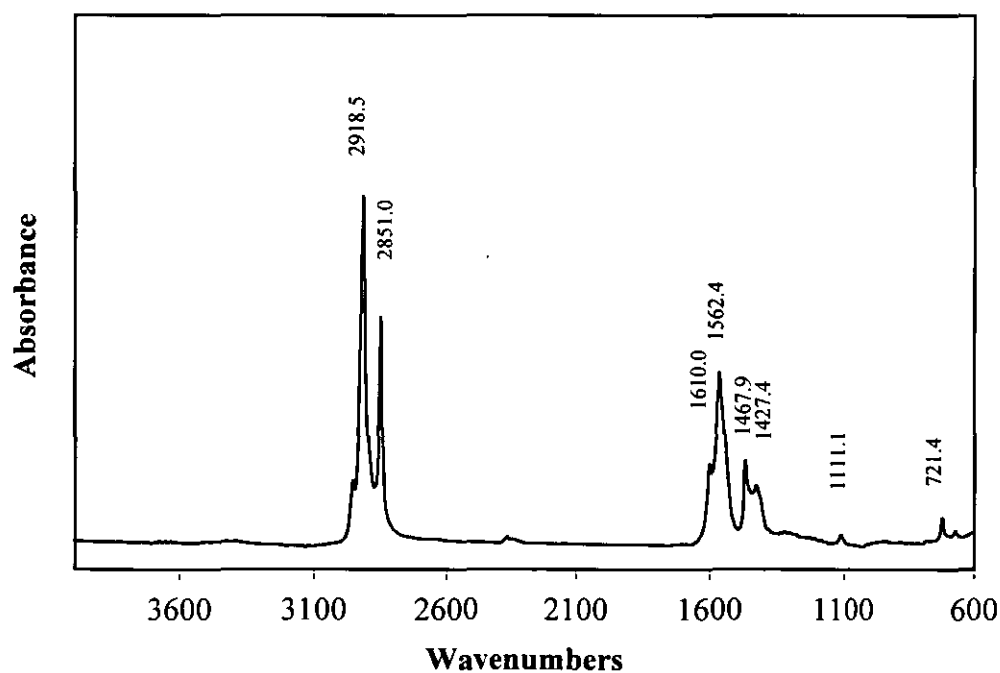
APPENDIX F: FTIR AND XPS SPECTRA

Appendix F.1: Transmission FTIR spectra of coating agents.

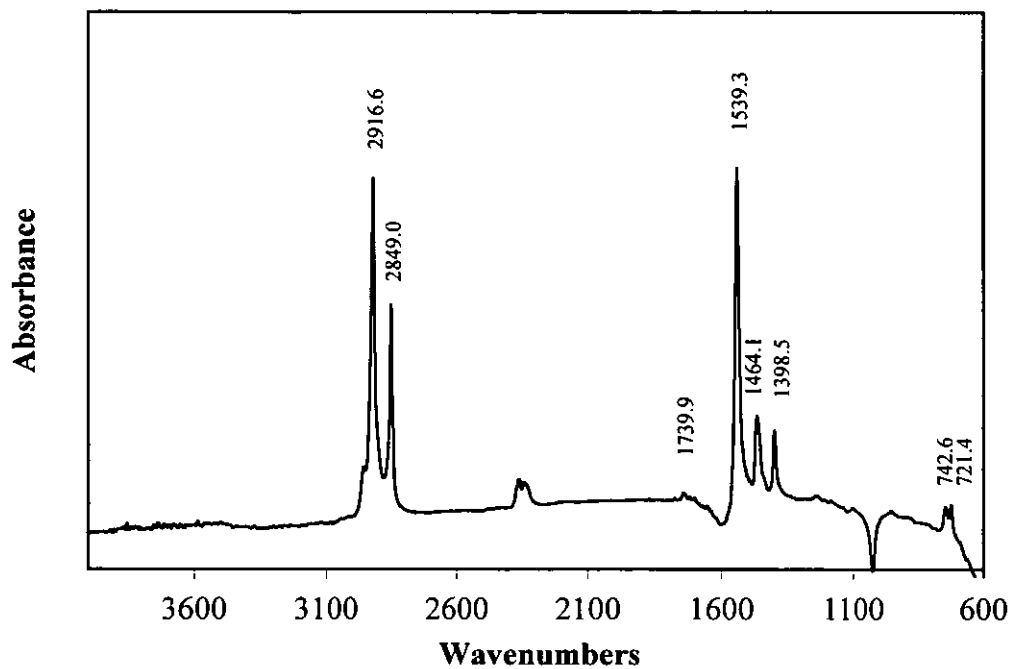
a.: Magnesium stearate.



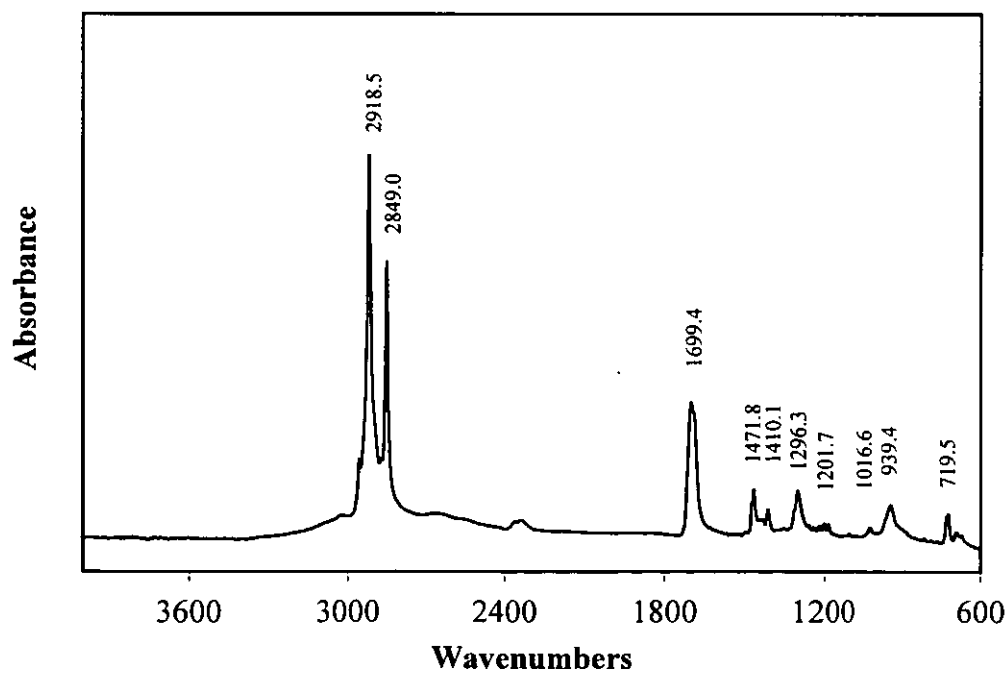
b.: Calcium stearate.



c.: Zinc stearate.

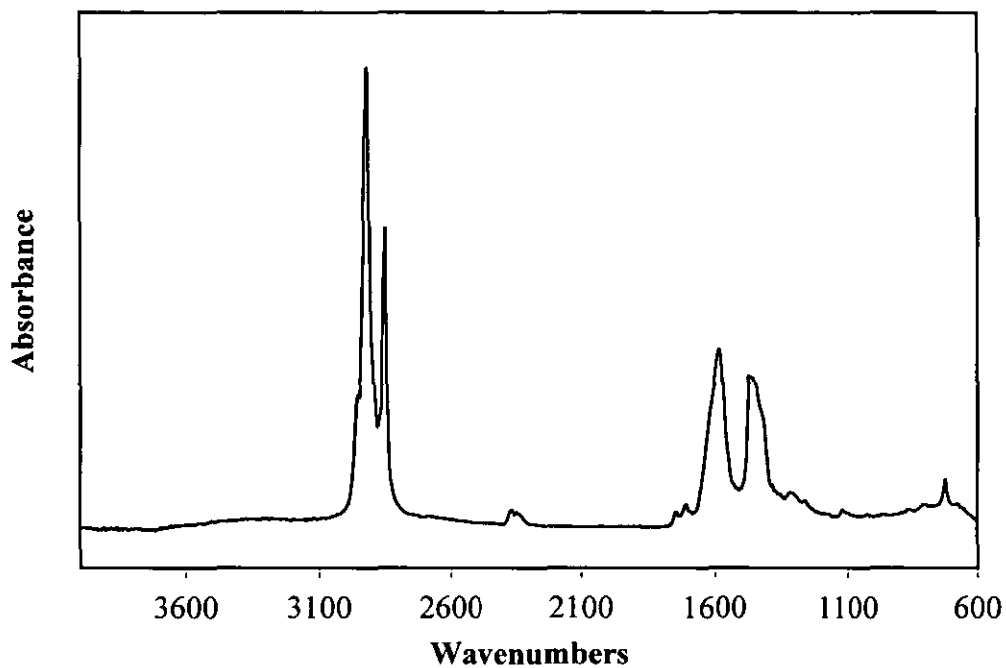


d.: Stearic acid.

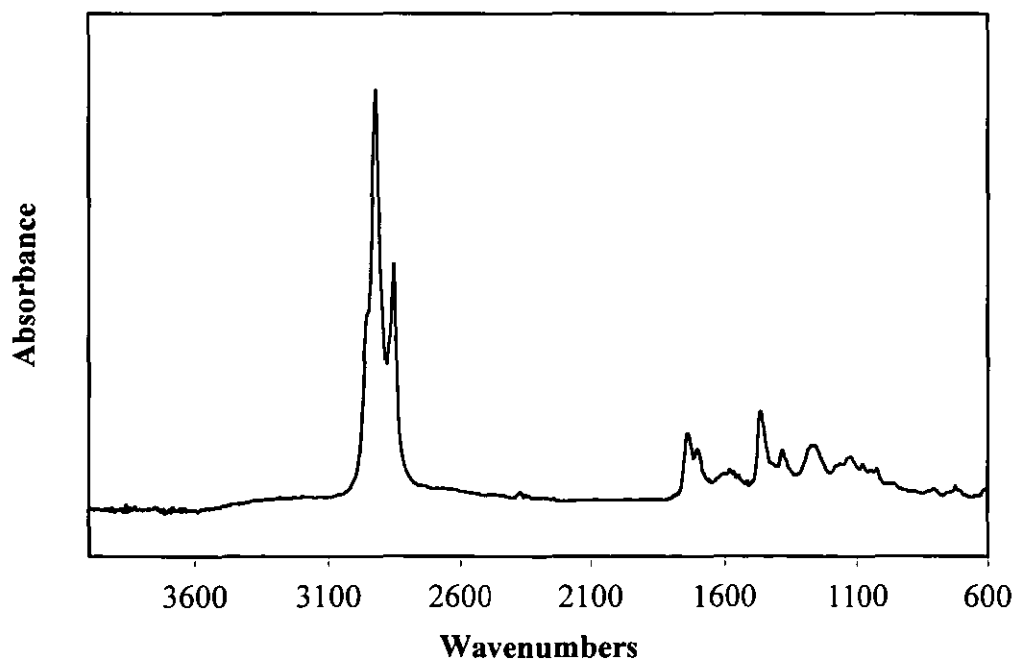


Appendix F.2: Transmission FTIR Spectra of extracted samples from coated magnesium hydroxide.

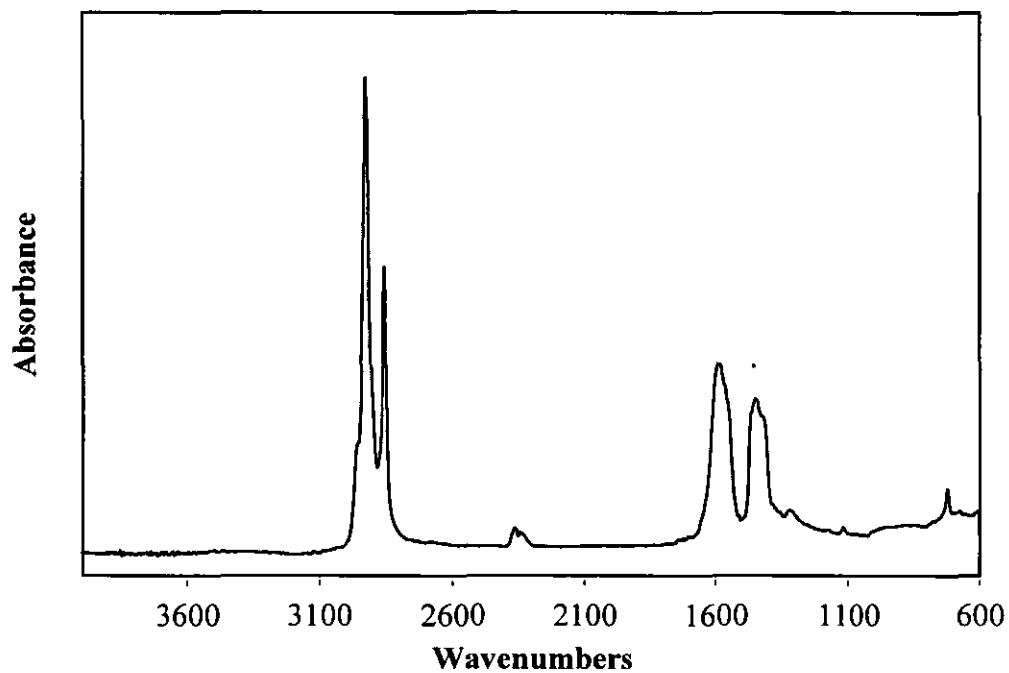
a.: 6.2% magnesium stearate coated on magnesium hydroxide.



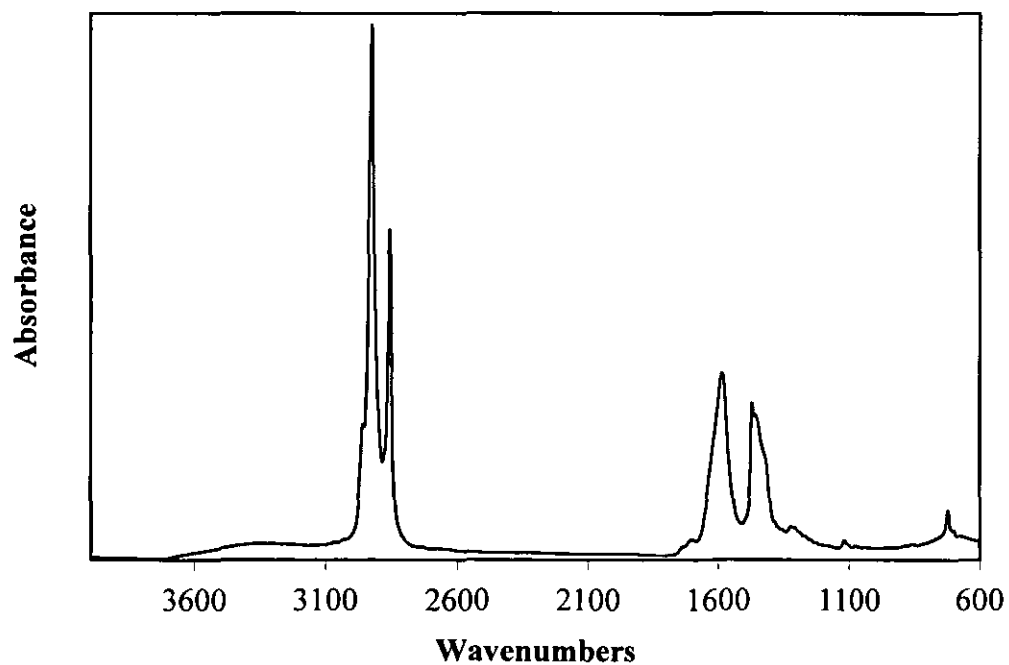
b.: 6.4% calcium stearate coated on magnesium hydroxide.



c.: 6.7% zinc stearate coated on magnesium hydroxide.

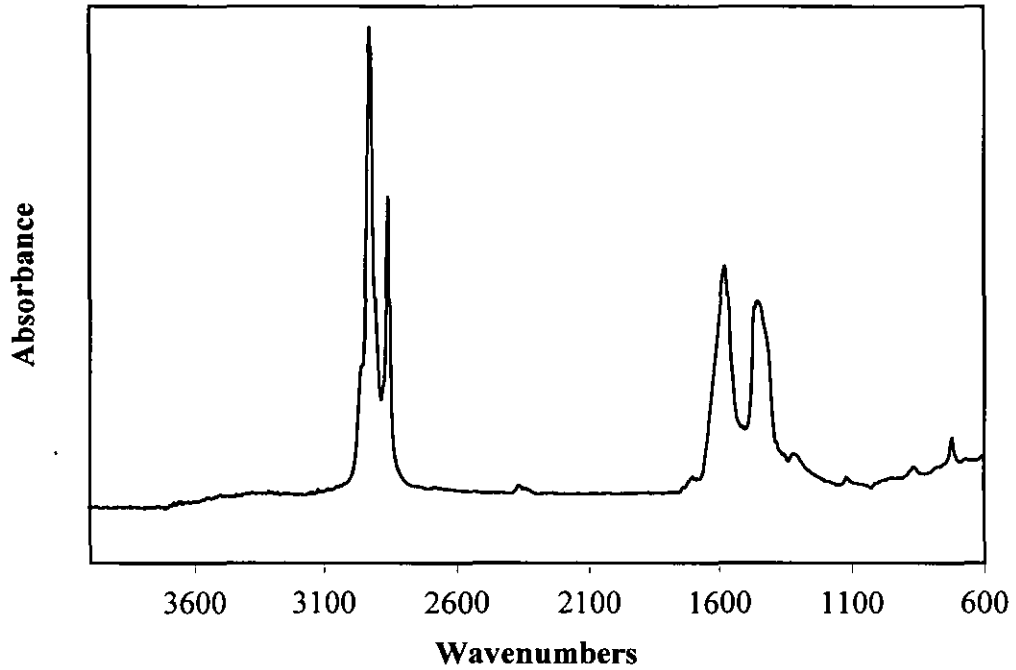


d.: 6.0% stearic acid coated on magnesium hydroxide.

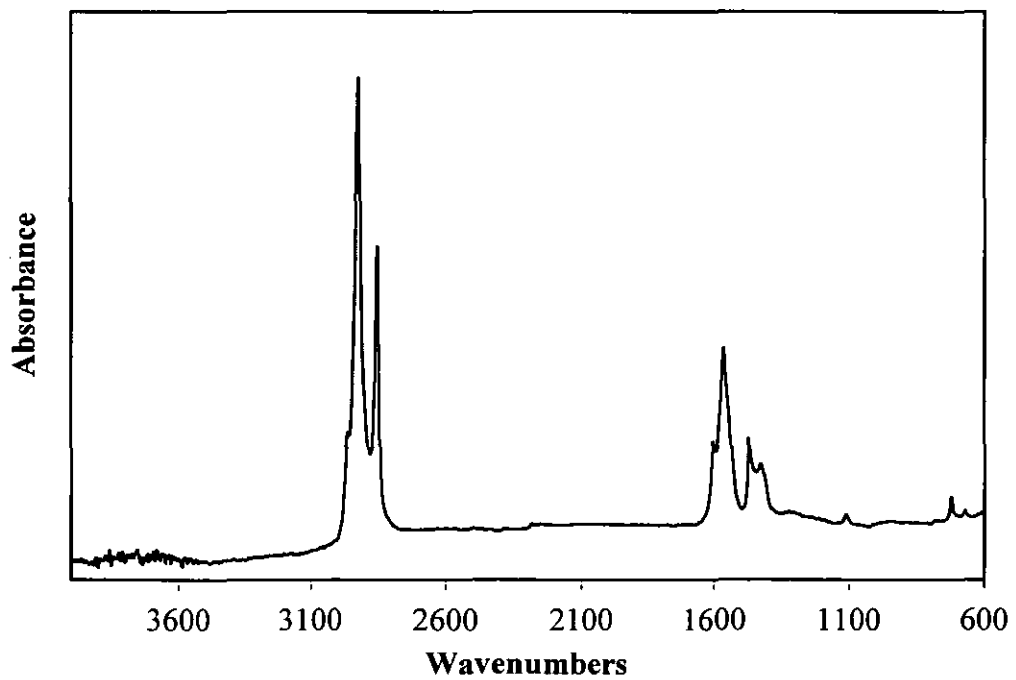


Appendix F.3: Transmission FTIR spectra of extracted samples from coated calcium carbonate.

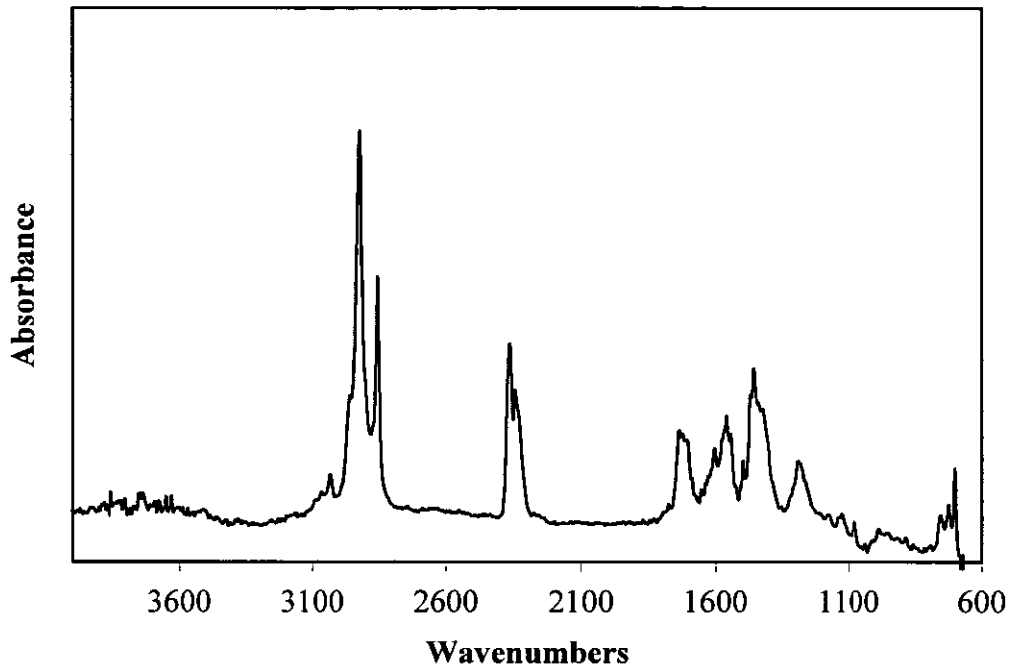
a.: 4.2% magnesium stearate coated on calcium carbonate.



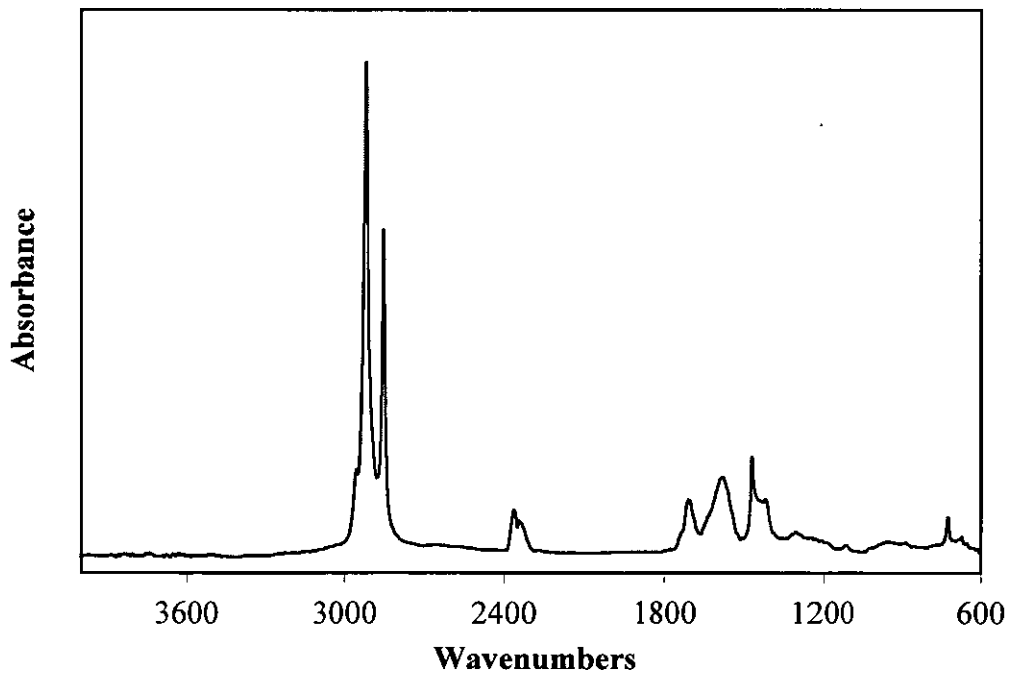
b.: 4.3% calcium stearate coated on calcium carbonate.



c.: 4.5% zinc stearate coated on calcium carbonate.

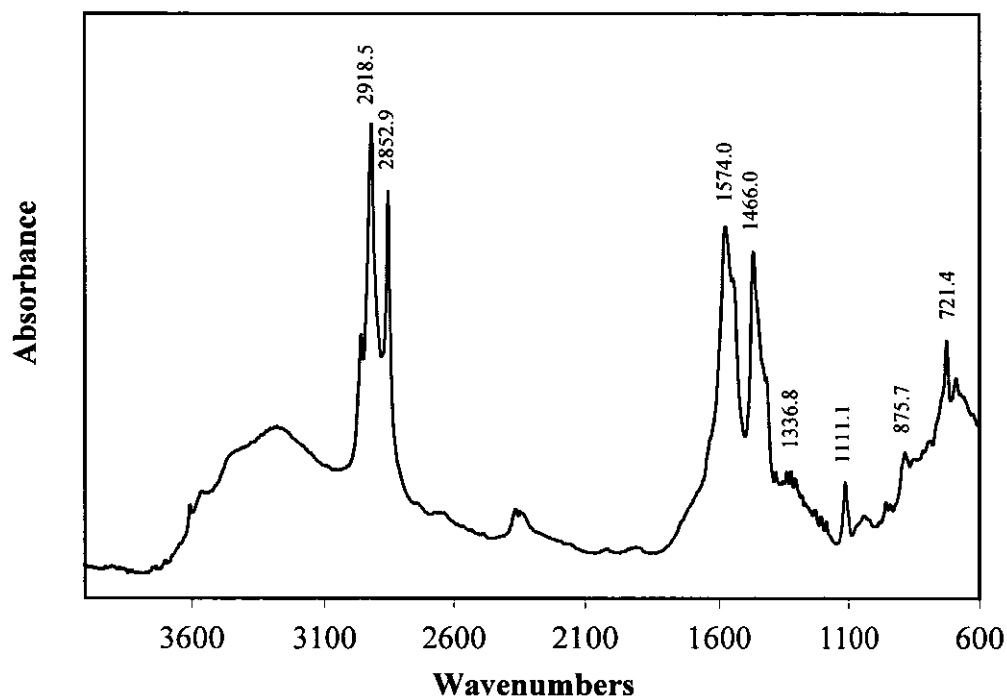


d.: 4.0% stearic acid coated on calcium carbonate.

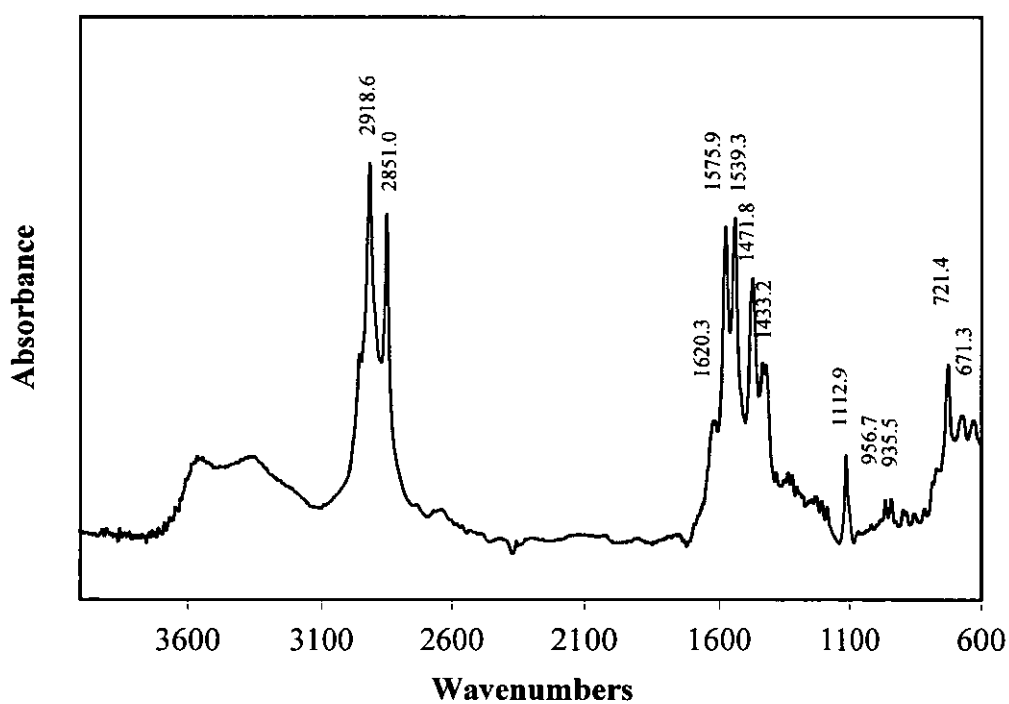


Appendix F.4: DRIFT spectra of coating agents.

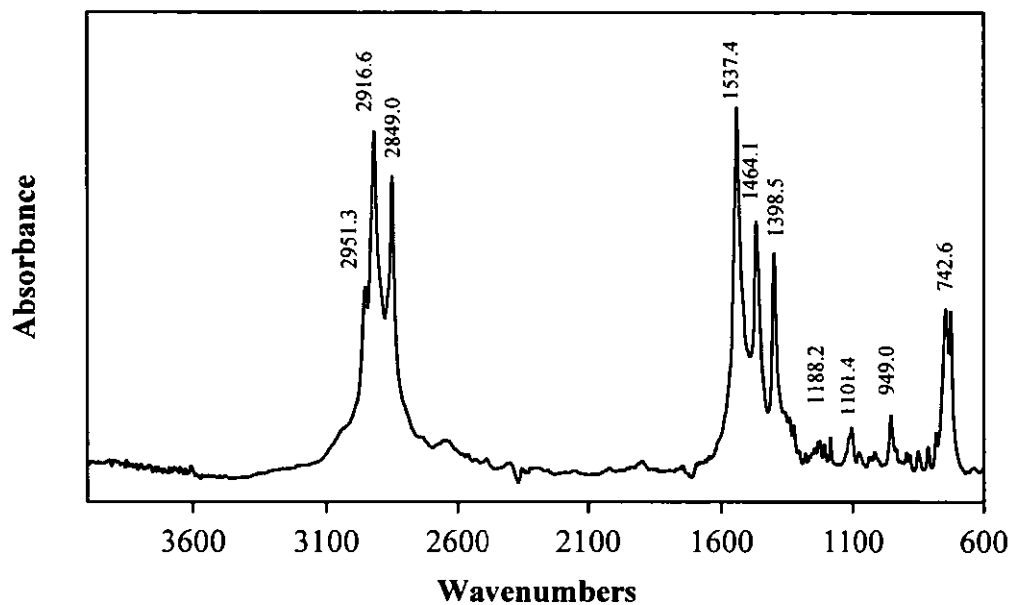
a: Magnesium stearate.



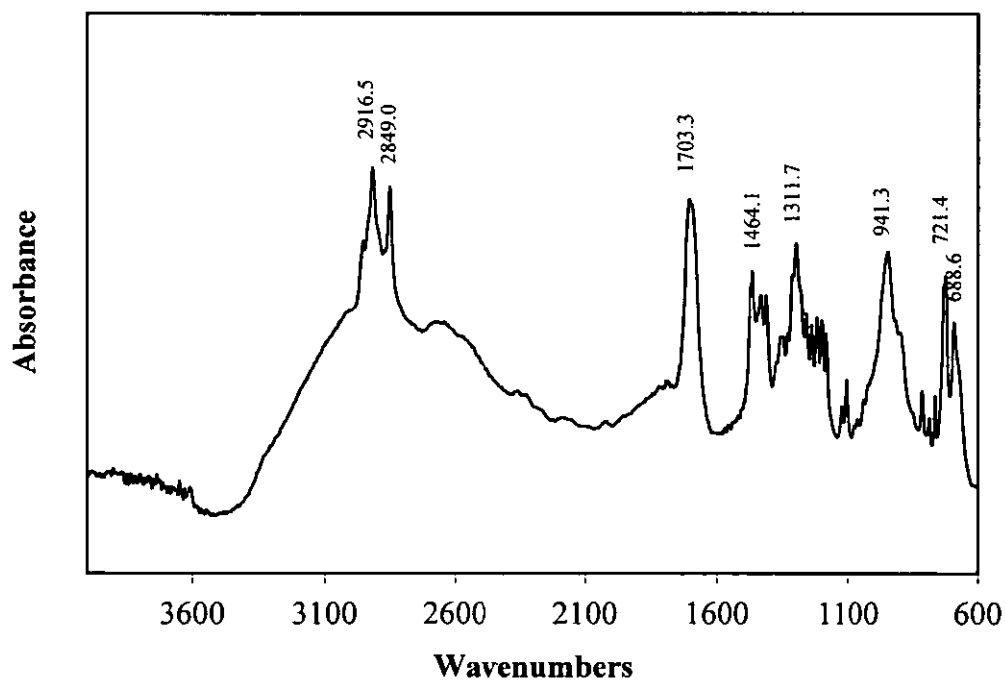
b: Calcium stearate.



c: Zinc stearate.

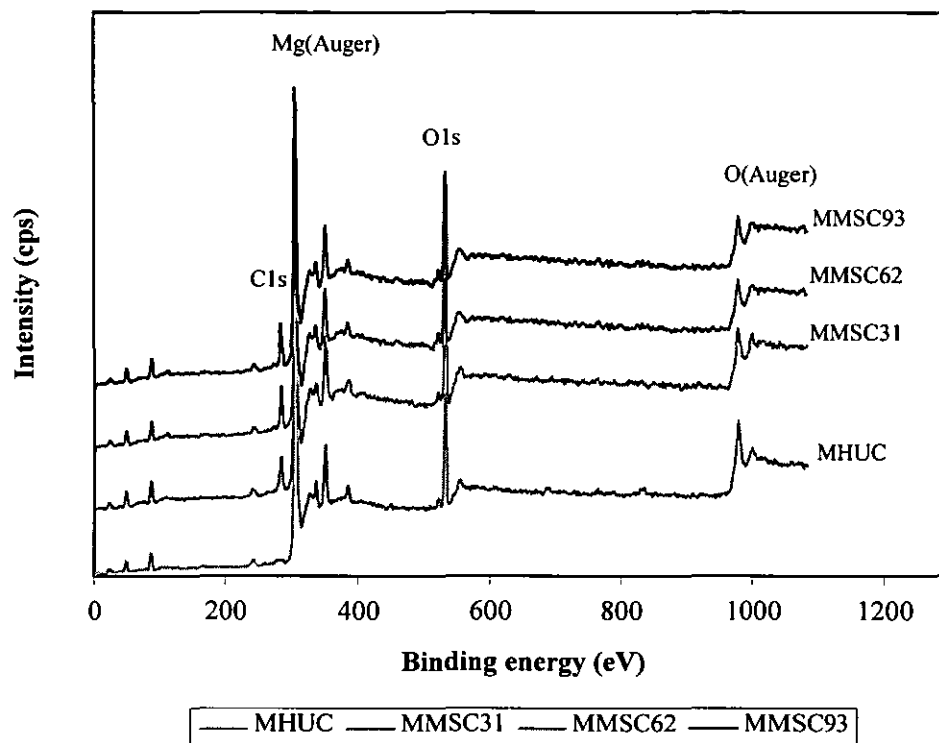


d.: Stearic acid.

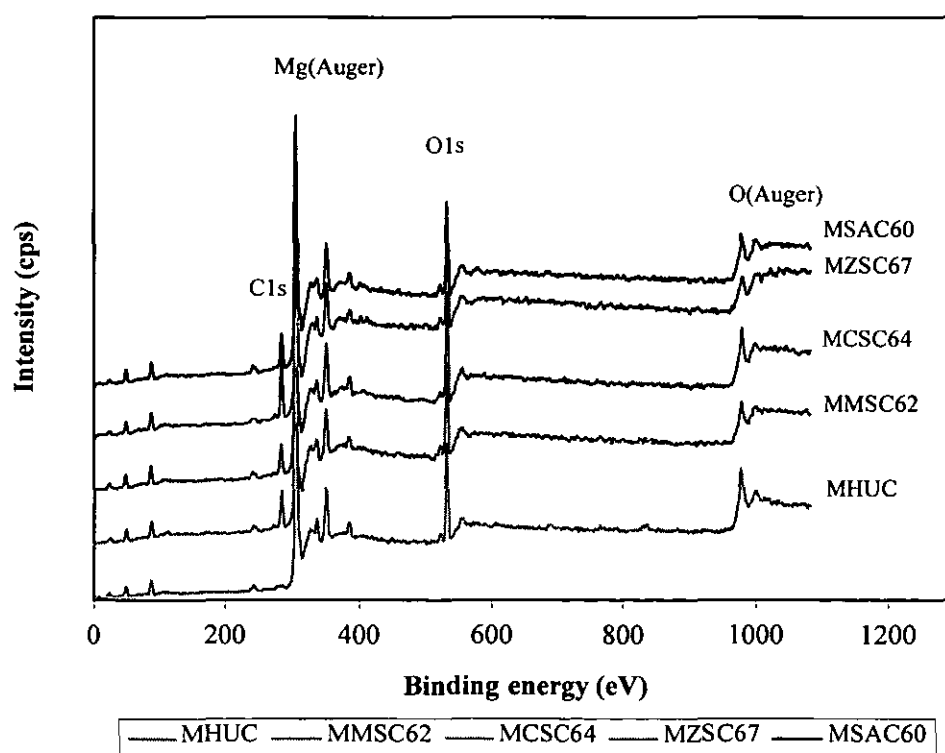


Appendix F.5: XPS spectra of uncoated/coated filler samples.

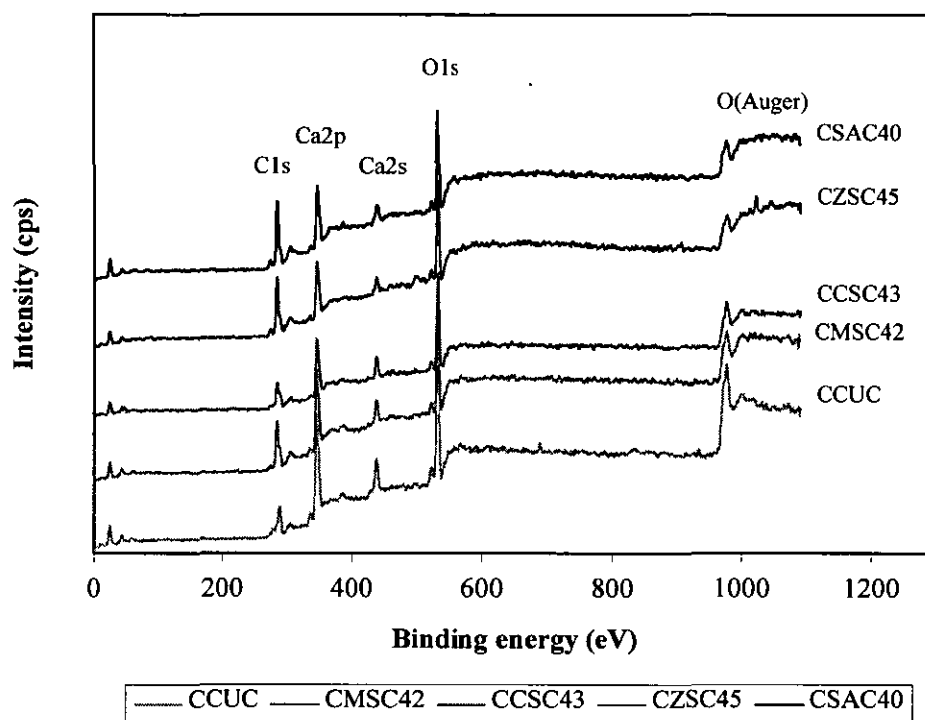
a.: Uncoated/coated magnesium hydroxide with various magnesium stearate concentrations.



b.: Uncoated/coated magnesium hydroxide with various coating agent types.



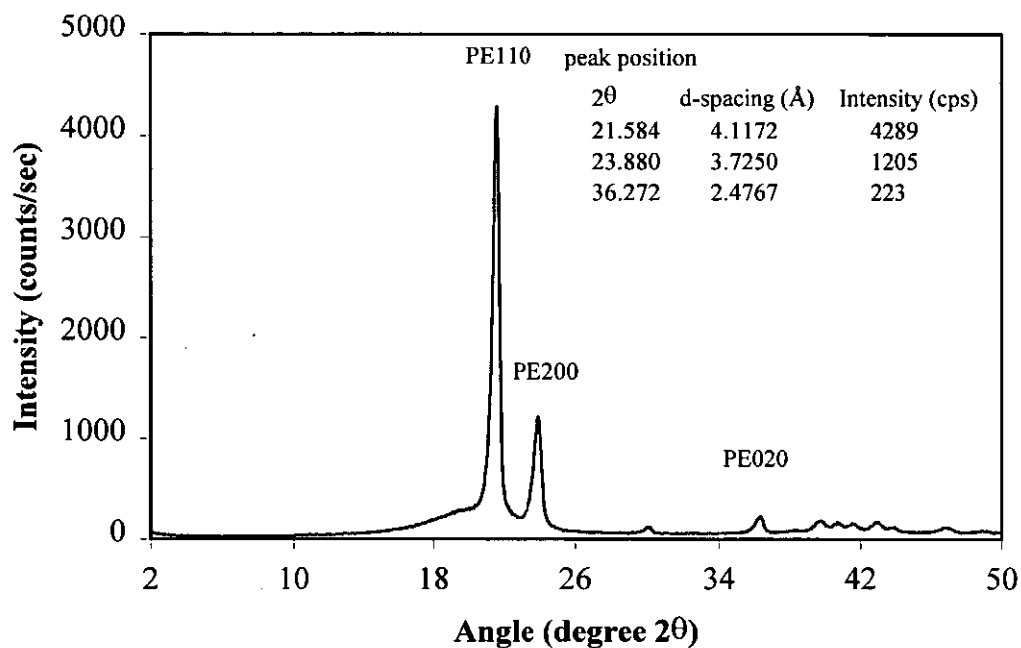
c.: Uncoated/coated calcium carbonate with various coating agent types.



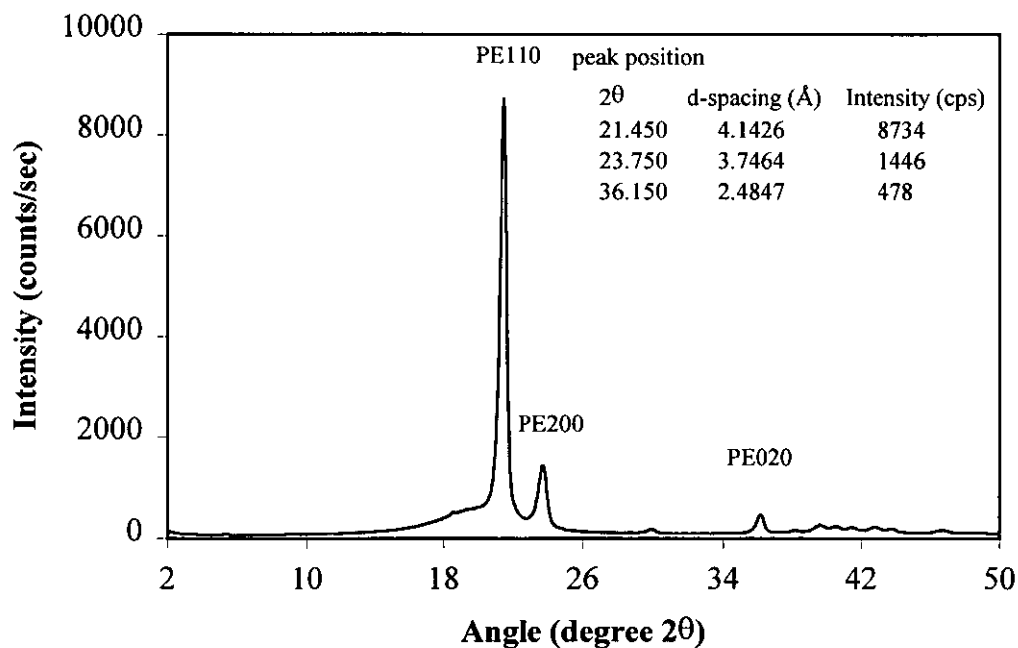
APPENDIX G: X-RAY DIFFRACTION PATTERNS

Appendix G.1: X-ray patterns of unfilled and Mg(OH)₂ filled HDPE composites.

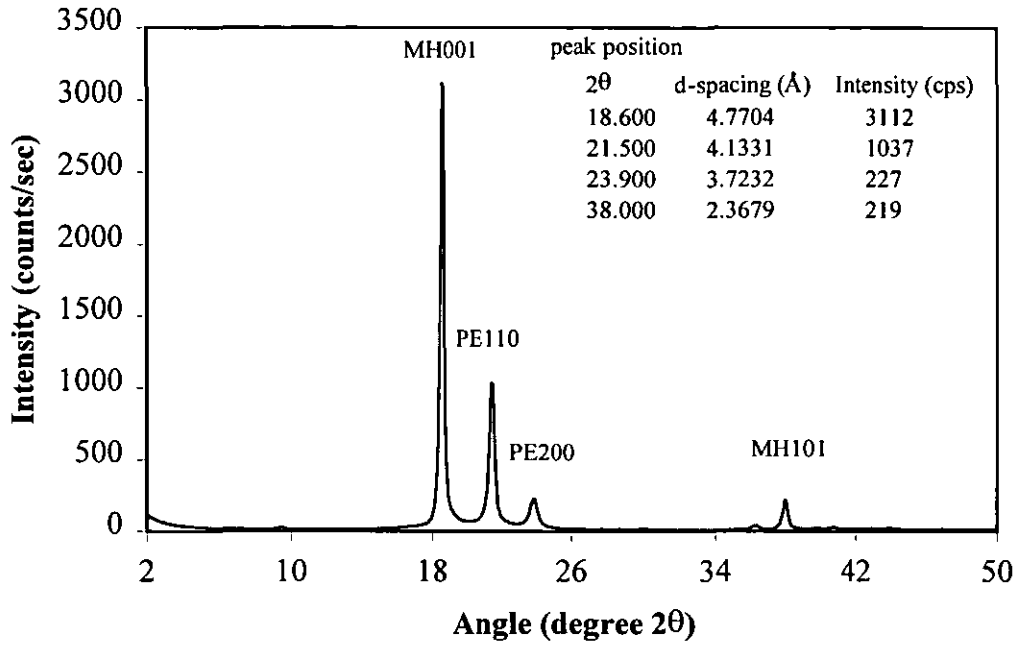
a.: HDPE isotropic structure (random orientation).



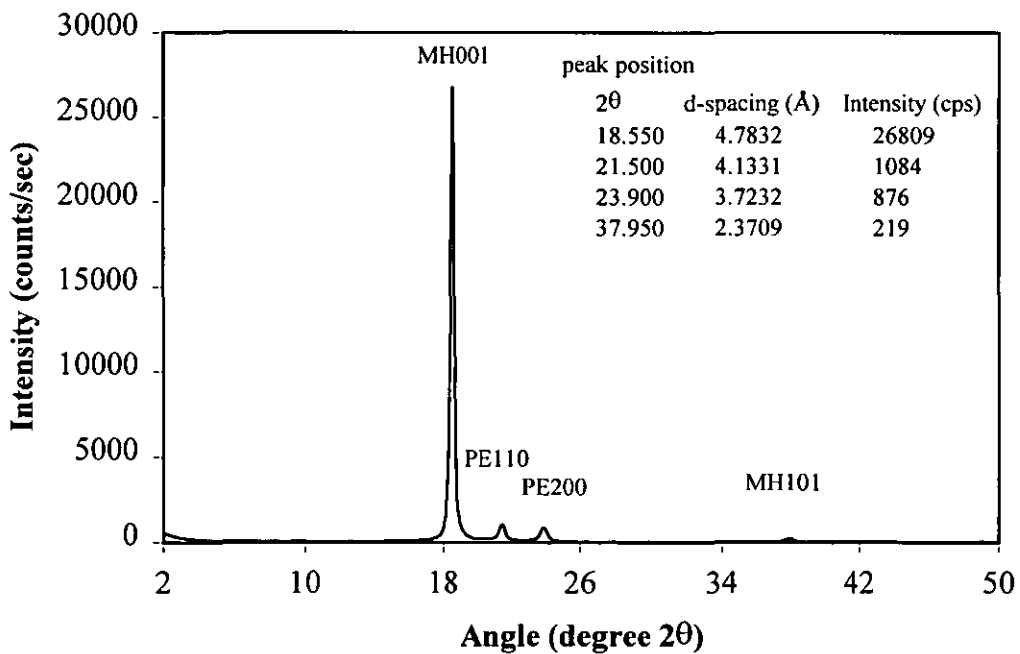
b.: HDPE unfilled (anisotropic orientation) using injection moulding.



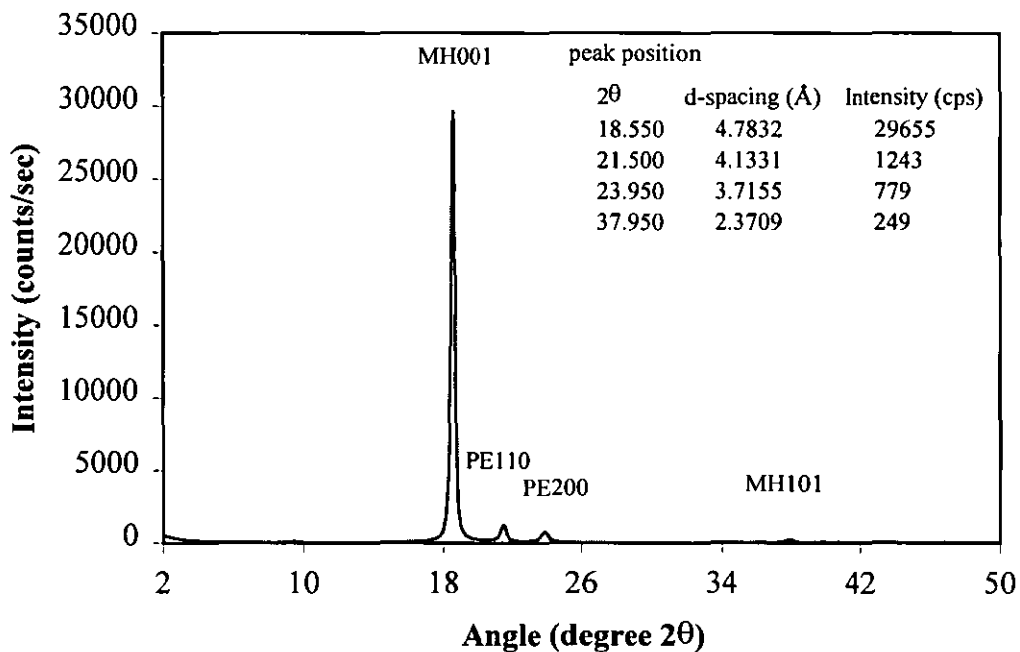
c.: HDPE containing uncoated $\text{Mg}(\text{OH})_2$.



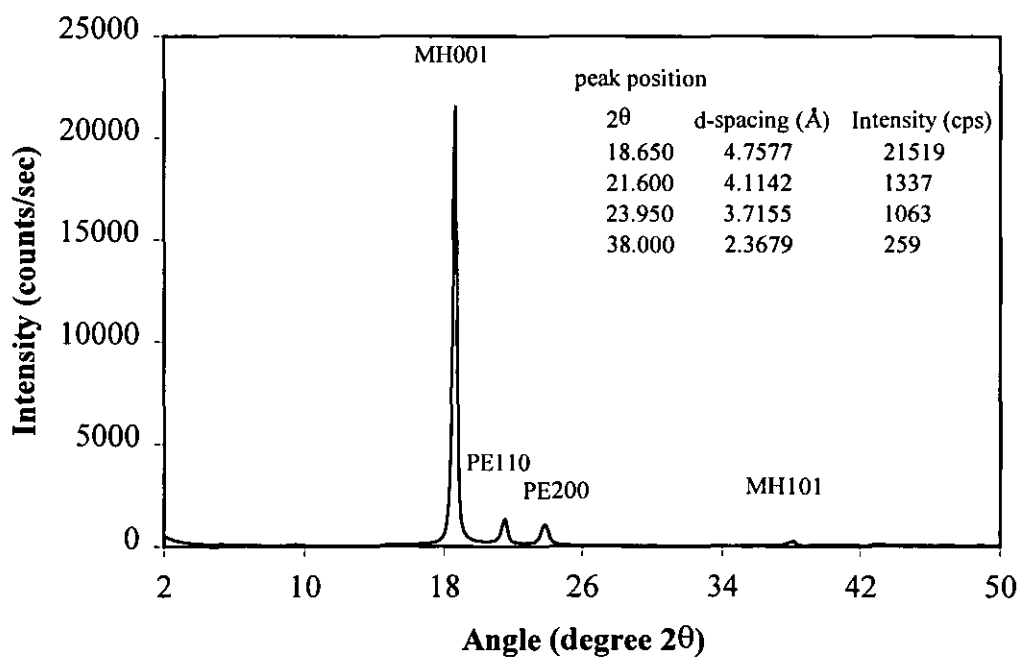
d.: HDPE containing magnesium hydroxide coated with 6.2% magnesium stearate.



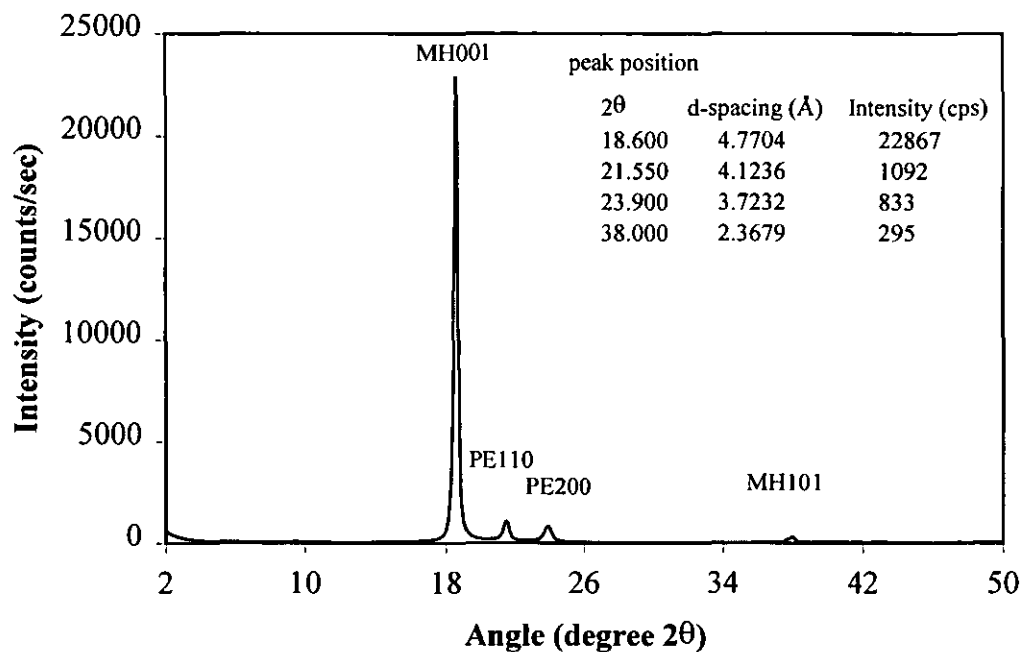
e.: HDPE containing magnesium hydroxide added with 6.2% magnesium stearate.



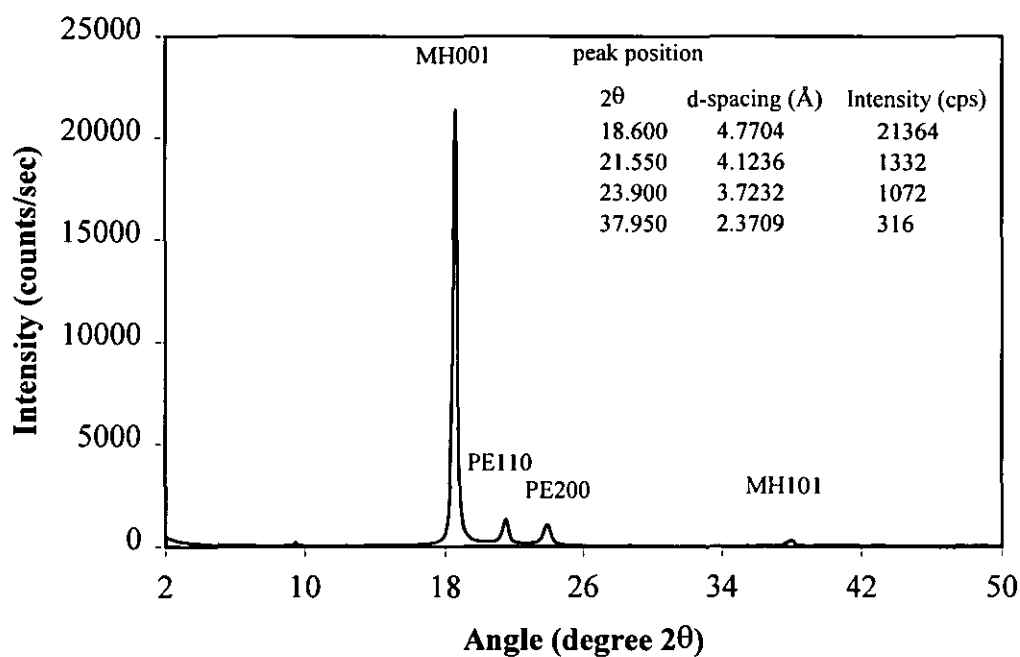
f.: HDPE containing magnesium hydroxide coated with 6.4% calcium stearate.

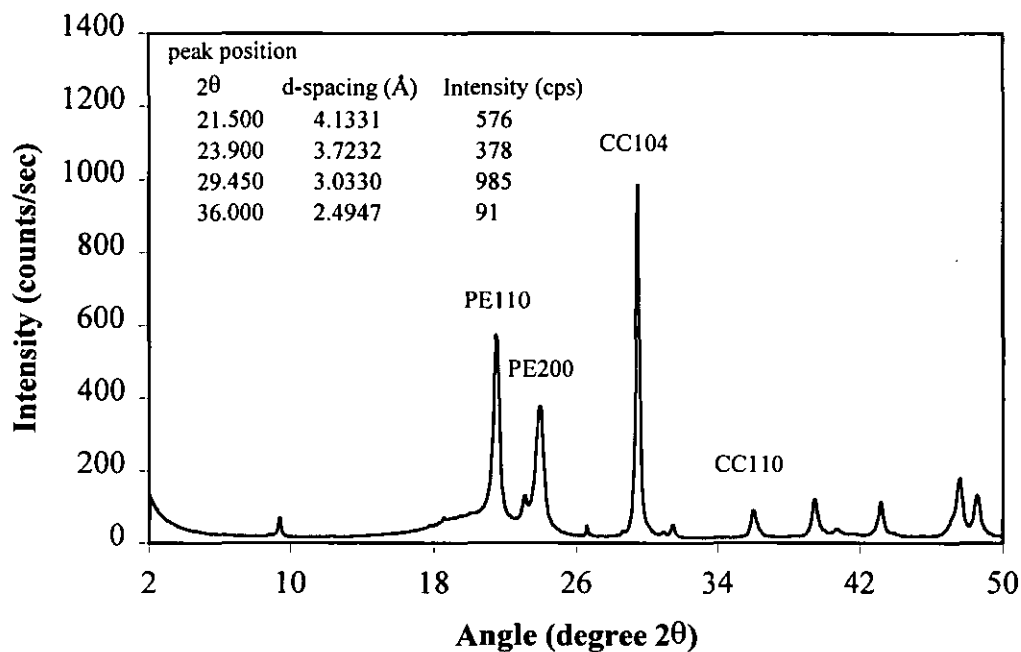


g.: HDPE containing magnesium hydroxide coated with 6.7% zinc stearate.

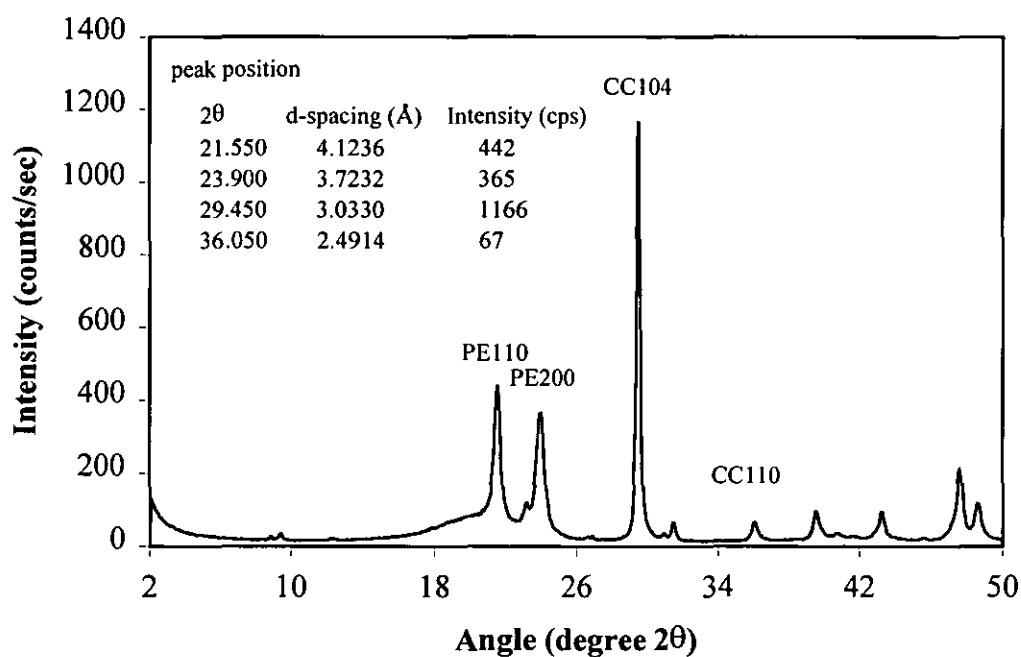


h.: HDPE containing magnesium hydroxide coated with 6.0% stearic acid.

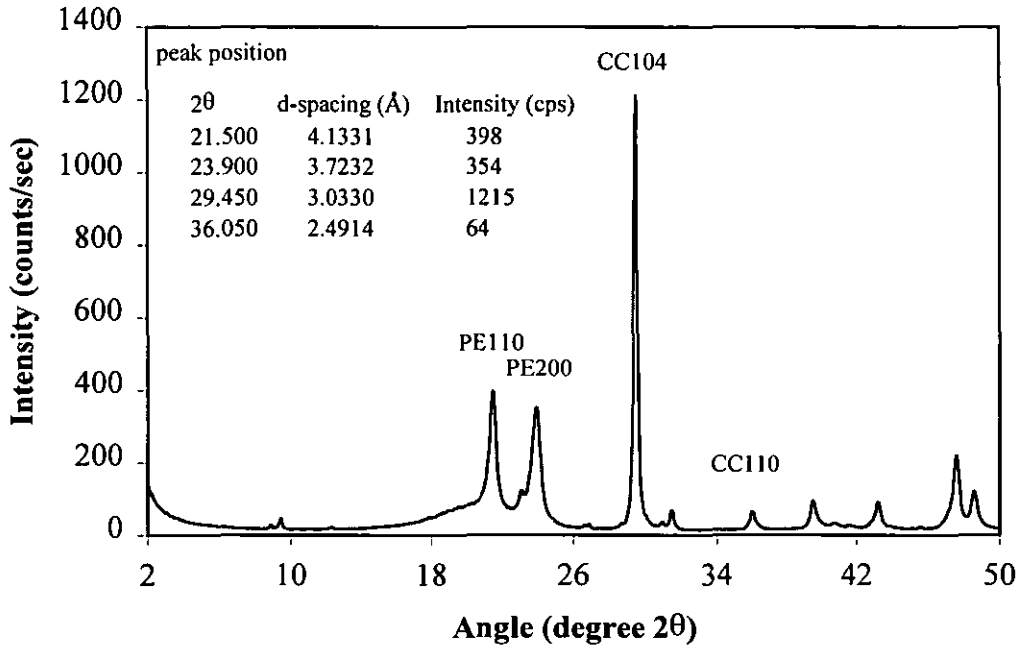


G.2: X-ray patterns of CaCO₃ filled HDPE composites.a.: HDPE containing uncoated CaCO₃.

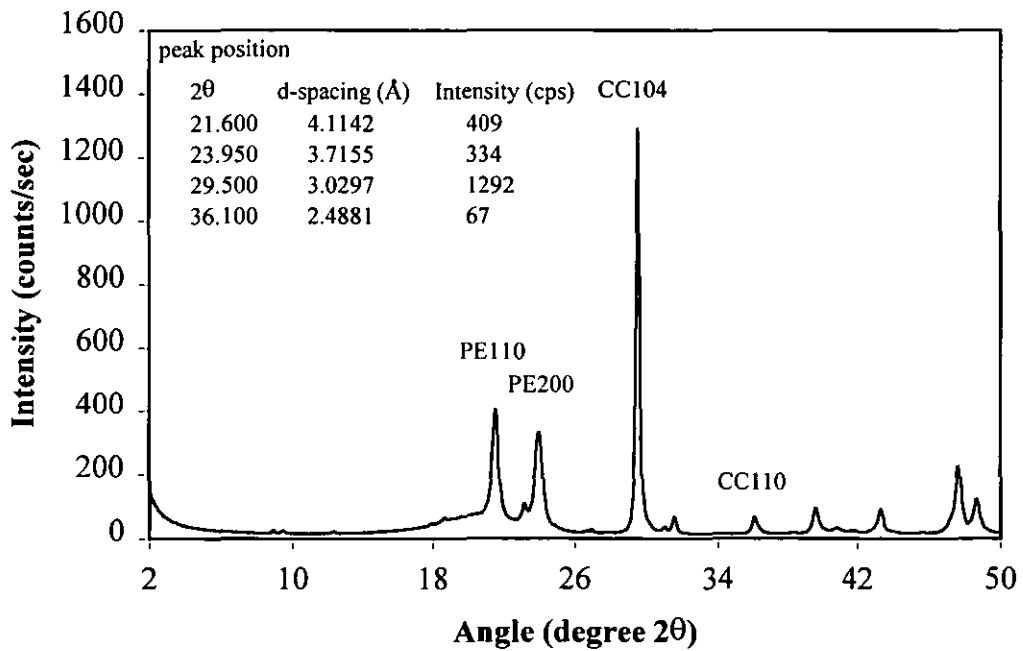
b.: HDPE containing calcium carbonate coated with 4.2% magnesium stearate.



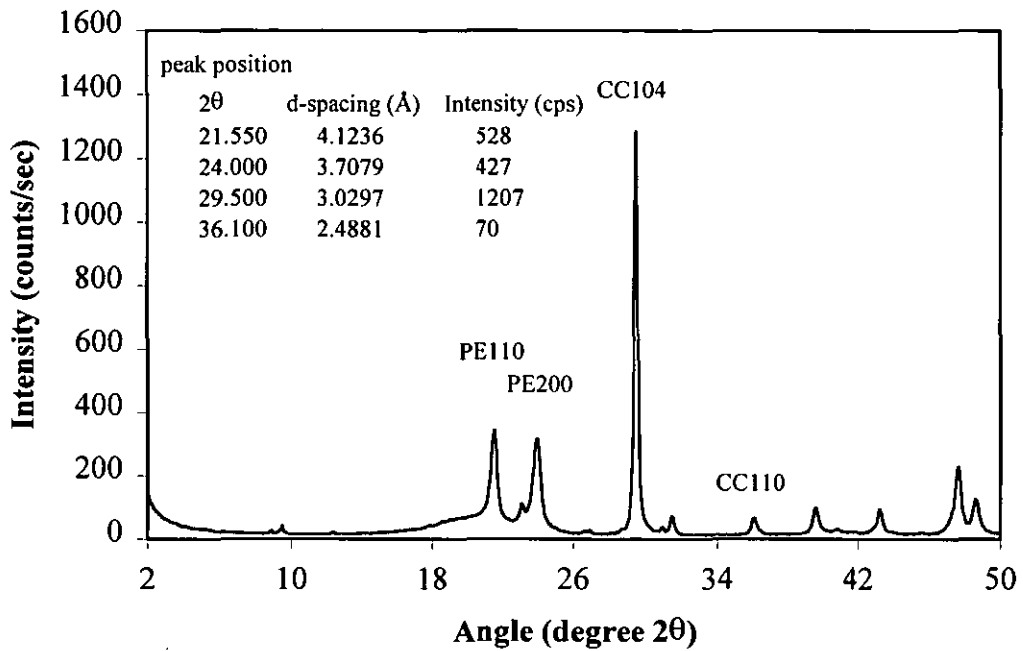
c.: HDPE containing calcium carbonate coated with 4.3% calcium stearate.



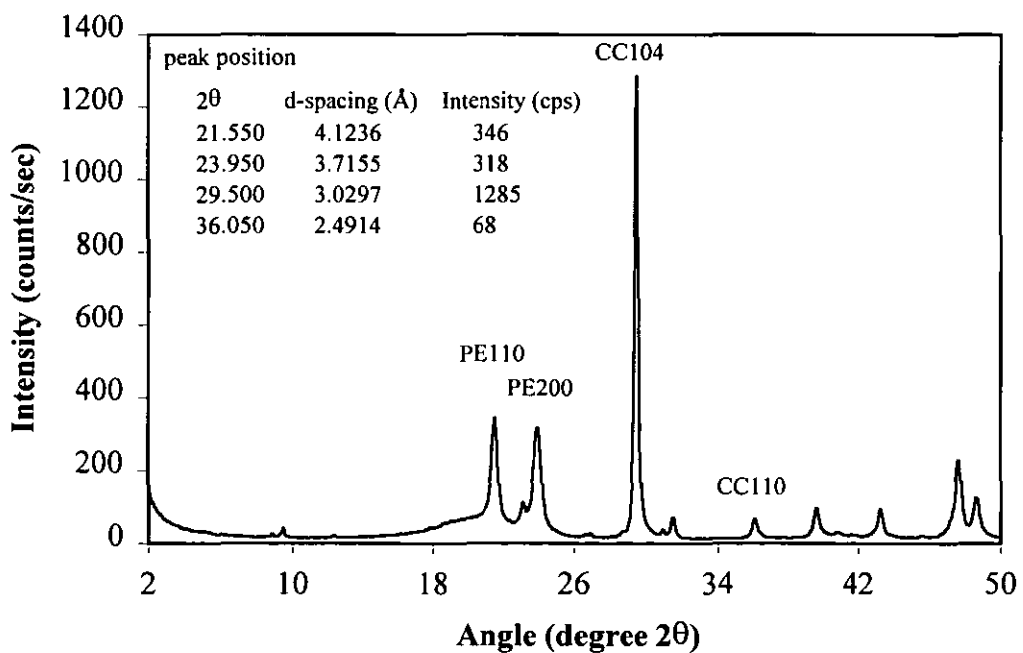
d.: HDPE containing calcium carbonate added with 4.3% calcium stearate.



e.: HDPE containing calcium carbonate coated with 4.5% zinc stearate.

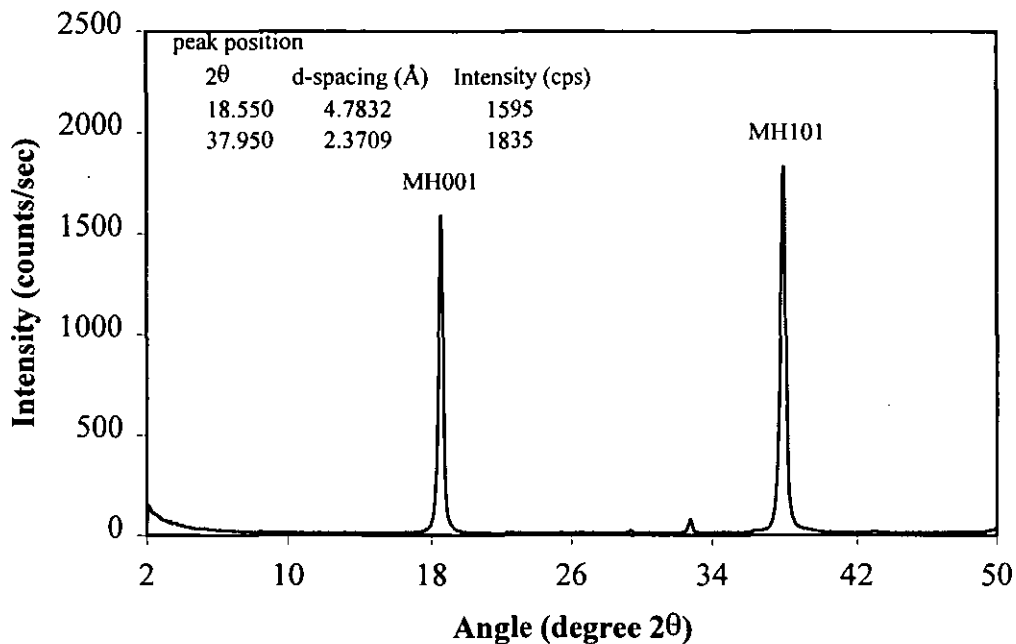


f.: HDPE containing calcium carbonate coated with 4.0% stearic acid.

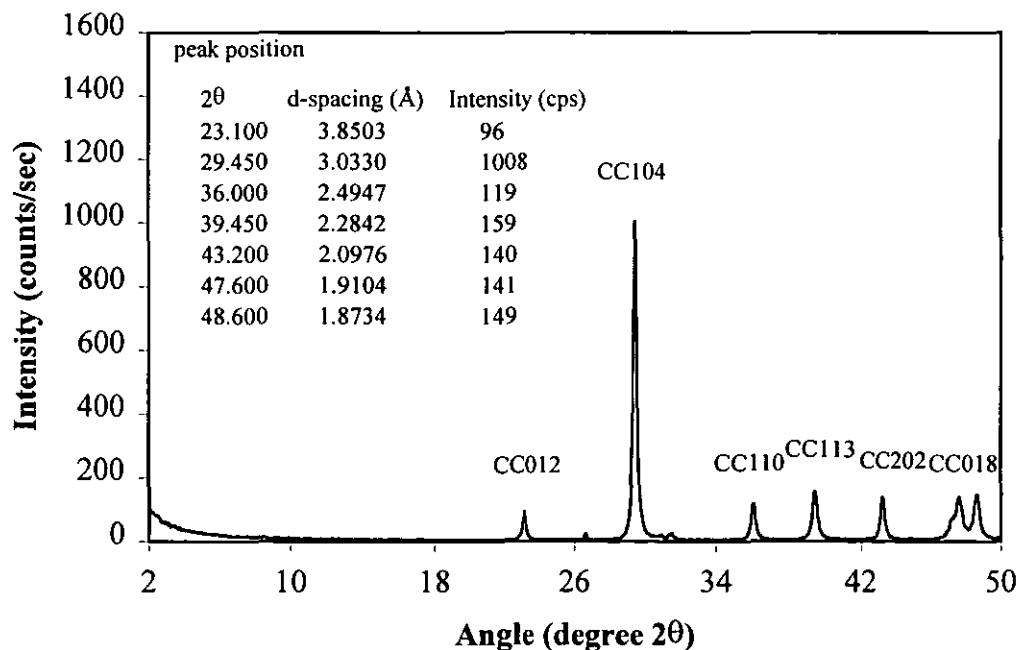


G.3: X-ray patterns of fillers.

a.: Magnesium hydroxide (random orientation).

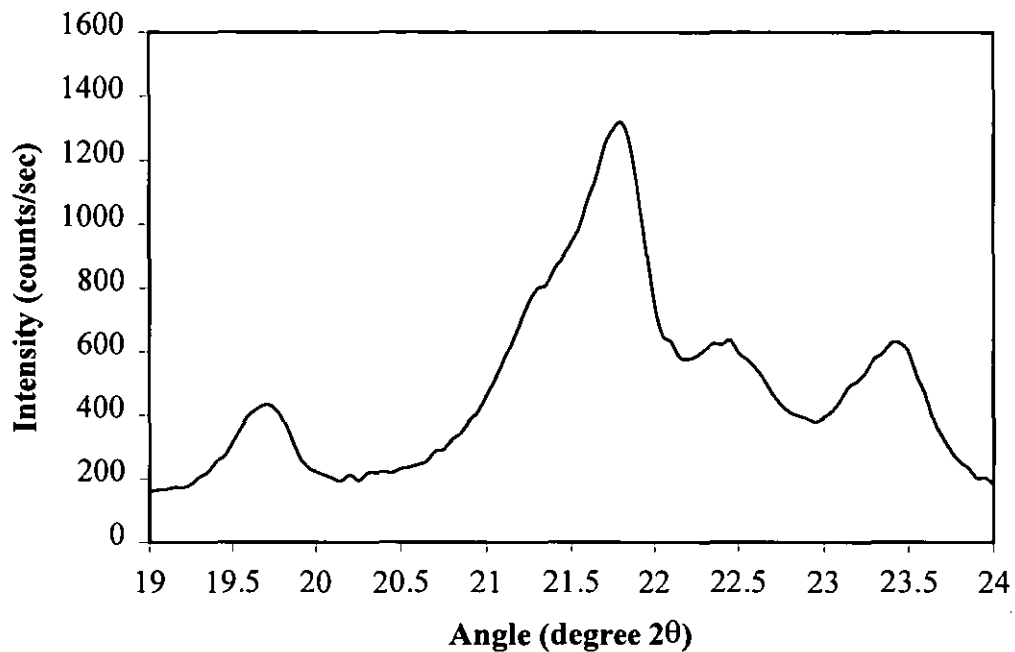


b.: Calcium carbonate (random orientation).

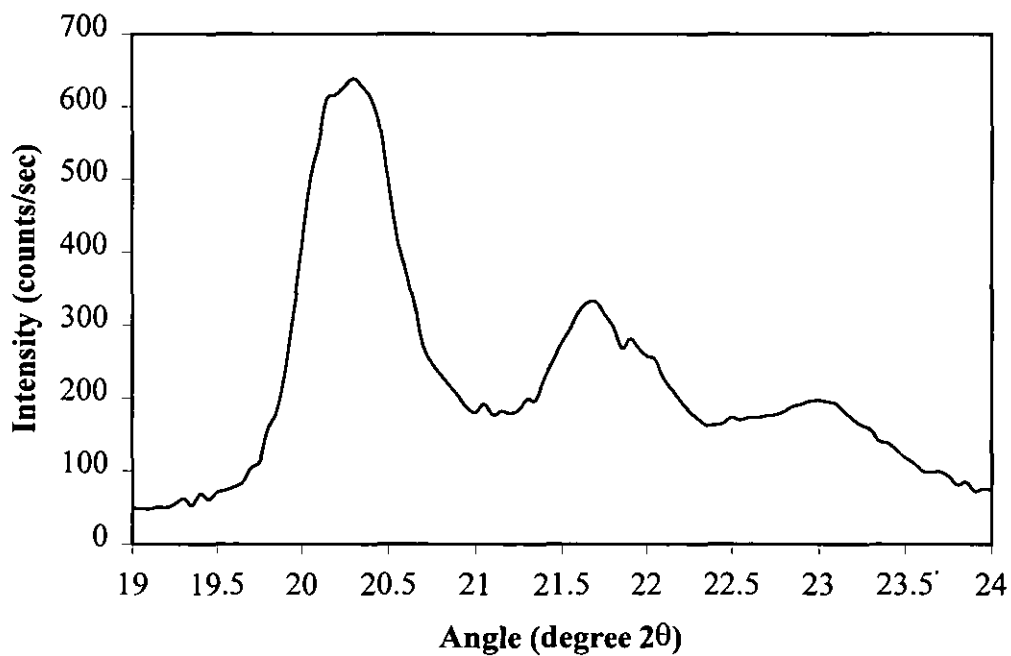


G.4: X-ray patterns of coating agents.

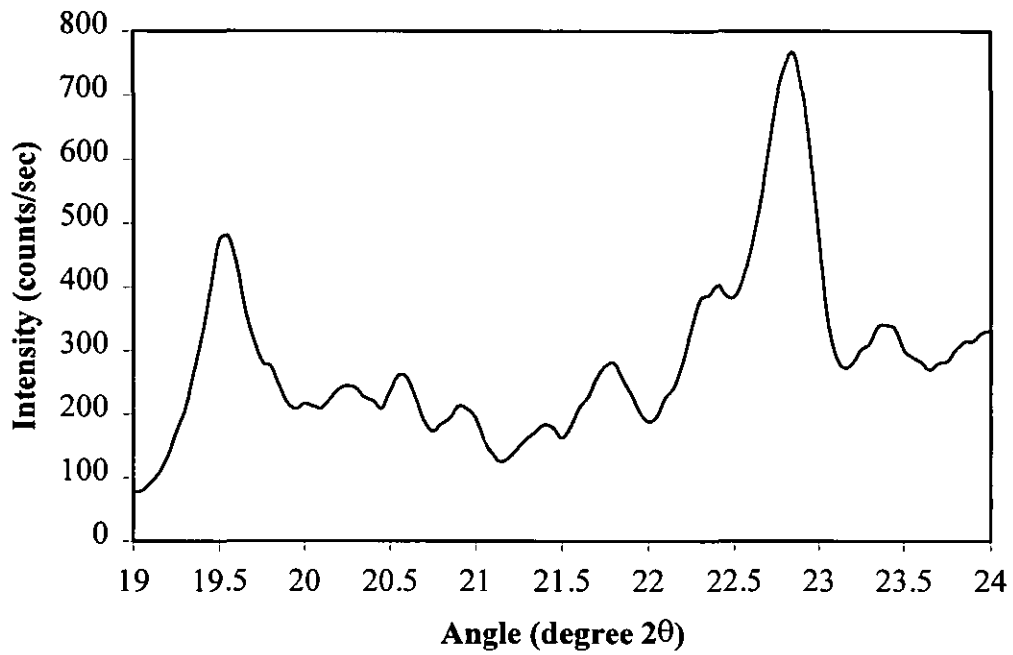
a.: Magnesium stearate.



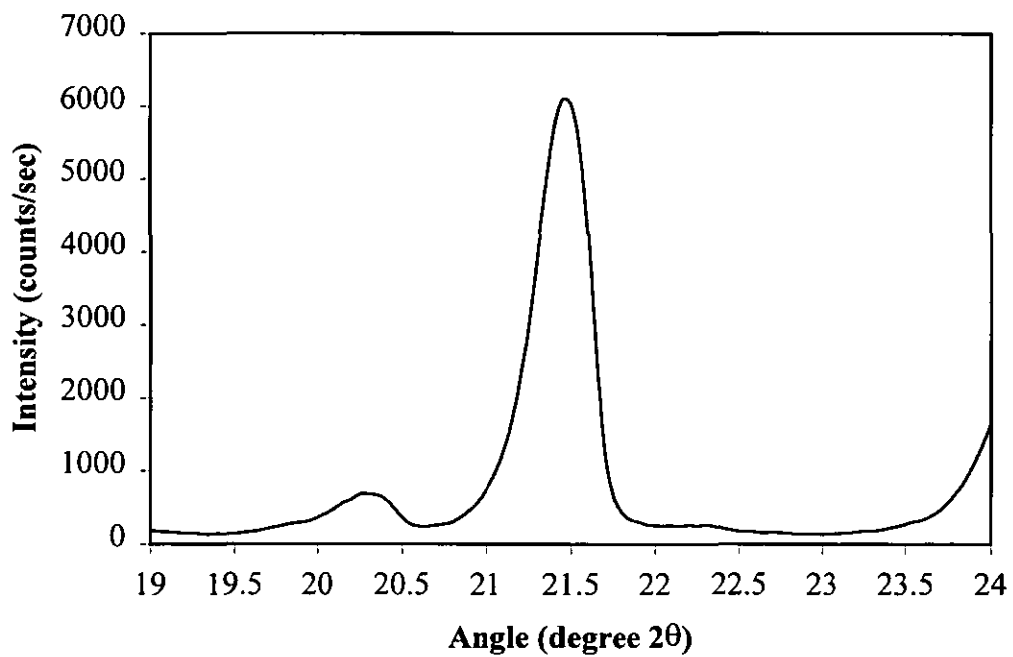
b.: Calcium stearate.



c.: Zinc stearate.

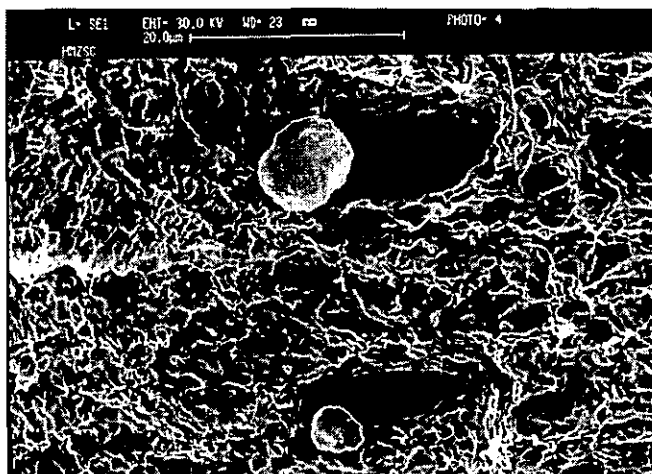


d.: Stearic acid.

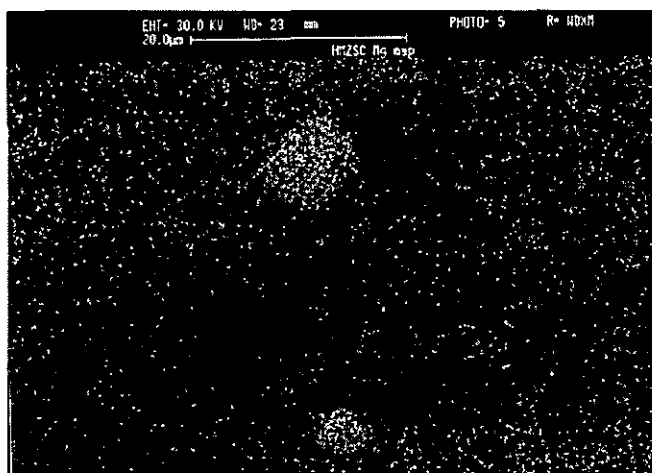


APPENDIX H: MICROGRAPHS

a) HMZSC67



b) HMZSC67 (Mg mapping)

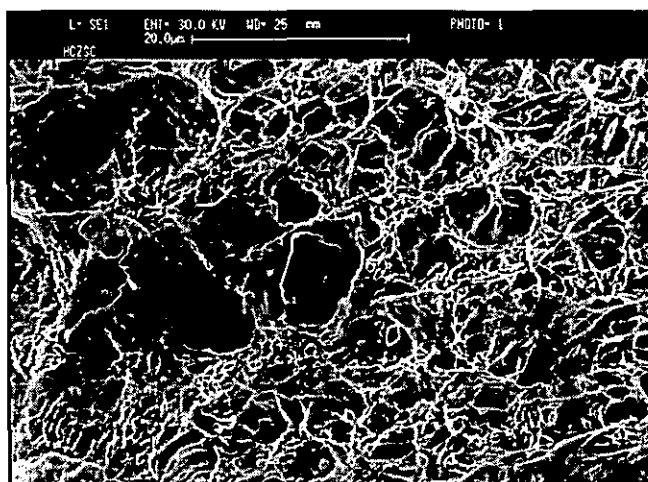


c) HMZSC67 (Zn mapping)

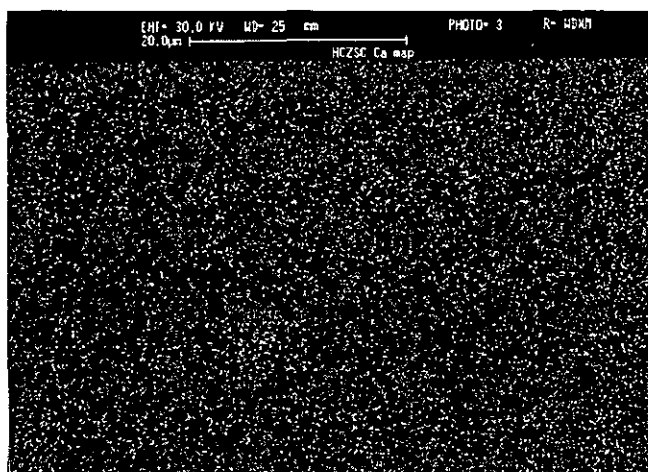


Figure H.1: Micrographs of HDPE compounds containing $Mg(OH)_2$ coated with 6.7%w/w zinc stearate a) image, b) Mg mapping, c) Zn mapping.

a) HCZSC45



b) HCZSC45 (Ca mapping)



c) HCZSC45 (Zn mapping)



Figure H.2: Micrographs of HDPE compounds containing CaCO_3 coated with 4.5%w/w zinc stearate a) image, b) Ca mapping, c) Zn mapping.

APPENDIX I: LIST OF PUBLICATIONS

1. M Gilbert and P Petiraksakul, "Magnesium stearate as a coating for magnesium hydroxide filler in polyethylene", paper presented at *Loughborough Fillers Symposium II*, 17th -18th, September, Loughborough, UK, 1996.
2. M Gilbert and P Petiraksakul, "Effect of type and level of stearate coating on properties of filled compounds", paper presented at *Eurofillers 97*, 8th-11th, September, Manchester, UK, 1997.
3. M Gilbert and P Petiraksakul, "Stearate coatings on particulate fillers-the effects on resulting compound properties", *Polymers & Polymer Composite*, Vol. 5, No. 8, p.535-539, paper presented at Addcon Asia '97 conference, 28th-29th, October, Singapore, 1997.
4. M Gilbert, P Petiraksakul, and I Matheson, "Stearate coating of magnesium hydroxide and calcium carbonate fillers", paper presented at *Eurofillers 99*, September, France, 1999.

